STUDIES OF ODD-A NUCLEI IN THE 2S-1D SHELL

by

Joseph P. Allen
(B. A., DePauw University, 1959)
(M.S., Yale University, 1961)

A Dissertation Presented to the Faculty of the
Graduate School of Yale University in
Candidacy for the Degree of
Doctor of Philosophy
1965

To my mother, my father,

and to Bonnie Jo

ABSTRACT

Experimental measurements of a number of level parameters in 2s-1d shell nuclei have been carried out, and attempts have been made to interpret these new data in terms of the corresponding predictions of currently existing nuclear models, including the asymmetric rotor model, the individual-particle spherical shell model, and the Nilsson unified model, which have been previously applied to this mass region.

Studies of gamma radiation following resonant proton capture by O^{18} have established the angular momentum of the 3.91 MeV state of F^{19} as 3/2 and, when coupled with previously reported data, have established the angular momentum of the 2.79 MeV F^{19} state as 9/2. Precise gamma deexcitation branching ratios of the 3.91 and 8.76 MeV levels of F^{19} have been determined.

Gamma radiation studies of the $O^{18}(d,p)O^{19}$ reaction have established the spin of the 0.096 MeV state of O^{19} as unambiguously 3/2 and the spin of the ground state as most probably 5/2. The deexcitation branching ratio of the O^{19} 1.47 MeV state has been accurately measured. No evidence for gamma radiation deexciting a recently reported 0.348 MeV state of O^{19} has been found.

Finally, measurements have been made of deexcitation branching ratios and radiation angular correlations of transitions originating from particular states in the systems Na^{21}, Ne^{21}, Na^{23}, and Ne^{23}. Qualitative investigations of proton angular distributions from the reaction $Ne^{22}(d,p)Ne^{23}$ have been carried out and suggest J^{π} assignments of $5/2^+$, $1/2^+$, $7/2^+$, and $1/2^+$ to the 0, 1.02, 1.83, and 2.32 MeV states of Ne^{23}, respectively. A number of further experimental investigations of interest as suggested by these and other related studies is discussed.

ACKNOWLEDGEMENTS

I would like to thank my thesis advisor, Prof. D. A. Bromley, for his guidance, encouragement, and active participation in all phases of this investigation. The assistance and advice given to me by Prof. Bromley over a number of years is, and will be, gratefully remembered.

It is a pleasure to thank Dr. A.J. Howard of Trinity College for his invaluable aid in the collection and interpretation of the data presented herein. The many hours of stimulating discussion with Dr. Howard are also appreciated.

The interest, guidance, and cooperation of Dr. J. W. Olness of Brookhaven National Laboratory during the experimental stages of this work is gratefully acknowledged.

The data reported herein was obtained in full at the Brookhaven National Laboratory Van de Graaff installation. I would like to thank the staff of the Van de Graaff Laboratory and in particular the director, Dr. D. E. Alburger, for the generosity and assistance extended to me during this investigation.

I wish to thank Dr. I. Kelson and Dr. G. Garvey for helpful discussions in connection with this work.

I am indebted to Miss Cathy Barton for the excellent preparation of the figures in this dissertation. In addition, special thanks are extended to my wife for the typing of a number of drafts and of this, the final manuscript.

Finally, I would like to thank the United States Atomic Energy Commission for financial support of this research.

PREFACE

Detailed calculations of the properties of a bound, many-body, quantum mechanical system such as an atomic nucleus in principle must be based on (i) a precise knowledge of the nucleon-nucleon (or perhaps nucleon-nucleus) force, and (ii) an adequate mathematical technique for handling a many-bodied system. Unfortunately, very little beyond the general features of the nuclear force is yet known; furthermore, no exact mathematical treatment has been developed to represent the great complexity of a many-particle structure. Hence the problem of theoretically understanding and describing the nuclear constitution can at present be solved only through relatively crude, but improving, mathematical approximations known as "nuclear models".

A nuclear model is formulated on the basis of postulates, assumptions, and approximations which reduce the insoluble problem to a soluble one and, hopefully, introduce as little error as possible into the problem. The model selected is then used to generate, through the appropriate mathematical operations, specific nuclear wave functions and eigenvalues, leading in turn to the predictions of such properties of nuclear states as angular momenta, parities, electromagnetic moments, deexcitation transition rates, and reduced widths. Comparison of these predictions with the corresponding experimental quantities then provides a measure of the validity of the model and, through this, an indication of the validity of the initial assumptions on which the model is based.

A successful model is, first of all, a mathematical framework which serves to catalogue and to correlate large quantities of experimental information. More basically, however, the success of a model is found in the physical consistency of its assumptions and in its anticipation and prediction of trends in nuclear properties. Since an approximate solution replaces real solutions of the nuclear system, exact agreement between model predictions and experimental measurement cannot be expected. On the other hand, as complete as possible a knowledge of the relationship between the model and the actual nucleus is essential to knowing both the limitations of the model and the possible means of extending these limitations

in order that the model represent more closely the exact description of the nucleus.

It is with several recently formulated nuclear models and their relationship to experimental measurements that this thesis is concerned. Studies of various level parameters have been carried out via a number of standard experimental techniques on nuclei in the low end of the sd shell, a mass region in which a single particle model, whether within the shell or collective frameworks, is thought to have particular validity; consequently, such models have been applied to specific nuclear systems in this region with a high degree of sophistication. Attempts are then made to compare detailed model predictions to these experimental measurements in order to understand where, and for what reasons, different model formulations are compatible and where, and from what causes, serious incompatibilities in these model formulations emerge. In particular, studies on O^{19} and F^{19} have been carried out in an effort to understand more fully to what extent the asymptotic Nilsson model and to what extent the spherical shell model are applicable in these nuclear systems. Measurements on nuclei of odd-nucleon number 11, Ne^{21}, Na^{21}, and Na^{23}, have been carried out to provide data on these nuclear systems which should be analogous in the Nilsson model sense and, therefore, which should have similar experimental properties provided the model is applicable in this region. Finally, initial experimental investigations of Ne^{23} have been undertaken to obtain information to be compared within the Nilsson model framework to the extensively studied, relatively well understood nuclei, Mg^{25} and Al^{25}.

TABLE OF CONTENTS

I. INTRODUCTORY CONSIDERATIONS OF THE SD-SHELL NUCLEI.

A. Orientation

Within the past several years there has been a striking increase in the amount of experimental information[1,2] available on nuclei between O^{16} and Ca^{40} in the region where the $2s_{1/2}$, $1d_{5/2}$, and $1d_{3/2}$ shells of the simple, single-particle shell model are filling. This reflects in part the recent technical advances necessary to the investigation of these nuclei which are clearly more complex than those in the p shell; specifically, the construction of higher energy accelerators of precisely controlled mono-energetic beams and the development of more sophisticated particle and gamma radiation detection equipment. However, the major incentive to experimental investigators has undoubtedly been the rather remarkable success of a variety of nuclear models[3,4,5] in providing a better understanding of the behavior of nuclei in this mass region and, at the same time, in pointing up areas where much more experimental information is needed. The research reported herein has been carried out in order to provide data necessary to further examination of the relative validity of various models which have been applied to selected odd-A nuclei in the sd shell.

This shell is theoretically interesting for several reasons. Unlike the p shell, the availability of the three subshells, $d_{5/2}$, $d_{3/2}$, and $s_{1/2}$, allows a large number of nucleon configurations and, consequently, provides a rich variety of experimental phenomena to be studied and correlated. Moreover, nuclei spanning this mass region contain up to 12 neutrons and 12 protons outside the doubly magic O^{16} core; this has been shown to be adequate to justify the application of various collective approaches, and yet is not such as to preclude shell model calculations whose complexity increases rapidly with the number of nucleons involved. That both the collective and the shell model interpretations have been shown to have considerable validity in the sd shell has led, in fact, to a major effort and to major progress in understanding and correlating the

interrelationship between these models which, although sharing various aspects of single particle motion, are not a priori closely related.

The remainder of this chapter is devoted to a brief review of several of the major theoretical approaches which have been applied with some success to sd-shell nuclei.

B. Individual Particle Spherical Shell Model

1. Basic Considerations:

The starting point for all shell model calculations, of which the individual particle shell model is a specific example, is the assumption that all nucleons move independently of each other within a central, static, potential field generated in some self-consistent fashion by all the nucleon-nucleon interactions present. The exact form of the central potential is not known; however, its general features are well represented by a three dimensional, harmonic oscillator well. In addition to this static potential each nucleon has been shown to be subject to the now famous strong spin-orbit interaction postulated by Mayer[6] and by Haxel, Jensen, and Suess[7]. A particularly successful shell model potential approximation may be written as

$$V = \frac{1}{2} M\omega_o^2 r^2 + D\,\vec{l}\cdot\vec{l} + C\,\vec{l}\cdot\vec{s} \qquad \text{(I-1)}$$

where M is the mass of the nucleon, ω_o the frequency of the classical oscillator, and $\vec{l}$ and $\vec{s}$ the orbital and intrinsic angular momenta, respectively. The first two terms are those of the harmonic oscillator well modified (by the second term) to resemble the shape of a finite square well for high angular momentum states. The third term is the spin-orbit interaction. This version of the potential V has been used by various authors on an ad hoc basis, but has since been shown from pairing and quadrupole force considerations[8] to include the terms which are indeed dominant within the "real" nuclear potential. It should be noted that, unlike the analogous shell model situation in atomic structure where residual, long range, electron interactions provide a positive $C\,\vec{l}\cdot\vec{s}$ term,

the parameter C in Equation I-1 is required phenomenalogically to be negative and of a magnitude such that it can be due only to strong, short range, nuclear forces.

Solution[9] of the problem of a single particle in this potential leads to a separable, single-particle wave function of the following product form

$$\varphi_{nlmm_s m_t} = R_{nl}(r)\, Y_l^m(\theta,\varphi)\,\sigma(m_s)\,\tau(m_t) \qquad \text{(I-2)}$$

where $R_{nl}(r)$ is the radial wave function[10] which is a solution of the equation

$$\frac{-h^2}{2M}\left[\frac{1}{r^2}\,\frac{d}{dr}\left(r^2\,\frac{d}{dr}R_{nl}\right) - \frac{l(l+1)}{r^2}\right]R_{nl} + \left[V - E_{nl}\right]R_{nl} = 0. \qquad \text{(I-3)}$$

$Y_l^m(\theta,\varphi)$ is the spherical harmonic function, $\sigma(m_s)$ the Pauli spin vector of angular momentum m_s along the z-axis, and $\tau(m_t)$ the analogous isotopic spin vector of fixed charge m_t. The orbital angular momentum and its component along z are specified by $\vec{l}$ and m respectively, (n—l) is the number of nodes in the radial wave functions.

The energy eigenvalues corresponding to these wave functions result in the familiar energy level diagram which successfully reproduces[11] the magic numbers found experimentally in many nuclear phenomena. If used in conjunction with several somewhat arbitrary rules[12] for determining the resultant spin of two or more extra-core nucleons, this simple model is also capable of reproducing the ground state spins and parities of almost all nuclei; and for odd-A nuclei it predicts with varying degrees of success[13] magnetic dipole moments, beta decay transition probabilities, and the islands of isomerism. But the model is much less successful in dealing with other nuclear properties such as the spacing and behavior of excited states, total binding energies, and both static and dynamic quadrupole strengths. Moreover, minor changes in the simple shell model formalism are not sufficient to bring the model into agreement with experiment; for this reason, several major modifications of this model have been necessary.

2. Inclusion of Residual Forces:

The first step in revision of the simple shell model is to take account of the obvious omission of interactions between nucleons with similar wave functions, particularly those outside a major core. Inclusion of these residual interactions is carried out in the following way. Rather than replacing the total nucleon-nucleon force by an average central potential as was done in the extreme single particle model, this generally assumed two-body interaction is divided arbitrarily into two components; the major part comprises the central potential V_i in which the i^{th} nucleon moves undisturbed, while the remaining portion provides a residual interaction v_{ij} between the nucleons i and j in the unfilled shell. The Hamiltonian of this system is written

$$H = \sum_i (T_i + V_i) + \sum_{i<j} v_{ij} \qquad \text{(I-4)}$$

where V_i is given by Equation I-1 and T_i is the kinetic energy of the i^{th} particle. As prescribed by first order perturbation theory, the wave functions for a nucleus with n nucleons in a partially filled orbit outside the closed core are then approximated by (1) coupling together the simple, single-particle wave functions $\varphi_{nlmmsmt}$ provided by the static central potential to form properly antisymmetrized states of n particles as given by the Slater determinant

$$\Phi_\nu \text{ (n particles)} = \sqrt{\frac{1}{N!}} \begin{vmatrix} \varphi_{\nu 1}(1) & - - - & \varphi_{\nu 1}(n) \\ \varphi_{\nu 2}(1) & & \\ & & \\ \varphi_{\nu n}(1) & & \varphi_{\nu n}(n) \end{vmatrix}, \qquad \text{(I-5)}$$

(these wave functions must of course be coupled together in such a way as to be eigenfunctions of both the total spin and isotopic spin of the system), (2) using the properly coupled, antisymmetrized wave functions to set up the energy matrix of the system, and (3) diagonalizing the energy matrix to obtain the eigenfunctions and eigenvalues of the system. In other words, the model energy levels of the

nucleus are obtained by including the residual interaction as a hopefully small perturbation on the simple shell model wave functions. It is these perturbations that result in mixing of pure shell model configurations. As will be demonstrated later, the residual forces which correlate the motions of the outer nucleons in general result also in polarization of the nuclear core, hence deformation of the nucleus and the corresponding deformation of the central shell model potential thus far ignored, but readily included in the formalism by appropriate generalization of the $\frac{1}{2} M\omega_o^2 r^2$ term of Equation I-1.

As in the case of the familiar intercombination of levels in the atomic models, nucleons in the last unfilled shell of the nuclear model can couple their individual angular momenta in a variety of ways to form states of differing total angular momentum J. In the absence of residual interactions, states of different J are degenerate; however, the residual interaction removes this degeneracy and thus determines the energy ordering of the multiplet states based on the same orbital configurations but having different total angular momentum J. This ordering and subsequent energy spacing of states depends on the form of the residual interactions. Unfortunately, just as the average central potential is a mathematical abstraction and clearly does not correspond exactly with the physical case, the residual forces may not a priori be assumed as real in the sense that they could be measured in, say, p-p or p-n scattering experiments. Consequently, these forces must either be estimated through some basic theory of nuclear matter or they must be determined empirically within the framework of a model. The latter method is the one traditionally used.

In such an approach, predictions of the model under consideration in which residual interactions (represented by operational parameters) have been included are compared to experimental level schemes of nuclei in the mass region of interest. If the experimental nuclei are such that the residual interactions are the dominant perturbation on otherwise simple shell model structures, then the form of the unknown residual interactions is reflected directly in the experimental level schemes, and the interactions may be approximately determined from these schemes. It is, of course, difficult to obtain useful information in this regard from complex many-bodied systems; for that reason, nuclei of hopefully simple

configurations are chosen for the level schemes with which to compare predictions: eg. Li^6 (2 p-shell particles) in the case of the p shell, F^{18} (2 sd-shell particles) in the case of the lower portion of the sd shell. Since a nuclear system n nucleons removed from a closed core can be represented mathematically in the same way as a system with n extra-core nucleons, equivalent simple "hole" configurations (such as K^{38} in the case of the upper sd shell) may likewise be used to determine the residual interactions between "hole" states.

If residual forces are primarily central interparticle forces, the outer nucleons will couple their angular momenta according to the L-S approximation well known in atomic physics; if the forces are predominately proportional to the $\vec{l} \cdot \vec{s}$ of the particle, j-j coupling of the nucleons results. The situation which lies intermediate between spin-orbit and central interactions is customarily referred to as intermediate coupling. It is this intermediate situation (represented as a ratio a/K of spin-orbit interaction strength to exchange integral magnitude) which has been used extensively by Inglis[14] and by Kurath[15] in representing nuclei in the p shell, by Elliott and Flowers[16], by Redlich[17], and quite recently by Flowers and Wilmore[18], and by Inoue et al.[19] for selected nuclei in the sd shell.

Bouten, Pullen and Elliott[20] have recently carried out a more extensive, but approximate, intermediate coupling model calculation for all sd-shell nuclei using computational methods similar to those applied by Inglis in the p shell in which the level energies and the first derivative of the energies with respect to the coupling parameters are calculated for the nuclei under consideration in both the j-j and L-S coupling limits. The situation of intermediate coupling is then approximated by interpolating between corresponding levels in the two limits. It should be noted that in spite of the sweeping approximations inherent in the intermediate-coupled shell model itself, rigorous solution of four particle systems within its framework already taxes severely the largest computers readily available for such problems.

Other model calculations utilizing the j-j coupling approximation with a limited number of nucleon configurations have been applied by Talmi and Unna[21] to several nuclei at the low end of the sd shell while McCullen, Bayman, and Zamick[22] have extended this work into the $1f_{7/2}$ shell. In addition, a very recent

investigation of the sd-shell nuclei in the range Si^{29} to Ca^{40} has been carried out within the j-j coupling approximation by Glaudemans, Weichers, and Brussard[23] in which all two-particle interactions between outer nucleons in the $1d_{3/2}$ and $2s_{1/2}$ shells are taken into account.

The individual particle shell model just discussed is found to improve qualitatively on a number of the simple shell model predictions in the areas of nuclear phenomena previously listed. It shows good success in reproducing many experimental properties of the ground and low-lying states of nuclei near closed shell configurations and also leads to an increased understanding of certain nuclear reaction data.

The model's success is marred, however, by its complete inability to reproduce correctly the electric quadrupole matrix elements necessary for generating both static quadrupole moments and E2 transition probabilities. The basis of this difficulty lies at the very foundations of the shell model; namely, the assumptions that individual nucleon states are essentially uncorrelated and that the central potential is both spherical and static. It is therefore not surprising that the initial solution to these problems comes from a model that emphasizes an entirely different aspect of nuclear behavior by attributing nuclear properties to all nucleons of a nucleus, not to just the few nucleons in an unfilled shell.

C. Collective Model

The initial concepts of the nuclear model to be considered in this section were first formulated by Bohr and Wheeler[24], who compared the behavior of a dense liquid drop to that of a nucleus undergoing fission. Rainwater[25] modified this liquid drop model by considering the polarization of the deformable core caused by a single nucleon moving in an external orbit about the core, thus providing a semi-qualitative explanation of experimentally observed large quadrupole moments. A. Bohr[26] and his co-workers have extended these ideas still further to include detailed detailed descriptions of both static and dynamic properties of the hydrodynamical, or collective, model as this extended formulation

is now known.

The basic premise of the collective model is that the nucleus is composed of closely coupled, strongly interacting particles. Any energy acquired by a particular nucleon is quickly shared with all other nucleons in the system, hence all nuclear phenomena (within this model) arise from the coordinated motion of many nucleons. Nuclear excitations are considered as oscillations of the nuclear surface about its equilibrium shape, or, if the equilibrium shape is aspherical, as rotations of the surface about an axis not identical with that of symmetry, if such symmetry exists in the deformation. For small deviations from sphericity the nuclear surface may be represented by

$$R = R_o\left[1 + \sum_{\lambda=0}^{\infty} \sum_{\nu=-\lambda}^{\lambda} \alpha_{\lambda\nu} Y_\lambda^\nu(\theta,\varphi)\right] \tag{I-6}$$

where θ and φ are angles with respect to a space-fixed coordinate system, $Y_\lambda^\nu(\theta,\varphi)$ are the spherical harmonics, and $\alpha_{\lambda\nu}$ are deformation parameters which are functions of time. It is usually assumed, in the simple case at least, that the nucleus does not depart drastically from sphericity; hence deformations only up to $\lambda = 2$, corresponding to quadrupole deformations known experimentally to be important, are considered. Furthermore, since $\lambda = 0$ deformations do not conserve the nuclear volume and are consequently thought to be physically unrealistic, and since $\lambda = 1$ deformations correspond to the physically uninteresting case of translation of the nuclear center of mass, these terms are neglected.

Under these assumptions, the Hamiltonian of the collective system may be written as

$$H_{\text{collective}} = \sum_\nu \left[\frac{1}{2} B \left|\dot{\alpha}_{2\nu}\right|^2 + \frac{1}{2} C \left|\alpha_{2\nu}\right|^2\right] \tag{I-7}$$

where B and C are parameters analogous to mass and surface tension in the problem of a continuous liquid drop. Terms higher than those quadratic in $\alpha_{\lambda\nu}$ and $\dot{\alpha}_{\lambda\nu}$ have been neglected. The frequency associated with the time dependent variable is $\omega = \sqrt{C/B}$.

It is convenient to express the nuclear surface with respect to its own

principal axes. Thus with θ' and φ' being the polar angles measured with respect to the body-fixed axes, Equation I-6 is rewritten as

$$R = R_o\left[1 + \sum_{\mu} a_{2\mu}\, Y_2^{\mu}(\theta', \varphi')\right]. \tag{I-8}$$

The $a_{2\mu}$ and the $\alpha_{2\mu}$ are related through the rotation matrix D which is a function of the Euler angles (Θ, Φ, Ψ) specifying the relative orientation of the space-fixed and body-fixed axes

$$a_{2\mu} = \sum_{\nu} \alpha_{2\nu} D^{2}_{\nu\mu}(\Theta, \Phi, \Psi). \tag{I-9}$$

Since the principal body axes were selected, the inertia tensor is necessarily symmetrical and the a coefficients simplify according to $a_{21} = a_{2-1} = 0$ and $a_{22} = a_{2-2}$. Thus the nuclear shape may be completely described by specifying a_{22} and a_{20} while its orientation in space is given by the Euler angles.

By rewriting the deformation parameters in terms of β and γ according to

$$\begin{aligned} a_{20} &= \beta \cos\gamma \\ a_{22} &= \sqrt{\frac{1}{2}}\,\beta \sin\gamma \end{aligned} \tag{I-10}$$

where β is a measure of the total deformation of the nucleus because $\sum_{\nu} \alpha_{2\nu}^{2} = \beta^2$, and γ indicates the degree of axial asymmetry, the Hamiltonian of the deformed system may be expressed in terms of these new parameters as

$$H_{\text{collective}} = \frac{1}{2} C\beta^2 + \frac{1}{2} B\,(\dot{\beta}^2 + \beta^2\dot{\gamma}^2) + \hbar^2 \sum_{\chi=1}^{3} \frac{R_{\chi}^2}{2I_{\chi}}. \tag{I-11}$$

R_{χ} is the χ-component of the angular momentum along the χ-axis (body-fixed) and

$$I_{\chi} = 4B\beta^2 \sin^2(\gamma - \chi\frac{2\pi}{3}). \tag{I-12}$$

The form of this equation shows I_{χ} to be periodic in γ with a modulus of 60°;

moreover, it may be shown that one need consider only the range of angles between 0 and 30^{o} provided either sign of β is allowed.

The terms in this collective Hamiltonian may be identified with (i) the potential energy of the ellipsoidal body deformation $\frac{1}{2}C\beta^2$, (ii) the kinetic energy associated with the collective vibration $\frac{1}{2}B(\dot{\beta}^2 + \beta^2\dot{\gamma}^2)$, and (iii) the kinetic energy associated with the collective rotation $\hbar^2\Sigma R_\chi^2/2I_\chi$, where I_χ is interpreted as the χ-component of the moment of inertia. The nucleus is thus pictured by this model as a quantum mechanical body capable of both rotational and vibrational motion.

The state of a nuclear system which has one axis of symmetry and whose Hamiltonian is that of Equation I-11 may be specified by three quantum numbers; the square of the total angular momentum, $L^2 = R(R+1)$; the component of angular momentum along the fixed z-axis, $L_z = M$; and the component of angular momentum along the body-fixed symmetry axis, $L_3 = K$. Furthermore, if rigid rotation of the system is assumed, the rotational energy eigenvalues are given by the familiar expression

$$E_R = \frac{\hbar^2}{2I} R(R+1); \qquad R = 0, 2, 4, \text{---} \tag{I-13}$$

which reproduces both the spin sequence and the relative energy separation of levels found experimentally in many even-even nuclei belonging to regions of nuclear distortion in the periodic table. This simple model is capable also of reproducing with good success the large E2 matrix elements leading to the quadrupole moments and the transition probabilities encountered in these nuclear regions.

Thus far discussion has been limited to a semi-quantitative treatment of the collective motion of deformed, ellipsoidal nuclei; the energy eigenvalue E_J pertains only to a nucleus undergoing rotation with a fixed value of β and with $\gamma = 0$. This rather limited picture may be generalized to include collective rotational motion in which the $\gamma = 0$ restriction is relaxed[27], to include vibrational motion in which β is allowed to vary[28], and to include vibrational motion in which γ is allowed to vary[29]. Although all of these model extensions have possible

application in sd-shell nuclei, they have not in general been widely applied to particular cases and, consequently, will be mentioned only briefly. Furthermore, none of these possible modifications would alter the fact that, in spite of good agreement with experimental quadrupole moments and relative energy spacings, this simple collective model contains essentially no reference to the number of nucleons comprising the core, and thus it is inherently unable to reproduce any of the discontinuous nuclear phenomena associated with the magic numbers. For this reason, the model has only limited applicability, and more complicated descriptions of nuclear structure must be turned to.

D. Unified Model

1. Basic Considerations:

A major contribution to the understanding of nuclear behavior has been still another model formulation carried out in detail, first by A. Bohr[26] in 1952 and since then by many workers, in an attempt to combine the successful aspects of both the hydrodynamic picture and the single particle picture of nuclear behavior. The unified model, as this approach is sometimes called, is based on the recognition of the fact that, in order to represent with any adequacy the approximate constitution of a nuclear system, the mathematical framework must incorporate both collective and single particle degrees of freedom; furthermore, it must include the interaction between collective and particle degrees of freedom since the two clearly are basically related. The equilibrium shape of the collective core is, in fact, just the composite density distribution of the single nucleons determined by some self-consistent, nucleon-nucleon interaction.

Consideration of both collective and particle motions begins with the total Hamiltonian being separated into two terms

$$H = H_c + H_p \tag{I-14}$$

such that the first term depends predominantly on the collective coordinates and the second term depends predominantly on the particle coordinates. If the

fundamental assumption is made that the frequencies (and energies) of the particle motions are much greater than the frequencies (and energies) of the collective core motions, ie., the adiabatic assumption, H_p may be written in shell model notation as

$$H_p = \sum_{i=1}^{n} T_i + V(\beta, \gamma; r_i, \vec{l}_i, \vec{s}_i). \tag{I-15}$$

where n is the number of nucleons being considered. As before, the core deformation is given by the parameters β and γ. As like nucleons are added pairwise to fill the single particle states of the nucleus, they are assumed to be assimilated into the core. Thus, within the philosophy of the model, only a single outer nucleon need be considered and the total angular momentum of the system may be written

$$\vec{J} = \vec{R} + \vec{j} \tag{I-16}$$

wherein $\vec{R}$ is the angular momentum of the core and $\vec{j}$ is the angular momentum of the odd nucleon.

The solutions of the Hamiltonian H depend upon assumptions made about the dependence of H on the deformation parameters. In the case of nearly spherical nuclei, the influence of changes in the core deformations β and γ on $V(\beta, \gamma; r, \vec{l}, \vec{s})$ is hopefully small; the collective-particle motions then are termed "weakly-coupled" and perturbation techniques are employed. Within this approximation the Hamiltonian is separated specifically into terms representing collective motion, particle motion, and coupled collective and particle motion. Thus,

$$H = H_c + H_p^o + H_{int} \tag{I-17}$$

where H_p^o is the spherical, single-particle, shell model Hamiltonian of the odd nucleon

$$H_p^o = T + V_o(\bar{r}, \vec{l}, \vec{s}); \tag{I-18}$$

and the term H_{int} is simply assumed small enough to be treated adequately by perturbation methods. The unperturbed states of the odd-A system are formed by the appropreate angular momentum coupling of eigenfunctions of the collective core $|RM_R\rangle$ to eigenfunctions of the odd nucleon $|jm\rangle$. The H_{int} term then mixes to the ground state of the coupled system, $|J_o M_o\rangle$, all states for which the matrix element $\langle JM|H_{int}|J_o M_o\rangle$ is non-zero. The symbols M_R, m, and M indicate the projections of angular momenta $\vec{R}$, $\vec{j}$, and $\vec{J}$ along the space-fixed z-axis.

For the case of strong coupling between collective and particle coordinates, perturbation approximations can no longer be reliably used; and under these conditions it is convenient to rephrase the collective Hamiltonian. It may be shown that under the assumptions of axial symmetry and negligible vibrational contributions, assumptions normally introduced only to simplify the formalism and not because of some more basic physical reason, the expression for H becomes

$$H = \frac{1}{2}C\beta^2 + \hbar^2 \sum_{\chi=1}^{3} \frac{R_\chi^2}{2I_\chi} + H_p \qquad \text{(I-19)}$$

The first term contributes only an additive constant to the solution and is usually neglected. Using Equation I-16 and the fact that for axial symmetry $I_1=I_2=I$, $I_3 = 0$, and $J_3 = j_3$, the Hamiltonian is written[30] as

$$H = H_R + H_p + H_{RPC} \qquad \text{(I-20)}$$

wherein

$$H_R = \frac{\hbar^2}{2I}\left[J(J+1) - 2K^2\right],$$

$$H_p = T + V(\beta, \gamma;; r, \vec{l}, \vec{s}),$$

and

$$H_{RPC} = \frac{-\hbar^2}{I}(J_1 j_1 + J_2 j_2).$$

As before, K is the component of angular momentum along the symmetry axis. This Hamiltonian, which represents a single nucleon coupled strongly to a collective core, is of considerable complexity. Once again approximate solutions must be

considered.

If it is assumed that the H_{RPC} term is negligible with respect to the other two terms, the resulting energy eigenvalues of the system for a particular value of K are given by

$$E_J^K = \frac{\hbar^2}{2I}\left[J(J+1) - 2K^2\right] + E_p^K, \qquad J \geq K \tag{I-21}$$

where E_J^K is an eigenvalue of H_p. The energy level sequence is interpreted as a K-band of rotational states based on the intrinsic particle state of energy E_p^K. It must be emphasized that this expression is valid only in the case that H_{RPC} is negligible; ie., in the case that the wave function $|JMK\rangle$ of energy eigenvalue E_J^K supports no diagonal matrix element for the H_{RPC} operator. It may be shown that this is indeed a fair assumption with, however, one exception; for the value $K = 1/2$ the diagonal matrix element becomes

$$\left\langle JM\tfrac{1}{2}\left|H_{RPC}\right|JM\tfrac{1}{2}\right\rangle = \frac{\hbar^2}{2I}(-1)^{J+1/2}(J+\tfrac{1}{2})\,a \tag{I-22}$$

where a is the decoupling parameter determined by the exact form of the particle hamiltonian H_p. By treating this additional matrix element as a perturbation on members of $K = 1/2$ bands, Equation I-21 must be amended to read

$$E_J^K = \frac{\hbar^2}{2I}\left[J(J+1) - 2K^2 + \delta_{K,1/2}\,a(-1)^{J+1/2}(J+1/2)\right] + E_p^K \tag{I-23}$$

It may also be demonstrated that the H_{RPC} term supports non-zero matrix elements between eigenstates of equal J but belonging to K-bands differing by 1, thus H_{RPC} connects levels E_J^K and E_J^{K+1}. Specifically

$$\left\langle JM\,K+1\left|H_{RPC}\right|JMK\right\rangle = \frac{\hbar^2}{2I}\sqrt{J(J+1) - K(K+1)}\;b_K \tag{I-24}$$

wherein b_K is determined from the solutions of H_p. First order perturbation treatments of this interaction vanish; a second order perturbation calculation gives

$$E_J^{K'} = E_J^K - \Delta$$

$$E_J^{K'+1} = E_J^{K+1} + \Delta \qquad \text{(I-25)}$$

where $$\Delta = \frac{|\langle JM\,K+1 \mid H_{RPC} \mid JMK\rangle|^2}{E_J^{K+1} - E_J^K}$$

and the primes indicate the corrected energies.

The amount of wave function mixing and the degree to which the unperturbed states "repel" each other are thus determined by the difference of the unperturbed energy eigenvalues and the factor b_K which depends in turn on the exact form of H_p. Band mixing of this sort was first applied quantitatively by Kerman[31] in his consideration of the W^{183} level scheme. Because the H_{RPC} term is the precise quantum mechanical analog of the Coriolis force in classical mechanics, this mixing of K and K+1 bands is often called "Coriolis mixing".

2. Single Particle States in Distorted Potentials:

Nilsson[32] extended significantly the unified model calculations outlined above by considering quantitatively the behavior of a single particle within the non-spherical potential provided by the distorted, collective core. He introduced a specific ad hoc assumption concerning the form of the single particle Hamiltonian; namely,

$$H_p = \frac{p^2}{2M} + \frac{M}{2}\left[\omega^2(x_1^2 + x_2^2) + \omega_3^2 x_3^2\right] + C\vec{l}\cdot\vec{s} + D\vec{l}\cdot\vec{l} \qquad \text{(I-26)}$$

which will be recognized as a modified harmonic oscillator potential similar to that discussed in connection with the simple shell model except for the spheroidal shape of the potential imposed when $\omega_1 = \omega_2 = \omega$ and $\omega \neq \omega_3$. The frequencies ω and ω_3 are related through the expressions

$$\omega^2 = \omega_0^2\,(1 + \tfrac{2}{3}\delta)\,; \qquad \omega_3^2 = \omega_0^2\,(1 - \tfrac{4}{3}\delta) \qquad \text{(I-27)}$$

where ω_0 specifies the harmonic oscillator strength and δ is related to the core

distortion parameter β previously defined, viz. $\delta = \frac{3}{2}\sqrt{\frac{5}{4\pi}}\,\beta$. It should be noted that the H_p used here is not the exact Hamiltonian indicated in Equation I-20 because the term of this equation involving the product $\vec{j}\cdot\vec{j}$ has been neglected.

Nilsson solved numerically the single particle wave equation for the Hamiltonian given in Equation I-26 to obtain the single particle eigenvectors and the corresponding energy eigenvalues as functions of the core distortion δ. The parameters C and D were chosen empirically to reproduce the spherical shell model ordering of states for zero distortion of the core as determined by Klinkenberg[11]. The resulting energy eigenvalues of interest in sd-shell calculations are reproduced as functions of both δ and η in Figure I-1. η is still another parameter often used to characterize the core deformation and is defined as

$$\eta = \frac{\delta}{\varkappa}\left[1 - \frac{4}{3}\delta^2 - \frac{16}{27}\delta^3\right]^{-1/6} \qquad \text{(I-28)}$$

where $\varkappa$ is related directly to the spin-orbit coupling strength parameter C. The curves representing each of the eigenstates in Figure I-1 are identified at zero deformation according to standard, spherical shell model, spectroscopic notation. For non-zero deformation the eigenstates are specified by the previously defined quantum numbers K and π (parity), and the quantum number triad $\left[N, n_z, \Lambda\right]$ corresponding respectively to the total number of nodes in the radial wave function, and the number of nodal planes perpendicular to the symmetry axis, and the component of orbital angular momentum of the single particle along the symmetry axis. The last two quantities n_z and Λ are constants of motion only in the asymptotic limit when the nuclear potential becomes very anisotropic. However, for values of $\beta \gtrsim 0.3$ the actual states containing admixtures of values other than n_z and Λ have an overlap[33] of 90% or greater with the asymptotic states characterized exactly by n_z and Λ. These particular quantum numbers have furthermore been found to be advantageous in describing the selection rules relevant to the strengths of nuclear transitions linking intrinsic states of the Nilsson model. Since selection rules applicable in the strongly deformed nuclear model differ considerably from those applicable in the spherical model, experimental examination of nuclear transition strengths is one means of providing a measure of the relative validities

Figure I-1. Energy levels of the Nilsson model as functions of both deformation parameters η and δ (taken from Reference 32). The levels are identified at zero deformation by spherical shell model notation and at non-zero deformation by the quantum numbers $K^{\pi}\left[Nn_z\Lambda\right]$.

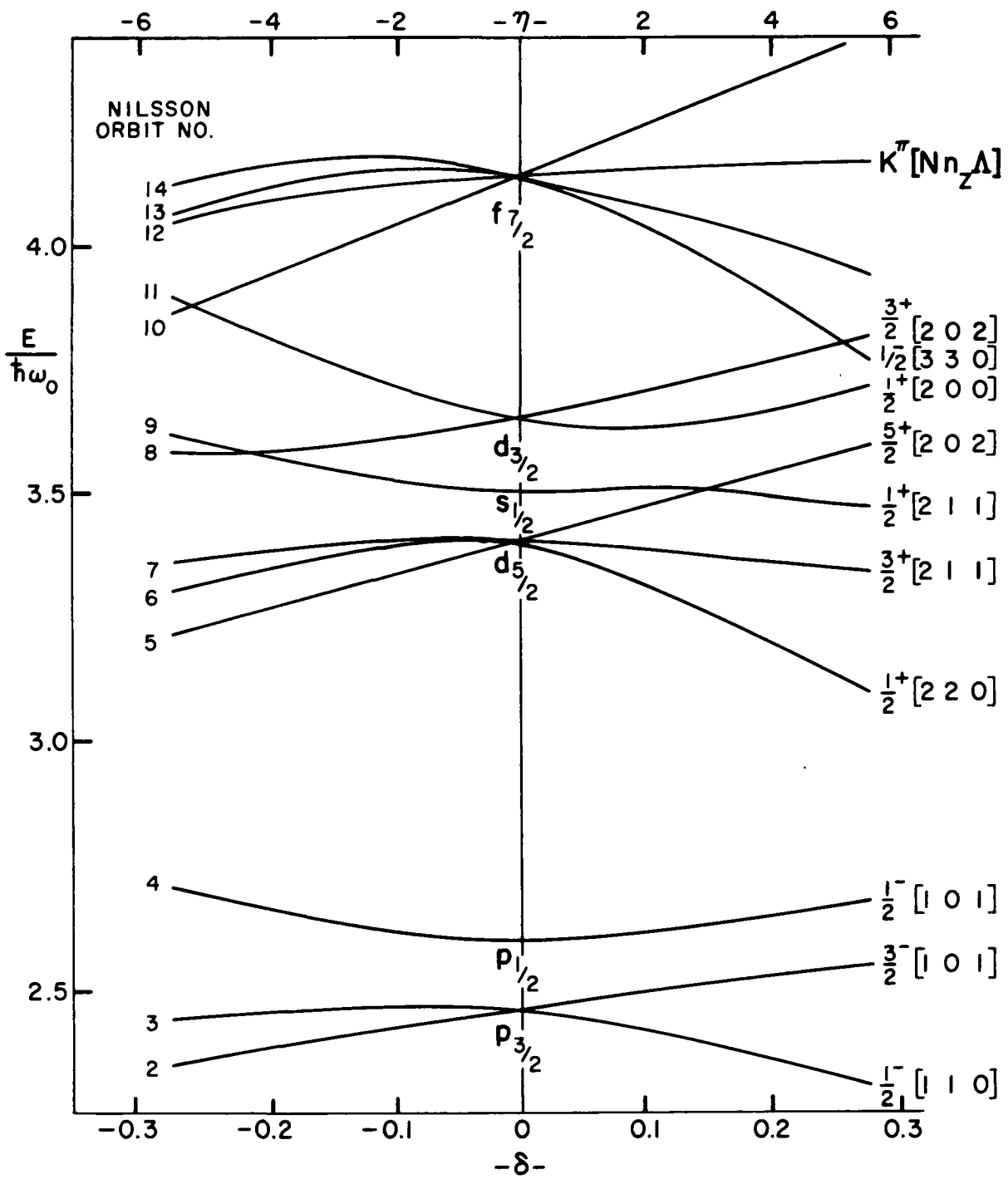
-6
-4
-2
-η-
2
4
6
NILSSON
ORBIT NO.
14
13
12
11
10
9
8
7
6
5
4
3
2
$f_{7/2}$
$d_{3/2}$
$s_{1/2}$
$d_{5/2}$
$p_{1/2}$
$p_{3/2}$
$K^{\pi}[Nn_z\Lambda]$
$\frac{3}{2}^+[2\ 0\ 2]$
$\frac{1}{2}^-[3\ 3\ 0]$
$\frac{1}{2}^+[2\ 0\ 0]$
$\frac{5}{2}^+[2\ 0\ 2]$
$\frac{1}{2}^+[2\ 1\ 1]$
$\frac{3}{2}^+[2\ 1\ 1]$
$\frac{1}{2}^+[2\ 2\ 0]$
$\frac{1}{2}^-[1\ 0\ 1]$
$\frac{3}{2}^-[1\ 0\ 1]$
$\frac{1}{2}^-[1\ 1\ 0]$
$\frac{E}{\hbar\omega_0}$
4.0
3.5
3.0
2.5
-0.3
-0.2
-0.1
0
0.1
0.2
0.3
-δ-

of each picture. The selection rules for electromagnetic single particle transitions pertinent to the discussion of Chapter II are reproduced in Table I-1. These rules, which are given in terms of the asymptotic quantum numbers, and their derivations have been extensively discussed by Mottelson and Nilsson[33], by Chasman and Rasmussen[34], and by Alaga[35].

TABLE I-1

Selection rules for single particle, electromagnetic transitions in the asymptotic limit.

Multipole	ΔK	$\Delta \Lambda$	Δn_z	ΔN
E1	1	1	0	± 1
	0	0	1	1
	0	0	-1	-1
M1	1	1	± 1	0
	0	0	0	0
E2	2	2	0	$0, \pm 2$
	1	1	± 1	0
	0	0	0	$0, \pm 2$
	0	0	2	2
	0	0	-2	-2

It should be noted that both the collective model and the more sophisticated unified model were first formulated to explain phenomena encountered in the study of much heavier nuclei; furthermore, it was generally believed that neither could be expected to have validity in the region of the periodic table below about atomic number of 100. The very meaningful applicability of the unified model formalism to considerably lighter nuclei was first established by Litherland et al.[36] in the interpretation of the level schemes of Mg^{25} and Al^{25}. The Nilsson model, including appropriate considerations for band mixing and band decoupling, has since been applied with notable success to a number of sd-shell nuclei, among them the odd-A systems of mass number 19, 21, and 23 which will be discussed in detail in subsequent chapters.

Newton[37], among others[38,39], has considered the case where one relinquishes the assumption of axial symmetry of the deformed core implicit in the form of H_p assumed by Nilsson. The term $\omega^2(x_1^2 + x_2^2)$ of Equation I-26 is generalized to read $(\omega_1^2 x_1^2 + \omega_2^2 x_2^2)$ which represents a distortion of the collective core in the same sense as that described by a non-zero value of the deformation parameter γ defined by Equation I-10. As would be anticipated, Newton's calculations generate families of Nilsson-like energy level diagrams for each value of γ.

All collective models discussed thus far have been based on solutions obtained by ignoring one or more terms of the strong-coupling Hamiltonian of Equation I-20. Chi and Davidson[40] have attempted to solve the complete Hamiltonian by diagonalizing the energy matrix representation of the Hamiltonian for odd-A, sd-shell nuclei. The energy matrix is constructed by these authors from base vectors which comprise the solutions of the isotropic harmonic oscillator. Approximations do enter their treatment, however; in order to mathematically formulate the collective model assumption that two like nucleons, when occupying a given level, are assimilated into the core, certain base vectors are removed from the basis as energy levels become filled, ie., the base system is truncated. The Nilsson level diagram (Fig. I-1) is used to determine the ordering of these energy levels and, consequently, the truncation procedure used in establishing the base vectors. Eigenvectors and eigenfunctions are given by these authors as surfaces in the parameter space of β, γ, and P, where β and γ are the core deformation parameters, and P is a direct measure of the effective mass of the core. Energy level diagrams, electromagnetic moments, and transition rates derived from the eigenvectors generated by this model have been applied to several nuclei in the sd shell and will be discussed later with regard to specific cases.

An extension of the Chi-Davidson approach has been formulated by Roessler[41] who has included approximately the possibility of collective vibrational motion represented by the term $\frac{1}{2}B\dot{\beta}^2$ in the collective Hamiltonian. This model has been applied to nuclear systems at the low end of the sd shell.

E. Other Model Variants Applied to SD-Shell Nuclei

1. Self-Consistent Model:

By requiring that the total binding energy of the single particle states determined by the Nilsson model is a maximum, the wave functions provided by the model for a particular nucleus predict the deformation parameter of that nucleus. However, the model in this form leaves unanswered a fundamental question; specifically, do the single particle orbits actually reproduce the particle density corresponding to the nuclear shape described by β; or, stating the question somewhat differently, does the average potential $V(\beta, \gamma; r, \vec{l}, \vec{s},)$ resulting from the single particle motions consistently represent the form of $V(\beta, \gamma; r, \vec{l}, \vec{s},)$ which was initially assumed?

The self-consistency problem of the single particle representation of deformed orbitals specifically in the sd shell has been investigated quite recently by Kelson and Levinson[42]. Unlike the Nilsson calculations in which the single particle Hamiltonian was simply assumed to be that of a spheroidal harmonic oscillator modified by $\vec{l} \cdot \vec{s}$ and $\vec{l} \cdot \vec{l}$ forces, these authors have started with the Rosenfeld two-body interaction, imposed a self-consistent criterion on the single particle Hamiltonian, and then utilized the Hartree-Fock method of iteration to obtain the resulting single particle representations. In this manner, shell model concepts and techniques have been used to evolve specific collective properties of nuclear spectra.

The self-consistent calculations applied to the first half of the sd shell lead to low-lying rotational energy spectra and single particle orbitals very similar to those given by the Nilsson model. However, the parameters which must be assumed for the Nilsson calculation are now understood directly in terms of the standard shell model Hamiltonian. Besides the appealing feature of applying shell model techniques to predict and explain collective parameters, the self-consistent approach offers another result which differs from that of the Nilsson model in a major way. The wave functions and energy levels of the self-consistent model may be used in conjunction with the "cranking formula" of Inglis[43] to evaluate the moment of inertia of the deformed nuclear core;

the agreement between the predicted[44] and the measured moments is quite impressive. This has not been the case with other model-generated calculations of moments of inertia, although prior to the self-consistent calculations the exact source of this theoretical inadequacy was not clearly understood.

Still another consequence of the self-consistent criterion is the prediction of the degree of core deformation caused by the addition of nucleons to the (assumed) spherical, doubly magic O^{16} core; the formalism predicts that as identical nucleons are added, the core is not significantly changed from sphericity while as non-identical nucleons are added, the core is substantially deformed by the close correlation of like neutron and proton orbits.

2. SU_3 Model:

Although the unified model, which is based on the long range features of the nuclear force and the assumption that the nucleon mean free path is considerably less than the nuclear radius, and the shell model, which is based on the short range features of the nuclear force and the assumption that the nucleon mean free path is considerably greater than the nuclear radius, appear on the surface to be completely incompatible, it was quickly recognized that the two approaches have common bases. This is especially true when one recognizes situations wherein short range forces cause strong band mixing in the collective model case and long range residual forces cause strong configuration mixing in the shell model case. Exact details of the interdependence of the two approaches, such as their relative ranges of validity, were not known for some time, however, partially because the models had been traditionaly applied in different regions of the periodic table.

The successful application of both the collective[45] and shell model[16] calculations to F^{19} provided the first real insight into this question of where the wave functions generated by the two models could be directly related. Paul[45] demonstrated the striking quantitative similarity in the shell and collective model wave functions by calculating their overlaps as shown in Table I-2. The probability of finding the last odd nucleon in a given configuration j is listed in the table as a percentage.

TABLE I-2

Configuration of the odd nucleon for the even parity states according to shell and collective model calculations in F^{19}.

State	j	Collective Model	Shell Model
J=1/2	1/2	29	49
	3/2	9	9
	5/2	62	42
J=3/2	1/2	15	21
	3/2	9	19
	5/2	76	60
J=5/2	1/2	23	19
	3/2	9	10
	5/2	68	71

Redlich[46] pointed out that in the specific cases of F^{19} and O^{18} a similar relationship between the models existed. Kurath and Picman[47] noted that shell model wave functions built up from nucleons in the p shell could likewise give rise to the collective-like structure inherent in a collective formulation.

The success of these initial efforts led Eliott[48,49] to introduce an approximation to the complex intermediate-coupled shell model which showed in a very general way the mathematical similarity between the shell and collective model descriptions of nuclei at the beginning of the sd shell. The approximation to the rigorous model enters through the assumption that low-lying states in these nuclei may be adequately represented as harmonic oscillator states having maximum orbital symmetry and a minimum number of excitation phonons. Such states are shown by Eilliott to belong to the irreducible group representation which maximizes the Casimir operator of the group; states with these properties are termed SU_3 states. The use of only SU_3 states in model considerations reduces considerably the number of nucleon configurations available in the sd shell and thus avoids the long variational calculations usually required. Moreover, within the validity of the SU_3 assumption, these states may be used to derive many of the gross properties of low-lying levels and have been shown to produce the same angular momentum sequence as rotational bands; namely, J=K, K$\mp$1, - - -.

The SU_3 techniques thus provide a computational method of selecting from a large number of complex, intermediate-coupled, spherical shell model states particular linear combinations of states which closely reproduce the rotational characteristics of band spectra.

The SU_3 approximation has been applied[50] to specific even-A, sd-shell nuclei (Mg^{24}, Ne^{20}) and has quite recently been used by Harvey[51] to make predictions about negative parity states in F^{19}, O^{18}, and O^{17}. The F^{19} predictions will be considered in some detail in Chapter II.

F. Summary

Results of SU_3 calculations and the work which preceded them point out clearly at least one region of the periodic table, the sd shell, in which there exists a definite overlap of the ranges of validity of nuclear models emphasizing basically different aspects of nuclear behavior. Self-consistent field calculations applied to this mass region are further providing quantitative insights into the coalescence of these models from a physically fundamental point of view.

The sd shell thus provides a rich area for experimental exploitation in that several theoretical frameworks already exists within which new data may be correlated; likewise new information may be used in critical evaluation of present model formulations and may provide the understanding of nuclear structure necessary for realistic extensions of these models in this, and perhaps in other, mass regions.

The chapters to follow describe experimental work carried out in the low end of the sd shell. Chapter II reports the measurements of previously unknown level parameters in F^{19}, then examines these paramenters in the light of both collective and shell model predictions. Experimental studies of static and dynamic properties of the first three states of O^{19} are described in Chapter III and the predictions of various models are compared with the measured deexcitation properties of the second excited state of this nucleus. The experimental properties of both the O^{19} and F^{19} systems are examined for characteristics with which the core deformation predictions of the self-consistent model may, or may not, be

in accord. Chapter IV and Chapter V describe investigations of selected excited states in Ne^{21}, Na^{21}, Ne^{23}, and Na^{23} carried out in an attempt to reveal any systematic changes of behavior which might be associated with the increasing number of paired nucleons in the nuclear core; similarly, various dynamic properties of these and of other nuclei with odd-nucleon number 11 (O^{19}, Ne^{21}, Na^{21}, Na^{23}) and with odd-nucleon number 13 (Ne^{23}, Mg^{25}, Al^{25}, Al^{27},) are examined for analogous behavior indicative of the validity of simple Nilsson model formulations in these systems. Chapter VI presents a brief discussion of open problems of current interest in both theoretical and experimental considerations of sd-shell nuclei and the last chapter provides a summary of the work presented herein.

II. STUDIES OF ENERGY LEVELS IN F^{19} FROM THE REACTION $O^{18}(p,\gamma)$ F^{19}.

A. Introduction

1. Theoretical:

The F^{19} nucleus was one of the first in the sd shell to be subjected to an extensive, individual particle shell model calculation. The work was carried out in 1954 by Elliott and Flowers[16] using methods similar to those applied earlier to nuclear systems in the p shell. In fact, it was in the F^{19} nucleus that the pioneering calculations of Paul demonstrated the remarkable similarity between the predictions of the experimental data set forth by the spherical shell model and those predictions produced by the strong-coupling collective model. As mentioned in Chapter I, this similarity led to the theoretical work of Elliott[49,50] on the SU_3 classification of shell model states to yield collective characteristics of nuclear systems and the subsequent increased understanding of the general relationships between collective and independent particle motions in the nucleus.

A wide variety of more recent calculations, emphasizing one or another of these aspects of behavior, has been reported for the F^{19} level spectrum. Among these are the calculations of Chi and Davidson[40], whose asymmetric rotor model was discussed briefly in Chapter I; of Inoue et al.[19], who have carried out an independent-particle calculation with somewhat different parameters than those used by Elliott and Flowers; of Dreizler[52], who has considered the coupling of a proton hole to a Ne^{20} core; and of Harvey[51], who has applied the SU_3 formalism to negative parity states in F^{19}.

2. Experimental:

Many of the experimental characteristics of F^{19} have been known for some time[1]; however, recent detailed $(p,p'\gamma)$ and other studies by Prentice et al.[53] have established unambiguous J^{π} assignments to the first six states up to and including the $3/2^+$ state at 1.56 MeV. These measurements have provided the bases for a collective model interpretation of these states as representing

highly decoupled, overlapping positive and negative parity K=1/2 rotational bands. This model is remarkably successful providing the state at 2.79 MeV has a value $J^{\pi} = 9/2^{+}$. A limit of $7/2^{+}$ or $9/2^{+}$ has, in fact, been placed on the 2.79 MeV state by Freeman[55] in her studies of the $F^{19}(n, n')F^{19}$ reaction. Although a further purported assignment of $9/2^{+}$ has been tentatively indicated by Huang et al.[55] in their investigations of the deexcitation radiation from the 1169 keV resonance in the $O^{18}(p,\gamma)F^{19}$ reaction, the data analysis leading to this conclusion is not supported by the work carried out herein. Figure II-1 summarizes the available information on these low levels.

At excitation energies in excess of 5 MeV extensive experimental data on F^{19} states have been obtained in studies on the $N^{15}+\alpha$ and O^{18} +p reactions;[56,57,58] for some six states in the intervening region between 3 and 5 MeV, however, essentially no data beyond their excitation energies have as yet been reported. These states are of particular interest in any attempt to elucidate the relative validity and interdependence of the various model calculations reviewed briefly in Chapter I. Although all such models applied to F^{19} give essentially overlapping predictions for the states below 3 MeV, and are not clearly distinguishable in that range, the predictions diverge in striking fashion (see Fig. II-16) for higher excitations.

The measurements reported in this chapter were carried out in an attempt to provide spectroscopic information on the states between 2 and 5 MeV. A major portion of this work involved a detailed study of gamma radiations from the resonant capture of 849 keV protons in O^{18}. Previous studies on the elastic scattering of protons in this energy range by Carlson et al.[57] and by Yagi et al.[58] have demonstrated that this resonance has a $1/2^{+}$ assignment making it particularly attractive in terms of correlation studies on cascade deexcitations. Previous measurements on this radiative capture reaction have been reported by Huang et al.[55], by Butler and Holmgren[59], and by Nelson and Hudspeth[60]. However, in these measurements attention has been given to those resonances which deexcite almost exclusively via the two, low-lying triplet states in F^{19}; and no detailed studies have been reported on resonances, including that at 849 keV, which demonstrated a more complex deexcitation. Incidental to the information

Figure II-1. Partial energy level diagram of F^{19} showing the experimental deexcitation scheme of the lower levels. Energies are in MeV.

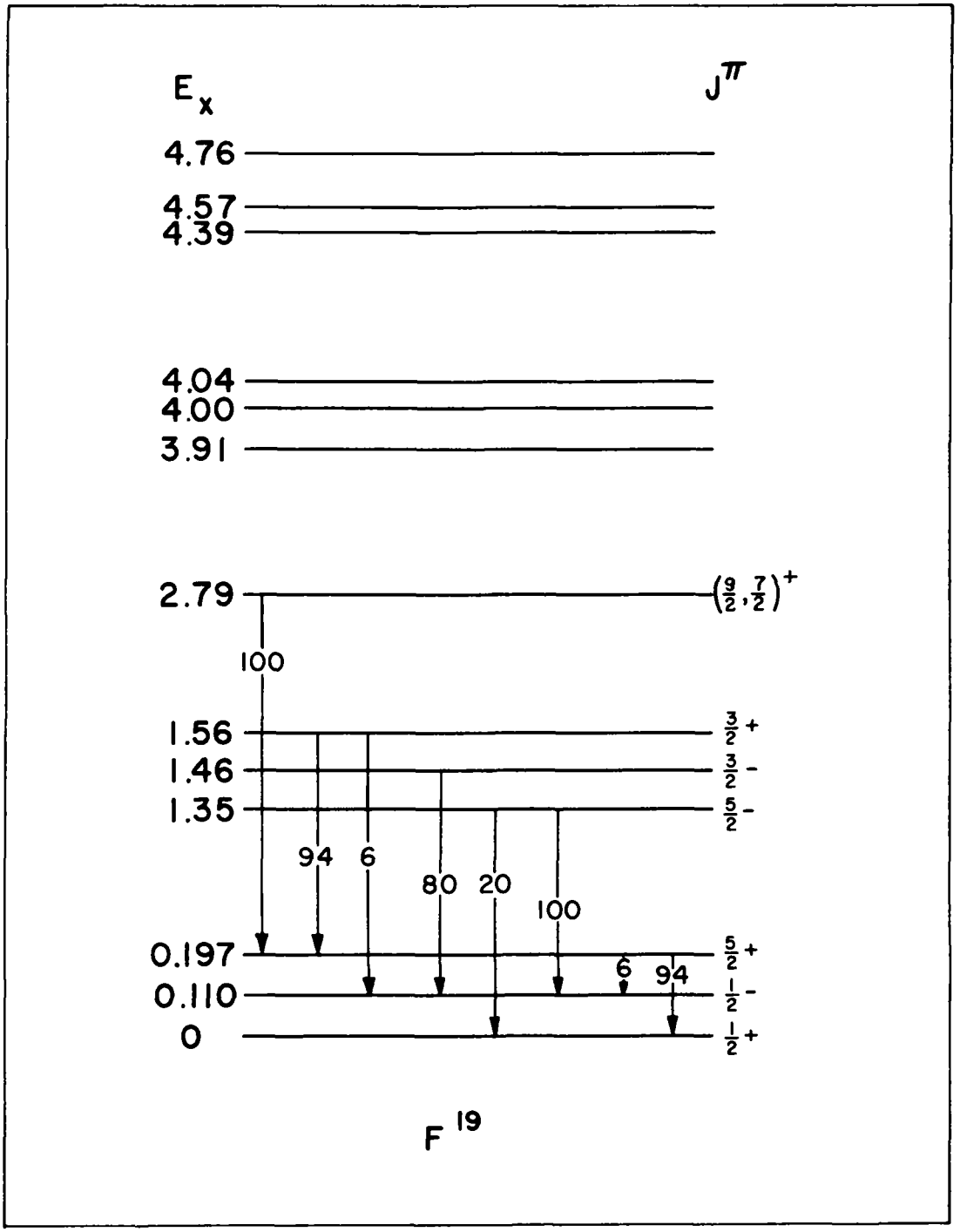
E_x
J^π
4.76
4.57
4.39
4.04
4.00
3.91
2.79
$(\frac{9}{2},\frac{7}{2})^+$
100
1.56
$\frac{3}{2}+$
1.46
$\frac{3}{2}-$
1.35
$\frac{5}{2}-$
94
6
80
20
100
0.197
$\frac{5}{2}+$
6
94
0.110
$\frac{1}{2}-$
0
$\frac{1}{2}+$

F^{19}

which has been obtained concerning the angular momentum and deexcitation branching of the 3.91 MeV state has been a determination of the branching from the resonance itself.

Preliminary measurements on the cascade deexcitation of the 9.07 MeV state corresponding to the 1169 keV resonance in this reaction have also been carried out to provide information concerning the tentative $9/2^+$ assignment to the 2.79 MeV state. Finally, the gamma radiations from the 1769 and 1932 keV resonances in the O^{18} (p, γ) F^{19} reaction have received preliminary study.

B. Experimental Equipment

1. Accelerator:

Excited states in F^{19} were populated via the resonant radiative capture of protons by O^{18} using the proton beam of the Brookhaven National Laboratory Van de Graff accelerator. This accelerator provided for both the F^{19} studies and the experimental studies to be described in subsequent chapters, either proton or deuteron beams of continuously variable energy from 0.6 to 3 MeV with a beam energy spread of not more than 2 keV. Calibration of the accelerator energy scale is described in section C1 of this chapter.

2. Gas Target:

A gas target cell containing 99.5% isotopically pure O^{18} gas at 20 cm of mercury absolute pressure was used throughout this experiment. The target cell consisted of a cylinder of 0.05 inch thick brass mounted with its axis along the horizontal beam axis. The cell was sealed on one side by a flat end plate, also of 0.05 inch brass, and on the other by a beam entrance window of 0.00025 cm thick nickel foil epoxied to a brass collar and O-ring assembly. The design of the entrance window unit permitted easy replacement in case of window breakage. The volume of the cell was about 2. cm^3. A lucite spacer was inserted between the target volume and the beam tube, thus providing electrical isolation of the scattering cell and allowing beam current integration

directly from it. Although the cross section of the target cell was not entirely symmetrical in the plane in which angular correlation and distribution measurements were made, angular dependent differences in the attenuation of gamma radiations of interest were found to be entirely negligible ($< 0.1\%$).

In order to minimize carbon build-up on the entrance window of the target cell, a liquid nitrogen filled trap was installed in the beam line immediately forward of the target. To further reduce background radiation the cell was lined along the sides and ends with 0.001 inch tantalum foil.

A gas handling system designed and constructed by A. J. Howard[61] was used throughout these experimental investigations. The system operated around a 200 cm^3 volume mercury Töpler pump and permitted easy transfer of the gas samples between the target cell and the glass break-seal storage volumes. The option of recovery of a gas sample from the target cell after a run was essential because of the expense involved in acquiring highly pure, mono-isotopic gases.

3. Gamma Radiation Detectors and Associated Equipment:

Gamma radiation was detected using two standard 5" x 5" NaI (Tl) spectrometers having a measured energy resolution of 9.2% and 12% for the 661 keV Cs^{137} radiation. Both spectrometers were mounted in heavy lead housings constructed specifically to shield all surfaces of the crystals except the front faces. Additional radiation shielding between the spectrometers and the beam collimators which immediately preceded the target was provided by appropriately placed lead bricks. For coincidence measurements the crystals and shielding assemblies were mounted at $\pm 90^{\circ}$ to the beam vector with their exposed faces 2.5 cm from the center of the target cell. Correlation and distribution measurements were carried out with one crystal set permanently at 90° to the beam and the second mounted on an angular correlation table whose axis of rotation passed through the target center perpendicular to the beam direction. The procedure for aligning the correlation table is described in Section C3.

Standard transistorized equipment was used throughout the experiments reported herein. This instrumentation included a number of fast-slow coincidence

circuits, single channel pulse-height analyzers, discriminators, double-delay line linear amplifiers, pulse scalers, and 400 channel (RIDL) analyzers. Also employed were pulse-height stabilizers[62] which operated on prominent spectral peaks to control the applied voltage to, hence the gain of, the spectrometer assemblies. The stabilizer units essentially eliminated the well known pulse height dependence of photomultiplier tubes on both radiation counting rate and physical proximity to magnetic materials. This feature of constant spectrometer gain simplified greatly the analysis of all gamma radiation spectra.

C. Experimental Measurements and Results

1. Location of Resonances:

A typical excitation function of the reaction O^{18} (p,γ) F^{19} for all gamma radiations of energy greater than 4 MeV is shown in Figure II-2. The indicated proton energy scale has been corrected for energy loss in the gas-cell window and in the target gas to give the resultant energy at the center of the target. The target pressure was 68 cm of mercury absolute for the main curve; 3.8 cm for the inset curves. From these results it is clear that the resonance widths shown in the insets are still purely instrumental and reflect the finite target thickness. The resonances in this excitation function at 849, 1169, 1397, 1769, and 1932 keV have also been reported by Butler and Holmgren[59] and by Nelson and Hudspeth[60], among others. In the present measurements the voltage scale of the accelerator was calibrated by observation of the 4.43 MeV gamma radiation from the N^{15} (p,$\alpha\gamma$) C^{12} reaction induced in the target volume when filled with air. In particular, the known resonances at 429 ± 1, 898 ± 1 and 1210 ± 3 keV were used to establish this calibration.

2. Deexcitation Branching Ratios of States at 8.76 and 3.91 MeV:

The branching ratios of the states in F^{19} at 8.76 and 3.91 MeV excitation have been determined by a detailed investigation of the gamma deexcitation of the 849 keV resonance state. In the coincidence measurements to establish these deexcitation characteristics the NaI crystals were mounted at $\pm 90^{o}$ to the

Figure II-2. Excitation function for O^{18} (p,γ) F^{19} with the yield of gamma radiation of energy greater than 4 MeV plotted against proton energy in keV. The gas target pressure was 68 cm of Hg absolute for the main curve; 3.8 cm of Hg for the inset curves.

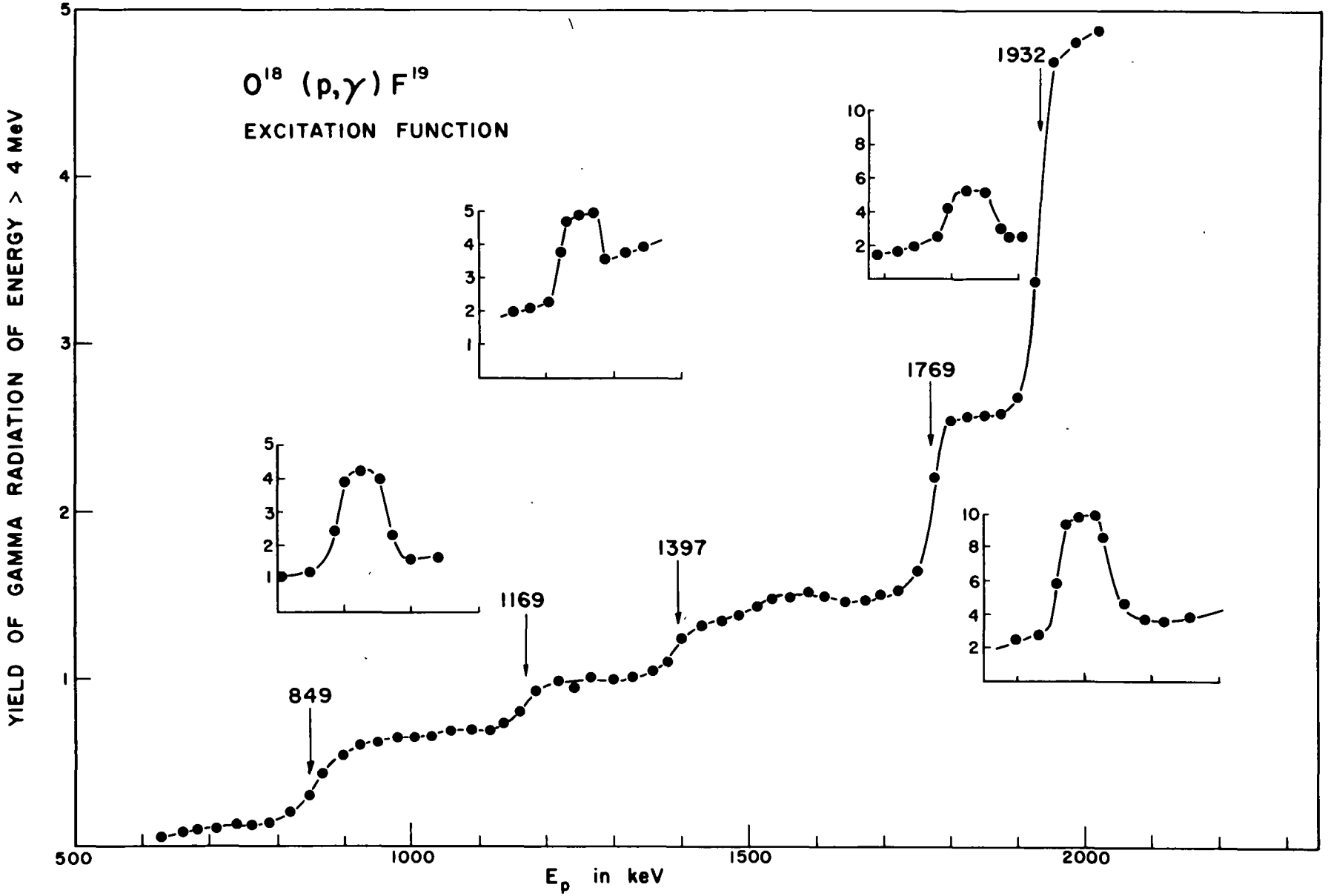
O^{18} (p,γ) F^{19}
EXCITATION FUNCTION
YIELD OF GAMMA RADIATION OF ENERGY > 4 MeV
E_p in keV
849
1169
1397
1769
1932
500
1000
1500
2000
1
2
3
4
5

proton beam with their front faces 2.5 cm from the reaction volume. This close geometry effectively averaged any anisotropies in the angular distribution of the radiations. The proton beam current was approximately 1 μa, limited by the transmission capabilities of the nickel entrance window in the target cell.

Figure II-3 presents a direct gamma radiation spectrum of the 849 keV resonance in the better of the two NaI spectrometers. This figure also includes an expanded spectrum of the low energy radiation showing transitions of 0.110 and 0.197 MeV which are involved in the cascade deexcitations. The energy scale calibration was accomplished using standard radioactive sources (Co^{60}, ThC', and PuBe) in addition to radiations of known energy from the 1769 and 1932 keV capture resonances in O^{18} +p.

The system resolution was inadequate to resolve the primary transitions to members of the low-lying triplets. However, the spectrum of Figure II-3 indicates strong transitions of mean energies 8.7 and 7.4 MeV corresponding to primary deexcitation transitions to one or more members of each of these triplets.

In order to establish the substructure of these transitions, coincidence measurements were carried out using the two crystal spectrometers. To minimize spurious coincidences a 0.5 inch lead filter was inserted between the target and the crystal on whose output voltage discrimination gates, defining the high energy members of the coincidence cascades, were established.

During each coincidence measurement the real-to-random coincidence corrections were examined by insertion of a fixed 0.4 μsec delay into one channel of the fast coincidence circuit. It was found that by operating with a resolving time of 50 μsec the accidental coincidence rate was entirely negligible. Off-resonance measurements at proton energies just below the 849 keV resonance established that corrections for non-resonant proton captures were also negligible except where specifically included hereafter. Through use of parallel multichannel analyzers and voltage gates, it was possible to record several coincidence spectra simultaneously.

The direct gamma radiation spectrum in Figure II-3 shows strong radiations of energies 8.6, 7.3, 4.85, 3.91, and 2.35 MeV corresponding to

Figure II-3. O^{18} + p direct gamma radiation spectrum at E_p = 849 keV. Approximate energies are indicated in MeV. The inset shows a high gain (low-energy) spectrum at the same resonance.

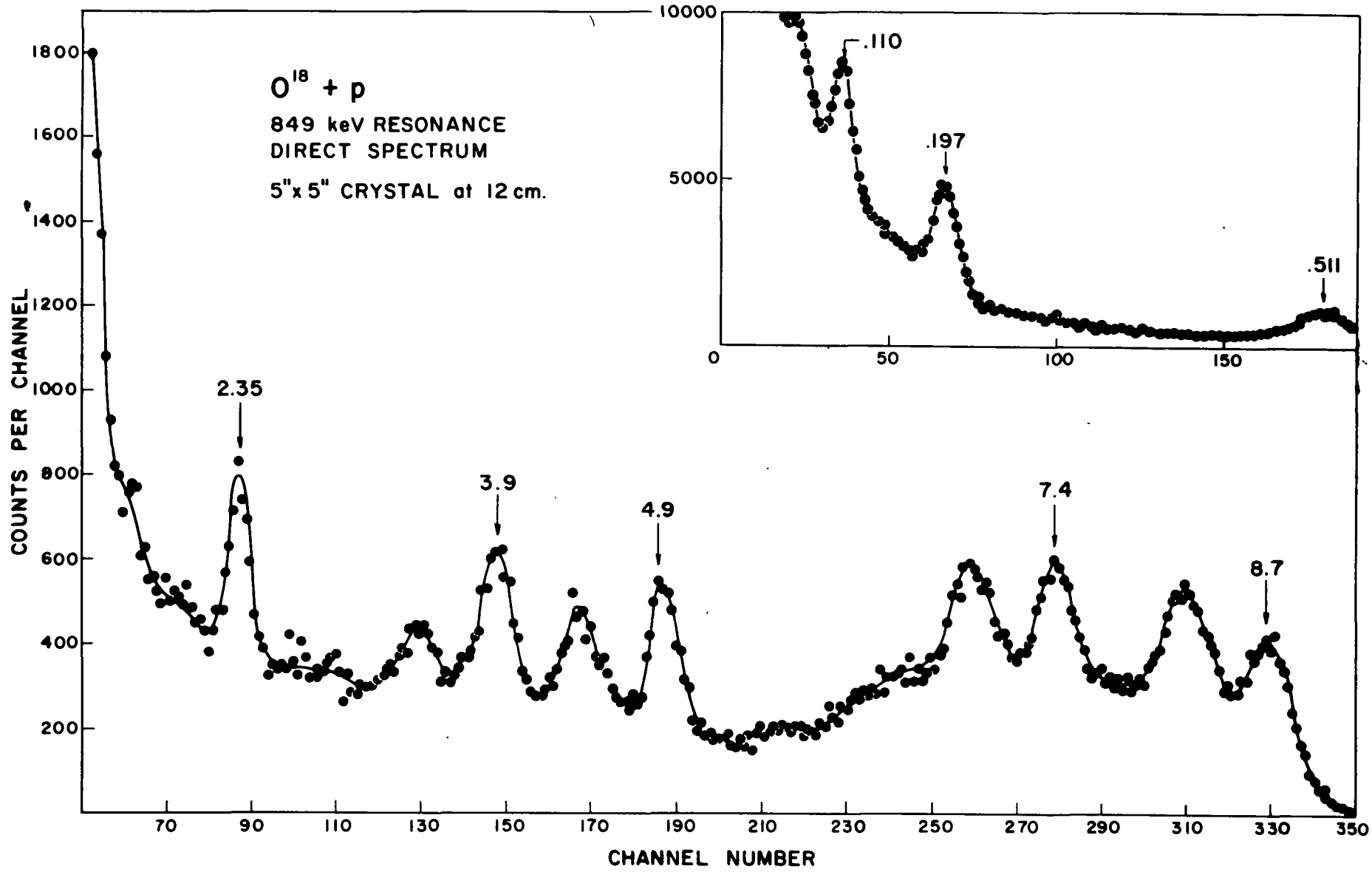
O^{18} + p
849 keV RESONANCE
DIRECT SPECTRUM
5"x 5" CRYSTAL at 12 cm.
COUNTS PER CHANNEL
CHANNEL NUMBER
2.35
3.9
4.9
7.4
8.7
.110
.197
.511

deexcitations of the capture state to members of the low triplets and to a state at 3.91 MeV. Evidence that a state at 4.85 MeV was not involved is obtained directly from the fact that the intensity of the 3.91 MeV radiation is significantly less than that of the 4.85 MeV radiation reflecting branching in the deexcitation of the 3.91 MeV state.

In order to separate transitions to individual members of the low-lying triplets and to clarify further the excited state deexcitations, a systematic program of gamma-gamma coincidence studies was undertaken as previously indicated. Figure II-4 is a spectrum measured in coincidence with a voltage gate set on the photopeak of the 8.6 MeV radiation. The figure also displays a portion of the spectrum obtained under identical conditions except with the proton energy 100 keV below resonance. The dominant 0.110 MeV transition observed in the on-resonance data demonstrates that the deexcitation proceeds strongly via a direct cascade involving the first excited state. From the known efficiency of the spectrometers[63] for gamma radiation in the energy range of interest, these data, and others to be presented in subsequent figures, were analyzed to provide the detailed branching ratios. The off-resonance portion of this figure demonstrates the absence, within experimental accuracy, of any direct E2 transitions to the $5/2^+$ state at 197 keV, since the observed 197 keV peak intensity has been shown to be entirely attributable to non-resonant capture.

Figure II-5 presents the gamma radiation spectrum coincident with radiation $\cong 7.3$ MeV showing 0.110, 0.197, and 1.35 MeV transitions. From the relative intensity of the 0.110 and the 0.197 MeV radiations, corrected for real, but unwanted, coincidence yield from the "tails" of higher energy pulse-height distributions falling within the voltage gate, and from the known detailed deexcitation characteristics of the triplet states in F^{19} (Fig. II-1), it has been possible to obtain the branching shown in a later summary diagram (Fig. II-15). The absence of any significant 0.511 MeV radiation in this spectrum taken with opposed NaI (Tl) crystals demonstrates the effectiveness of the 0.5 inch inter-crystal lead filter in removing these unwanted coincidences.

Figure II-6 shows the spectrum coincident with 4.85 MeV radiation composing primarily transitions of 3.91, 2.35, and 1.35 MeV from the 3.91 MeV state.

Figure II-4. O^{18} + p gamma radiation spectrum at E_p = 849 keV in time coincidence with the 8.6 MeV transition into the ground state triplet. Energies are in MeV. The inset displays portion of a spectrum obtained under similar conditions except with the proton energy 100 keV below the resonance energy ($E_p \cong$ 750 keV).

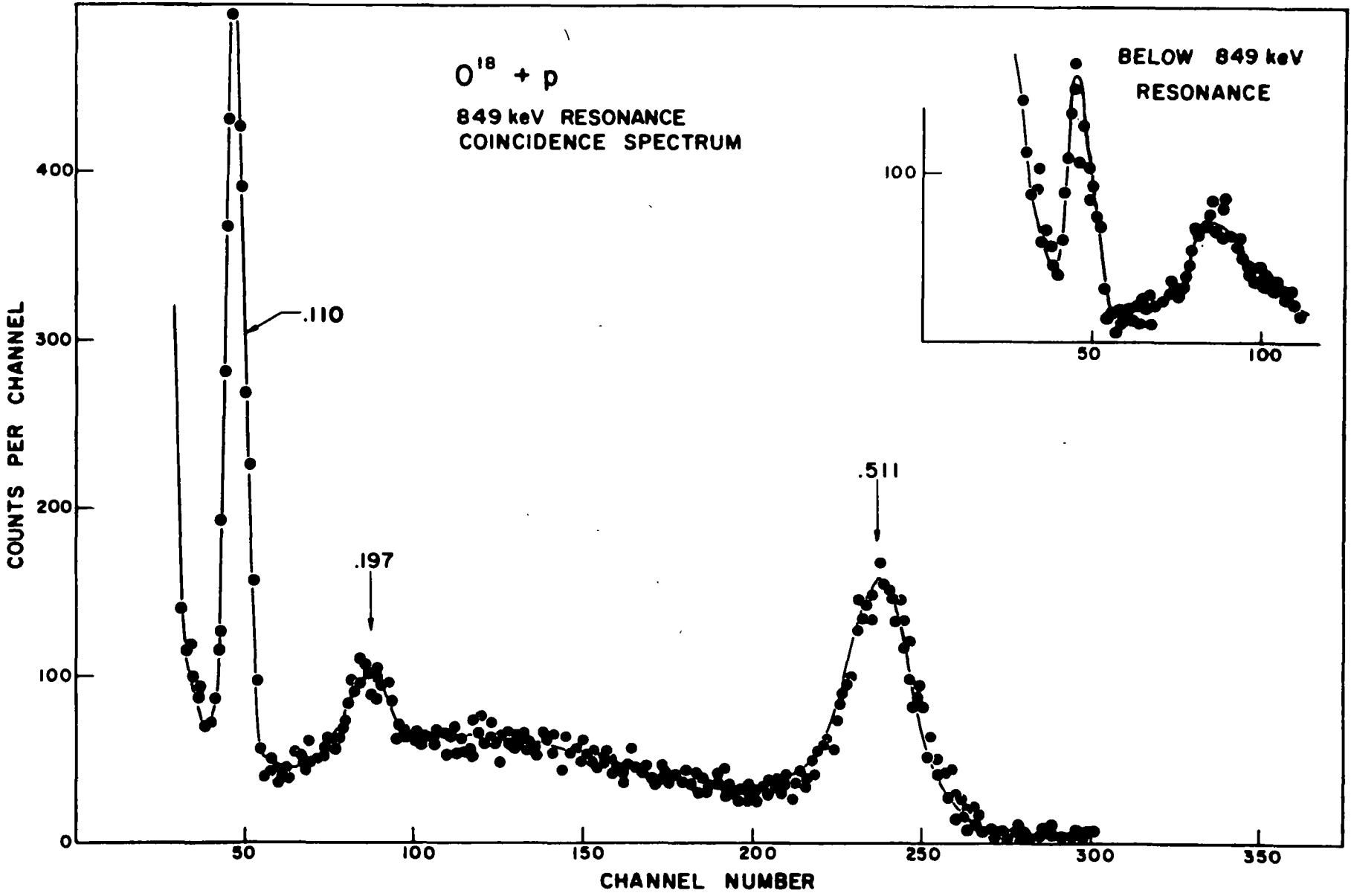
O^{18} + p
849 keV RESONANCE
COINCIDENCE SPECTRUM
BELOW 849 keV
RESONANCE
.110
.197
.511
COUNTS PER CHANNEL
CHANNEL NUMBER
0
100
200
300
400
50
100
150
200
250
300
350

For comparison, the data obtained with an identical voltage gate set just above the 4.85 MeV photopeak are also indicated by the open circles in the figure. Careful energy calibration of this spectrum and of the direct gamma spectrum (Fig. II-3) establishes unambiguously the 4.9 and 3.9 MeV radiations as members of the two-step deexcitation cascade through the 3.91 MeV state. Figures II-7A (voltage gate on photopeak) and II-7B (voltage gate above photopeak) present the expanded low energy sections of these same coincidence spectra showing the 0.110 and 0.197 MeV radiations. Comparison of these two spectra demonstrates that the 3.91 MeV state has no strong branches to the first or second excited states and that the observed 0.110 and 0.197 MeV radiations are largely in coincidence with higher radiation tails, primarily that of the 8.65 MeV transition, falling in the coincidence gates. It should be noted, however, that the intense 8.65 MeV radiation provides sufficient unwanted coincidences with the 0.110 MeV radiation to make difficult the determination of the intensity of real 3.91 - 0.110 MeV coincidences. On the other hand, energy calibration of the spectrum in coincidence with 4.85 MeV radiation (Fig. II-6) favors deexcitations of the 3.91 MeV state directly to the ground state and indicates that the 3.91 to 0.110 MeV branch is small with respect to the 3.91 MeV to ground state transition.

Figures II-8A and II-8B present, respectively, coincidence spectra with gates set on, and directly above, the 0.197 MeV photopeak. Intensity analysis of these spectra corroborates the branching ratios established from the above spectra. Figures II-9A and II-9B present, respectively, similar results obtained by gating on, and immediately above, the 0.110 MeV photopeak. (To facilitate comparison, the latter spectrum (B) has been expanded vertically by a factor of 2.) These spectra confirm in particular the dominance of the cascade deexcitations involving the 0.110 MeV state

In the analysis of the above spectra, standard spectral shapes, determined by using appropriate radioactive sources and the 5 x 5 inch NaI (Tl) spectrometers, have been used together with efficiency data interpolated from those of Vegors et al.[63].

Figure II-5. O^{18} + p gamma radiation spectrum at E_p = 849 keV in time coincidence with the 7.3 MeV transition into the first excited triplet.

Figure II-6. O^{18} + p gamma radiation spectrum at E_p = 849 keV in time coincidence with the 4.85 MeV transition. Careful energy calibration of this spectrum and the direct gamma spectrum establish the prominent 4.9 and 3.9 MeV radiations as members of the two-step cascade through the 3.91 MeV state. The open circles indicate the coincident spectrum obtained with a similar voltage gate set just above the 4.85 MeV photopeak.

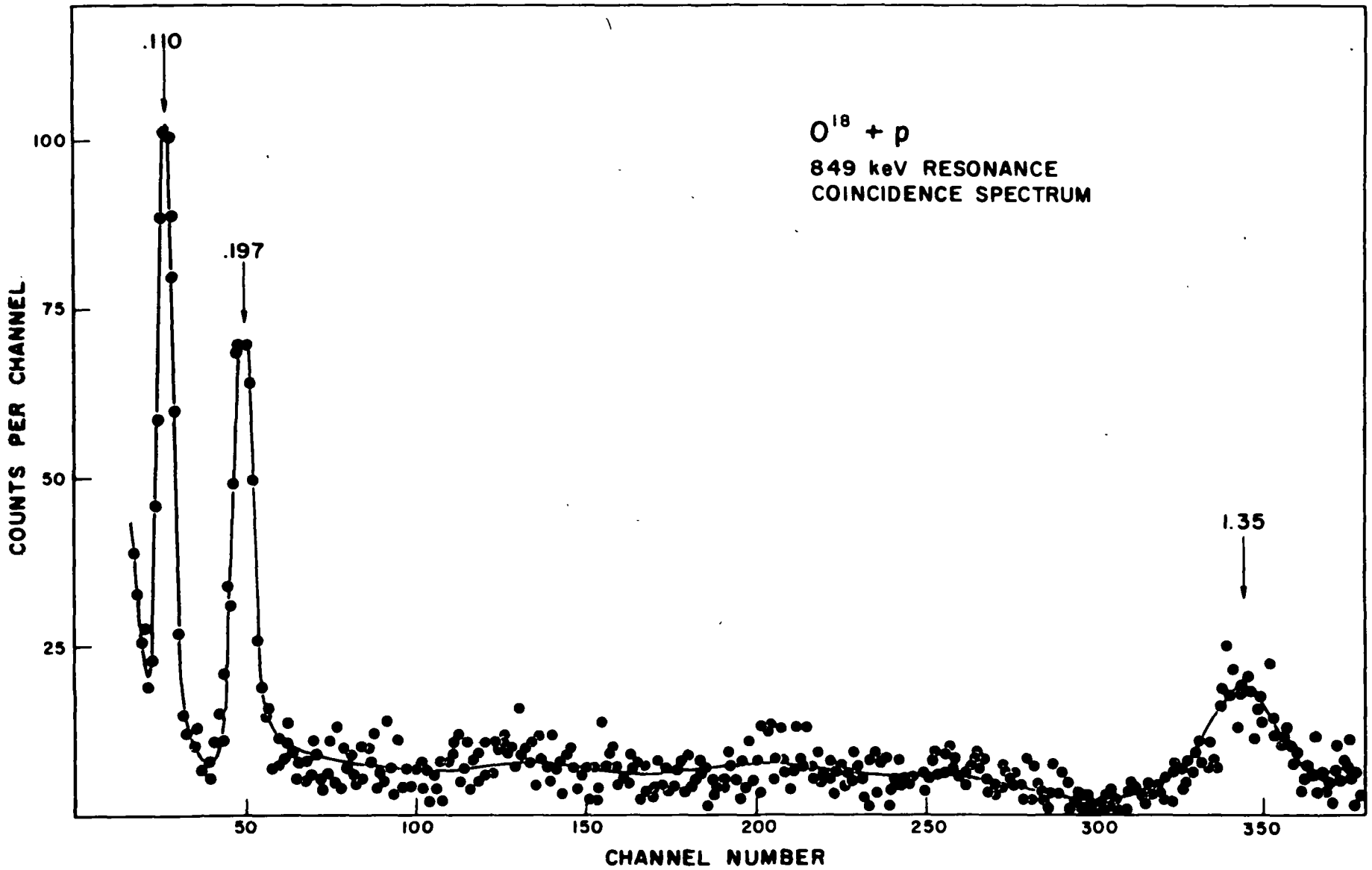
.110
.197
1.35
$O^{18} + p$
849 keV RESONANCE
COINCIDENCE SPECTRUM
COUNTS PER CHANNEL
100
75
50
25
50
100
150
200
250
300
350
CHANNEL NUMBER

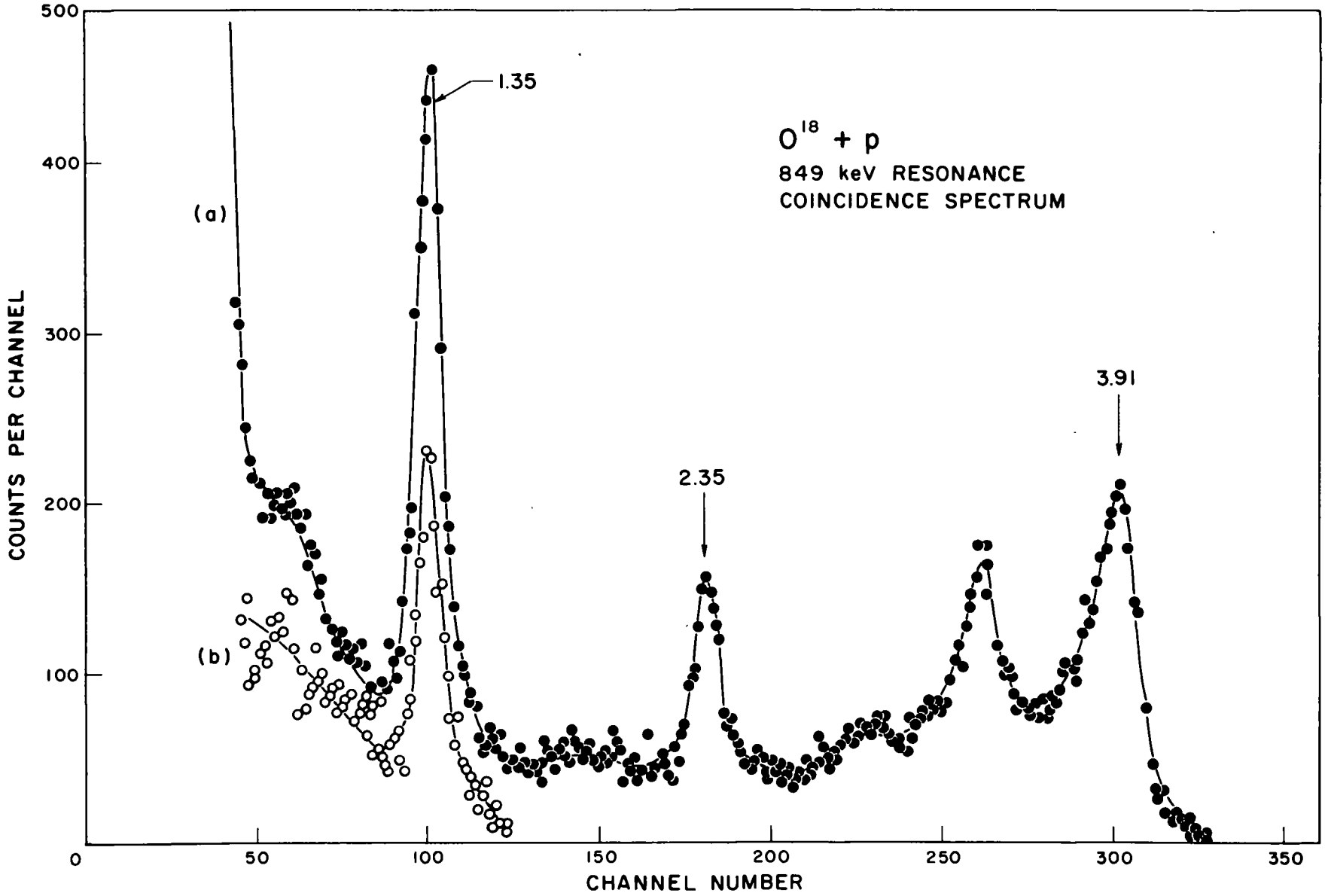
500
400
300
200
100
0
50
100
150
200
250
300
350
COUNTS PER CHANNEL
CHANNEL NUMBER
(a)
(b)
1.35
2.35
3.91
O18 + p
849 keV RESONANCE
COINCIDENCE SPECTRUM

Figure II-7. (A) O^{18} + p gamma radiation spectrum at high gain obtained under the same conditions as in Fig. 6, and (B) gamma radiation spectrum obtained under conditions identical to (A) except with the voltage gate set just above the 4.85 MeV photopeak.

Figure II-8. (A) O^{18} + p gamma radiation spectrum in time coincidence with the 0.197 MeV transition, and (B) gamma radiation spectrum obtained under conditions identical to (A) except with the voltage gate set just above the 0.197 MeV photopeak.

Figure II-9. (A) O^{18} + p gamma radiation spectrum in time coincidence with the 0.110 MeV transition, and (B) gamma radiation spectrum obtained under conditions identical to (A) except with the voltage gate set just above the 0.110 MeV photopeak. To facilitate comparison, spectrum (B) has been expanded vertically by a factor of 2.

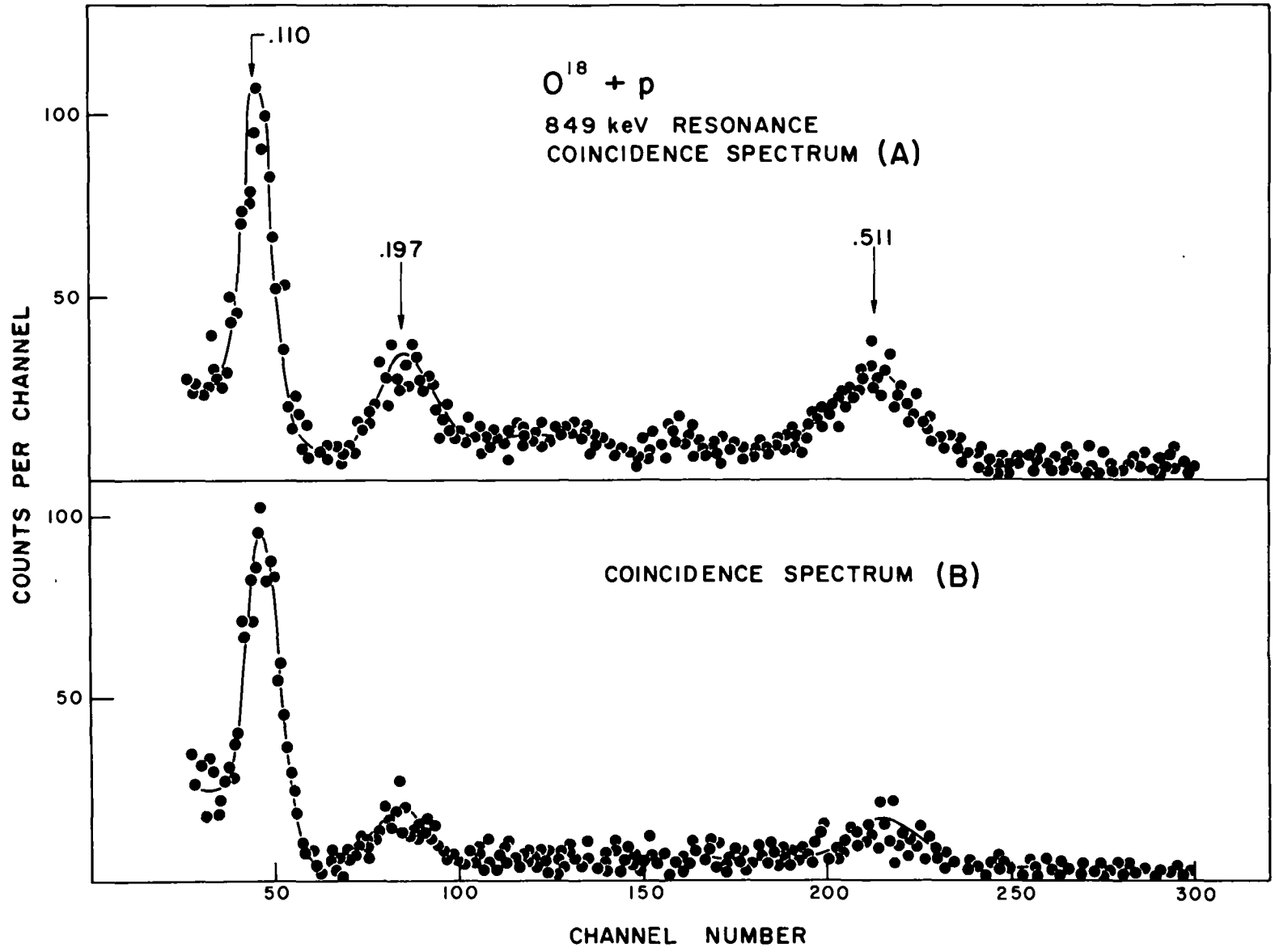
.110
O^{18} + p
849 keV RESONANCE
COINCIDENCE SPECTRUM (A)
.197
.511
100
50
COUNTS PER CHANNEL
100
50
COINCIDENCE SPECTRUM (B)
50
100
150
200
250
300
CHANNEL NUMBER

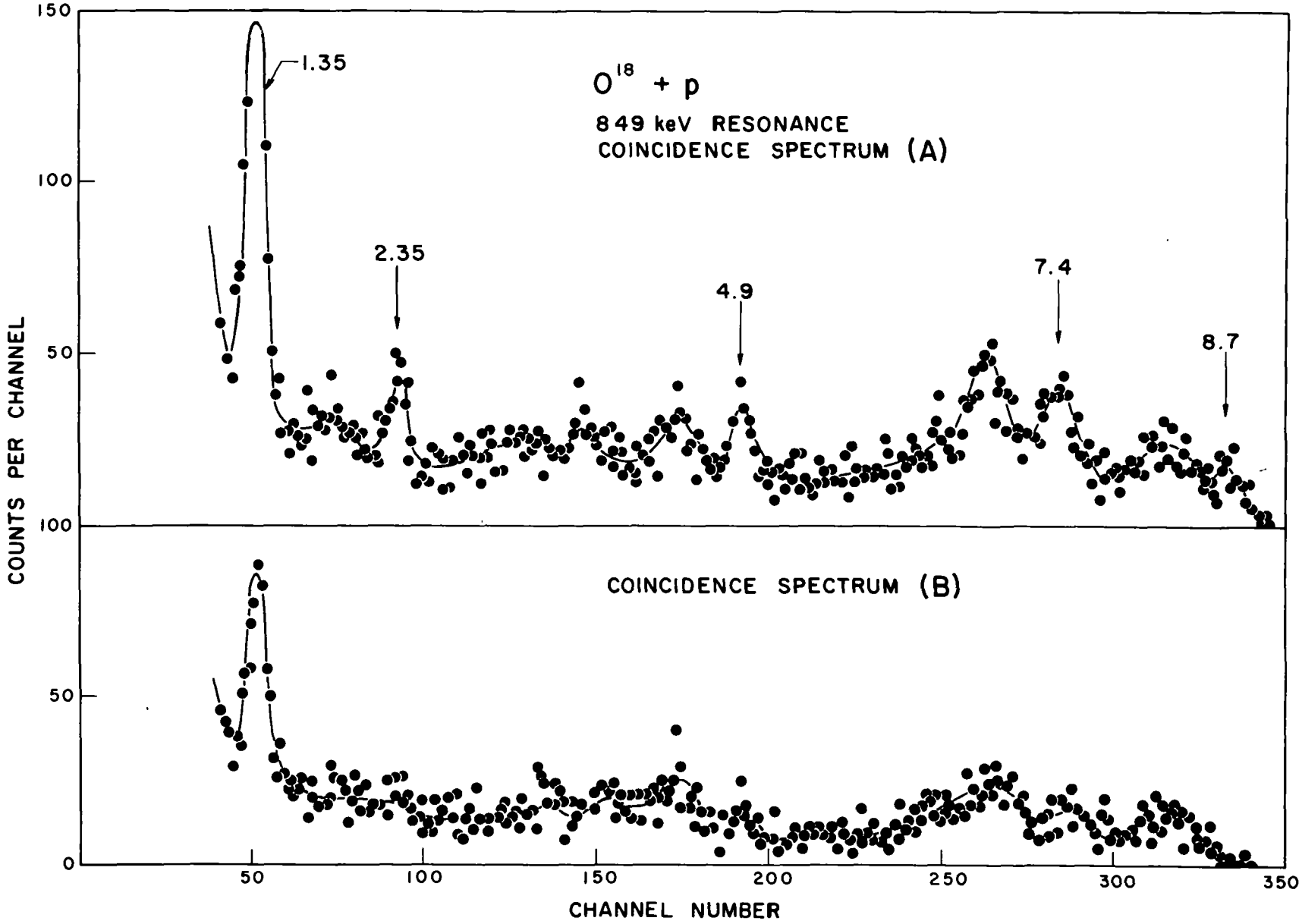
150
100
50
100
50
0
1.35
2.35
4.9
7.4
8.7
O^{18} + p
849 keV RESONANCE
COINCIDENCE SPECTRUM (A)
COINCIDENCE SPECTRUM (B)
COUNTS PER CHANNEL
50
100
150
200
250
300
350
CHANNEL NUMBER

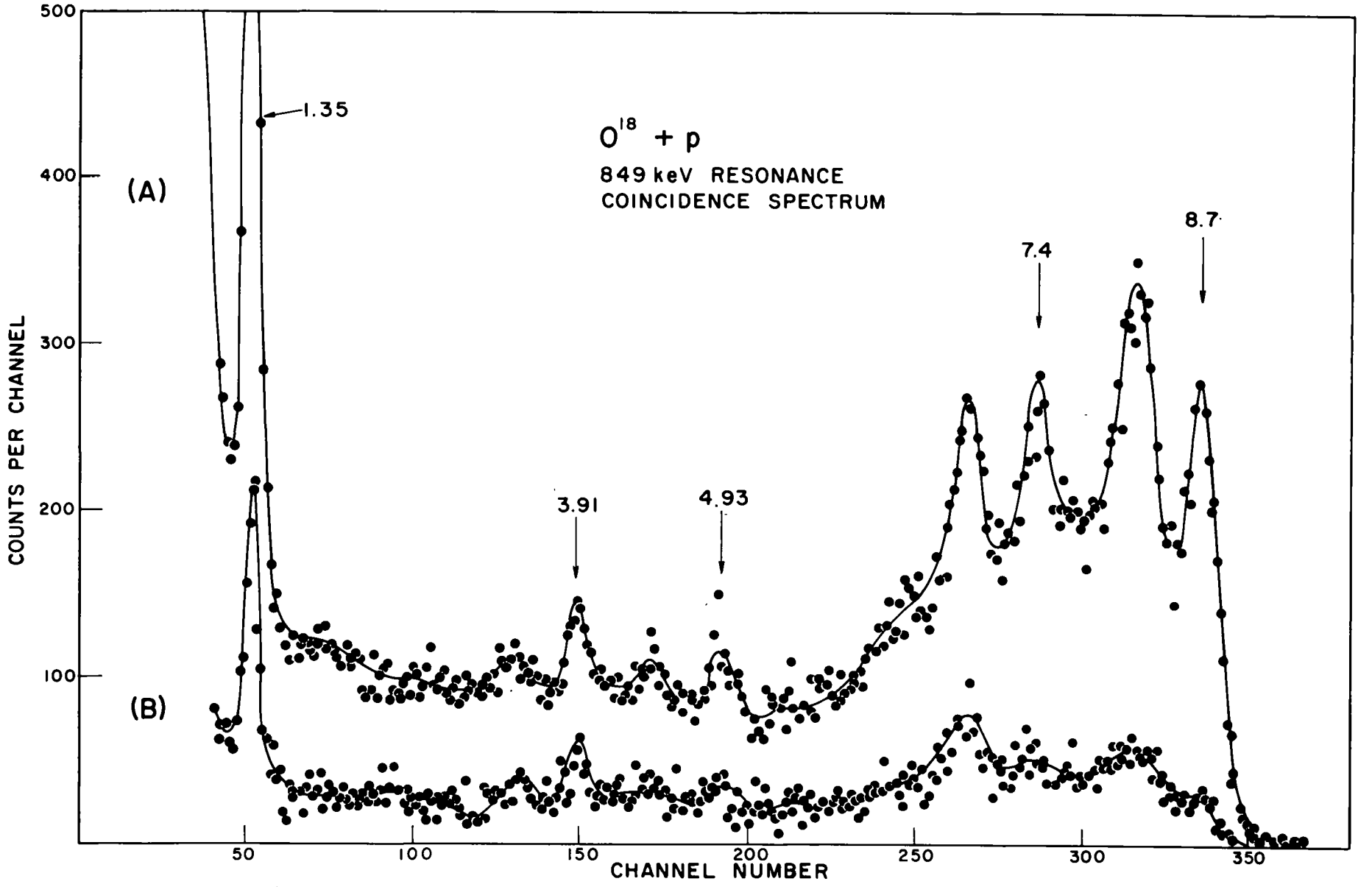
500
400
300
200
100
(A)
(B)
1.35
O^{18} + p
849 keV RESONANCE
COINCIDENCE SPECTRUM
3.91
4.93
7.4
8.7
COUNTS PER CHANNEL
50
100
150
200
250
300
350
CHANNEL NUMBER

3. 8.76 → 3.91 → 0 MeV Angular Correlation:

The correlation table used for this and subsequent angular correlation and distribution measurements has been described briefly in section B3. For this measurement the NaI (Tl) spectrometers were mounted at a face-to-reaction volume distance of 12 cm. Since the resonance assignment of $1/2^+$ is firmly established from the elastic proton scattering measurements, the cascade correlations from this resonance are necessarily functions only of θ, the angle between the crystal axes, and are consequently independent of the beam orientation. Furthermore, observation of the isotropic direct radiations from this $1/2^+$ state provided a convenient means of centering the axis of the correlation table about the reaction volume. Careful positioning of the table yielded gamma radiations which were isotropic to within 0.5%.

The correlation between the 4.85 and the 3.91 MeV radiations was effectively measured twice by establishing gates on both of these transitions in the counter fixed at 90° to the incident beam and recording the coincident spectra from the moving counter in two parallel multichannel analyzers. Four sets of data for each of the five values of θ were recorded and then averaged for each value of θ. The position of the moving spectrometer was alternated between large and small θ values during the measurement to eliminate any possible systematic, time-dependent error with a period of the same order as that of the correlation measurement (8 hours). Relative intensities of the 3.91 and 4.85 MeV radiations were computed from the areas under the photo and first-escape peaks of spectra similar to that shown in Figure II-6.

Figure II-10 shows the experimental correlation obtained, a theoretical least squares fit of the function

$$W(\theta) = 1 + \frac{A_2}{A_0} P_2(\cos\theta) + \frac{A_4}{A_0} P_4(\cos\theta) \qquad \text{(II-1)}$$

to the correlation data, and a schematic illustration of the geometry used in the measurement.

The experimental coefficient ratio A_4/A_0 is zero within the accuracy of this measurement ($\pm$ 0.05) whereas $A_2/A_0 = 0.22 \pm 0.03$ after a 38% correction[61]

Figure II-10. Angular correlation of the $8.76 \rightarrow 3.91 \rightarrow 0$ MeV cascade deexcitations in the $O^{18}(p, \gamma_{12}\gamma_2)F^{19}$ reaction with $E_p = 849$ keV. The solid curve is the result of the least squares fit to the data of the correlation function given by Equation II-1.

ANGULAR CORRELATION OF
8.76 MeV → 3.91 MeV → GROUND STATE
CASCADE IN $O^{18}(p,\gamma\gamma)F^{19}$

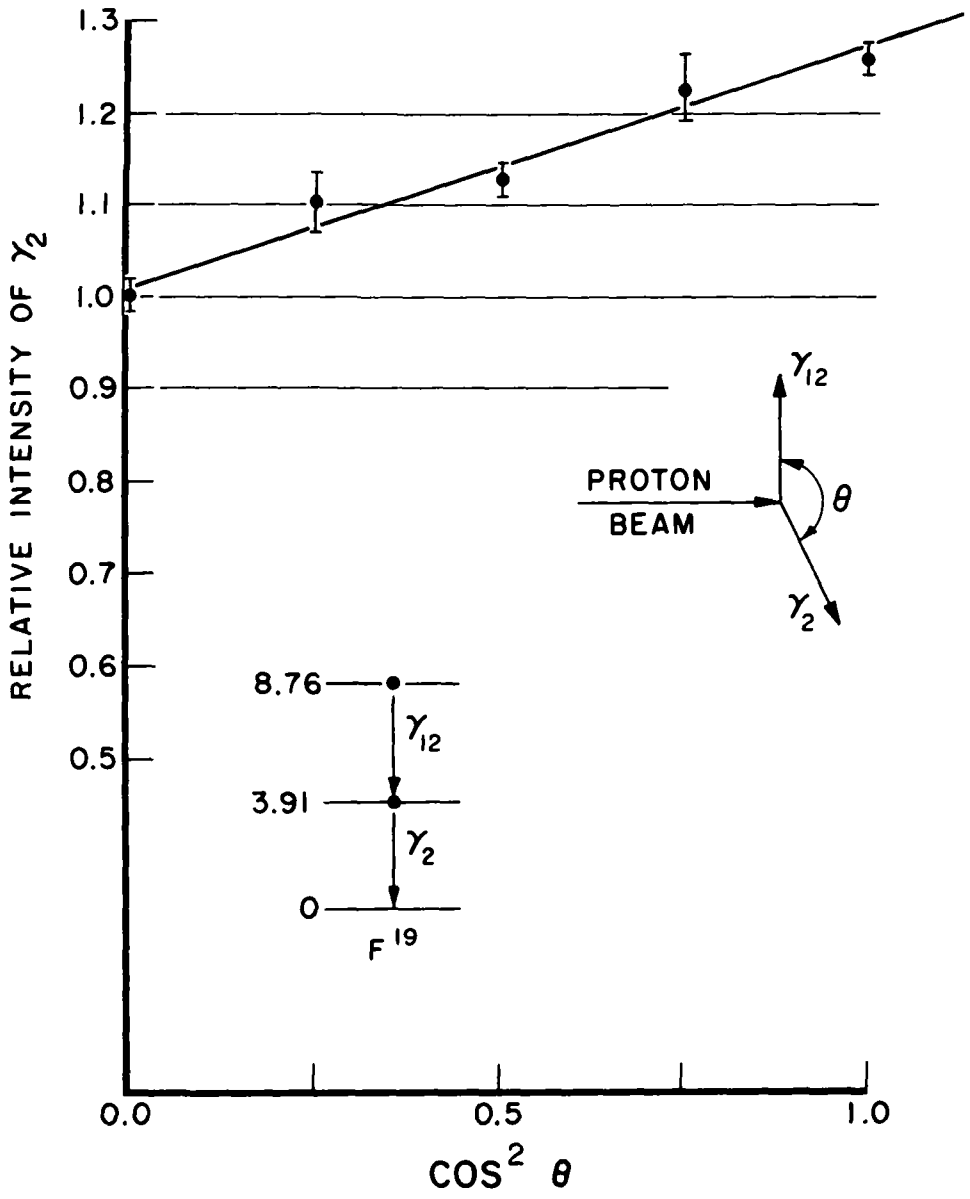

for the finite solid angle of the spectrometers.

The correlations of other cascades from this resonance were not examined in detail since all the other levels involved have previously received unambiguous assignments.

4. 2.79 → 0.197 MeV Angular Distribution:

With the correlation table alignment unchanged from that of the previous measurement, the energy of the proton beam was increased to populate states in F^{19} from the proton capture resonance in O^{18} at 1169 keV. The direct spectrum of gamma radiation deexciting this resonant state is shown in Figure II-11; the dominant transitions of 8.9, 7.7, and 6.28 and 2.59 MeV in the spectrum establish strong deexcitation branches from the 9.07 MeV state into the 0.197 MeV state, into the first excited triplet, and into the 2.79 MeV state, respectively. The 6 MeV region of this spectrum is complicated by the presence of a 6.13 MeV transition not associated with the 1169 keV O^{18} + p resonance as demonstrated by the off-resonance spectrum shown also in Figure II-11. The source of the contaminant radiation is almost certainly the $(p,\alpha\gamma)$ reaction on an F^{19} target impurity. It is thought that this unwanted radiation does not significantly affect the distribution measurement of the 2.59 MeV transition.

The angular distribution of the 2.59 MeV radiation corresponding to the 2.79 to 0.197 MeV transition was extracted from a number of direct gamma spectra taken by the movable spectrometer at a series of five angles φ, where φ specifies the angle between the spectrometer and the beam axis. The crystal face-to-reaction site distance was 16 cm. Both the integrated beam current and the gamma radiation detected in the fixed counter at 90^{o} were used to normalize the data recorded by the movable crystal. Throughout the distribution measurement the ratio of these two independent monitors proved to be constant to within the statistical accuracy of the measurement, thus providing a check against systematic errors due to, say, a possible energy shift in the proton beam. As in the correlation measurement, data was recorded several times at each of the angles.

The observed relative intensities of the 2.59 MeV radiation are shown in

Figure II-11. $O^{18} + p$ direct gamma radiation spectra at the resonance energy $E_p = 1169$ keV and 100 keV below the resonance energy. Energies of prominent peaks are indicated in MeV.

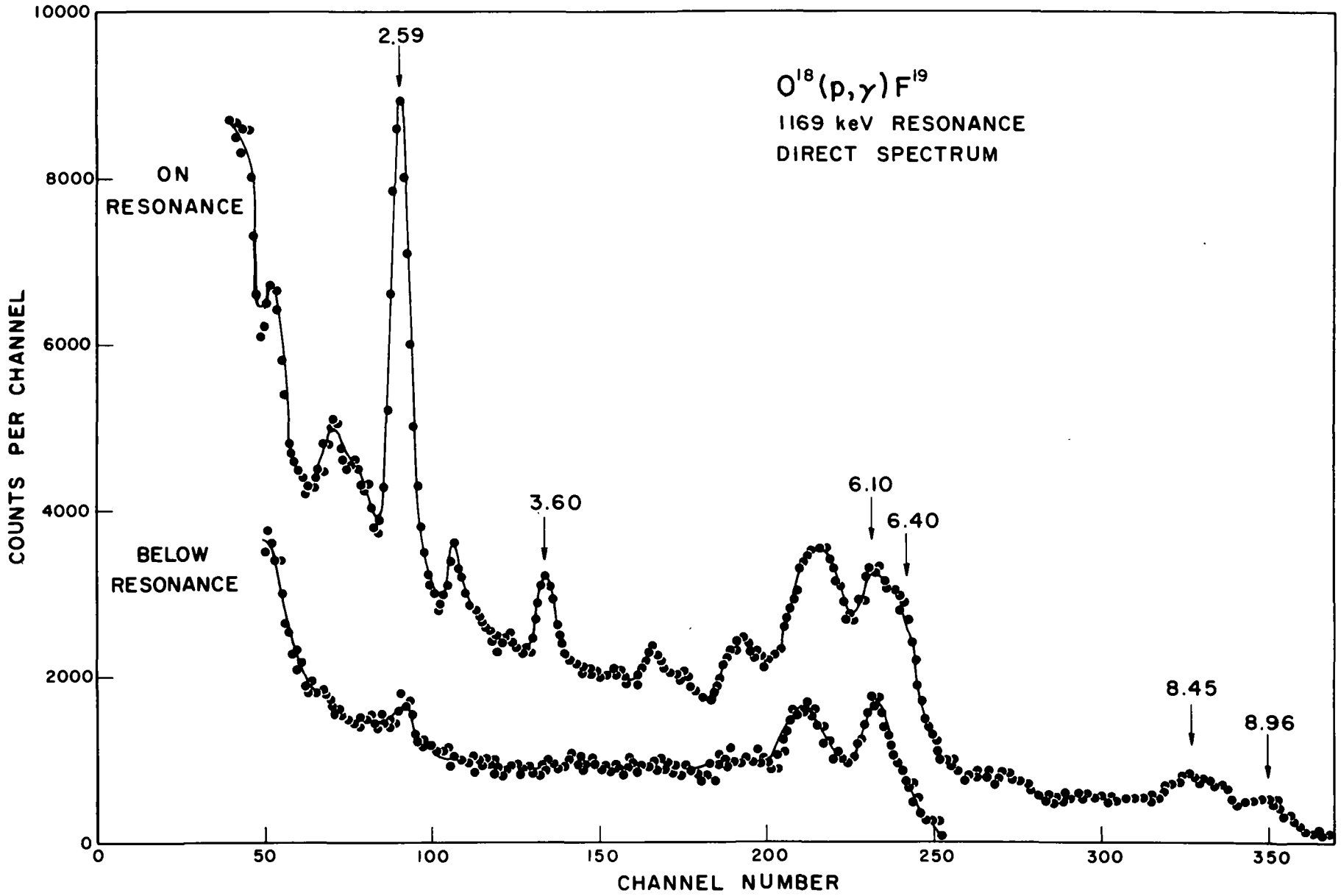
$O^{18}(p,\gamma)F^{19}$
1169 keV RESONANCE
DIRECT SPECTRUM
ON RESONANCE
BELOW RESONANCE
2.59
3.60
6.10
6.40
8.45
8.96
COUNTS PER CHANNEL
CHANNEL NUMBER
0
2000
4000
6000
8000
10000
0
50
100
150
200
250
300
350

Figure II-12. Angular distribution of the $2.79 \rightarrow 0.197$ MeV radiation following the resonant capture reaction $O^{18}(p,\gamma)F^{19}$ at $E_p = 1169$ keV. The solid curve is the result of the least squares fit to the data of the correlation function given by Equation II-1.

ANGULAR DISTRIBUTION OF
THE 2.79 → 0.197 MeV RADIATION
IN $O^{18}(p,\gamma)F^{19}$.

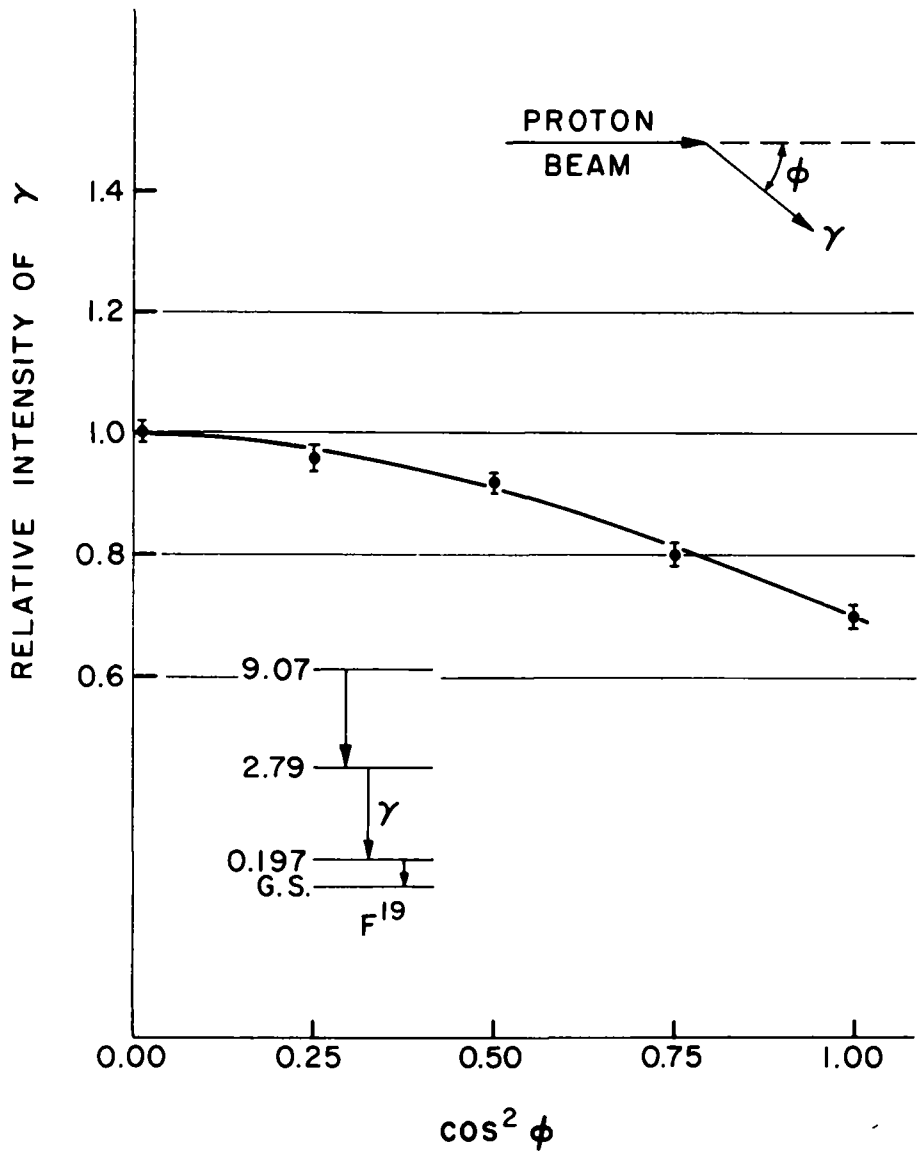

Figure II-12. A least squares fit to these data after solid angle corrections[61] yields $A_2/A_0 = 0.300 \pm 0.015$ and $A_4/A_0 = -0.097 \pm 0.023$ where the coefficients are those in the distribution function of Equation II-1. It should be emphasized that in spite of the unrealistic data interpretation of Huang et al.[55], to be discussed further in Section D, these authors obtained under markedly different experimental conditions (solid target, much smaller NaI(Tl) crystal spectrometers, etc.) essentially the same A_2/A_0 and A_4/A_0 distribtuion coefficients as those obtained herein giving further credence to the distribution data.

5. Other Resonances:

The resonances at 1769 and 1932 keV have also received preliminary study. In agreement with earlier reports[60], it has been found that the 1769 keV resonance state exhibits a very complex deexcitation. The direct gamma radiation spectrum of the 1769 resonance is illustrated in Figure II-13. It is clear that many cascades involving levels in the interesting 4-5 MeV range of excitation in F^{19} are present. This results, in fact, in the rather featureless spectrum shown in the figure. The same deexcitation complexity is true of the 1932 keV resonance for which a direct spectrum is also included in Figure II-13 along with a 849 keV resonance spectrum for purposes of comparison. These spectra were measured under identical conditions with the gain of the entire system stabilized on an 0.835 MeV spectral line from a Mn^{54} source exposed to the spectrometer in parallel with the bombarded cell.

Weak radiation at 4.43 MeV is evident in both the higher energy spectra and is attributable to the prolific N^{15} $(p,\alpha\gamma)$ C^{12} reaction on the 0.37% abundant N^{15} component of a nitrogen contaminant of the O^{18} target gas. Unfortunately, an N^{15} contamination can be particularly bothersome since the N^{15} $(p,\alpha\gamma)$ C^{12} cross section is some 800 mb compared to the (p,γ) resonance cross sections of $\sim$50 μb as measured herein.

No detailed attempt was made to establish more carefully the deexcitation of these two higher resonances.

Figure II-13. O^{18} + p direct gamma radiation spectra obtained at the three proton resonances E_p = 849, 1769, and 1932 keV. The 1769 and 1932 curves have been displaced vertically to facilitate spectra comparison. Energies of prominent peaks are indicated in MeV. The 5 x 5 inch sodium iodide spectrometer was placed at 90^o to the beam direction and 3 cm from the target center for each of the spectra.

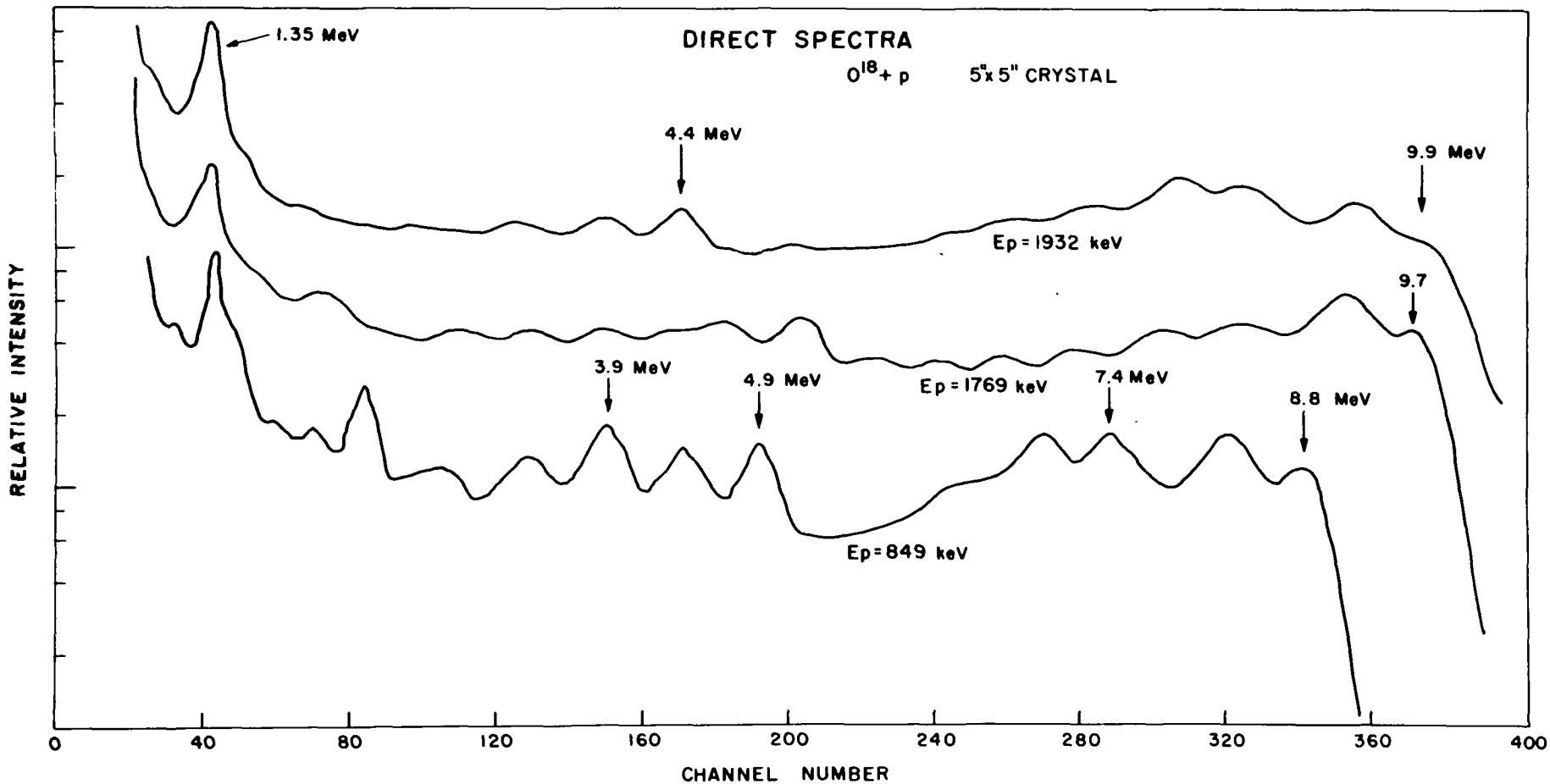
DIRECT SPECTRA
O^{18} + p
5"x5" CRYSTAL
1.35 MeV
4.4 MeV
9.9 MeV
Ep = 1932 keV
9.7
3.9 MeV
4.9 MeV
Ep = 1769 keV
7.4 MeV
8.8 MeV
Ep = 849 keV
RELATIVE INTENSITY
0
40
80
120
160
200
240
280
320
360
400
CHANNEL NUMBER

D. Analysis of Experimental Results

1. Angular Momentum of the 2.79 MeV State:

Several authors[55, 59, 60] have examined the 1169 keV proton capture resonance in the O^{18} (p, γ) F^{19} reaction. This resonance shows a strong deexcitation branch of 6.3 MeV which populates the state at 2.79 MeV in F^{19}. Huang et al.[55] have studied the angular distribution of the radiation from the resonance state and the distribution of the 2.59 MeV radiation from the 2.79 MeV state, and, on the basis of these measurements, have assigned the value $J^{\pi} = 9/2^{\pm}$ to the 2.79 MeV state.

Close examination of the work of these authors, however, indicates that in their data analysis they have unrealistically neglected the definite possibility of multipole mixing in the unobserved 6.3 MeV member of the 9.07 → 2.79 → 0.197 MeV cascade while considering instead a physically improbable mixture of M3 with E2 radiation in the 2.59 MeV members.

In view of the immediate theoretical importance of establishing correctly the angular momentum assignment of the 2.79 MeV state, which has universally been identified with the $9/2^+$ member of the positive parity K = 1/2 band based on the ground state except in the case of a recent calculation by Unna[65] where it has been identified as a $7/2^+$ state, it is clear that the experimental information at hand concerning this state should be reexamined. The levels involved in the deexcitation cascade through the 2.79 MeV state are the state at 0.197 MeV, the state at 2.79 MeV, and the resonance state at 9.07 MeV. The first of these is known from a number of measurements[1] to have an unambiguous J^{π} assignment of $5/2^+$.

As mentioned previously, the spin of the 2.79 MeV state has been limited to 7/2 or 9/2 by inelastically scattered neutron data[54] on an F^{19} target. That the angular momentum is at least 7/2 is further supported by a number of measurements of deexcitation branchings in which this state in involved; in particular, (i) the 2.79 MeV state deexcites almost entirely to the $5/2^+$ state with no observable branches to the states of $J^{\pi} = 5/2^-$, $3/2^-$, $3/2^+$, $1/2^+$, or $1/2^-$ available well below the 2.79 MeV state, and (ii) the 2.79 MeV state is fed

strongly by gamma radiation from the 9.07 MeV state known to have spin $7/2^+$ with spin $9/2^+$ less probable. A spin assignment to the 2.79 MeV state greater than 9/2 is made highly unlikely by very recent two-parameter, gamma-gamma coincidence measurements[66] following the beta decay of O^{19}. A weak beta-branch is found from the ground state of O^{19} to the 4.39 MeV state in F^{19} limiting the spin of the latter to J = 3/2, 5/2, or 7/2. The 4.39 MeV state then deexcites by cascading through the 2.79 MeV level, thus placing a reasonable upper limit of 9/2 on this level.

The O^{18} (p,p) O^{18} data of Yagi et al.[58] establish the 9.07 MeV state as being excited by g-wave protons indicating a J^π value of $7/2^+$ or $9/2^+$ for this state. The higher value is inconsistent[67] with the measured cross section of the (p,α_0) reaction at the same resonance, although the $9/2^+$ assignment perhaps cannot be ruled out entirely on this basis. Amsel and Bishop[68] indicate a spin of $7/2^-$ for the 9.07 MeV state. They do not indicate, however, on what grounds the 9/2 possibility was eliminated from consideration.

From the above arguments, the possible spin sequences which must be considered in analyzing the angular distribution of the 2.79 MeV transition are (a) $7/2 \xrightarrow{Q} 9/2 \rightarrow 5/2$, (b) $7/2 \xrightarrow{Q} 7/2 \xrightarrow{\delta} 5/2$, (c) $9/2 \xrightarrow{Q} 9/2 \rightarrow 5/2$, (d) $9/2 \xrightarrow{Q} 7/2 \xrightarrow{\delta} 5/2$ with sequences (a) and (b) more consistent with the experimental (p,α_0) data. The symbols ρ and δ are the multipole mixture parameters for the upper and lower members of the cascade. The distribution functions[69] for each of the possible sequences are plotted in Figure II-14 a, b, c, and d. The experimental distribution coefficients are indicated by the shaded horizontal bands. The experimental A_4/A_0 coefficient rules out the possible spin sequence $9/2 \rightarrow 7/2 \rightarrow 5/2$ because of the positive $P_4(\cos\theta)$ term required by this sequence for all but highest values of E2 mixing in the upper transition. Reference to the remaining three possibilities (Fig. II-14 a, b, and c) indicates that the theoretical coefficients are in accord with experiment under the conditions listed in Table II-1.

Figure II-14a. The gamma radiation angular distribution coefficients, A_2/A_0 and A_4/A_0, for the second member of the deexcitation cascade $7/2 \rightarrow 9/2 \rightarrow 5/2$ as a function of the E2-M1 mixing parameter ρ. The shaded bands indicate the experimentally measured coefficient values; the dashed vertical lines indicate the mixing parameter values compatible with the distribution measurements.

Figure II-14b. The gamma radiation angular distribution coefficients, A_2/A_0 and A_4/A_0, for the second member of the deexcitation cascade $7/2 \rightarrow 7/2 \rightarrow 5/2$ as a function of the E2-M1 mixing parameter δ at particular values of the E2-M1 mixing parameter ρ.

Figure II-14c. The gamma radiation angular distribution coefficients, A_2/A_0 and A_4/A_0, for the second member of the deexcitation cascade $9/2 \rightarrow 9/2 \rightarrow 5/2$ as a function of the E2-M1 mixing parameter ρ.

Figure II-14d. The gamma radiation angular distribution coefficients, A_2/A_0 and A_4/A_0, for the second member of the deexcitation cascade $9/2 \rightarrow 7/2 \rightarrow 5/2$ as a function of the E2-M1 mixing parameter δ at particular values of the E2-M1 mixing parameter ρ.

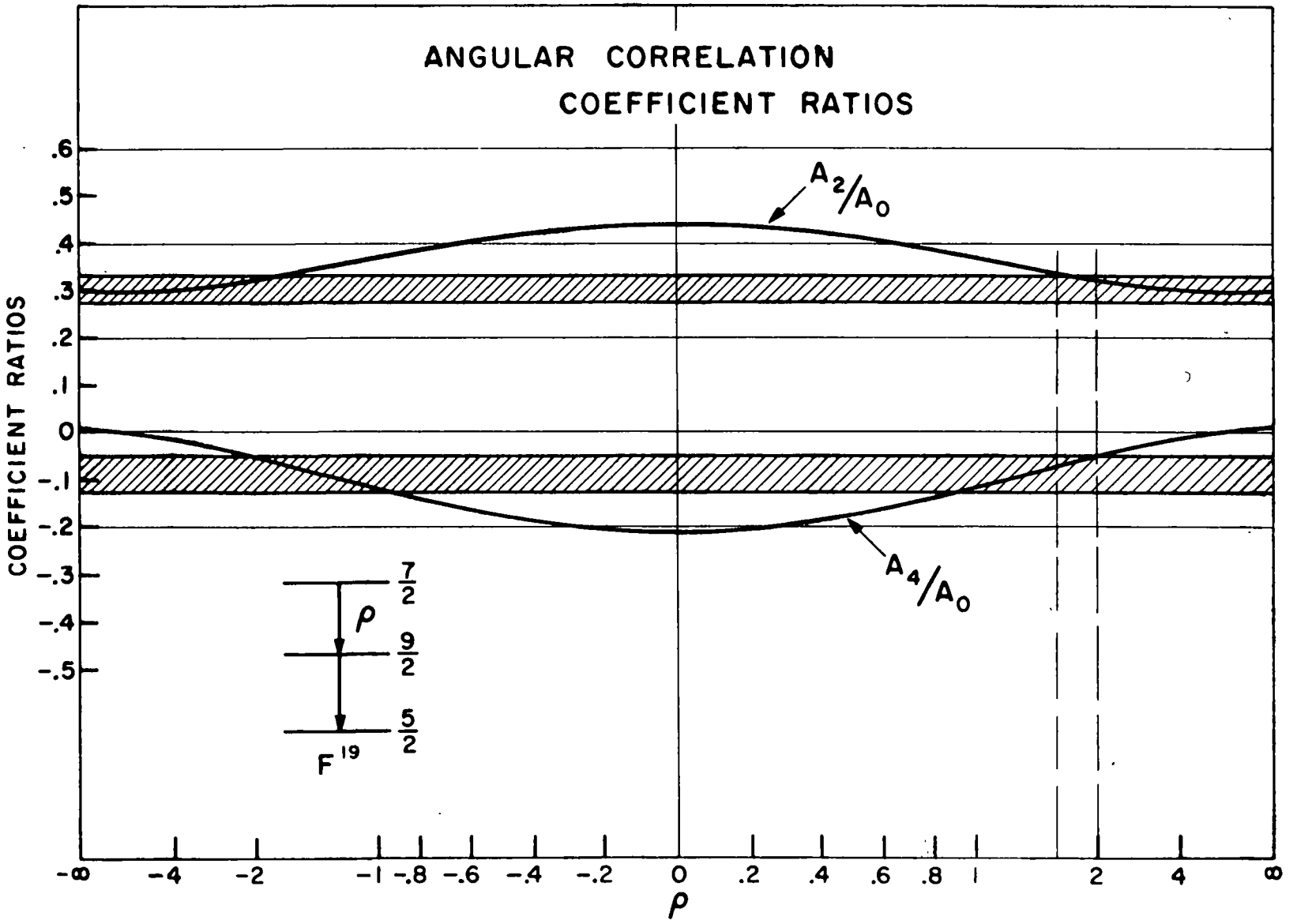
ANGULAR CORRELATION
COEFFICIENT RATIOS
COEFFICIENT RATIOS
.6
.5
.4
.3
.2
.1
0
-.1
-.2
-.3
-.4
-.5
A_2/A_0
A_4/A_0
$\frac{7}{2}$
ρ
$\frac{9}{2}$
$\frac{5}{2}$
F^{19}
-∞ -4 -2 -1 -.8 -.6 -.4 -.2 0 .2 .4 .6 .8 1 2 4 ∞
ρ

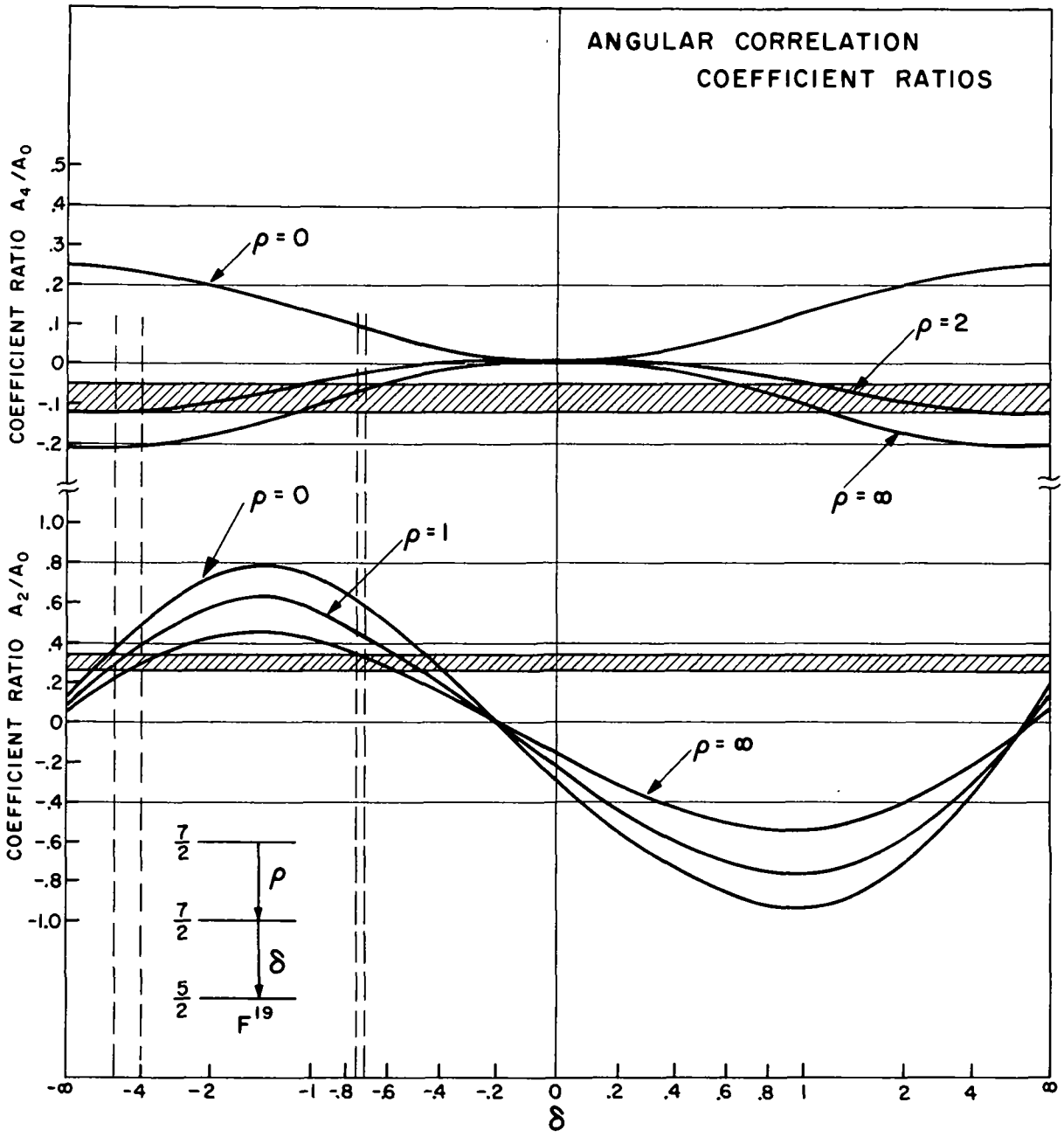
ANGULAR CORRELATION
COEFFICIENT RATIOS
COEFFICIENT RATIO A_4/A_0
$\rho = 0$
$\rho = 2$
$\rho = \infty$
COEFFICIENT RATIO A_2/A_0
$\rho = 0$
$\rho = 1$
$\rho = \infty$
$\frac{7}{2}$
ρ
$\frac{7}{2}$
δ
$\frac{5}{2}$
F^{19}
δ

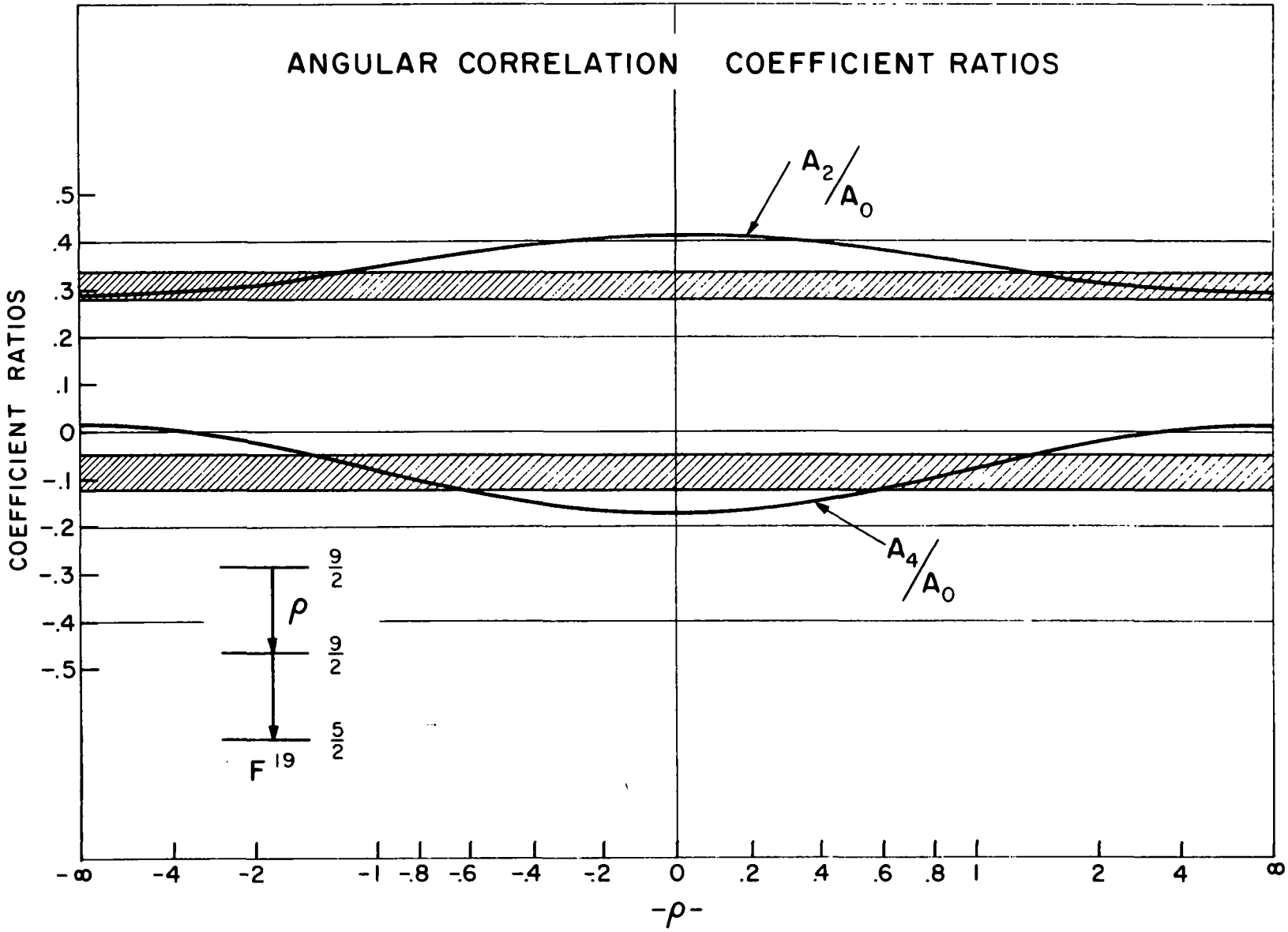
ANGULAR CORRELATION COEFFICIENT RATIOS
COEFFICIENT RATIOS
.5
.4
.3
.2
.1
0
-.1
-.2
-.3
-.4
-.5
A_2/A_0
A_4/A_0
$\frac{9}{2}$
ρ
$\frac{9}{2}$
$\frac{5}{2}$
F^{19}
-∞ -4 -2 -1 -.8 -.6 -.4 -.2 0 .2 .4 .6 .8 1 2 4 ∞
$-\rho-$

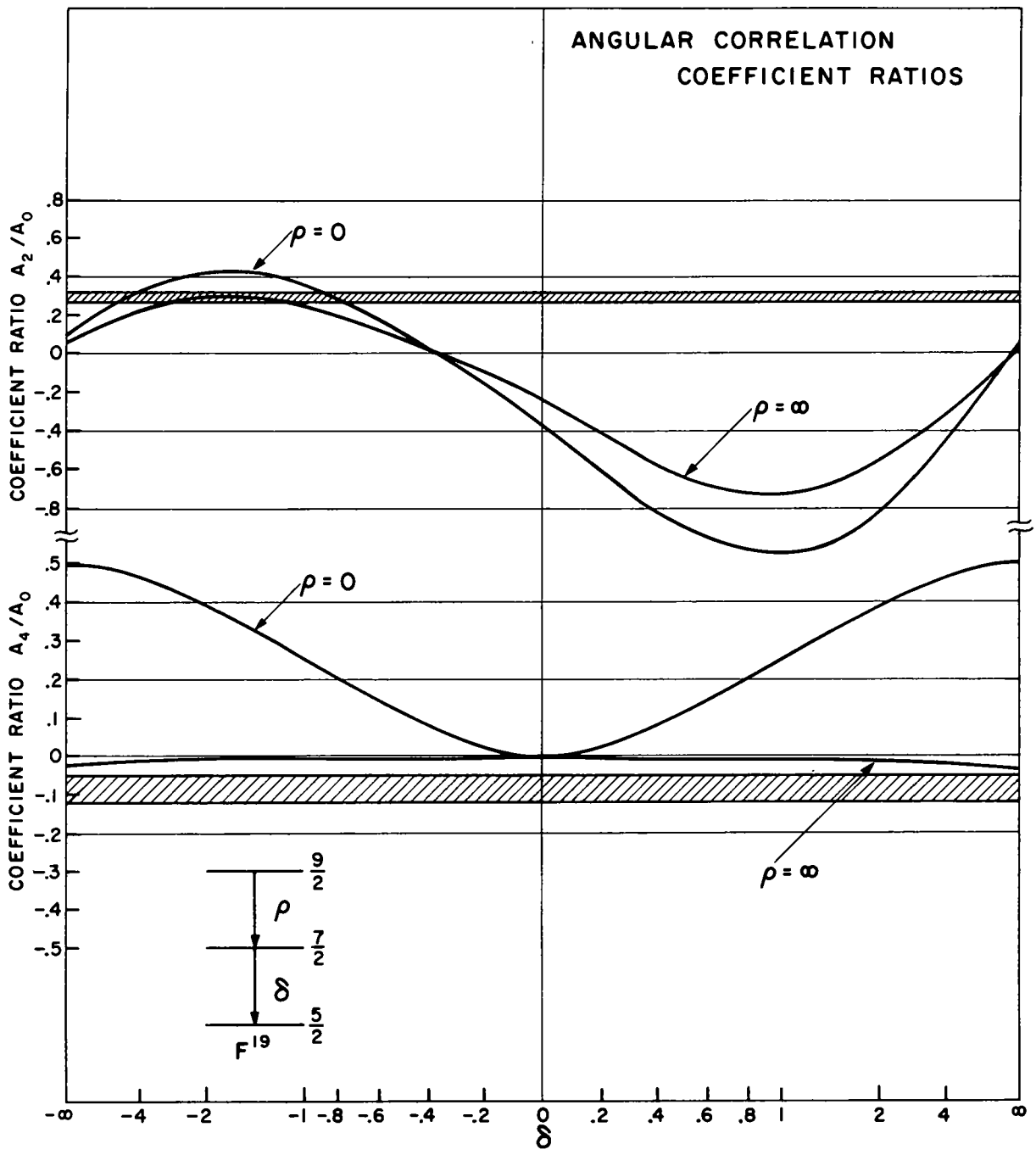
ANGULAR CORRELATION
COEFFICIENT RATIOS
COEFFICIENT RATIO A_2/A_0
$\rho = 0$
$\rho = \infty$
COEFFICIENT RATIO A_4/A_0
$\rho = 0$
$\rho = \infty$
$\frac{9}{2}$
ρ
$\frac{7}{2}$
δ
$\frac{5}{2}$
F^{19}
δ

TABLE II-1

Mixing ratios in the 6.28 and the 2.59 MeV members of the 9.07 $\rightarrow$ 2.79 $\rightarrow$ 0.197 MeV deexcitation cascade in F^{19} permitted by the angular distribution measurement of the 2.59 MeV radiation.

Spin sequence	Allowed ρ and δ values from the experimental A_2/A_0 coefficient	Allowed ρ and δ values from the experimental A_4/A_0 coefficient	Allowed ρ and δ values from both A_2/A_0 and A_4/A_0 coefficients
7/2→9/2→5/2	$1.5 < \lvert\rho\rvert < \infty$ $\delta = 0$	$0.7 < \lvert\rho\rvert < 2.0$ $\delta = 0$	$1.5 < \lvert\rho\rvert < 2.0$ $\delta = 0$
7/2→7/2→ 5/2	$0 < \lvert\rho\rvert < \infty$ $-0.7 < \delta < -0.4$ or $0 < \lvert\rho\rvert < \infty$ $-10 < \delta < -3$	$1.2 < \lvert\rho\rvert < \infty$ $0.6 < \lvert\delta\rvert < \infty$	$\lvert\rho\rvert \cong \infty$ $-0.75 < \delta < -0.60$ or $1.2 < \lvert\rho\rvert < 2$ $-10 < \delta < -4$
9/2→9/2→5/2	$1.5 < \lvert\rho\rvert < \infty$ $\delta = 0$	$0.5 < \lvert\rho\rvert < 1.4$ $\delta = 0$	no allowed value of ρ

The sequence 9/2 → 5/2 may be eliminated with $\cong$70% certainty since the measurement of either A_4/A_0 or A_2/A_0 must be in error by more than one standard deviation in order that δ have a value compatible with both distribution coefficients. On this basis, the spin of the 9.07 MeV state is 7/2 in accord with assignment of Yagi[67].

Examination of the remaining two spin sequences indicates that no unambiguous determination between the spin possibilities of 7/2 or 9/2 for the 2.79 MeV state can be made from these data, although the value 7/2 would appear the less probable of the two because of the specific combinations required in both the 6.28 and 2.59 MeV members of the cascade in order that the predicted distribution agree with experiment. However, since the work reported herein was initiated, further experiments utilizing the F^{19} (p,p'γ) F^{19} reaction with coincident p' - γ detection have been carried out and are reported[70] to limit the spin assignment of the 2.79 MeV state to possible values of 5/2, 9/2, or 11/2. Of these, only the 9/2 assignment is compatible with the data presented above; thus, the angular momentum of the 2.79 MeV state is established as

most certainly 9/2. Furthermore, reference to Table II-1 shows that for the $7/2 \rightarrow 9/2 \rightarrow 5/2$ sequence, the multipole mixing parameter for E2 radiation in the upper member of the cascade has a value of between 1.5 and 2.0.

2. Angular Momenta and Deexcitation Properties of the 8.76 and 3.91 MeV States:

Figure II-15 presents the branching ratios determined in the present measurements for the 8.76 and the 3.91 MeV states. The occurrence of the relatively strong primary transition (18%) to the 3.91 MeV state and the anisotropy of the correlation shown in Figure II-10 limit the possible angular momentum assignments of the 3.91 MeV state to 3/2 or 5/2.

In view of the strength of this transition to the 3.91 MeV state, as compared to the higher energy transitions to lower states in F^{19} where known level assignments require dipole transitions, it appears reasonable to assume essentially pure dipole character for the 4.85 MeV transition if a 3/2 assignment to the 3.91 MeV state is considered. A 5/2 assignment would clearly require pure quadrupole transitions for both cascade members.

For a 5/2 assignment to the 3.91 MeV level it follows simply that the angular correlation would be predicted to have the form

$$W(\theta) = 1 + 0.286\, P_2(\cos\theta) + 0.381\, P_4(\cos\theta). \qquad \text{(II-2)}$$

For a 3/2 assignment and a pure dipole primary transition, it also follows that the correlation would be predicted[69] to have the form

$$W(\theta) = \frac{1 + 1\text{-}2\sqrt{3}\,\delta - \delta^2 \cdot P_2(\cos\theta)}{4\,(1+\delta^2)} \qquad \text{(II-3)}$$

where δ is the multipole amplitude ratio in the second member of the cascade.

The least squares fit to the correlation data described in Section C3 established the correlation coefficients as $A_2/A_0 = 0.22 \pm 0.03$ and $A_4/A_0 \cong 0$, and the absence of a $P_4(\cos\theta)$ term excludes completely a 5/2 assignment to the 3.91 MeV state. The results are consistent, however, with a 3/2 assignment

Figure II-15. Energy level spectrum of F^{19} including the deexcitation branching ratios of the states at 8.76 and 3.91 MeV. Relative transition intensities are indicated in % with 100% comprising the total gamma deexcitation of a state. Excitation energies in MeV and J^{π} assignments are shown on the left. The asymptotic Nilsson model quantum numbers $\left[Nn_z\Lambda\right]$, which have been identified in the text with particular F^{19} states, are included for easy reference.

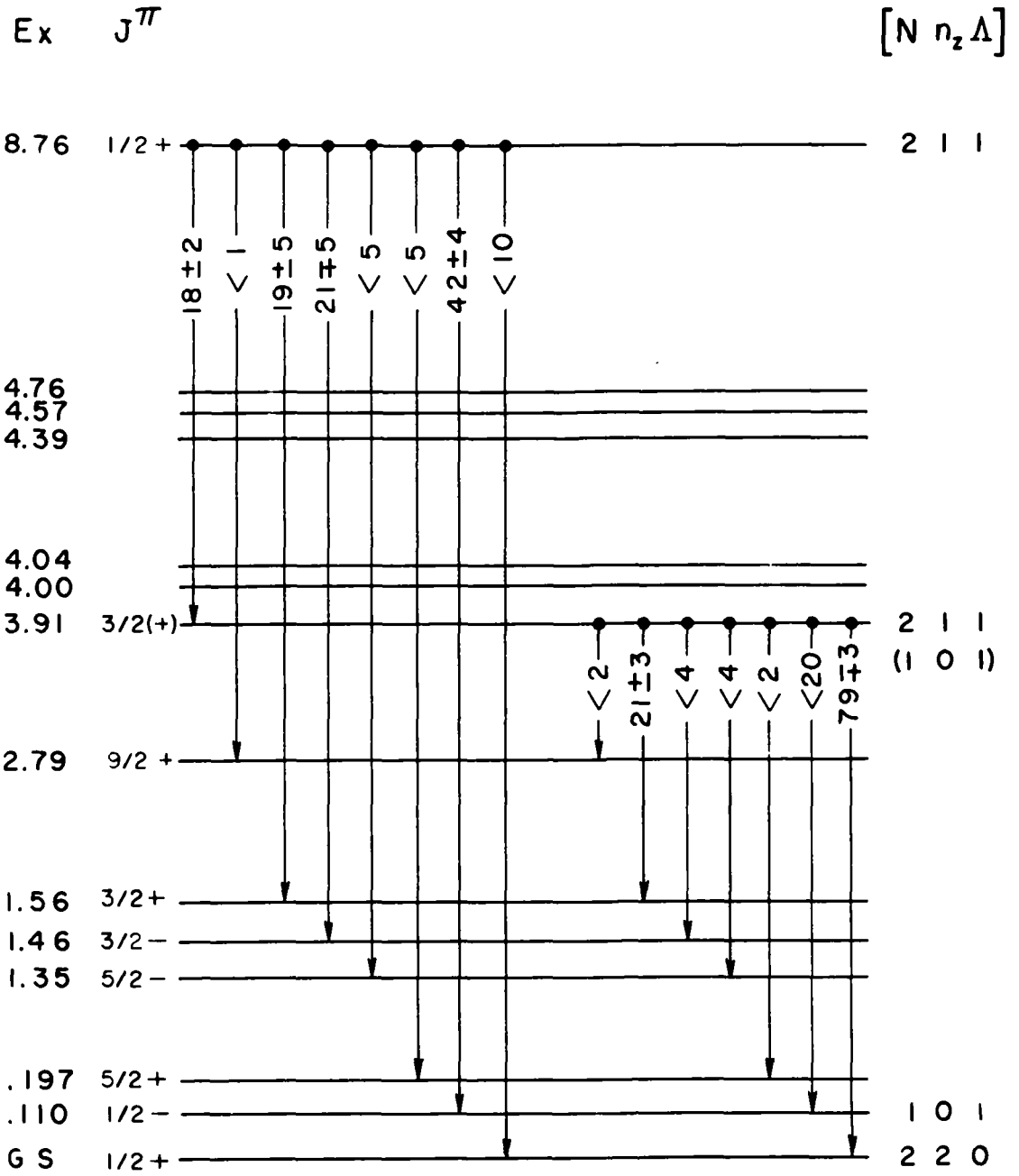
Ex
J^{π}
$[N\ n_z\ \Lambda]$
8.76
1/2+
2 1 1
18±2
<1
19±5
21±5
<5
<5
42±4
<10
4.76
4.57
4.39
4.04
4.00
3.91
3/2(+)
2 1 1
(1 0 1)
<2
21±3
<4
<4
<2
<20
79±3
2.79
9/2+
1.56
3/2+
1.46
3/2−
1.35
5/2−
.197
5/2+
.110
1/2−
1 0 1
G S
1/2+
2 2 0

F^{19}

with either $\delta \cong 0$ or $\delta \cong -2.0$ as may be demonstrated by equating the coefficient of $P_2(\cos\theta)$ in Equation II-3 with the experimental coefficient A_2/A_0. The $\delta = 0$ value is consistent with either positive or negative parity for the intermediate state whereas the $\delta \cong -2.0$ value would require positive parity only. The angular momentum assignment of 3/2 to the 3.91 MeV state is unambiguous.

E. Discussion

1. Orientation:

For reasons outlined briefly in Chapter I of this work, it is of considerable interest to investigate just what significance the branching ratios and spin assignments here made have within the framework of the wide variety of model calculations which have been applied to F^{19}. To facilitate theoretical and experimental comparisons Figure II-16 presents (A) the experimentally observed energy level scheme of F^{19} on either side of the theoretically generated level schemes of (B) Rakavy[71], (C) Redlich[17], (D) Chi and Davidson[40], (E) Harvey[51], (F) Paul[45], (G) Elliott and Flowers[16], and (H) Inoue et al.[19]. Not shown in this figure are the predictions of Abraham and Warke[72], who have qualitatively fit the $1/2^+$, $5/2^+$, and $3/2^+$ states of F^{19} by considering the odd nucleon as weakly coupled to surface oscillations of the O^{18} core; and the predictions of Wildermuth and Kanelloupoulos[73], who have carried out a cluster model calculation in which the low energy, positive parity states of F^{19} are represented as the coupling of two unexcited O^{16} and H^3 clusters to produce the level ordering $1/2^+$, $5/2^+$, $3/2^+$, $9/2^+$, $7/2^+$, $13/2^+$, and $11/2^+$. The negative parity states are represented in turn as the coupling of unexcited N^{15} and He^4 clusters which results in the same level order as the positive parity states. No quantitative statements concerning the energy spacing of the states are predicted by this cluster calculation, however.

2. Model Interpretations of the 2.79 MeV State:

As indicated in Figure II-16, the model calculations of F^{19} presented herein, whether collective or shell model based, all predict correctly the existence of a $9/2^+$ state in the energy region of 2.8 MeV. An exception to this is a more recent

Figure II-16. Comparison of (A) the experimentally observed energy level spectrum of F^{19} with the model-generated energy level spectra of (B) Rakavy, (C) Redlich, (D) Chi and Davidson, (E) Harvey (F) Paul, (G) Elliott and Flowers, and (H) Inoue et al.

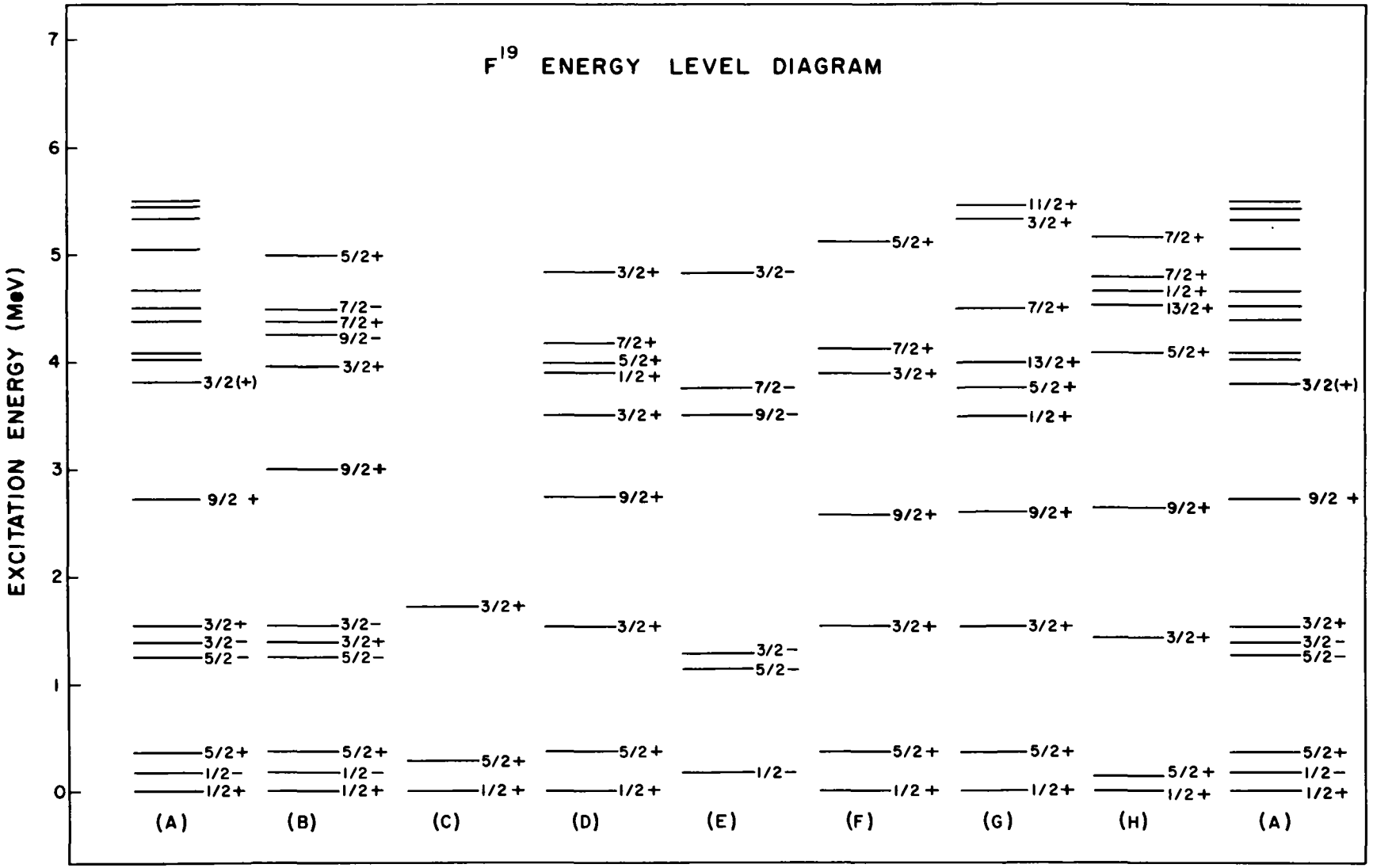
F19 ENERGY LEVEL DIAGRAM
EXCITATION ENERGY (MeV)
7
6
5
4
3
2
1
0
3/2(+)
9/2 +
3/2+
3/2−
5/2−
5/2+
1/2−
1/2+
5/2+
7/2−
7/2+
9/2−
3/2+
9/2+
3/2+
5/2+
1/2+
3/2+
3/2−
5/2−
3/2+
7/2+
5/2+
1/2+
3/2+
9/2+
3/2+
5/2+
1/2+
3/2−
9/2−
7/2−
3/2−
5/2−
1/2−
5/2+
7/2+
3/2+
9/2+
3/2+
5/2+
1/2+
11/2+
3/2+
7/2+
13/2+
5/2+
1/2+
9/2+
3/2+
5/2+
1/2+
7/2+
7/2+
1/2+
13/2+
5/2+
9/2+
3/2+
5/2+
1/2+
3/2(+)
9/2 +
3/2+
3/2−
5/2−
5/2+
1/2−
1/2+
(A)
(B)
(C)
(D)
(E)
(F)
(G)
(H)
(A)

model formulation (not shown in Figure II-16) of F^{19} by Unna[65], who states that for a pure $(d_{5/2})^3$ configuration the $7/2^+$ state should lie lower than the $9/2^+$ state. The experimentally observed $9/2^+$ state is thus a signature of strong configuration interaction in this nucleus; considerable configuration mixing has, in fact, been assumed in the other shell model calculations.

In addition to the generally successful model predictions of the experimentally confirmed $9/2^+$ state, of further interest here is the enhanced E2 radiation (or the inhibited M1 radiation) from the resonant 9.07 MeV state itself into the 2.79 MeV level. As noted in the previous section, the distribution measurement establishes the E2/M1 mixing ratio δ of this radiation as lying between 1.5 and 2.0, although the same transition, when considered in terms of the extreme single particle model, would be expected to have a mixing parameter of $\delta \cong 10^{-2}$ where the single particle transition probabilities of Moszkowski[74] have been used; $T_{sp}(M1) = 2.8 \times 10^{13} E^3$ and $T_{sp}(E2) = 1.6 \times 10^{8} (1+Z/A^2)\ A^{4/3} E^5\ sec^{-1}$. Reference to the compilations of previously determined E2 and M1 transition rates as given by Wilkinson[75] indicates that an appropriate combination of enhanced E2 and inhibited M1 transitions could easily give rise to the relative E2 enhancement factor of 10^{+2} observed above and that such a combination would not be "unphysical" on the basis of past measurements. On the other hand, the high density of states at 9 MeV would be expected to lead to very strongly mixed intrinsic and collective wave functions, hence no presently available model calculations would anticipate a priori such a large mixing ratio.

Work is presently in progress to reproduce and thus reconfirm this angular distribution measurement under a number of different experimental conditions. Pending the results of these investigations, a triple correlation study of the 9.07 to 2.79 to 0.197 MeV cascade is planned in hopes of obtaining further information concerning this interesting transition.

3. Model Interpretations* of the 3.91 MeV State:

The theoretical implications of the J = 3/2 assignment of the 3.91 MeV state in F^{19} must be considered from two different points of view depending upon whether the unknown parity of this state is positive or negative.

As indicated in Figure II-16, model calculations dealing with states of negative parity have been carried out only within the collective and the SU_3 frameworks. The low-lying negative parity states, for example, have been subjected to a detailed SU_3 treatment by Harvey[51], who has obtained excellent theoretical agreement with the experimental data. The SU_3 calculation, which attributes the low-lying negative parity states to promotion of a $p_{1/2}$ proton from the O^{16} core into the sd shell, lends credence to the corresponding rotational interpretation wherein a proton is promoted from Nilsson orbit 4 (see Fig. I-1) to fill orbit 6, thereby generating a $K^{\pi} = 1/2^-$ band head. The alternative of forming such a configuration through promotion of the odd proton from orbit 6 to 14 is not attractive because of the extreme deformation which would be required to bring down the energy of this configuration adequately.

A collective model calculation including the possibility of both positive and negative parity states has been examined by Rakavy[71]. This author shows that satisfactory fits to the experimental data may be obtained by considering three rotational bands $K=1/2^+$, $K= 1/2^-$, and $K=3/2^+$ with mixing between the positive parity band members. Reference to Figure II-16 indicates no $3/2^-$ states predicted by either of these models to lie near 3.9 MeV, except for possibly the SU_3 $3/2^-$ level at 4.85 MeV.

In contrast to the situation regarding negative parity states, a number of model calculations on the positive parity states of F^{19} have been carried out in detail, and it is evident from Figure II-16 that none of the shell model formulations presently available predict a 3/2 state in the energy region of 4 MeV. On the other hand, all of the collective calculations reproduce a 3/2 state of energy $\cong 4$ MeV. For example, Paul[45] achieved quite reasonable fits to the then available experimental data (and remarkably good predictions of data subsequently obtained including the assignments 9/2 and 3/2 presented above) by invoking strong Coriolis mixing of two rotational bands, $K^{\pi} = 1/2^+$ and $3/2^+$, corresponding within the framework of the Nilsson model to intrinsic configurations with the odd proton

*The author is particularly indebted to Professor D.A. Bromley for many helpful discussions concerning these model interpretations.

occupying 6 and 7, respectively. The Coriolis mixing required to achieve agreement is quite large; the J = 3/2 member of the $K = 1/2^+$ band is found, for example, to have 46% of intensity of K = 3/2 configuration. Newton, Clegg, and Salmon[76] have concluded that, on the basis of their studies on inelastic scattering of 150 MeV protons on F^{19}, the band mixing must be considerably less than this, attributing the strong mixing required in Paul's calculation to the fact that the Nilsson model predicts too close a level spacing, hence to high a mixing of the original configurations. In spite of the uncertainties in the collective model parameters, its general implications and predictions remain basically unchanged.

Because of the success of the collective calculation in reproducing a spin 3/2 state in the proper energy region, it is of interest to probe the validity of the model more deeply by investigating, qualitatively at least, the deexcitation behavior of the 3.91 MeV state in terms of the same collective picture. Since the asymptotic form of the model wave functions are most easily applied, the states of F^{19} shown in Figure II-15 have been labeled with the appropriate $[Nn_z\Lambda]$ quantum numbers corresponding to the same numbers which characterize the intrinsic Nilsson states of Figure I-1. As discussed above, the state at 3.91 MeV is to be considered either as the positive parity band head corresponding to promotion of a proton from orbit 6 to orbit 7, with quantum numbers $[2\ 1\ 1]$, or as the negative parity band head with $K^\pi = 3/2^-$ and $[1\ 0\ 1]$ corresponding to the promotion of a proton from orbit 4 into orbit 6 and the coupling of the resultant $p_{1/2}$ hole to a K=1 rather than K = 0 resultant of the two protons in the latter orbit. This type of $K = 3/2^-$ hole configuration is the one predicted by the SU_3 calculation[51] at approximately 4.85 MeV, significantly above the excitation of the state under discussion.

In terms of the Nilsson model the observed branching of the 3.91 MeV state is consistent with the positive parity assignment. The observed transitions, corresponding to $\Delta K = 1$, $\Delta N = 0$, $\Delta n_z = -1$, and $\Delta\Lambda = 1$, do not violate the asymptotic selection rules (listed in Table I-1) for either M1 or E2 multipoles; moreover, E1 transitions to members of the negative parity band, whose apparent absence is <u>a priori</u> somewhat puzzling, would correspond to $\Delta K = 1$, $\Delta n_z = 1$ and $\Delta\Lambda = 0$, violating the asymptotic selection rules $\Delta K=1$, $\Delta N = \pm 1$, $\Delta n_z = 0$,

and $\Delta\Lambda = 1$ on two separate counts.

On the assumption of negative parity and a $[1\ 0\ 1]$ configuration, it would be anticipated that relatively strong M1 transitions would be observed to the members of the $K = 1/2^-$ band in addition to those to the members of the $1/2^+$ band, contrary to the experimental observation.

Furthermore, on this assumption of negative parity, the observed transitions into the $K^\pi = 1/2^+$ rotational band would necessarily be E1 in character with $\Delta K \mp 0$, $\Delta N = -1$, $\Delta n_z = -2$, and $\Delta\Lambda = 1$ in violation of the Δn_z and $\Delta\Lambda$ asymptotic selection rules, so that E1 competition with the allowed M1 branches to the $K = 1/2^-$ band would be further inhibited. It should be noted that, within the assumptions of the SU_3 model, all E1 transition amplitudes vanish since the effective dipole operator is written[51] as $\vec{p} = Ze\vec{R}$ where Z is the atomic number, e the charge on the proton, and $\vec{R}$ the position vector for the center of mass of the proton distribution within the nucleus. To the extent that the center of mass of the proton distribution is in an S state, as is assumed in the SU_3 model for both positive and negative parity bands, $\vec{R} = 0$ and the E1 transition amplitudes vanish. Even if the restriction of a pure S state is relaxed, it follows that E1 transitions would be markedly inhibited as is indeed observed in the transition between the $K^\pi = 1/2^-$ and $1/2^+$ band heads in F^{19}.

The observed branching of the 3.91 MeV state is thus entirely consistent with a $3/2^+$ assignment wherein the forbidden E1 transitions do not compete with allowed M1 (or E2) transitions. On the other hand, within the Nilsson model the experimental data would be in qualitative disagreement with a $3/2^-$ assignment to the state, since this would require that the forbidden E1 transitions completely mask any competition from allowed M1 transitions.

The absence of a third branch from the 3.91 MeV state to the $5/2^+$ member of the $K = 1/2$ band is somewhat puzzling. Considering only the dipole component of the transition, and noting that the $b_{E\lambda}$ (or $b_{M\lambda}$) term vanishes for this particular case in the Nilsson expression for the reduced transition matrix elements[77], the B(M1) ratios for the transitions into the ground state band would be expected to be as follows; $3/2 \rightarrow 1/2$, $3/2 \rightarrow 3/2$, $3/2 \rightarrow 5/2$: 1, 0.8 , 0.2. Experimentally these ratios are found to be; 1, 1.25, < 0.1.

The apparent enhancement of the $3/2 \rightarrow 3/2$ transition over the predictions of this simple model may well reflect the admixture of these two states which is undoubtedly present if the 3.91 MeV state has positive parity. It should be noted in this connection that the $1/2^+$ ground state, on this basis, remains a pure configuration.

4. Model Interpretations of the 8.76 MeV State:

It follows necessarily, within any collective model, that the 8.76 MeV resonance state must be assigned K=1/2 since higher K-bands exclude this J value. Although a priori it would be anticipated that at this excitation wave functions would be extremely complex, reflecting widespread mixing of bands built on a number of single particle intrinsic states, the case of the $J=1/2^+$ member of a band is somewhat anomalous in that mixing is only possible with other J^π, $K^\pi = 1/2^\pm$, $1/2^+$ configurations. The anticipated low density of such configurations even at this excitation suggests that the configuration may be relatively pure, in which case the relevance of the asymptotic selection rules to the deexcitation of the 8.76 MeV state may be considered.

The experimental branching ratios shown in Figure II-15 include strong E1 transitions into the low-lying $K^\pi = 1/2^-$ band, apparently inhibited M1 transitions into the $K^\pi = 1/2^+$ band, and a transition (presumed M1) into the 3.91 MeV state.

Assuming the $\left[Nn_z\ \Lambda\right] K^\pi$ assignments of $\left[2\ 2\ 0\right]\ 1/2^+$, $\left[1\ 0\ 1\right]\ 1/2^-$, and $\left[2\ 1\ 1\right]\ 3/2^+$ noted previously for the positive and negative $K = 1/2$ band heads and the 3.91 MeV state, respectively, and considering the asymptotic selction rules of Table I-1 appropriate to the transitions above, it follows that an assignment of $\left[2\ 1\ 1\right]\ 1/2^+$ to the 849 keV resonance encompasses the observed branching. Moreover, an orbit with just these quantum numbers (orbit 9) is available in the appropriate energy region. If this identification is meaningful, the experimentally absent 8.76 MeV to ground state transition is the signature of the $\Delta K = \Delta N = \Delta n_z = \Delta\Lambda = 0$ selection rule for M1 transitions; likewise the 19% transition from the resonance to the 1.56 MeV state would be expected to show E2 enhancement. All other transitions observed are completely allowed as M1

or E2 radiations.

F. Conclusions and Summary

Angular distribution measurements of radiation from the 2.79 MeV state of F^{19} have corroborated the limitation of J= 7/2 or 9/2 placed on this state by other workers but cannot uniquely distinguish between these two possibilities. When coupled with recently obtained (p, p$'\gamma$) data, however, the distribution measurements allow only the angular momentum value of 9/2 for this state.

Studies on the O^{18} (p,γ) F^{19} reaction at the 849 keV resonance have established the angular momentum of the 3.91 MeV state in F^{19} as 3/2 and strongly suggest positive parity for the state.

Both shell and collective model calculations of F^{19} are able to predict the correct level ordering up to and including the now confirmed $9/2^+$, 2.79 MeV state. Furthermore, the collective calculations continue successfully up to the 3.91 MeV state now known to be 3/2, provided that this state has positive parity. The observed features of gamma deexcitation of the 3/2, 3.91 MeV state and the higher-lying resonance state studied here are also correlated in reasonable fashion by the electromagnetic selection rules of the strongly deformed, collective model. On the other hand, shell model calculations fail with regard to predictions of the 3/2 state at values of model parameters appropriate to the description of the lower excited states. Since the predicted excitation of a particular state is only slowly dependent on the model parameters in this energy region of interest, a major modification of, say the spin-orbit / central-strength ratio would be required to bring a predicted 3/2 state down into agreement with the known 3/2, 3.91 MeV state.

The success of the collective model in reproducing these newly established level parameters and branching ratios adds to be accumulating evidence for pronounced nuclear deformations, particularly for low T_z - nuclei, even at this low a mass number. The predictions of the self-consistent model calculations are, however, in complete accordance with this observed behavior. It perhaps should be noted with regard to this core deformation that very recent C^{12} + α

scattering experiments[78] provide data which have been interpreted as indicating pronounced distortion in the O^{16} nucleus at excitations at and above MeV. If such an interpretation concerning O^{16} proves correct, strong distortion of the F^{19} nucleus would certainly be anticipated.

Another indication of strong core deformation is found in the effective representation of the observed deexcitation branching ratios provided by the asymptotic quantum number selection rules. Equally successful predictions are not enjoyed by spherical or slightly deformed shell model calculations which favor E1 transitions over M1 or E2 transitions in all radiations of $\Delta L \leq 1$.

Clearly a number of further measurements concerning F^{19} would be of interest. A direct measurement of the parity of the 3/2 state at 3.91 MeV could confirm the interpretation of this state as the $K = 3/2^+$ band head. Unfortunately, determination of the linear polarization of radiation through this state from the 849 keV resonance would not yield the desired parity information because of the 1/2 character of the resonance[79]. Establishment of the properties of the remaining levels in F^{19} in the 4-5 MeV range, specifically those at 4.00, 4.04, 4.39, 4.58, and 4.76 MeV, would be important to provide still more data for stringent comparison with the numerous model-generated predictions in this energy region.

III. STUDIES OF THE LOW-LYING STATES OF O^{19}

A. Introduction

1. Theoretical:

Just as in the case of F^{19}, extensive theoretical calculations have been carried out on the O^{19} nuclear system. Elliott and Flowers[16] have applied their intermediate-coupled shell model calculations and have found that parameter choices appropriate to F^{19} were not successful in O^{19}. Talmi and Unna[21] calculated the energy level schemes of O^{17}, O^{18}, O^{19}, and O^{20} using only the $d_{5/2}$ and $s_{1/2}$ configurations with considerable success in O^{19}, although Inoue et al.[19] with their extension of the Elliott and Flowers calculation suggested that the agreement attained by Talmi and Unna may have been fortuitous.

Also like F^{19}, the O^{19} system has been approached from the collective model point of view. Armstrong and Quisenberry[80] have carried out a very detailed examination of the predictions of the Nilsson model in the O^{19} case. Assuming strong Coriolis mixing of the K=1/2, 3/2, and 5/2 bands corresponding to orbits 9, 7, and 5, respectively, these authors were able to obtain a reasonable description of the available data. In this treatment it was assumed that the 1.47 MeV level had a dominant Nilsson assignment $\left[N n_z \Lambda\right] K^{\pi}$ of $\left[2\,1\,1\right]\ 1/2^+$, the 0.096 MeV level an assignment of $\left[2\,1\,1\right]\ 3/2^+$, and the ground state an assignment of $\left[2\,0\,2\right]\ 5/2^+$. Rakavy[71] has reported an attempt to describe the level spectrum of O^{19} within the framework of a strongly-coupled rotational model. Chi and Davidson[40] have applied their model, including the possibility of asymmetric core deformations, to O^{19} and have found that the most acceptable fit to the first three levels occurs for axial symmetry in the model.

Intercomparisons and extensions of these theoretical calculations are made difficult because the experimental situation is far from clear at present. In view of the extensive theoretical interest in O^{19}, it is in fact somewhat surprising that so few data on this nucleus were available until quite recently. This in large measure reflected the relative inaccessibility of O^{19} to low energy reaction studies involving convenient targets.

2. Experimental:

With the availability within the last few years of isotopically pure O^{18}, several laboratories have reported studies on the $O^{18}(d,p)O^{19}$ and $O^{18}(d,p\gamma)O^{19}$ reactions. A brief survey of the results of these experiments follows.

Zimmerman[78] has carried out measurements on both protons and gamma radiations involving the ground and first two excited states at incident deuteron energies of 1.74 and 2.50 MeV. These measurements suggested the J^{π} assignments of $3/2^+$ or $5/2^+$ to the ground state and $1/2^+$ to the state at 1.47 MeV; experimental results for the state at 0.096 MeV in this reaction were not amenable to stripping analysis. Although quantitative data were not obtained, it was suggested that the deexcitation of the 1.47 MeV state proceeded almost entirely via the 0.096 MeV state whose mean life was measured to be 1.7×10^{-9} sec. Measurement of the internal conversion coefficient for the deexcitation of this state by Givens et al.[82] has established a dominant M1 character for the transition radiation, hence positive parity for the 0.096 MeV state.

Absolute and differential cross sections for proton groups to some twelve states in O^{19} were studied by Armstrong and Quisenberry[80], and by Yagi et al.[83] with 15 MeV deuterons, by Wickenberg et al.[84] with 7 MeV deuterons, and most recently by El Bedewi et al.[85] with 10 MeV deuterons. In none of these studies has the proton angular distribution to the 0.096 MeV state displayed stripping characteristics, although the results are not inconsistent with an angular momentum transfer $l_n = 2$, hence an assignment of $5/2^+$ or $3/2^+$ to this state.

Preliminary measurements on the gamma-gamma angular correlation involving cascade radiations from the 1.47 MeV, $1/2^+$ state have been reported by Rollefson et al.[87] as being consistent with a $1/2^+ \rightarrow 3/2^+ \rightarrow 5/2^+$ level sequence but inconsistent with $1/2^+ \rightarrow 5/2^+ \rightarrow 5/2^+$, $1/2^+ \rightarrow 3/2^+ \rightarrow 3/2^+$, or $1/2^+ \rightarrow 5/2^+ \rightarrow 3/2^+$. The recent suggestion of El Bedewi et al.[85], based on relative intensity considerations in their studies of the $O^{18}(d,p)O^{19}$ proton groups, that the O^{19} ground state is in fact $3/2^+$ is thus in conflict with these preliminary measurements on the angular correlation. A $3/2^+$

ground state assignment is also in conflict with the measurements of Alburger et al.[87] on the beta decay of O^{19}, which was found to be forbidden to the $1/2^+$ F^{19} ground state and thus indicated a $5/2^+$ ground state assignment.

Even the experimental data regarding the existence of levels in O^{19} have been remarkably contradictory considering that in almost all cases high resolution magnetic spectrometry has been involved. States at 1.257 and 3.791 MeV were reported and later withdrawn by the same investigators.[84] Quite recently evidence has been found[85] for nine new states at excitations below 5.6 MeV including one at 0.348 MeV, all of which are populated in the (d,p) reaction with 10 MeV deuterons.

The experimental measurements to be reported in this chapter were intended to provide a precise determination of the branching ratio of the 1.47 MeV deexcitation in order to test which, if any, of the various model wave functions provide a valid representation of dynamic characteristics of low-lying states in O^{19}; to investigate the deexcitation behavior of the newly reported 0.348 MeV state which would possibly be the lowest negative parity state appearing in this nucleus at a startlingly low energy; and to reexamine the $1.47 \rightarrow 0.096 \rightarrow 0$ MeV cascade angular correlation to further establish the relative ordering of the low-lying $3/2^+$ and $5/2^+$ states in view of the above mentioned uncertainties concerning this ordering.

B. Experimental Equipment

The target gas cell and angular correlation table assemblies used in the $O^{18}(d,p\gamma)O^{19}$ measurements have been described in Chapter II. Except where otherwise indicated, the target cell contained 12.5 cm of mercury absolute pressure of O^{18} gas and was bombarded with 2.2 MeV deuterons. Since the gamma radiations of interest were of relatively low energies, two 3 x 3 inch NaI(Tl) crystals were used. The integral crystal-photomultiplier units provided 7.5% and 8% energy resolution of the 661 keV Cs^{137} radiation.

For the branching ratio measurement of the 1.47 MeV state it was necessary to require a proton-gamma radiation coincidence in order to separate

radiations produced in the $O^{18}(d,p\gamma)O^{19}$ reaction from the more intense radiations of almost identical energy resulting from the $O^{18}(d,n\gamma)F^{19}$ reaction. For this purpose a second, somewhat larger gas target cell was . This cell consisted of a 3 cm diameter by 4 cm long cylindrical brass shell mounted with its axis perpendicular to the beam axis. The walls were internally lined with tantalum to reduce background radiation. The top of the chamber was removable and was fitted with vacuum-sealed, electrical feedthroughs which permitted a solid state particle detector to be mounted and operated directly in the target cell.

Reaction protons were detected in a small, gold surface barrier, silicon counter (ORTEC SBE007-300) at 90^{o} to the incident beam and 1 cm from the reaction site. The detector was collimated to intercept a solid angle of about 10^{-2} sr. Since the Q-value of the $O^{18}(d,p)O^{19*}$ (1.47 MeV) reaction is such as to give very similar energies for both protons and elastically scattered deuterons at 90^{o}, a 0.001 inch aluminum absorber was used to degrade the scattered deuterons to below the energy region of interest, thus avoiding unnecessary deuteron-gamma radiation accidental coincidences.

Gamma radiation was detected in one of the 3 x 3 inch NaI(Tl) crystals placed at -90^{o} to the beam direction with its front face 8 cm from the target center. It should be noted that, in consequence of the J=1/2 character of the 1.47 MeV state, all radiations from it are necessarily isotropic so that only a single angle measurement was required to determine the branching ratio.

C. Experimental Results

1. Investigations of the 0.348 MeV State:

Measurements of El Bedewi et al.[85] suggested that the 0.348 MeV state is populated with roughly the same intensity as that at 0.096 MeV in the $O^{18}(d,p)O^{19}$ reaction with 10 MeV deuterons. This state would necessarily deexcite to one or both of the 0.096 MeV and ground states; further, if the model considerations to be discussed in Section D1 are valid, dominant El deexcitation of the 0.348 MeV to the 0.096 MeV state would be expected. A search was therefore carried out for radiations of 0.252 MeV (and of 0.348 MeV) in the direct radiation spectrum

from the bombarded target. Figure III-1 shows the spectrum obtained. The 0.096 MeV transition from O^{19} and the 0.110 and 0.197 MeV transitions from F^{19} produced in the $O^{18}(d,n\gamma)F^{19}$ reaction are clearly evident. Also shown is a spectrum obtained under identical conditions with a Na^{22} source to establish a standard 0.511 MeV spectral shape in the experimental configuration used.

Comparison of the two spectra of Figure III-1 shows no evidence of a 0.348 MeV state deexcitation in O^{19}. If present, the transitions from this state are less that 5% of those involving the 0.096 MeV state.

The spectrum of low energy radiation from the O^{18} + d reaction in time coincidence with all radiation in the energy range 0.075 to 0.120 MeV was examined in an effort at revealing the 0.348 → 0.096 → 0 MeV cascade. This spectrum is presented in Figure III-2. No evidence for a cascade deexcitation from the 350 keV energy region was found. From the data of Zimmerman[81] on the relative populations of the 1.47 and 0.096 MeV states at bombarding energies of 2.5 MeV and from the branching ratio measurement of the 1.47 MeV state reported below, it may be concluded that the cascade branch of the 0.348 MeV deexcitation cannot be more than 0.5% of the 1.47 MeV cascade intensity.

Careful examination of data available on the $F^{19}(t,\alpha)O^{18}$ reaction as measured by Hinds and Middleton[88] and of data available on the $O^{17}(d,p)O^{18}$ reaction as measured by Yagi et al.[83] strongly suggests that the state observed previously at an apparent excitation of 0.348 MeV in O^{19} is, in fact, spurious and that the proton group involved corresponds to the 4.45 MeV state in O^{18} populated via an $l_n = 1$ neutron capture. If this hypothesis is correct, it would imply that others of the new levels in O^{19} reported by these authors[85] might also be incorrectly identified with proton groups from the $O^{17}(d,p)O^{18}$ contaminant reaction.

2. 1.47 → 0.096 → 0 MeV Angular Correlation:

In examining the angular correlation in the cascade deexcitation of the 1.47 MeV level, advantage was taken once again of the $1/2^+$ nature of the cascading state and the resultant dependence of the correlation only on the angle included between the axes of the detectors. The 3 x 3 inch NaI(Tl) crystals

Figure III-1. O^{18} + d direct gamma radiation in the energy region 0 to 500 keV obtained with a 3 x 3 inch NaI(Tl) crystal at 90^{o} to the beam axis. A standard 511 keV spectrum taken with a Na^{22} source is shown for comparison. The indicated X-radiation peaks reflect the presence of the tantalum liner in the target chamber and the lead shielding enclosing the crystal.

Figure III-2. O^{18} + d gamma radiation spectrum observed in time coincidence with radiation in the energy range 0.075 to 0.120 MeV. The radiations at 0.272 and 0.295 MeV correspond to transitions in N^{16} from the $O^{18}(d, \alpha) N^{16}$ reaction, the radiation at 0.197 MeV corresponds to a transition in F^{19}, and those at 1.37 and 0.096 MeV correspond to transitions in O^{19}. The yield of 0.096 MeV radiation reflects the presence of "tails" of the 1.37 MeV radiation falling within the coincidence gate.

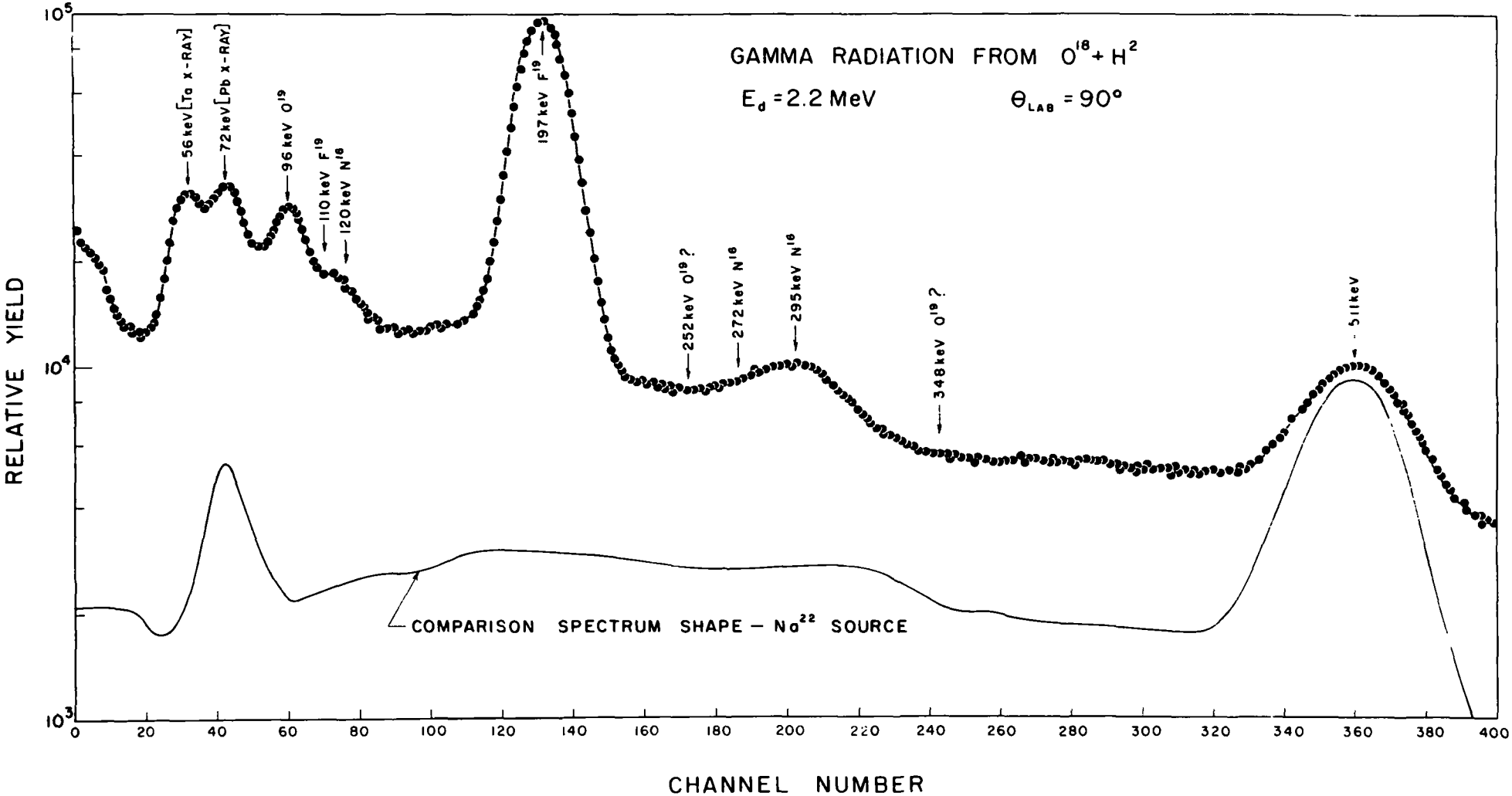
GAMMA RADIATION FROM $O^{18}+H^2$
$E_d = 2.2$ MeV
$\theta_{LAB} = 90°$
56 keV [Ta X-RAY]
72 keV [Pb X-RAY]
96 keV O^{19}
110 keV F^{19}
120 keV N^{16}
197 keV F^{19}
252 keV O^{19} ?
272 keV N^{16}
295 keV N^{16}
348 keV O^{19} ?
511 keV
COMPARISON SPECTRUM SHAPE – Na^{22} SOURCE
RELATIVE YIELD
10^5
10^4
10^3
0
20
40
60
80
100
120
140
160
180
200
220
240
260
280
300
320
340
360
380
400
CHANNEL NUMBER

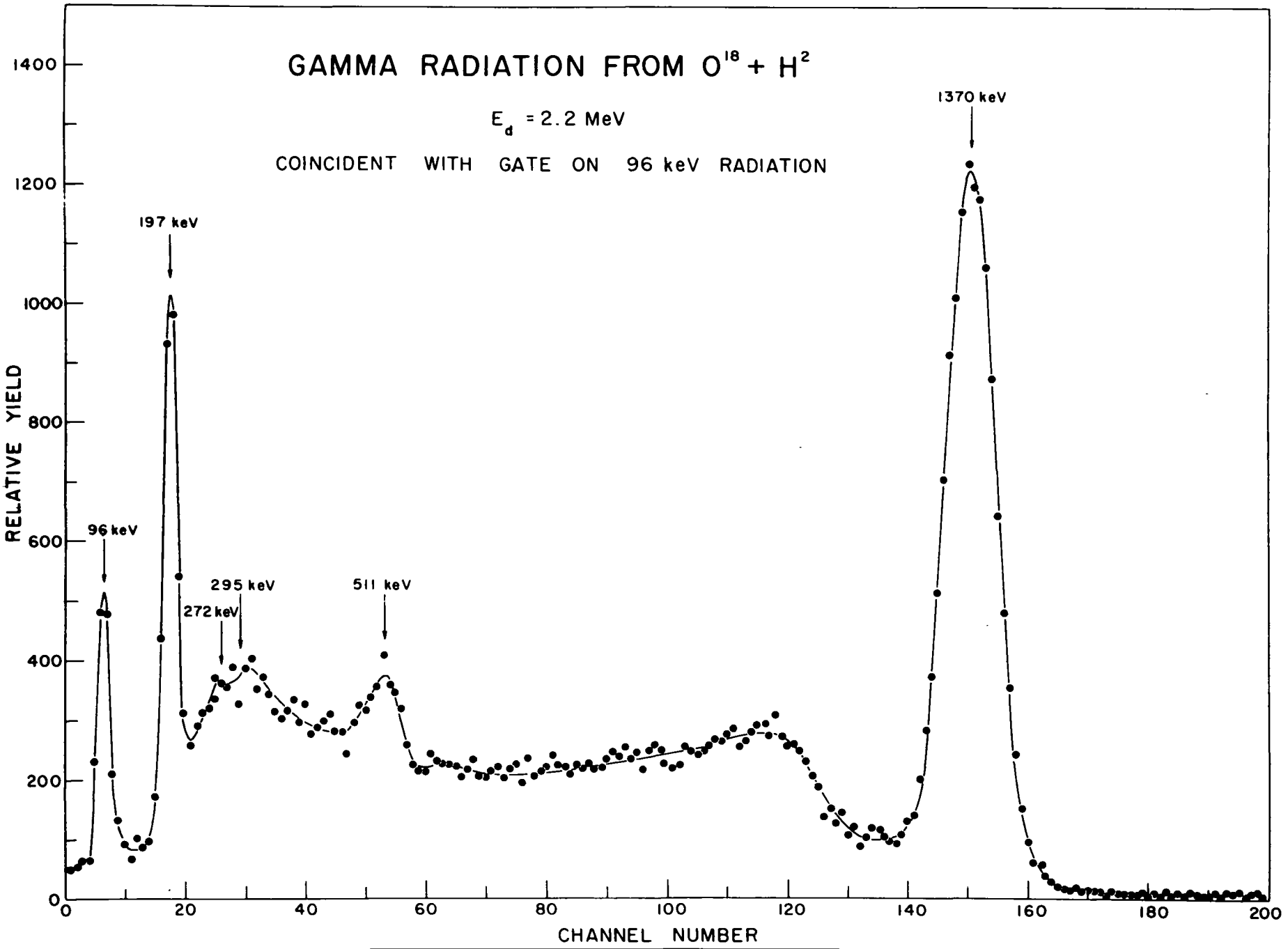
GAMMA RADIATION FROM $O^{18} + H^2$
E_d = 2.2 MeV
COINCIDENT WITH GATE ON 96 keV RADIATION
1370 keV
197 keV
96 keV
295 keV
272 keV
511 keV
RELATIVE YIELD
CHANNEL NUMBER
0
200
400
600
800
1000
1200
1400
0
20
40
60
80
100
120
140
160
180
200

were mounted on the correlation table with their front faces 12 cm from the center of the reaction volume. While the instrumental resolution of the crystals was not adequate to resolve the 1.37 MeV cascade transition from the dominant 1.35 MeV radiation of the competing $O^{18}(d,n)F^{19}$ reaction, it was possible to separate the 0.096 MeV radiation of O^{19} from that at 0.110 MeV from F^{19}. Because of the marked absorption of the 0.096 MeV radiation in material of medium - to - high atomic number, this radiation was detected at a fixed angle of 90^{o} to the beam while the 1.37 MeV radiation was detected in the moving crystal, thus eliminating any uncertainties which slight non-uniformities in chamber walls or linings might have introduced. The fast-slow coincidence circuit, adjusted for 40 nsec resolving time, imposed the gamma-gamma coincidence condition.

It was not possible to align the axis of the correlation table by observing directly the isotropic 1.37 MeV deexcitation radiation of the $1/2^{+}$ O^{19} state because of the intense, anisotropic, 1.35 MeV radiation originating from the 1.46 and 1.56 MeV states of F^{19}. In order to avoid this problem and to establish with certainty the centering of the correlation table about the reaction site, the O^{18} target gas was replaced temporarily with pure Ne^{20} gas at the same absolute pressure, and the angular distribution of the 2.80 MeV radiation from the known $1/2^{+}$ state in Ne^{21} was examined. Under the alignment condition used in this measurement, the Ne^{21} radiation showed an angular distribution isotropic to within 0.5%; the axis of the aligned correlation table was found to correspond to the geometrical center of the target chamber to within 0.7 mm.

Figure III-3 shows one of a series of gamma radiation spectra in coincidence with the 1.37 MeV radiation from O^{19}. Each spectrum was corrected for the presence of the isotropic $1/2^{-} \rightarrow 1/2^{+}$, 0.110 MeV radiation from the $O^{18}(d,n)F^{19}$ reaction and was then analyzed to determine the 0.096 MeV radiation intensity.

The correlation data thus obtained is shown in Figure III-4. A least-squares fit of this data to the standard Legendre polynomial expansion

$$W(\theta) = 1 + \frac{A_2}{A_0} P_2(\cos\theta) + \frac{A_4}{A_0} P_4(\cos\theta) \qquad \text{(III-1)}$$

Figure III-3. O^{18} + d gamma radiation in time coincidence with radiation in the energy region of 1.37 MeV. The 0.096 MeV transitions originate in O^{19}, the 0.110 MeV transitions originate in F^{19}. X-radiations from tantalum and lead in the vicinity of the crystals are also evident.

Figure III-4. Angular correlation of the 1.47→0.096→0 MeV cascade deexcitation in the O^{18} (d, p $\gamma_1 \gamma_2$) O^{19} reaction. The solid curve is the result of a least squares fit to the data of the polynomial expansion of Equation III-1.

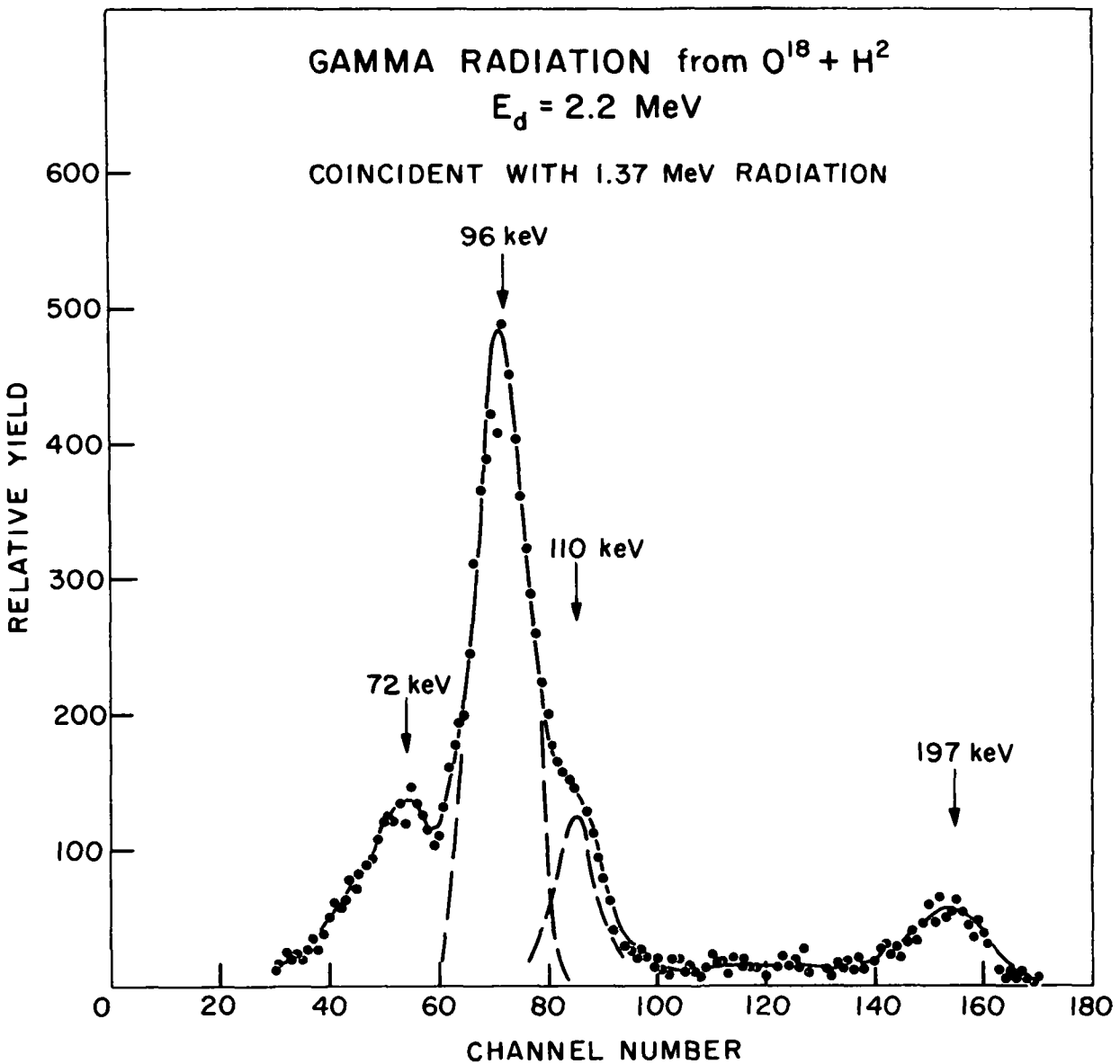
GAMMA RADIATION from $O^{18} + H^2$
E_d = 2.2 MeV
COINCIDENT WITH 1.37 MeV RADIATION
96 keV
110 keV
72 keV
197 keV
RELATIVE YIELD
CHANNEL NUMBER
600
500
400
300
200
100
0
20
40
60
80
100
120
140
160
180

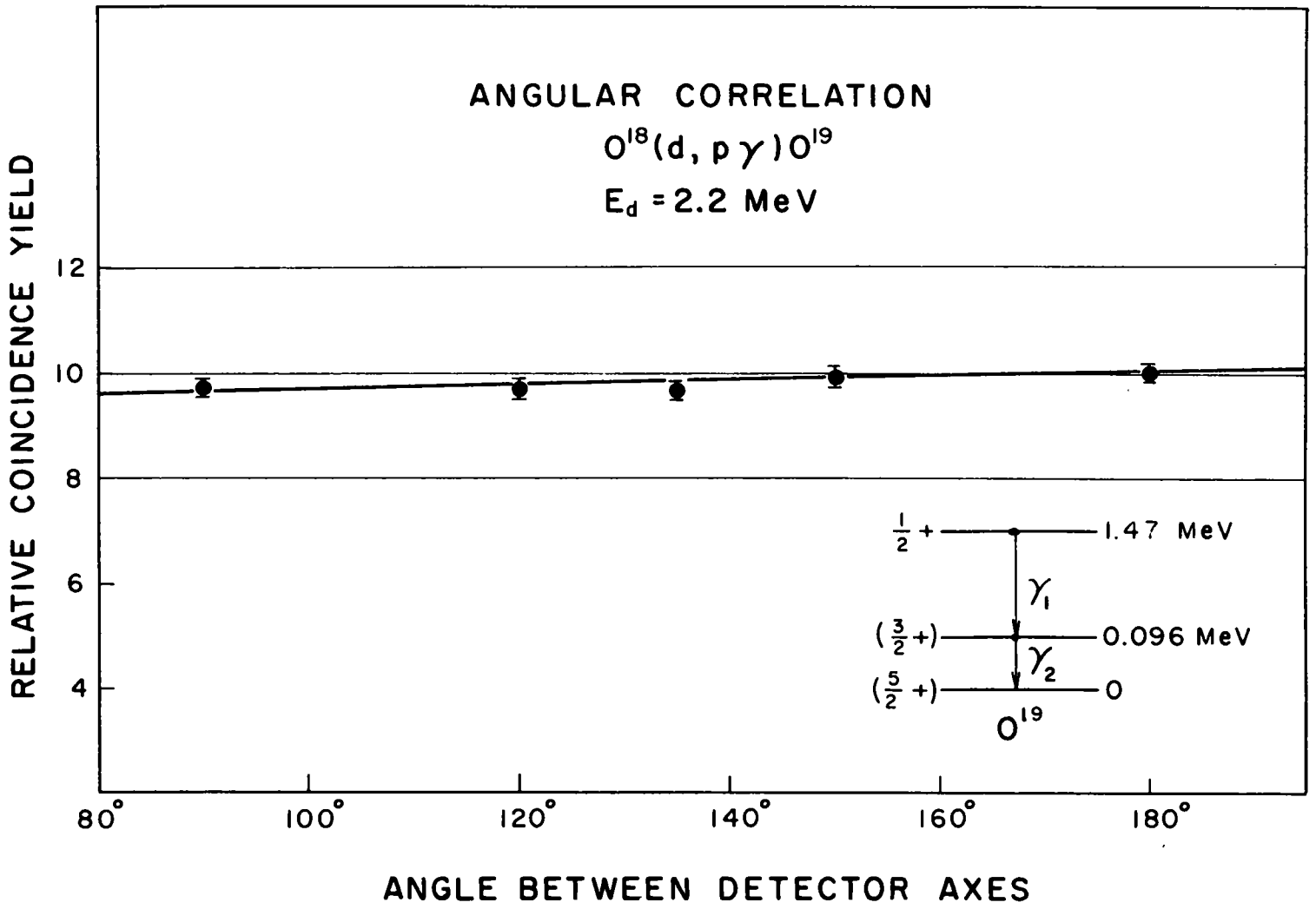
ANGULAR CORRELATION
$O^{18}(d, p\gamma)O^{19}$
E_d = 2.2 MeV
RELATIVE COINCIDENCE YIELD
12
10
8
6
4
80°
100°
120°
140°
160°
180°
ANGLE BETWEEN DETECTOR AXES
$\frac{1}{2}$+
1.47 MeV
γ_1
$(\frac{3}{2}+)$
0.096 MeV
γ_2
$(\frac{5}{2}+)$
0
O^{19}

resulted in the coefficient ratios $A_2/A_0 = 0.029 \pm 0.020$ and $A_4/A_0 \cong 0$ where finite solid angle corrections[64] have been applied.

To demonstrate that this angular correlation was not being affected by a rapidly varying $O^{18}(d,p\gamma\gamma)O^{19}$ excitation function, and thus a possible shifting of the effective target center, the measurements were repeated at an absolute target pressure of 6.2 cm of mercury. Identical results were obtained within experimental accuracy.

3. Deexcitation Branching Ratio of the 1.47 MeV State:

The gamma radiation spectrum in time coincidence with proton groups corresponding to the 1.47 MeV state in O^{19} is shown in Figure III-5. Since the individual detector counting rates were large in this measurement, Figure III-5 also includes the spectrum of accidental coincidences obtained by inserting a fixed 0.4 μsec delay in the fast proton channel.

The system resolution was inadequate to separate 1.47 and 1.37 MeV radiations from the direct and cascade deexcitations of the 1.47 MeV state. For this reason it was convenient to utilize a Gaussian fitting program[89] to obtain an objective measure of the relative intensities. The fitting program used here permitted inclusion of a smooth background (random coincidences) and a Gaussian representation of the Compton distribution in the region of the photopeaks in addition to the two Gaussians representing the photopeaks themselves. The Gaussian widths were fixed a priori from the measured characteristics of the spectrometer, so that the four parameters searched over during the fit were the two peak locations and the two peak areas. The "correct" peak locations were also known from the energy calibration of the spectrometer and were used as a consistency check on the peak locations provided by the computer fit. The resultant fitted curve is that superposed on the data points of Figure III-5; the dashed curves show the individual components.

It was necessary to correct the apparent intensity of the 1.47 MeV radiation for accidental summing of the two cascade radiations. Absolute 3 x 3 inch spectrometer efficiencies of Vegors et al.[63], together with the $1/2 \rightarrow 3/2 \rightarrow 5/2$ angular correlation function[69], assuming dominant dipole

Figure III-5. O^{18} + d gamma radiation observed at $\theta = 270^{o}$ in time coincidence with the proton group populating the O^{19} state at 1.47 MeV. The solid curve (A) indicates the background spectrum of random coincidences, curve (B) shows the theoretical least squares fit to the data points, dashed curves (C) and (D) indicate the two Gaussian components at 1.37 and 1.47 MeV which comprise curve (B).

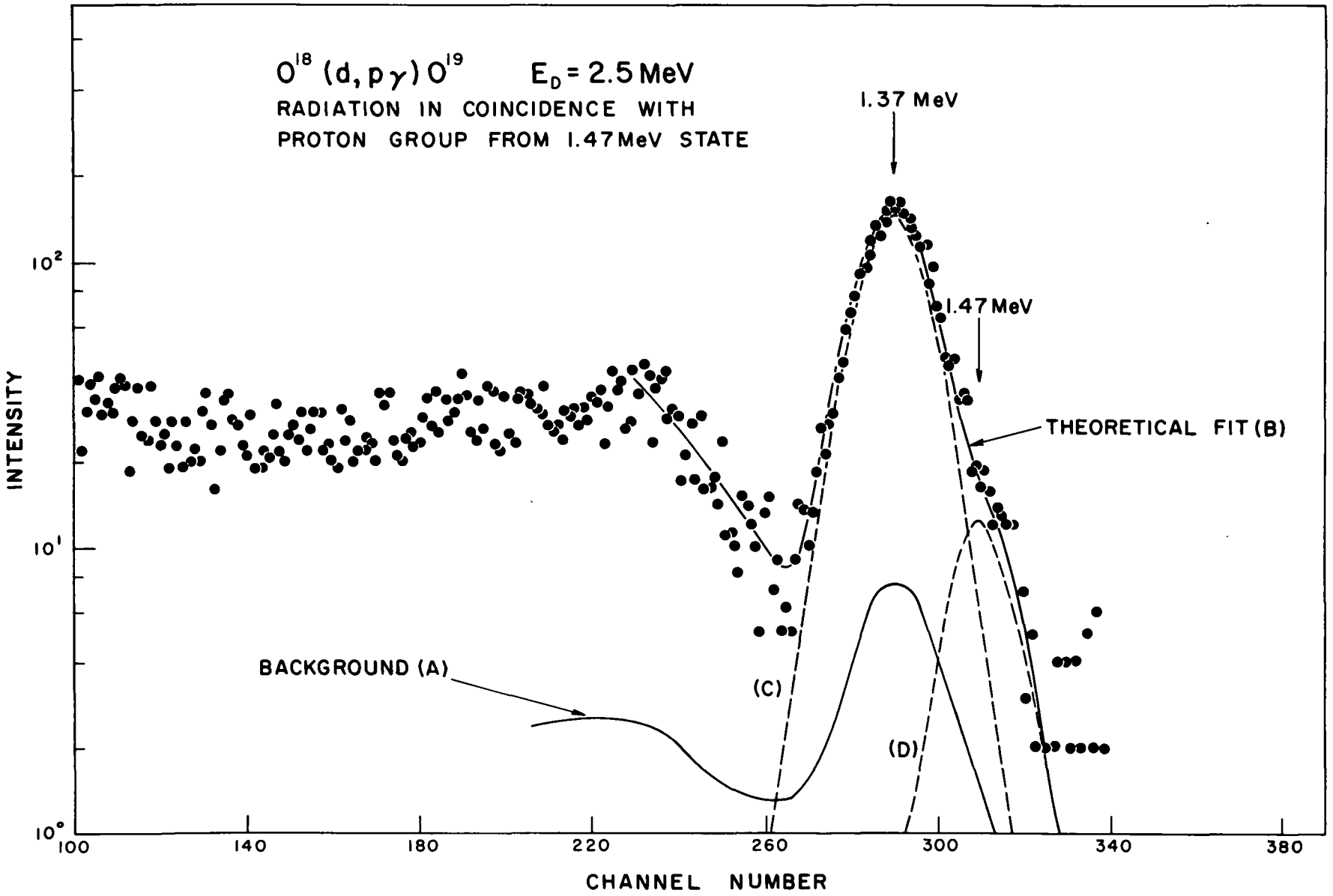
$O^{18}(d,p\gamma)O^{19}$ $E_D = 2.5$ MeV
RADIATION IN COINCIDENCE WITH
PROTON GROUP FROM 1.47 MeV STATE
1.37 MeV
1.47 MeV
THEORETICAL FIT (B)
BACKGROUND (A)
(C)
(D)
INTENSITY
10^2
10^1
10^0
100
140
180
220
260
300
340
380
CHANNEL NUMBER

transitions for both cascade steps (and correcting this function for the finite solid angle of the detector), were used to calculate this summing correction of 4.2% of the total cascading radiation. The summing correction was checked experimentally by examining known, radioactive, coincidence sources including Co^{60} and Na^{22}; in these cases the experimental and calculated summation corrections were found to agree to within 15%.

The resulting corrected branching ratio for the 1.47 MeV state is found to be $3.3 \pm 1.6\%$ for the crossover and $96.7 \pm 1.6\%$ for the cascade deexcitation. The quoted uncertainty reflects primarily the standard deviation of the computer-derived 1.47 MeV photopeak area.

D. Interpretation and Discussion of Experimental Results:

1. Orientation:

Figure III-6 presents a comparative compilation of the theoretical energy level schemes of O^{19} as indicated by (B) the intermediate-coupled shell model calculations of Elliott and Flowers[16], (C) the j-j coupled shell model calculations of Talmi and Unna[21] and (D) of Shah[90], (E) the rotor model calculation of Chi and Davidson[40], and (F) the strongly-coupled rotational band calculation of Armstrong and Quisenberry[81]. The experimental level scheme (A) is shown on each side of the figure and includes level parameters established in this work.

2. Implications of a 0.348 MeV State in O^{19}:

Specific model calculations applied to the O^{19} system have to date dealt only with positive parity states. Examination of Figure III-6, which includes all currently available calculations pertaining to O^{19}, indicates that on the basis of any one model only three positive parity states are predicted to exist below 1.7 MeV in excitation. Within each model, the three low-lying states are tentatively identified with the experimentally observed levels at 1.47, 0.096, and 0 MeV. It is therefore reasonable to make a preliminary assignment of negative parity to any newly observed state below 1.5 MeV entirely on the strength of the existing model predictions and the fact that the existing positive parity states are

Figure III-6. Comparison of (A) the experimentally observed energy spectrum of O^{19} with the model - generated energy spectra of (B) Elliott and Flowers, (C) Talmi and Unna, (D) Shah, (E) Chi and Davidson, and (F) Armstrong and Quisenberry.

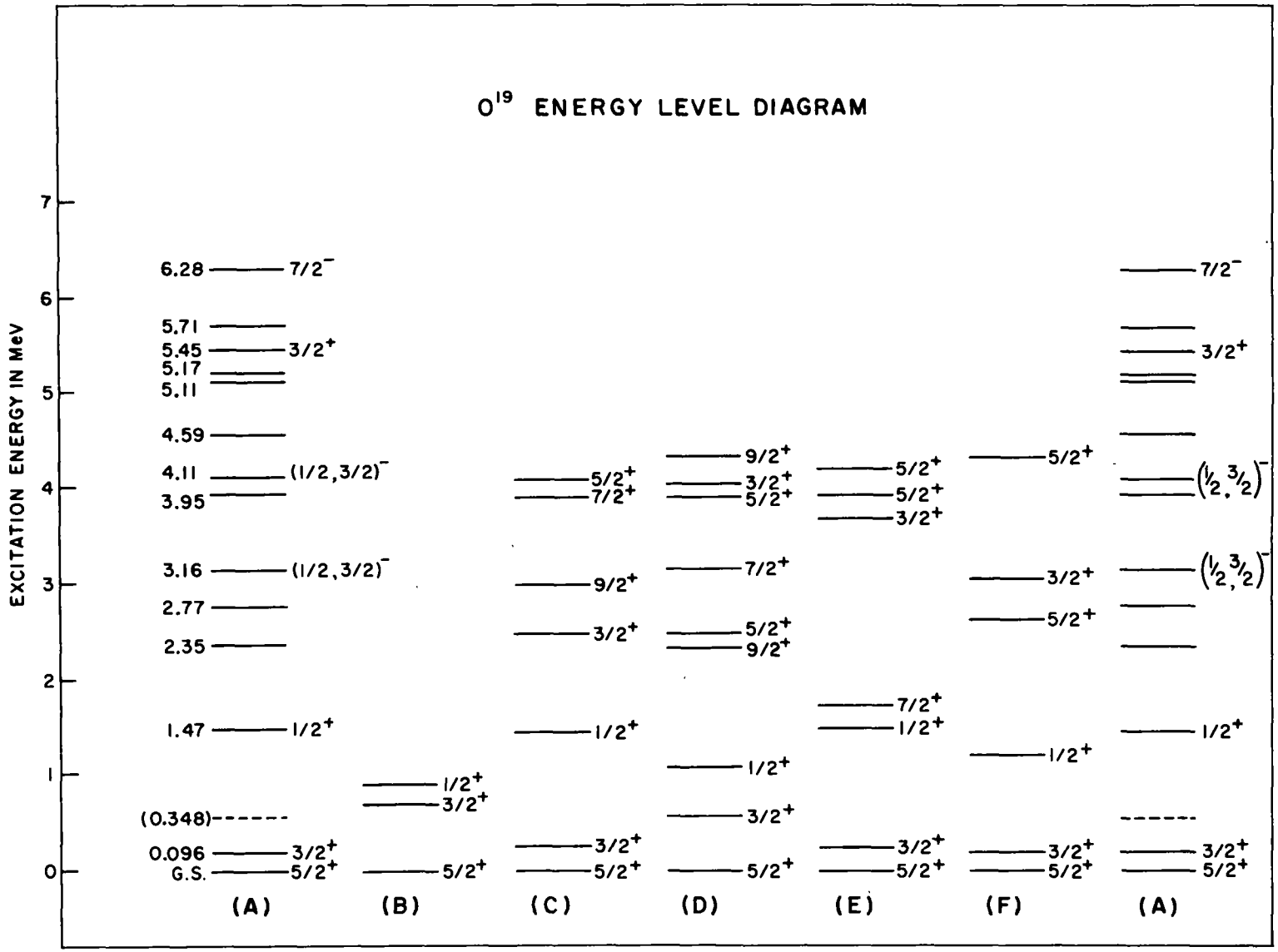
O19 ENERGY LEVEL DIAGRAM
EXCITATION ENERGY IN MeV
7
6
5
4
3
2
1
0
6.28
7/2−
5.71
5.45
3/2+
5.17
5.11
4.59
4.11
(1/2,3/2)−
3.95
3.16
(1/2,3/2)−
2.77
2.35
1.47
1/2+
(0.348)
0.096
3/2+
G.S.
5/2+
(A)
1/2+
3/2+
5/2+
(B)
5/2+
7/2+
9/2+
3/2+
1/2+
3/2+
5/2+
(C)
9/2+
3/2+
5/2+
7/2+
5/2+
9/2+
1/2+
3/2+
5/2+
(D)
5/2+
5/2+
3/2+
7/2+
1/2+
3/2+
5/2+
(E)
5/2+
3/2+
5/2+
1/2+
3/2+
5/2+
(F)
7/2−
3/2+
(1/2, 3/2)−
(1/2, 3/2)−
1/2+
3/2+
5/2+
(A)

accounted for within the framework of a number of these models.

It follows that the reported state at 0.348 MeV has most probably negative parity. However, this tentative parity assignment is only slightly less puzzling than that of positive parity for the following reason. A survey[1] of the neighboring nuclei shows that the lowest experimentally identified negative parity states occur at 3.06 MeV in O^{17} ($1/2^-$), 3.10 MeV in F^{17} ($1/2^-$), 4.45 MeV in O^{18} (3^-), and somewhere above 3.8 MeV in F^{18}. Arguing from systematics alone, it would be surprising to find the lowest-lying negative parity state below, say conservatively, 2 MeV in O^{19}; 0.348 MeV is astonishingly low.

It should be noted that F^{19} is not an exception to the systematic energy trend cited above. The presence of two protons and two neutrons outside the O^{16} core provides a unique opportunity to form very highly symmetric, thus tightly bound, negative parity configurations. The relatively low excitation of the $1/2^-$ state in F^{19} can in fact be quantitatively predicted[51] from considerations of the large residual interactions acting between symmetric pairs in the four nucleon, sd configurations.

There exists of course the possibility that two or even three particles may be excited from the p shell into the sd shell, if the situation is such that a particularly stable extra-core configuration may be formed to make up for the pairing energy lost by the particles in leaving the closed core. In fact, the shell model calculations already applied to this mass region would be of questionable validity if the possibility of numerous other particle configurations of like parity and comparable energies had been unrealistically neglected; there is, however, no previous evidence for multiple excitations in this mass and energy region. It is therefore gratifying to note that the measurements reported herein make highly speculative all evidence for the existence of a state which would be somewhat disturbing from a theoretical point of view.

3. Angular Momenta of the 0.096 MeV and Ground States:

In view of the renewed uncertainty concerning the assignments to the two lowest states in O^{19}, it has been necessary to consider possible cascade correlations from the known $1/2^+$, second excited state at 1.47 MeV of the following

forms; (a) $1/2 \rightarrow 3/2 \rightarrow 5/2$, (b) $1/2 \rightarrow 5/2 \rightarrow 3/2$, (c) $1/2 \rightarrow 3/2 \rightarrow 3/2$, and (d) $1/2 \rightarrow 5/2 \rightarrow 5/2$, since the stripping data already referred to suggested that the lowest two states were populated via $l_n = 2$ neutron capture with lesser possibility of an $l_n = 1$ capture to the 0.096 MeV state.

The internal conversion studies of Givens et al.[82] preclude the $l_n = 1$ capture on parity grounds and in addition establish limits on the multipole amplitude ratio in the $0.096 \rightarrow 0$ MeV transition. From the measured k-shell internal conversion coefficient for this transition, $\alpha_k = 6.27\ (1 \pm 0.18) \times 10^{-4}$ and from the theoretically expected values of this coefficient for M1 and E2 transitions[92], $\alpha_k(M1) = 6.99 \pm 0.70 \times 10^{-4}$ and $\alpha_k(E2) = 2.83 \pm 0.28 \times 10^{-2}$, respectively. The usual amplitude ratio δ may be computed from the expression

$$\alpha_k = \left[\alpha_k(M1) + \delta^2 \alpha_k(E2)\right] \left[1 + \delta^2\right]^{-1}. \qquad \text{(III-2)}$$

Since δ is necessarily real, assuming time reveral invariance holds, substitution of the experimental and theoretical coefficients just listed into this expression requires that $|\delta| \leq 0.07$.

This conclusion is in accord with the mean life of $1.75\ (1 \pm 0.16) \times 10^{-9}$ seconds which Zimmerman[81] has reported for the 0.096 MeV level.

Correlation functions for the four possible assignment sequences listed above were calculated[69] using this maximum value of δ for the lower cascade member to establish single parameter plots in terms of ρ, the mixing in the upper member for cases (a) and (c) where multipole mixtures would be anticipated in both cascade members; in cases (b) and (d) where no mixing is anticipated in the assumed pure E2 upper radiation, the correlation plots are given in terms of δ as defined above and the corresponding limitations on the correlation coefficients may be obtained directly from them.

Figures III-7a, b, c, and d present these plots on standard inverse tangent grids. The experimental value of A_2/A_0 lies between the dashed horizontal lines; the experimental value of A_4/A_0 is not shown but lies within 0 ± 0.05 and therefore would form a band of appropriate width on either side of the center axis. Although the parameter δ is allowed to vary in plots b and d from

Figure III-7a. $1/2 \rightarrow 3/2 \rightarrow 5/2$ angular correlation coefficient ratios as a function of the E2-M1 mixing parameter ρ for particular values of the E2-M1 mixing parameter δ. The horizontal band indicates the region allowed by the correlation measurement; the dashed vertical lines enclose the values of ρ compatible with this allowed region.

Figure III-7b. $1/2 \rightarrow 5/2 \rightarrow 3/2$ angular correlation coefficient ratios as a function of the E2-M1 mixing parameter δ. The shaded area indicates the region of the $(A_2/A_0, \delta)$ - plane allowed by both the correlation measurement and the previously reported internal conversion measurement.

Figure III-7c. $1/2 \rightarrow 3/2 \rightarrow 3/2$ angular correlation coefficient ratios as a function of the E2-M1 mixing parameter ρ for particular values of the E2-M1 mixing parameter δ. The horizontal band indicates the region allowed by the correlation measurement; the dashed vertical lines enclose the values of ρ compatible with this allowed region.

Figure III-7d. $1/2 \rightarrow 5/2 \rightarrow 5/2$ angular correlation coefficient ratios as a function of the E2-M1 mixing parameter δ. The shaded area indicates the region of the $(A_2/A_0, \delta)$ - plane allowed by both the correlation measurement and the previously reported internal conversion measurement.

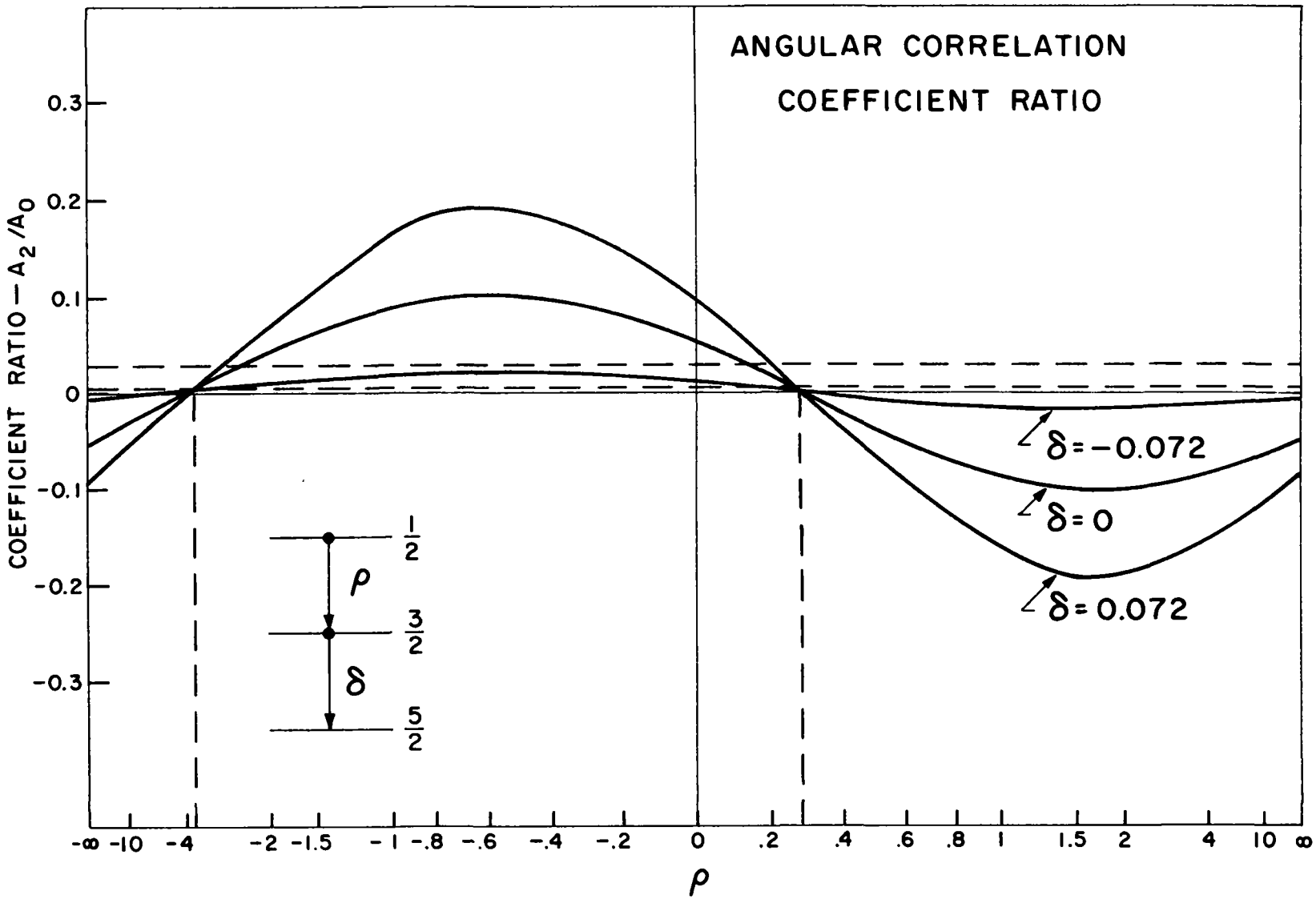
ANGULAR CORRELATION
COEFFICIENT RATIO
COEFFICIENT RATIO — A_2/A_0
0.3
0.2
0.1
0
-0.1
-0.2
-0.3
$\delta = -0.072$
$\delta = 0$
$\delta = 0.072$
$\frac{1}{2}$
ρ
$\frac{3}{2}$
δ
$\frac{5}{2}$
$-\infty$ -10 -4 -2 -1.5 -1 -.8 -.6 -.4 -.2 0 .2 .4 .6 .8 1 1.5 2 4 10 ∞
ρ

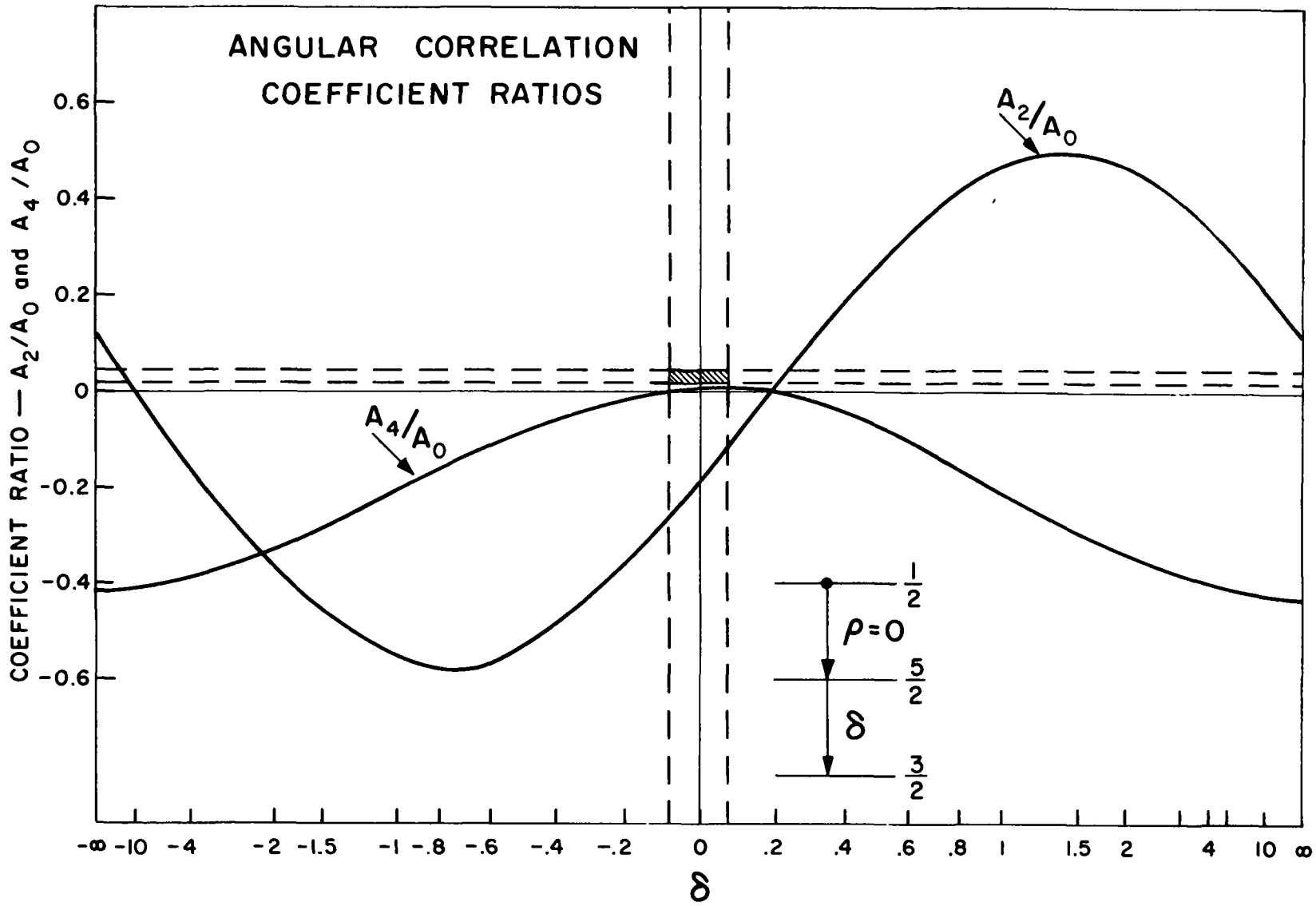
ANGULAR CORRELATION
COEFFICIENT RATIOS
COEFFICIENT RATIO — A_2/A_0 and A_4/A_0
A_2/A_0
A_4/A_0
0.6
0.4
0.2
0
-0.2
-0.4
-0.6
$\rho=0$
$\frac{1}{2}$
$\frac{5}{2}$
δ
$\frac{3}{2}$
-∞ -10 -4 -2 -1.5 -1 -.8 -.6 -.4 -.2 0 .2 .4 .6 .8 1 1.5 2 4 10 ∞
δ

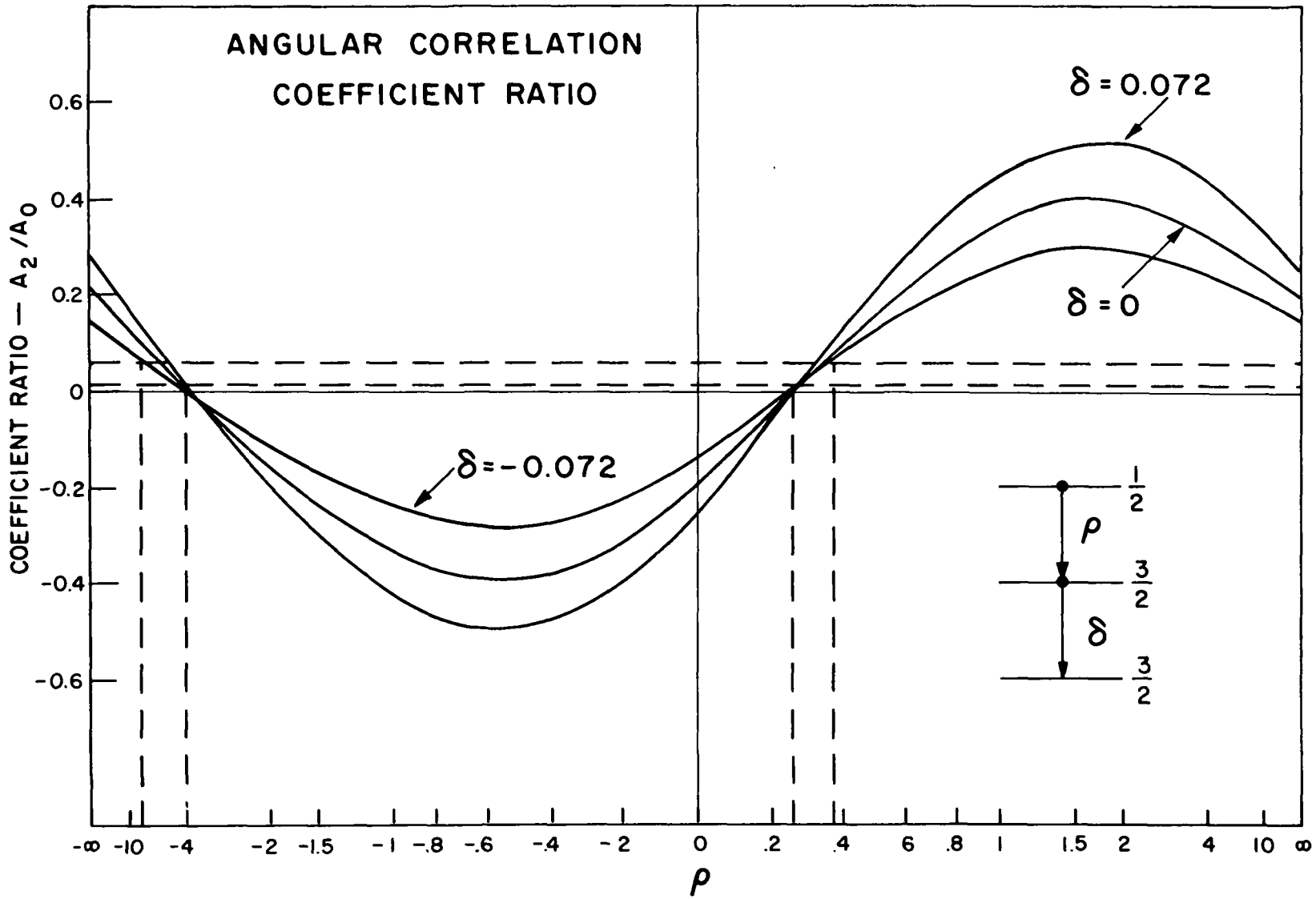
ANGULAR CORRELATION
COEFFICIENT RATIO
δ = 0.072
δ = 0
δ = -0.072
COEFFICIENT RATIO — A_2/A_0
0.6
0.4
0.2
0
-0.2
-0.4
-0.6
-∞ -10 -4 -2 -1.5 -1 -.8 -.6 -.4 -2 0 .2 .4 .6 .8 1 1.5 2 4 10 ∞
ρ
1/2
ρ
3/2
δ
3/2

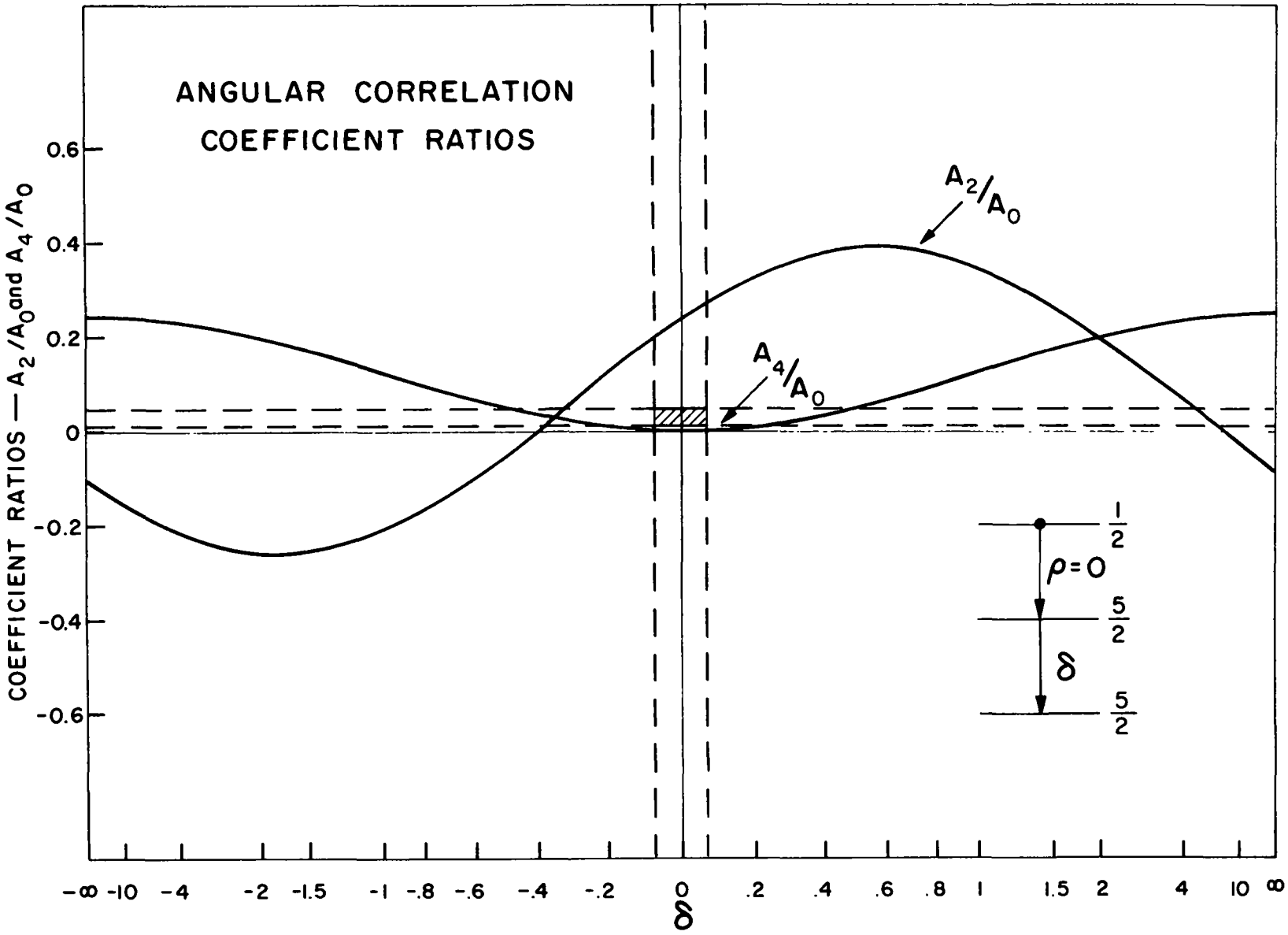
ANGULAR CORRELATION
COEFFICIENT RATIOS
COEFFICIENT RATIOS — A_2/A_0 and A_4/A_0
0.6
0.4
0.2
0
-0.2
-0.4
-0.6
A_2/A_0
A_4/A_0
$\frac{1}{2}$
$\rho=0$
$\frac{5}{2}$
δ
$\frac{5}{2}$
$-\infty$ -10 -4 -2 -1.5 -1 -.8 -.6 -.4 -.2 0 .2 .4 .6 .8 1 1.5 2 4 10 ∞
δ

∞ to $-\infty$, δ is limited experimentally (internal conversion measurement) to between ± 0.07 as indicated by the dashed vertical lines. Thus the shaded regions in plots b and d enclose the only areas in the $(A_2/A_0, \delta)$-plane permitted by experiment. Since the curves in neither spin sequence pass through the allowed area, both sequence possibilities are ruled out and a 5/2 assignment to the 0.096 MeV state is completely excluded.

Reference to Figure III-7a shows that the experimentally established A_2/A_0 ratio is entirely in accord with assignments of 3/2 and 5/2 to the 0.096 MeV and ground states, respectively, with any value between -4.0 and 0.3 (dashed vertical lines) of the multipole amplitude ratio ρ for the upper 1.37 MeV cascade transition provided there is sufficient mixing in the 0.096 MeV transition. This is in accord with the qualitative reports available on the measurements of Rollefson et al.[86]. Contrary to the result reported by these authors, however, the present data, and indeed theirs, cannot a priori exclude the possibility that both the 0.096 MeV and ground states have angular momenta of 3/2. This is indicated in Figure III-7c which shows that for $|\delta| \leq 0.07$ for the 0.096 MeV ground state transition as discussed above, the experimental correlation ratios would be in accord with a 1/2, 3/2, 3/2 spin sequence if the multipole ratio ρ of the upper 1.37 MeV transition were in either of the ranges $-10 < \rho < -4$ or $0.25 < \rho < 0.38$.

Considerable experimental evidence may be adduced, however, to support the 1/2, 3/2, 5/2 assignments and to argue against a 3/2 assignment to the O^{19} ground state. Three of these arguments now follow.

(1) The measurements of Alburger et al.[87] of the beta decay of O^{19} have already been mentioned. The experimentally determined lower limit of 6.5 on the log ft value for the decay branch, if present, to the F^{19} ground state indicates that this decay is at least first forbidden (mean log ft ~ 7) and, since there is no change of parity in the transition, suggests $\Delta J \geq 2$. These data have been taken as establishing the $5/2^+$ assignment to the O^{19} ground state; but it must be borne in mind that such an assignment is at the mercy of an accidental cancellation in the transition matrix elements. The assignment is further jeopardized by the experimental difficulty unavoidably encountered in measuring a weak O^{19} ground state to F^{19} ground state beta branch which is strongly masked by the intense branches to

higher-lying F^{19} states.

(2) The measured branching ratio for the 1.47 MeV state, as reported herein and discussed quantitatively in Section D4, provides additional evidence favoring the 5/2 assignment to the ground state. The correlation results noted above, combined with the measured internal conversion coefficient from the 0.096 MeV state, establish unambiguously a $3/2^+$ assignment for this state. If the ground state were also $3/2^+$, it follows that extensive mixing of the two state wave functions would be present reflecting the small energy denominator appearing in the mixing perturbations. Such strong admixing might be expected to give rise to comparable electromagnetic transition probabilities from the 1.47 MeV state contrary to the observation, here reported, of only a 3.5% direct ground state deexcitation. It must be recognized however that this argument is flawed by the possibility of coherent addition and subtraction of component transition amplitudes in the configuration, leading to enhancement of one transition and corresponding inhibition of the other.

(3) Similar arguments follow in the case of the proton spectroscopic factors appropriate to the (d,p) stripping reaction on O^{18}. If the two low-lying states were strongly mixed it might be anticipated that roughly comparable spectroscopic factors would be observed; particularly since in this case the contributions corresponding to different components add incoherently. Experimentally, the spectroscopic factors for the ground and 0.096 MeV states differ by a factor ~ 200, arguing against strong mixing and hence against equivalent spins of the state wave functions; moreover, the shell model predictions of these spectroscopic factors[81,84,85] are in good accord with the experimental results on the assumption of the 5/2, 3/2, 1/2 sequence.

It is worth noting that although certain collective model variants have predicted inversion of a low-lying 3/2, 5/2 pair from the shell model order, no model with relevance to this mass region can readily generate two low-lying $3/2^+$ states. In the Nilsson model, for example, it would be necessary to postulate that one of the states was the second member of a $K = 1/2$ band based on Nilsson orbit 9 with the assumed $1/2^+$ band head at 1.47 MeV. This would require a band decoupling parameter of $-3 < a < -1$ and would also require a corresponding low-lying

$7/2^+$ state for which there is no evidence. Of course, this model-dependent argument cannot be considered as experimental evidence for such a spin assignment.

It might be noted that any residual ambiguity between $3/2^+$ and $5/2^+$ assignments to the O^{19} ground state could, in principle, be removed through study of the $O^{18}(d,p\gamma\gamma)O^{19}$ angular correlation through a higher excited state with $J \geq 3/2$. In the case of the 0.096 MeV state, which is the only one other than the $1/2^+$ state at 1.47 MeV accessible to the deuteron energies here available, the lack of either resonant structure in the excitation curves or a well defined stripping angular distribution precludes application of correlation techniques of this type.

4. Deexcitation Properties of the 1.47 MeV State:

Experimental measurement of the deexcitation branching of the 1.47 MeV state described in Section C3 indicated a cross-over transition of intensity $3.3 \pm 1.6\%$ where 100% is the total deexcitation intensity of the state. To the extent that model-generated wave functions describe the states of O^{19}, it should be possible to predict from the wave functions this observed branching of the gamma deexcitation. It is well known that the dynamic characteristics of a nucleus reflected in its electromagnetic transition rates, among other phenomena, are much more sensitive to small wave function admixtures than are its static properties. It was therefore of special interest to examine to what degree several of the existing model calculations dealing with O^{19} were capable of reproducing the experimental result stated above.

Table III-1 lists the 1.47 MeV state branching ratio predicted within the framework of the extreme single particle model, the Chi and Davidson[40] asymmetric rotor model, and the intermediate-coupling shell model. The ratio is expressed in each case as the intensity of the crossover transitions to that of the total transitions. Details of each of these calculations are outlined below the table.

TABLE III-1

Deexcitation branching ratio of the 1.47 MeV state in O^{19}.

Extreme single particle model	Chi and Davidson rotor model	Inoue et al. shell model	Experimental value
0.0003	0.76	0.03	0.035

(A) The branching based on the extreme single particle model[92] was calculated from the ratio for E2 and M1 radiative widths as given by the expressions

$$\Gamma(E2) = 4.9 \times 10^{-8} A^{4/3} E^{5} \text{ eV}$$
$$\Gamma(M1) = 2.1 \times 10^{-2} E^{3} \text{ eV} \qquad \text{(III-3)}$$

where $A = 19$ in this case and E is the transition energy in MeV.

(B) The branching based on the Chi and Davidson model[40] was calculated from the reduced matrix elements, $B(E2) = 1.14 \times 10^{-6}$ barns and $B(M1) = 1.31 \times 10^{-9}$ nm, calculated by these authors from their model fit to O^{19}.

(C) The branching predicted by the shell model[93] may be obtained from any set of a number of wave functions generated by shell model formulations of O^{19}. For example, Elliott and Flowers[16], Talmi and Unna[21], and Inoue et al.[19] all provide wave functions for the O^{19} system which are identical to within 1 part in 10 of their configuration coefficients in spite of the different model variants used in each case. In consequence, because those of Inoue et al. are based on the most comprehensive model thus far carried out, the wave functions of these authors are listed in Table III-2 and were utilized in the calculation presented herein. Configuration admixtures of intensity less that 1% have been neglected.

The branching ratio is given by the expression

$$\text{B.R.} = \frac{T(E2,\ 1/2 \text{ to } 5/2)}{T(E2,\ 1/2 \text{ to } 5/2) + T(M1,\ 1/2 \text{ to } 3/2)} \qquad \text{(III-4)}$$

where the E2 amplitude in the 1/2 to 3/2 transition has been neglected. The

TABLE III-2

Wave functions of O^{19} based on the intermediate-coupled shell model calculations of Inoue et al.

Configuration	T	3/2	3/2	3/2
	J	1/2	3/2	5/2
$d_{5/2}^3$		—	0.73	-0.89
$d_{5/2}^2 s_{1/2}$		-0.96	-0.65	—
$d_{5/2} s_{1/2}^2$		—	—	0.36
$d_{5/2} d_{3/2} s_{1/2}$		0.15	—	—
$d_{5/2} d_{3/2}^2$		—	-0.12	-0.19
$d_{3/2}^2 s_{1/2}$		0.22	—	—

transition probability[94] between a final state $|J_f\rangle$ and an initial state $|J_i\rangle$ is

$$T(E2) = \frac{4\pi}{75}\left(\frac{E}{hc}\right)^5 \frac{1}{\hbar}\left|\langle J_f \| Q^2 \| J_i\rangle\right|^2 \qquad \text{(III-5)}$$

for E2 radiation, and

$$T(M1) = \frac{e^2 E^3}{3M^2\hbar^2 c^5}\left|\langle J_f \| M^1 \| J_i\rangle\right|^2$$

for M1 radiation. The reduced matrix elements are defined as

$$\begin{aligned}\langle J_f M_f | Q_\mu^2 | J_i M_i\rangle &= (J_i 2 M_i \mu | J_f M_f)\langle J_f \| Q^2 \| J_i\rangle \\ \langle J_f M_f | M_\mu^1 | J_i M_i\rangle &= (J_i 1 M_i \mu | J_f M_f)\langle J_f \| M^1 \| J_i\rangle\end{aligned} \qquad \text{(III-6)}$$

In the above expressions Q_μ^2 and M_μ^1 are the μ-components of the electric quadrupole and magnetic dipole operators, respectively, M is the nucleon mass,

E is the energy of the deexcitation, and the notation for Clebsch-Gordan coefficients $(J_1 J_2 M_1 M_2 | JM)$ follows from the angular momentum coupling $\vec{J}_1 + \vec{J}_2 = \vec{J}$; $M_1 + M_2 = M$.

The matrix elements of Equation III-6 are calculated from the single-body multipole operators

$$\begin{aligned} Q^2_\mu &= e\sum_p r_p^2 Y_2^\mu(p) + e\alpha \sum_{p,n} r_{p,n}^2 Y_2^\mu(p,n) \\ \vec{M}^1 &= \sum_p g_l(p)\vec{l}(p) + g_s(p)\vec{\sigma}(p) + \sum_n g_s(n)\vec{\sigma}(n) \end{aligned} \qquad \text{(III-7)}$$

which become for the O^{19} case of three valence neutrons

$$\begin{aligned} Q^2_\mu &= e\alpha\sum_{n=1}^{3} r_n^2 Y_2^\mu(n) \\ \vec{M}^1 &= \sum_{n=1}^{3} g_s(n)\vec{\sigma}(n). \end{aligned} \qquad \text{(III-8)}$$

The coefficient α is the "effective charge" of the neutron included to represent the polarizibility of the nuclear core and to a lesser extent the core recoil contributions to the transition moments. In the above expressions, Y_2^μ is the usual associated Legendre polynomial of order 2, $g_s = -1.91$ nm, and $\vec{\sigma}$ is the Pauli spin matrix.

Employing methods described by Talmi and de Shalit[95] each term of the wave functions may be written as

$$\Phi^J_M = \sum_{\substack{m_1+m_2+m_3 \\ m_\alpha \leq j_\alpha}} b^{JM}_{m_1 m_2 m_3} \varphi^{j_1}_{m_1}(1)\,\varphi^{j_2}_{m_2}(2)\,\varphi^{j_3}_{m_3}(3) \qquad \text{(III-9)}$$

wherein $\varphi^{j_i}_{m_i}(i)$ is the wave function of the single i^{th} particle in a simple harmonic oscillator potential as given by Equation I-2, and $b^{JM}_{m_1 m_2 m_3}$ is the product of two Clebsch-Gordan coefficients which couple the three single-particle wave functions to a state of angular momentum $\vec{J}$ and projection M. Linear combinations of appropriate Φ^J_M terms summed according to the amplitude coefficients listed in Table III-2 form the wave functions of the O^{19}

states of interest. The pertinent matrix elements of the Pauli spin operator $\vec{\sigma}$ upon which the magnetic dipole operator depends are easily calculated; the matrix elements of the r^2 operator upon which the electric quadrupole operator depends have been previously calculated for all single particle transitions within the sd shell by Raz[96] and these matrix element values have been used in this computation.

The process of calculating the matrix elements representing the M1 and E2 transitions between initial and final states is further simplified by the fact that, because of the single-body nature of the transition operators, a particular matrix element is non-zero only if at least two of the three single particle states in the initial product wave function are identical to two of the three single states in the final product wave function.

A calculation analogous to that just described may be carried out for the equivalent $1/2 \rightarrow 5/2$ transition from the first excited state in O^{17} where a fit to the experimentally measured transition probability[97] determines the effective charge parameter to be $\alpha \cong 0.5$. If this same charge parameter is taken over directly into the O^{19} calculation, the predicted branching ratio of $\cong 3\%$ given in Table III-1 follows immediately.

The good agreement between the shell model predictions and the experimental results further supports the validity of this model for O^{19} and thus may be adduced as still more evidence supporting the $5/2^+$ assignment to the ground state of this nucleus. Of perhaps greater interest, however, is the fact that the same effective E2 operator, $Q^2_\mu = e\alpha r^2 Y^\mu_2$, with α approximately equal to one half the proton charge, reproduces the transition probabilities in the "neutron" transitions between (1) the 0^-, 0.12 MeV state and the 2^-, ground state in N^{16}; (2) the $1/2^+$, 0.87 MeV state and the $5/2^+$, ground state in O^{17}; (3) the $1/2^+$, 0.58 MeV state and the $5/2^+$, ground state in Mg^{25}; and (4) the $1/2^+$, 1.47 MeV state and the most probably $5/2^+$, ground state in O^{19}. Assigning an effective charge to the odd neutron in all these cases is equivalent[98] to invoking, within the framework of the collective model, a very weak coupling between the odd valence neutron and surface oscillations in the core. Thus in O^{19} the 1.47 MeV cross-over transition, which is quite strong with respect to that expected on the basis

of the extreme single-particle model, is simply the signature of collective motion of the O^{19} nucleus or, differently stated, of collective polarization of the O^{18} core by the extra-core nucleon.

The fact that essentially the same value of effective charge leads to good agreement between theoretical predictions of E2 transition rates and experimental measurements over a considerable range of mass numbers should be especially noted. In particular, the addition of two neutrons to the core does not enhance the core polarizibility in O^{19} over that of the analogous case in O^{17} giving support to the picture of the two additional nucleons pairing to give a spherically symmetric contribution to the effective potential which binds the last neutron. Recent calculations of Kelson[99] are in accord with this behavior.

E. Summary

The measurements reported in this chapter have established an unambiguous assignment of $3/2^+$ to the 0.096 MeV state of O^{19} and an almost certain assignment of $5/2^+$ to the O^{19} ground state. It is demonstrated that the recently reported 0.348 MeV state in O^{19} is spurious and that the previous evidence supporting it corresponds instead to population of the 4.45 MeV state of O^{18} through the $O^{17}(d,p)O^{18}$ reaction on an O^{17} target contaminant.

It has been shown that shell model predictions are in excellent accord with available experimental data for this $T_z = 3/2$ nucleus giving further support to the j-j coupling approximation assumed valid for this system. Evidence is also obtained which demonstrates that the addition of two neutrons to the O^{17} structure does not contribute significantly to increased polarizibility of the core; and, therefore, that the effective charge in the E2 "neutron" transition of O^{19} may be represented by an effective E2 operator essentially identical to that required in the O^{17} case. This ineffectiveness of additional identical nucleons in increasing the core polarizibility is in striking contrast to the case of additional non-identical nucleons which lead to strong polarization, as for example in F^{19}, as discussed in the previous chapter. The self-consistent model calculations provide a theoreticas basis for expecting just this type of behavior.

IV. STUDIES OF LOW-LYING ENERGY LEVELS OF Ne^{21}, Na^{21}, AND Na^{23}

A. Introduction

1. Theoretical:

In Figure IV-1 the energy level diagrams of six nuclei of odd-nucleon number $\eta = 11$ are presented. It has long been realized that within the application of the Nilsson model the identification and subsequent interpretation of corresponding analogous states in adjacent $\eta = 11$ systems are greatly complicated by the possibility of strong K = 3/2 and K = 1/2 and/or K = 5/2 and K = 3/2 band mixing reflecting the normally neglected Coriolis term in the nuclear Hamiltonian. Nevertheless, a variety of Nilsson model calculations and extensions thereof have been applied to these nuclei; among the calculations are those of Roesser[41], of Kelson and Levinson[44], and of Benenson and Lidofsky[100] in the case of Na^{21}; of Roesser[41], of Kelson and Levinson[44], of Freeman[101], of Dreizler[102], and of Rakavy[71] in the case of Ne^{21}; and finally of Paul and Montague[103], of Clegg and Foley[104], of Litherland et al.[36], of Braben et al.[105], of Rakavy[71], and of Glöckle[106] in the case of Na^{23}. More generally, Chi and Davidson[40] and Bhatt[107] have carried out collective model calculations throughout the sd shell with specific treatments applied where data permitted to all the nuclear systems shown in Figure IV-1. Further calculations based on application of sophisticated group theoretical methods to the sd shell are being carried out currently by Moshinsky[108] and collaborators. This work has been restricted until now to even-A nuclei, but calculations are presently being initiated on the odd-A, $\eta = 11$ systems under consideration herein.

The extensive application of the Nilsson model in this mass region has already been noted as being due largely to the success achieved in the mass-25 nuclei. However, contrary to the relatively well understood experimental situation which exists in Al^{25} and Mg^{25}, measurements of many more level parameters of $\eta = 11$ nuclei are needed before equivalent quantitative comparison with model predictions may be carried out.

The measurements to be reported in this chapter were initiated in an effort

Figure IV-1. Experimentally observed energy level spectra for the odd-nucleon count $\eta = 11$ nuclear systems. Excitation energies are indicated in MeV.

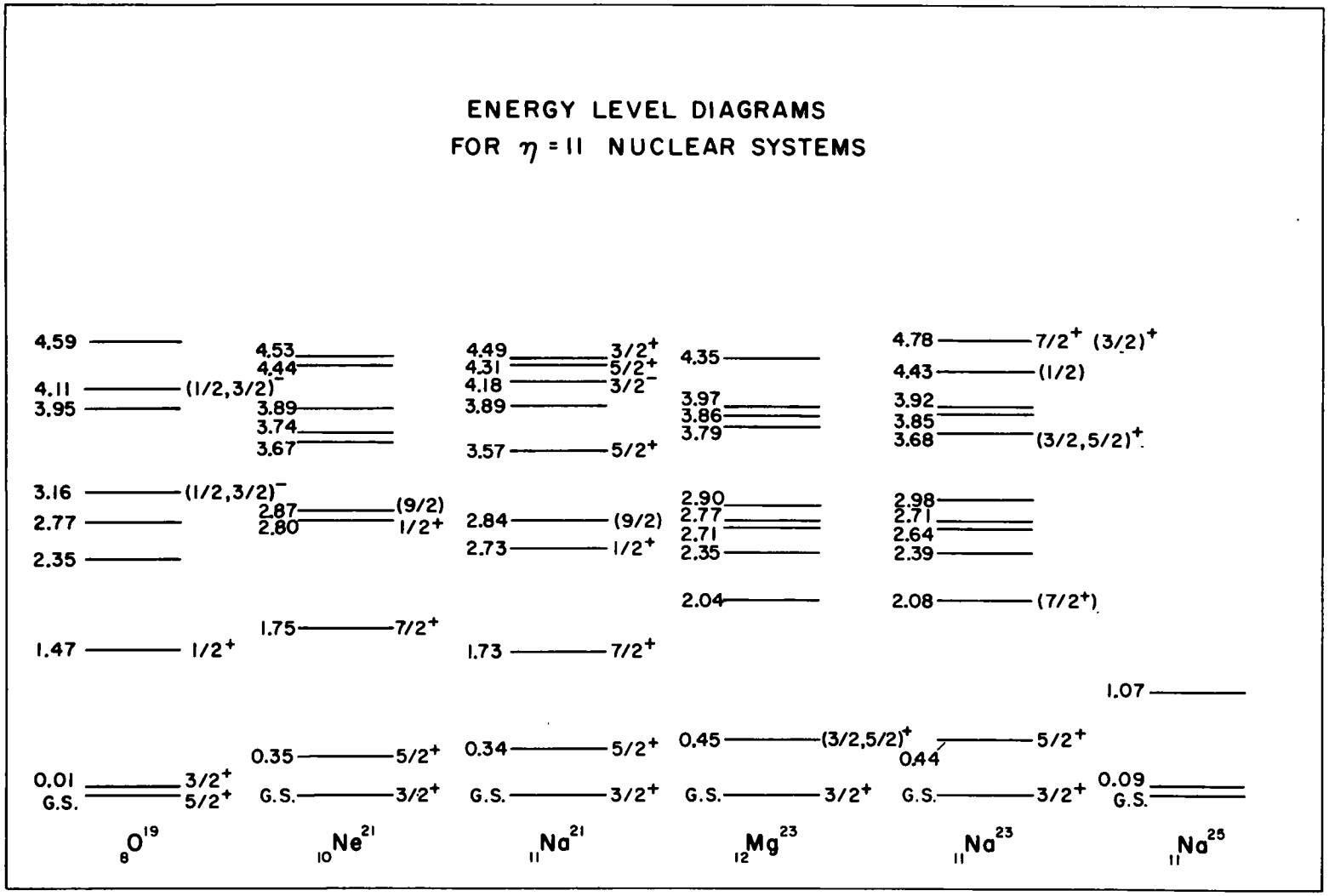
ENERGY LEVEL DIAGRAMS
FOR η = 11 NUCLEAR SYSTEMS
4.59
4.11
(1/2,3/2)⁻
3.95
3.16
(1/2,3/2)⁻
2.77
2.35
1.47
1/2⁺
0.01
3/2⁺
G.S.
5/2⁺
$_{8}O^{19}$
4.53
4.44
3.89
3.74
3.67
2.87
(9/2)
2.80
1/2⁺
1.75
7/2⁺
0.35
5/2⁺
G.S.
3/2⁺
$_{10}Ne^{21}$
4.49
3/2⁺
4.31
5/2⁺
4.18
3/2⁻
3.89
3.57
5/2⁺
2.84
(9/2)
2.73
1/2⁺
1.73
7/2⁺
0.34
5/2⁺
G.S.
3/2⁺
$_{11}Na^{21}$
4.35
3.97
3.86
3.79
2.90
2.77
2.71
2.35
2.04
0.45
(3/2,5/2)⁺
G.S.
3/2⁺
$_{12}Mg^{23}$
4.78
7/2⁺ (3/2)⁺
4.43
(1/2)
3.92
3.85
3.68
(3/2,5/2)⁺
2.98
2.71
2.64
2.39
2.08
(7/2⁺)
0.44
5/2⁺
G.S.
3/2⁺
$_{11}Na^{23}$
1.07
0.09
G.S.
$_{11}Na^{25}$

to provide information of the dynamic properties of several low-lying states in three of these nuclei, Ne^{21}, Na^{21}, and Na^{23}. The experimentally determined static properties of each of these nuclear systems (which must be very similar in the single-particle, Nilsson sense) are reviewed briefly in the next section.

2. Experimental:

(i) The Ne^{21} nucleus: The states of Ne^{21} as summarized in Figure IV-1 have recently been the subject of several extensive experimental investigations. Particle studies in the reactions Ne^{20} (d, p) Ne^{21} and F^{19} (He^3, p) Ne^{21} were carried out by Burrows et al.[109], by Freeman[101], and by Hinds and Middleton[110] to establish firmly the energy positions of the excited states and to limit the J^{π} assignments to several of these states. Recent observations, primarily those of Howard et al.[111], on the distributions and correlations of gamma radiations originating from these energy levels have determined the spin assignments to be $3/2^+$, $5/2^+$, $7/2^+$, $1/2^+$, and $3/2^-$ for the ground, 0.35 MeV, 1.75 MeV, 2.80 MeV, and 4.73 MeV, states, respectively. Gamma deexcitation branching of the states at 1.75, 2.80, 3.67, and 4.73 MeV have been established by the studies of Howard et al.[111] and of Pelte et al.[112]; these independent determinations are in good accord with one notable exception. The deexcitation branching of the 2.80 MeV state is found by the former group to be 90% and 10% to the ground state and first excited state, respectively, and by the latter group to be 50% to both the ground and first excited states. This discrepancy is well outside the limits of error assigned to each measurement and both measurements have been extensively checked experimentally by both groups of investigators. The Doppler shift of radiation from the four lowest states populated through both the Ne^{20} (d, p) Ne^{21} and the Be^9 (O^{16}, $\alpha\gamma$) Ne^{21} reaction have also been recently measured[107, 109] to provide approximate lifetimes of these states.

(ii) The Na^{21} nucleus: The experimentally established level scheme of Na^{21} presented in Figure IV-1 is, as expected, quite similar to that of its mirror nucleus Ne^{21}. The principle source of information on energy levels below 2.45 MeV in Na^{21} has been the study[100, 114] of neutron groups from the reaction Ne^{20} (d, n) Na^{21}. Above 2.45 MeV excitation this nucleus is unstable

against proton emission and studies[92, 100, 115, 116] concerning the unbound states have utilized the Ne^{20} (p,γ) Na^{21} and Ne^{20} (p,p) Ne^{20} reactions.

The ground state of Na^{21} has been firmly established[2] as $3/2^+$; the 0.335 MeV state is most probably $5/2^+$ by analogy with its equivalent state in Ne^{21}; the 1.73 MeV state is known to be $7/2^+$ from angular distribution studies[61] of the gamma deexcitation of the 3.57 MeV state through the 1.74 MeV state: and, finally, the 2.73 MeV level is known from (d, n) distribution data to have spin and parity $1/2^+$. Gamma radiation distribution studies show also the spin of the 3.57 MeV state to be very probably $5/2^+$. The detailed multipole mixing ratio of the 3.57 MeV to ground state radiation has been in considerable question, however, because of gross inconsistencies which exist between the various distribution measurements which have been used to determine this ratio.

(iii) The Na^{23} nucleus: The energy level excitations in Na^{23} are well known from the work of Beuchner and Sperduto[117] in which the energies of proton groups inelastically scattered from Na^{23} were determined by magnetic analysis. The J^π value of the ground state of this nucleus is firmly established[114] as $3/2^+$; the first excited state[2] as $5/2^+$. The remaining spin and parity limitations summarized in Figure IV-2 were determined from the study[119] of inelastic scattering of protons from NaI targets, from the investigation[105, 120] of gamma radiation distributions and correlations following proton capture by Ne^{22} at a number of proton capture resonances, and from the measurement[121] of angular distributions of neutron groups resulting in the reaction Ne^{22} (d, n) Na^{23} at $E_d = 3.0$ MeV.

Although the information presented above represents considerable progress in accumulating precise experimental data sufficient for extensive model interpretations of $\eta = 11$ nuclei, only fragmentary, and in several cases contradictory, results exist concerning the dynamic properties of these nuclei. For this reason, the experimental investigations to be reported in this chapter were undertaken to obtain further information on selected states in these nuclei which would be of interest in elucidating model applicability; in particular, an attempt has been made to provide (1) a consistent set of branching ratio measurements of deexcitation from the second excited $7/2^+$ state in each system for purposes of intercomparison, (2) a measurement of the 2.08 → 0.44 → 0 MeV cascade deexcitation correlation

in Na^{23} to permit perhaps a unique determination of the spin of the 2.08 MeV state and the mixing amplitude of the 2.08 → 0.44 MeV transition for detailed comparison with the known mixing amplitude of the assumed analogous $7/2^+ \rightarrow 5/2^+$ transition in Ne^{21}, (3) a remeasurement of the distribution of the ground state radiation originating from the 3.57 MeV state in Na^{21} in view of numerous discrepancies between the various experimental measurements thus far reported, and (4) a remeasurement of the deexcitation branching of the 2.80 MeV state in Ne^{21} for purposes of resolving the experimental inconsistencies present in the previous measurements of the branching.

B. Experimental Equipment

The electronic and detection equipment utilized in the particle-gamma coincidence, gamma-gamma coincidence, angular distribution, and angular correlation measurements to be reported in this chapter have been thoroughly described in previous sections. As before, gas targets[122] have been employed in this series of measurements; essentially pure Ne^{20} gas for the Ne^{21} and Na^{21} measurements, highly enriched Ne^{22} gas (isotopic purity $\cong 95\%$) for the Na^{23} measurements.

Because of the straightforward angular correlation methods which may be used in examining deexcitations of a state populated by a radioactive decay process, the beta decay branch of Ne^{23} to the 2.08 MeV state in Na^{23} was selected as the means of forming this state of interest. This particular technique of populating the 2.08 MeV level had the further advantage of avoiding the complex gamma deexcitation spectra normally resulting from direct proton or deuteron bombardment of Ne^{22}.

Ne^{23} was produced in the target cell by deuteron bombardment of the Ne^{22} target sample; the deuteron beam was periodically interrupted by a mechanical shutter system placed between the control slits of the accelerator and the target cell, and the detection equipment was automatically enabled during the beam-off period. The complete beam-on, beam-off cycle was controlled by a series of cams, relays, and microswitches synchronized to the mechanical drive of the

shutter system.

As will be more fully described in Section C3 of this chapter, a lifetime analysis of the radioactivity formed during the beam-on period was necessary. A 400 channel analyzer operated in the multi-scale mode was employed for this measurement. The sweep oscillator of a standard Tektronix oscilloscope provided the channel advance to the analyzer, and it was from this signal that the channel-to-time base was derived.

The timing of the irradiate-count cycle was adjusted to take advantage of the lifetimes of the two predominant radioactive products, F^{20} and Ne^{23}, formed by the (d,α) and (d,p) reactions on the Ne^{22} target; specifically

Time in seconds	Operation
0	beam on target
60	beam off target
90	detecting equipment on
178	detecting equipment off
180	beam on target

The irradiation time of 60 seconds ($\sim 2\tau_{1/2}$ of Ne^{23}) permitted formation of about 75% of the total Ne^{23} activity attainable under the given beam and target conditions; the waiting time of 30 seconds ($\sim 3\tau_{1/2}$ of F^{20}) permitted the ratio of the inital number of Ne^{23} nuclei to the initial number of F^{20} nuclei to increase by a factor of 4. The experimental advantage of increasing this ratio is discussed in the following section.

C. Experimental Results

1. The Ne^{21} System:

Branching ratio measurements for the states at 1.75 and 2.80 MeV in Ne^{21} were carried out by means of proton-gamma radiation coincidence studies. The target cell and particle detector assembly described in Chapter III, Section B was employed; the gamma radiation detector in this case consisted of a 3x3 inch

NaI (Tl) crystal positioned 4 cm from the target center and at 90^{o} to the incident beam. A deuteron beam accelerated to 2.2 MeV was used, and the Ne^{20} target pressure was held at 60 cm of Hg absolute throughout the measurement.

The two energy regions corresponding to the proton groups populating the 1.75 MeV state and the 2.80 and 2.87 MeV states in Ne^{21} were selected by the particle counter for coincidence measurements. The gamma radiation in coincidence with the proton group populating the 1.75 MeV level is illustrated in Figure IV-2, that in coincidence with the two groups populating the 2.80 and 2.87 MeV levels in Figure IV-3. These measurements were repeated at a second observation angle, $\theta = 0^{o}$, and at a higher incident deuteron energy of 2.90 MeV.

The coincidence spectra were corrected for crystal efficiencies[63], coincidence summing, and the slight ($\sim 3\%$) adjustment made necessary by the proton-gamma correlations and indicated by comparison of the two measurements at extreme angles. As expected, intercomparison of the spectra taken at the two bombarding energies suggested no deexcitation branching dependence on deuteron energy. Analysis of the data then established the deexcitation branching of the 1.75 MeV state in Ne^{21} to be $7 \pm 1\%$ crossover radiation to the ground state and $93 \pm 1\%$ cascade radiation through the 0.353 MeV state; the deexcitation branching of the 2.80 MeV state was established to be $90 \pm 2\%$ to the ground state and $10 \pm 2\%$ to the 0.353 MeV state. No evidence for 1.05 MeV radiation which would correspond to the $2.80 \rightarrow 1.75$ MeV transition was observed; similarly, no significant gamma radiations of energy suggesting depopulation of the 2.87 MeV state were detected indicating that the population of this state at deuteron energies of 2.20 and 2.90 MeV is less than 10% of the population of the 2.80 MeV state. The deexcitation branching ratios of these specific states in Ne^{21} are summarized in Figure IV-13.

2. The Na^{21} system:

Methods identical to those discussed in Chapter II in connection with the O^{18} + p resonances were used to locate and identify the 1170 keV proton capture resonance in the Ne^{20} + p reaction. This process was simplified greatly because of the nearly equal energies of the 1170 keV Ne^{20} (p,γ) Na^{21} and the 1169 keV O^{18} (p,γ) F^{19} resonances. The fact that all pertinant experimental quantities

Figure IV-2. Gamma radiation observed at $\theta = 90^{o}$ in coincidence with the proton group populating the 1.75 MeV state of Ne^{21} in the reaction $Ne^{20}(d,p)Ne^{21}$.

Figure IV-3. Gamma radiation observed at $\theta = 90^{o}$ in coincidence with the proton groups populating the 2.80 and 2.87 MeV states of Ne^{21}.

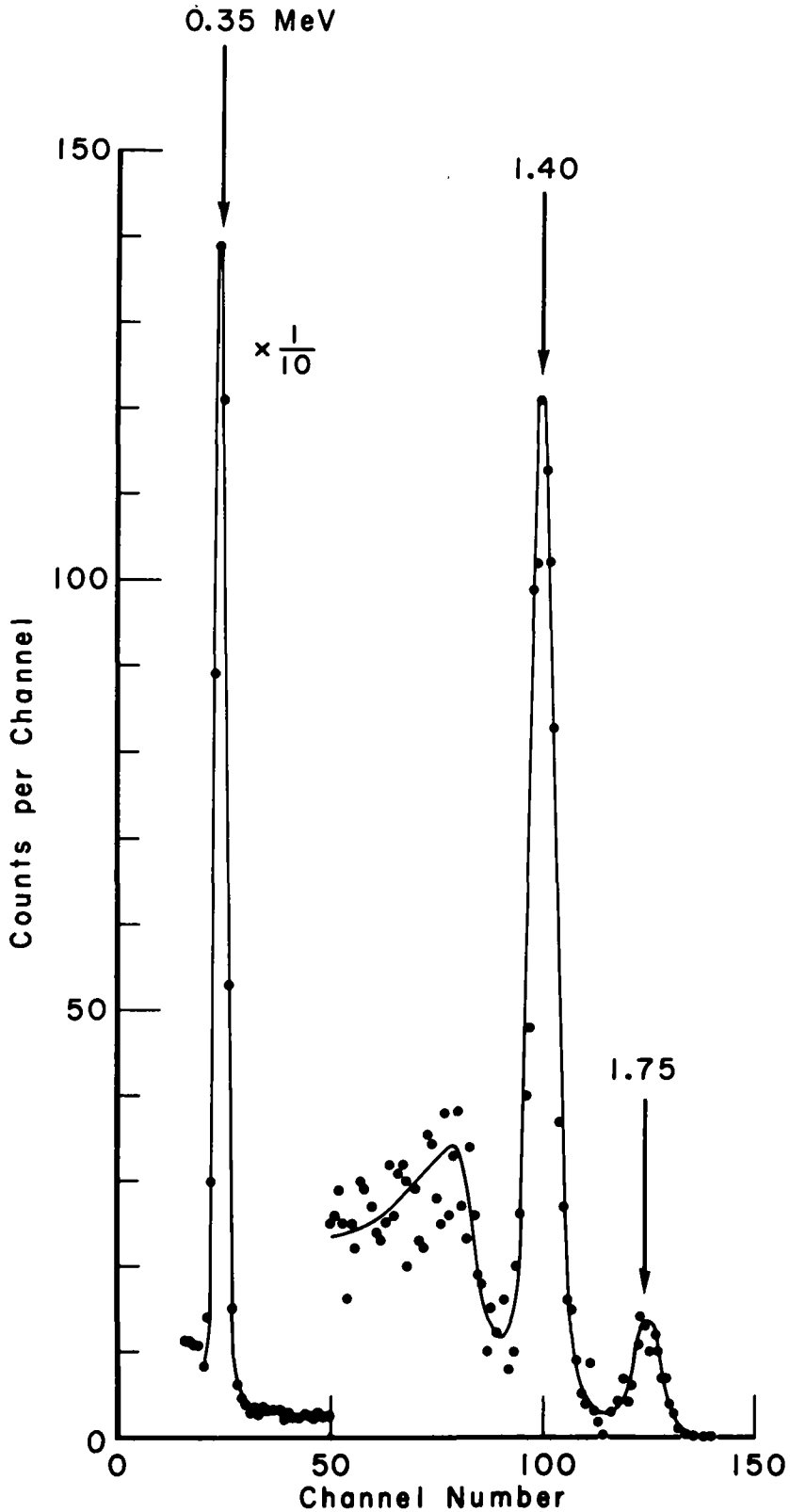
0.35 MeV
1.40
1.75
× 1/10
150
100
50
0
0
50
100
150
Counts per Channel
Channel Number

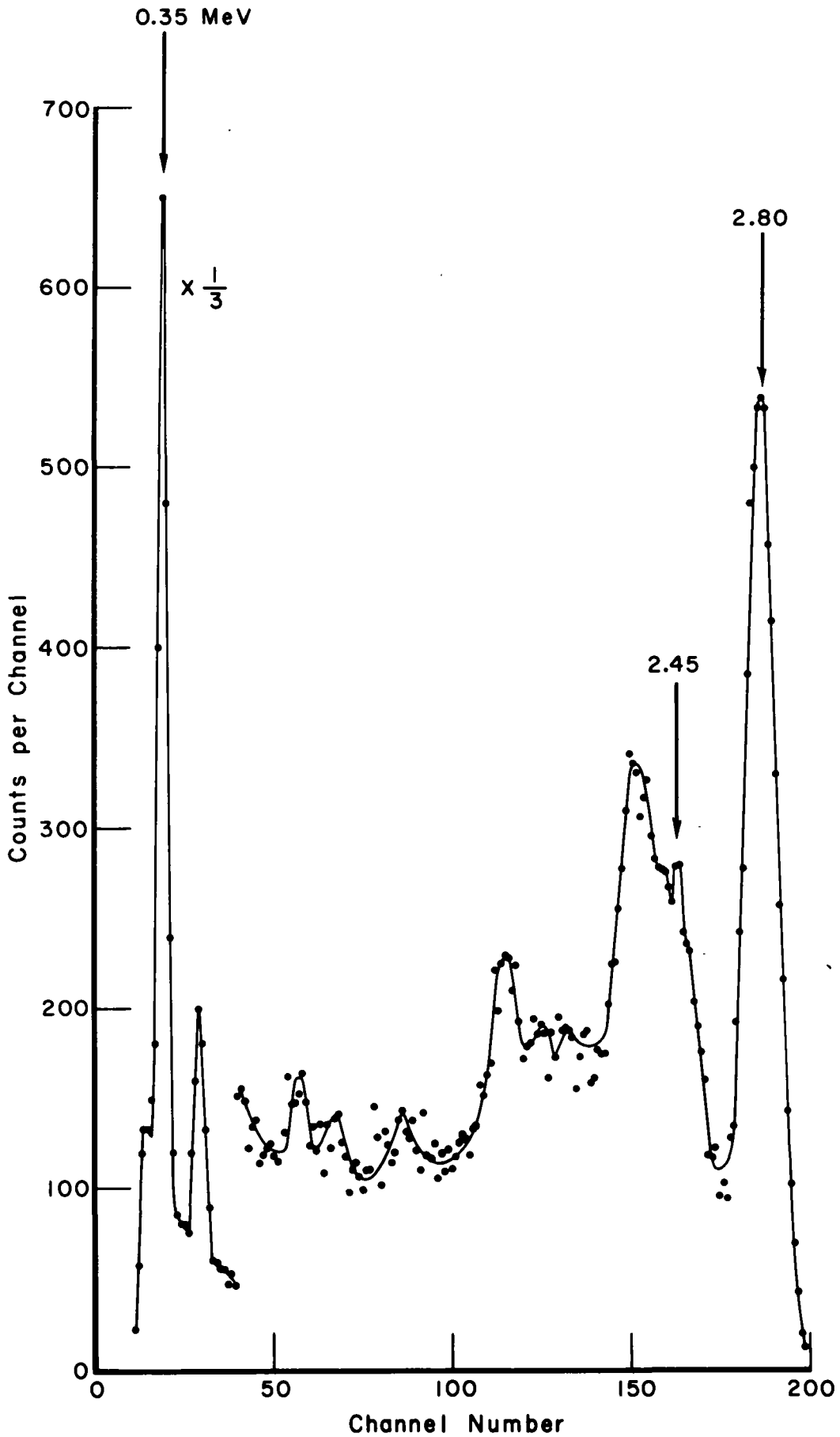
0.35 MeV
2.80
2.45
X 1/3
Counts per Channel
Channel Number
0
100
200
300
400
500
600
700
0
50
100
150
200

(target pressure, target chamber entrance window thickness, accelerator energy calibration) were unchanged between these sets of measurements served as still another check on the resonance identifications in both nuclear systems. Furthermore, the alignment of the correlation table was unchanged from that established in Chapter II.

A direct spectrum of the deexcitation of the 3.57 MeV state in Na^{21} populated by the 1170 keV proton capture of Ne^{20} is shown in Figure IV-4. This spectrum was obtained with the 3 x 3 inch NaI (Tl) spectrometer located at 90^{o} to the beam direction and 12 cm from the target center.

Energy calibration of the spectrometer (previously described) established the presence of prominent transitions of energies 0.335, 1.40, 1.84 and 3.57 MeV in satisfactory agreement with the deexcitations of the 3.57 MeV state previously reported by Howard.[61]

A series of direct spectra similar to that of Figure IV-4 were taken at angles $\theta = 0^{o}$, 30^{o}, 45^{o}, 60^{o}, 90^{o}, and 120^{o} where θ is the angle between the spectrometer and the beam direction. As in the previous angular distribution measurements, both a fixed monitor counter at $\theta = -90^{o}$ and a beam current integrator were used to obtain normalization data for these runs.

The observed intensities of the 3.57 MeV transition to the ground state of Na^{21} are shown in Figure IV-5 as a function of $\cos^{2}\theta$. The angular distribution coefficients A_2/A_0 and A_4/A_0, defined as in previous chapters, were found to be $A_2/A_0 = -0.26 \pm 0.02$ and $A_4/A_0 \cong 0$ from a least squares analysis of the data. A solid angle correction[64] of 5% appropriate for the 3 x 3 inch spectrometer at the quoted distance from the reaction site has been included in the above values.

In order to establish the detailed deexcitation branching of the Na^{21} state at 1.73 MeV excitation, a gamma-gamma coincidence measurement was carried out using 5 x 5 inch NaI(Tl) spectrometers. The deexcitation radiation spectrum in one crystal, which was in coincidence with a voltage gate spanning the pulse-height range corresponding to photopeaks of energy 1.6 to 1.9 MeV in the other, is presented in Figure IV-6. Unwanted coincidence contributions due to (a) higher energy tails falling within the coincidence gate (b) random coincidences, and (c) non-resonant coincidences were found to give essentially negligible corrections

Figure IV-4. Ne^{20} + p direct gamma radiation spectrum obtained with a 3 x 3 inch NaI(Tl) crystal at $\theta = 90^{o}$ and E_p = 1170 keV. Energies of the prominent peaks and their corresponding identification with transitions in the energy level spectrum of Na^{21} are indicated.

Figure IV-5. Angular distribution of the 3.57 MeV radiation originating in Na^{21} plotted as a function of $\cos^2\theta$. The solid curve is the result of a least squares fit to the data of the polynomial expansion of Equation III-1.

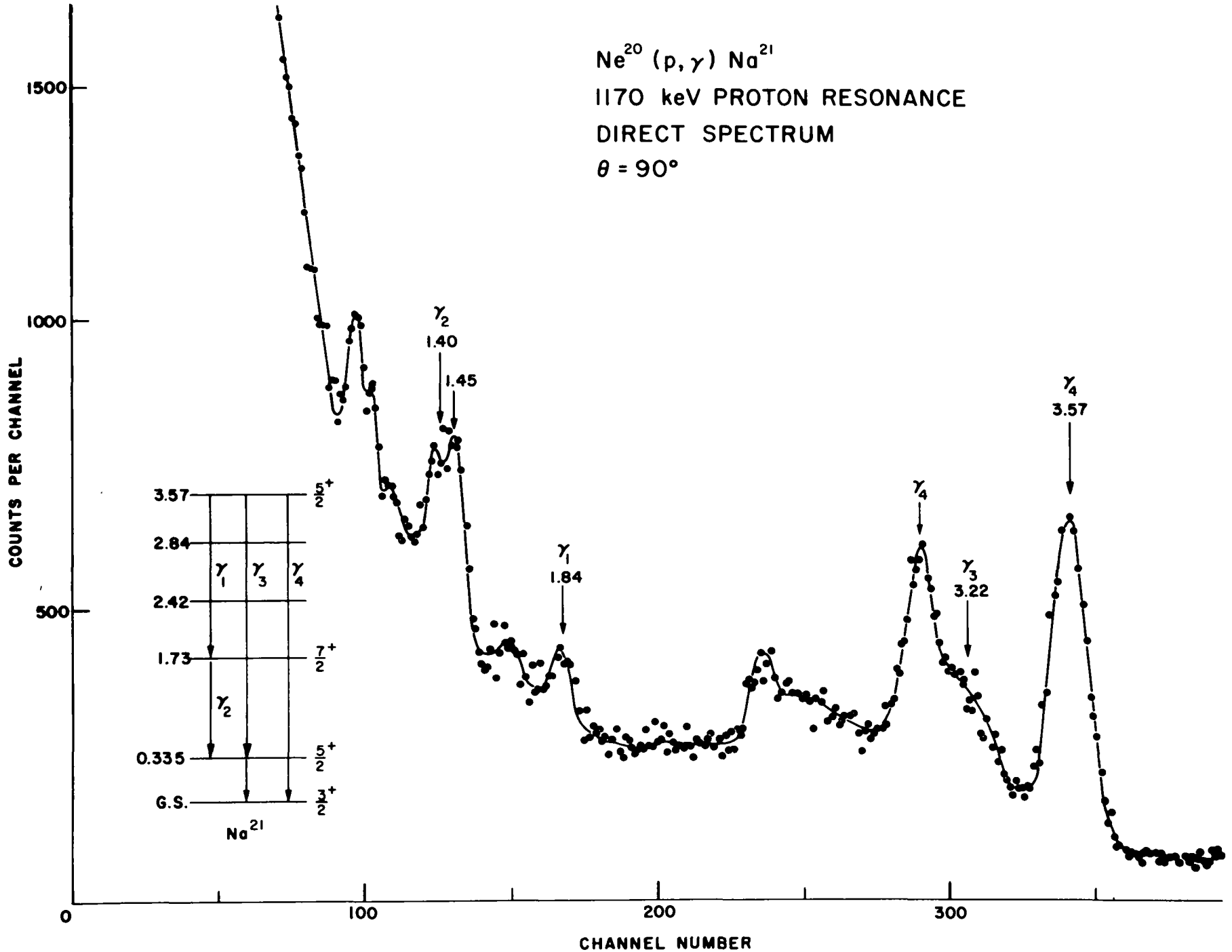
Ne^20 (p, γ) Na^21
1170 keV PROTON RESONANCE
DIRECT SPECTRUM
θ = 90°
COUNTS PER CHANNEL
CHANNEL NUMBER
1500
1000
500
0
100
200
300
γ2
1.40
1.45
γ1
1.84
γ4
3.57
γ4
γ3
3.22
3.57
2.84
2.42
1.73
0.335
G.S.
5/2+
7/2+
5/2+
3/2+
γ1
γ3
γ4
γ2
Na^21

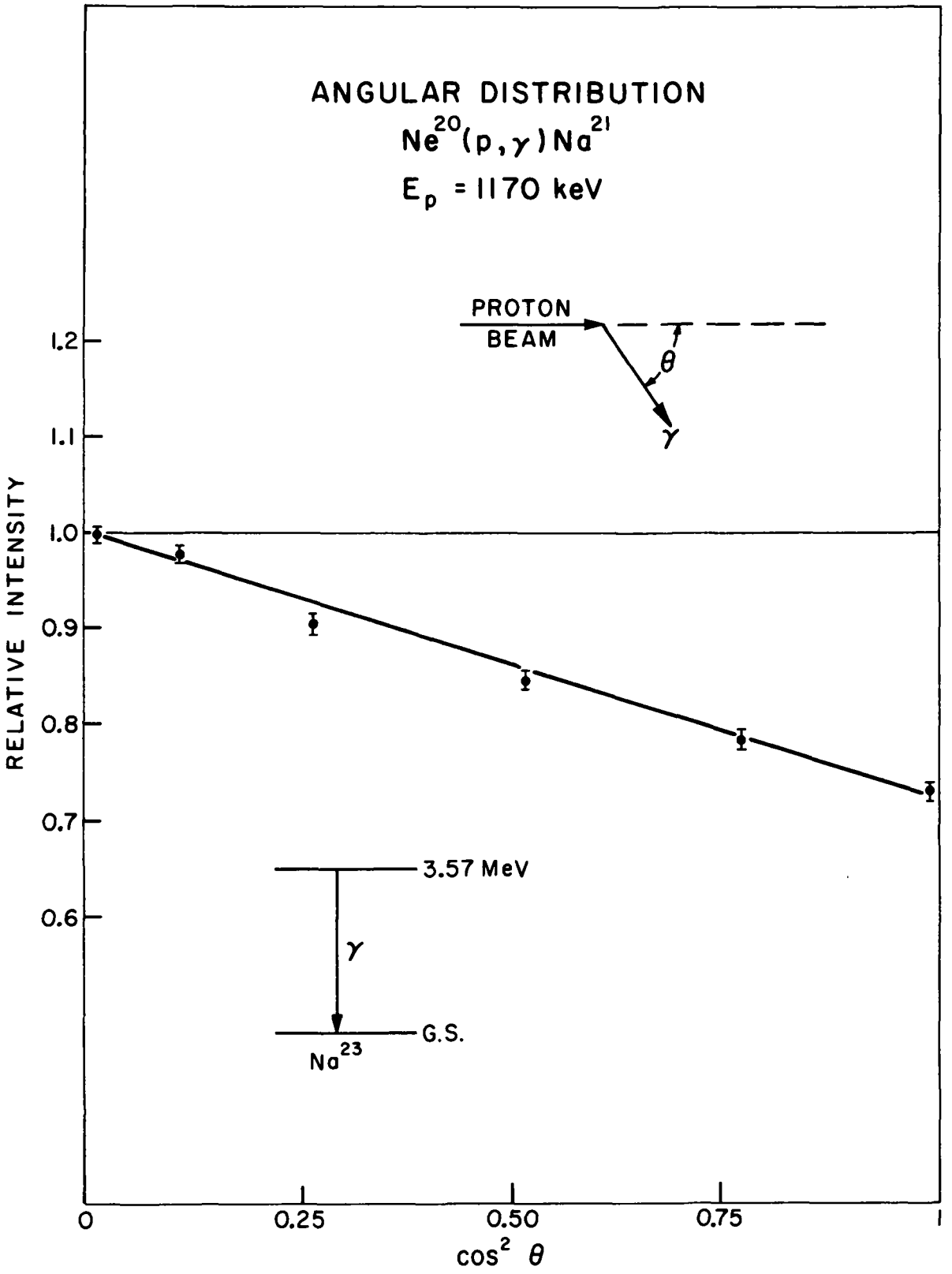
ANGULAR DISTRIBUTION
$Ne^{20}(p,\gamma)Na^{21}$
E_p = 1170 keV
PROTON
BEAM
θ
γ
RELATIVE INTENSITY
1.2
1.1
1.0
0.9
0.8
0.7
0.6
3.57 MeV
γ
G.S.
Na^{23}
0
0.25
0.50
0.75
1
$\cos^2\theta$

Figure IV-6. Ne^{20} + p gamma radiation spectrum observed in time coincidence with radiation in the energy region of 1.8 MeV. Prominent peaks of the spectrum are identified with particular transitions originating in Na^{21}.

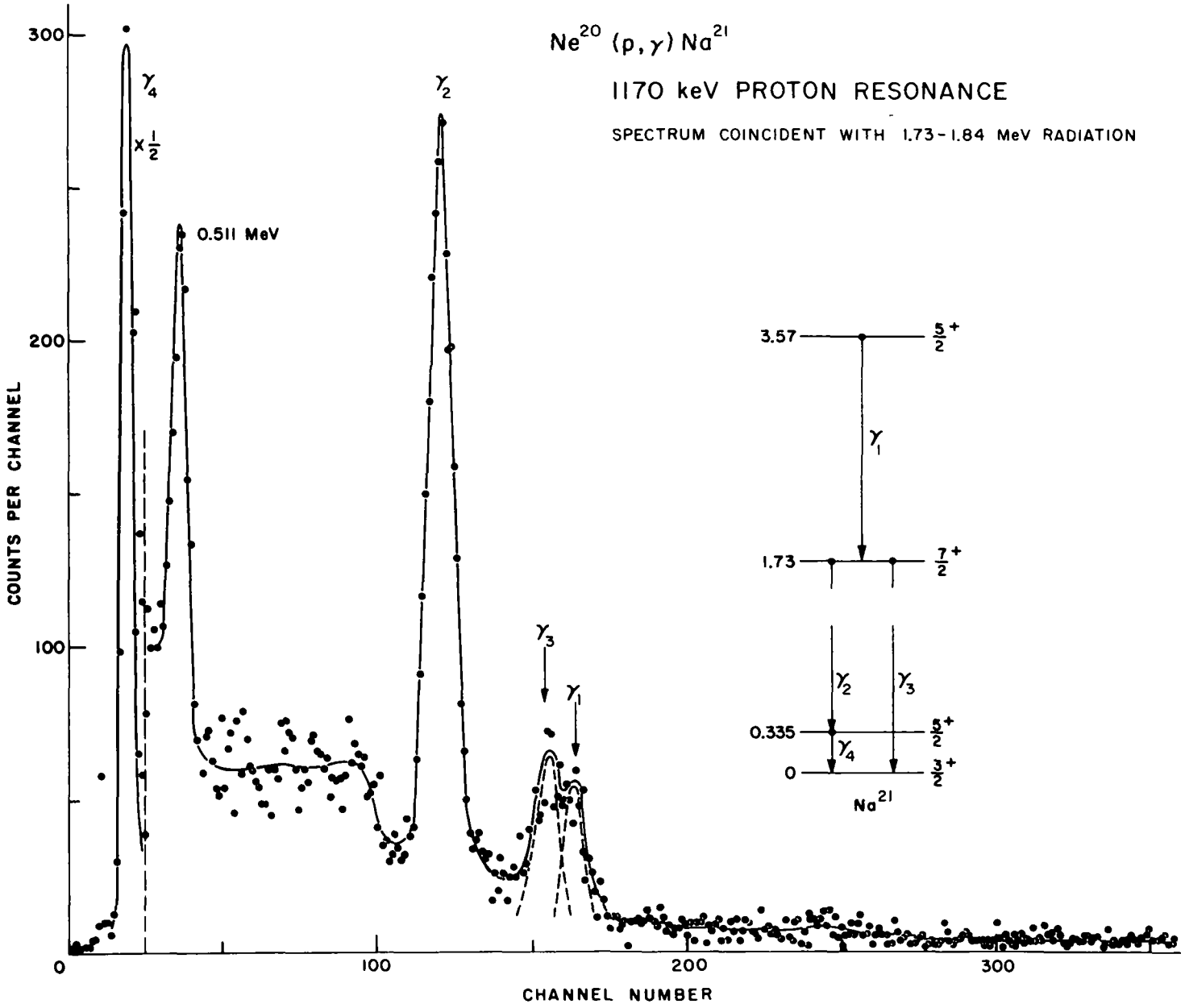
$Ne^{20}(p,\gamma)Na^{21}$
1170 keV PROTON RESONANCE
SPECTRUM COINCIDENT WITH 1.73-1.84 MeV RADIATION
COUNTS PER CHANNEL
CHANNEL NUMBER
0
100
200
300
γ_4
$\times\frac{1}{2}$
0.511 MeV
γ_2
γ_3
γ_1
3.57
$\frac{5}{2}^+$
1.73
$\frac{7}{2}^+$
0.335
$\frac{5}{2}^+$
0
$\frac{3}{2}^+$
Na^{21}

to this measurement. The small target-to-detector distance (4 cm) used for this run made unnecessary any angular correlation corrections which would otherwise have been required.

In analyzing the coincidence spectrum to obtain the branching ratio of $11 \pm 2\%$ crossover intensity and $89 \pm 2\%$ cascade intensity, the spectrometer efficiency calculation of Vegor et al.[63] were used. The fact that the $3.57 \rightarrow 1.73 \rightarrow 0$ MeV cascade was experimentally "counted" twice because of the nearly equivalent energies of the two branches involved was recognized and duely considered in the data analysis. This deexcitation branching is summarized in Figure IV-13.

2. The Na^{23} system:

The beam-on, beam-off technique of populating the first two excited states in Na^{23} was discussed briefly in Section B. A direct gamma radiation spectrum obtained with this method is shown in Figure IV-7. The gas target pressure was 60 cm of Hg absolute; the beam intensity and energy during the irradiation portion of the cycle were 1 μa at 2.75 MeV. The 3 x 3 inch NaI crystal employed for this measurement was 12 cm from the target. The spectrum shown with open circles is that obtained with the target chamber evacuated.

The beta decay branches in the decay of the ground state of Ne^{23} have been previously reported[2] as 67%, and 32%, and 1% to the ground, 0.439 MeV and 2.08 MeV states in Na^{23}, respectively; thus, the 0.44 MeV photopeak in the spectrum originates predominantly from direct beta decay population of the 0.44 MeV state. The 1.64 MeV photopeak originates from two sources; deexcitation of the 1.64 MeV first excited state of Ne^{20} formed by the reaction Ne^{22} (d, α) $F^{20} \xrightarrow{\beta^-} Ne^{20*}$ (1.64 MeV) and deexcitation of the state formed by the reaction Ne^{22} (d, p) $Ne^{23} \xrightarrow{\beta^-} Na^{23*}$ (2.08 MeV). Since the 2.08 MeV state in Na^{23} was of major interest in this investigation, it was necessary to first minimize the unwanted "contaminant" 1.64 MeV radiation by careful selection of the beam-on, beam-off cycle times and then to account accurately for the relative amounts of Ne^{23} and F^{20} activities present during the count period. The cycle times employed and the basis upon which they were selected were discussed in Section B. The fraction of the 1.64 MeV photopeak corresponding to Ne^{23} radiations and that corresponding to Na^{23} radiations were

Figure IV-7. Direct gamma radiation spectrum following 2.75 MeV deuteron bombardment of Ne^{22}. Energies of prominent transitions are indicated in MeV.

Figure IV-8. Decay of 1.64 MeV gamma radiation intensity following deuteron bombardment of Ne^{22}. The raw data is indicated in curve A. Curve B results from subtraction from the raw data of the longest lived radioactive component determined by a least squares fit to the data. Curve C results from subtraction from the raw data of both the 25 minute and the 37.5 sec components.

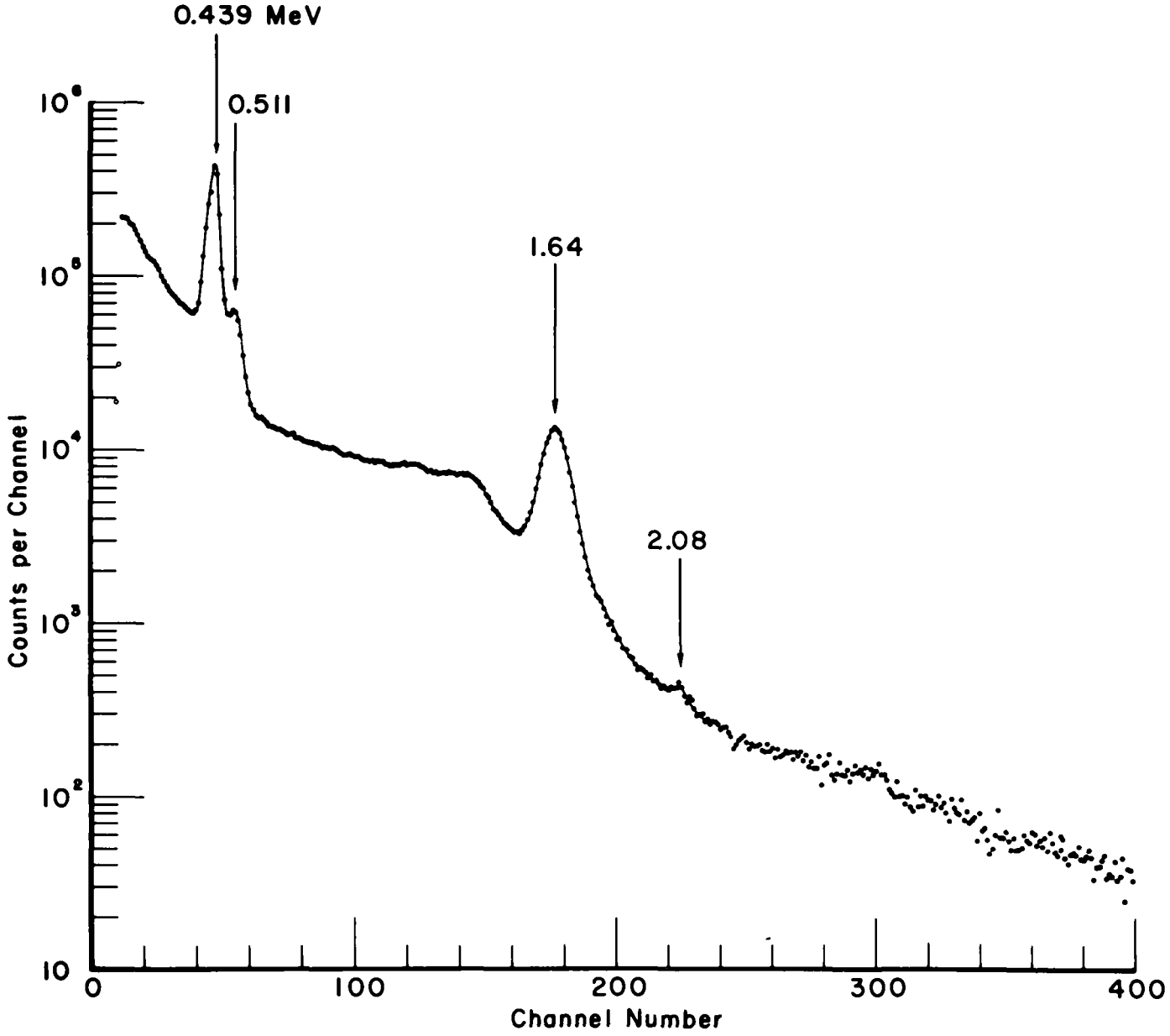
0.439 MeV
0.511
1.64
2.08
Counts per Channel
Channel Number
10
10²
10³
10⁴
10⁵
10⁶
0
100
200
300
400

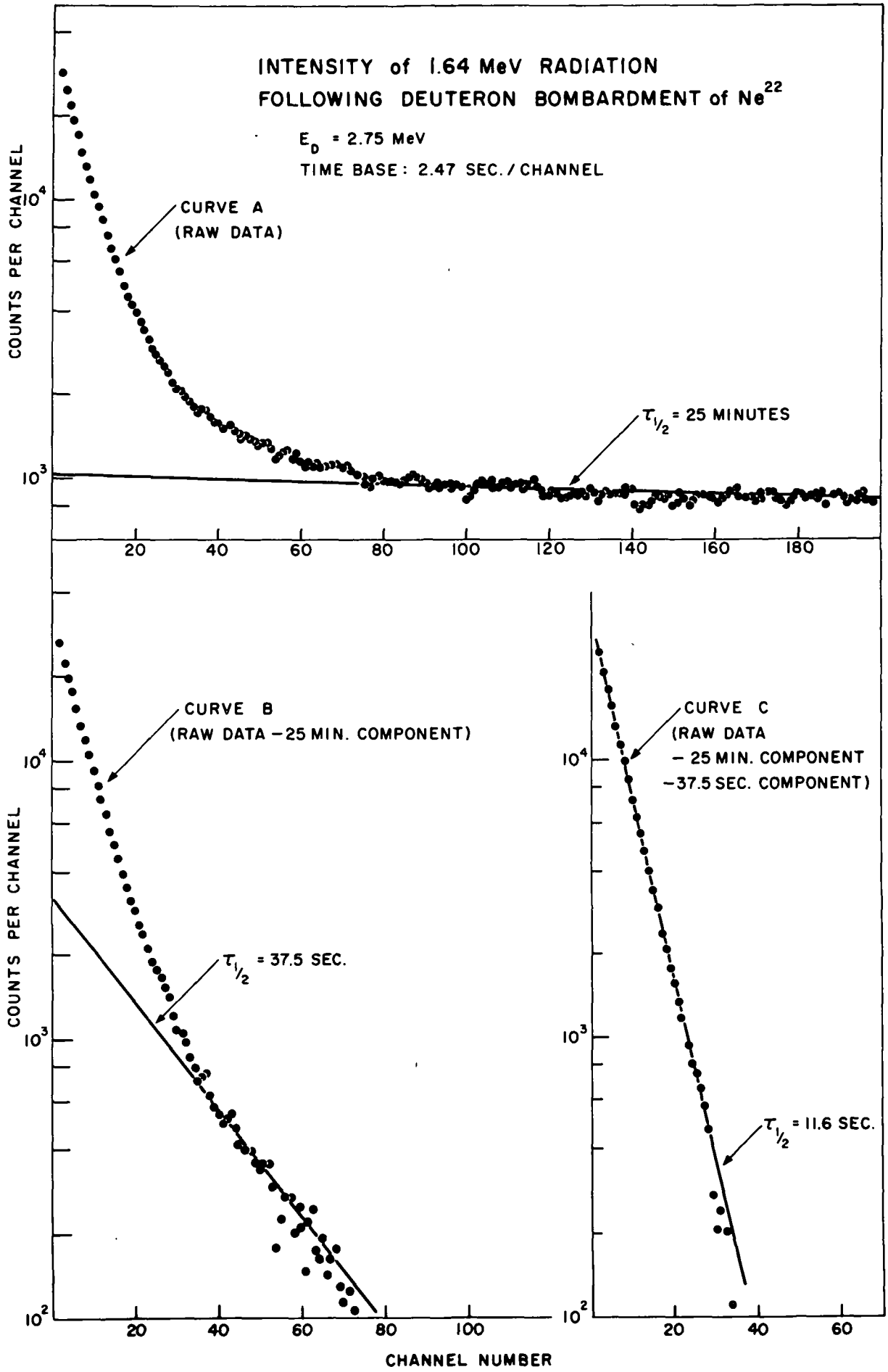
INTENSITY of 1.64 MeV RADIATION
FOLLOWING DEUTERON BOMBARDMENT of Ne^{22}
E_D = 2.75 MeV
TIME BASE: 2.47 SEC./CHANNEL
CURVE A
(RAW DATA)
$\tau_{1/2}$ = 25 MINUTES
CURVE B
(RAW DATA − 25 MIN. COMPONENT)
$\tau_{1/2}$ = 37.5 SEC.
CURVE C
(RAW DATA
− 25 MIN. COMPONENT
−37.5 SEC. COMPONENT)
$\tau_{1/2}$ = 11.6 SEC.
COUNTS PER CHANNEL
CHANNEL NUMBER

determined by multi-time scale analysis of the 1.64 MeV region of the radiation spectrum. The 400 channel analyzer in the multi-scale mode of operation described briefly in Section B was employed for this purpose; the decay curve of 1.64 MeV radiation is shown in Figure IV-8. Similar time-scale analyses were made of the portion of the radiation spectrum just above the 1.64 MeV region, and of the 1.64 MeV region of the spectrum obtained under identical experimental conditions but with a target of He^4 gas. Within the accuracy of the experiment, no corrections to the data of Figure IV-8 were indicated by these additional measurements. A least squares fitting[123] code was used to decompose the decay curve into a number of component halflives and thus determine the halflives of the sources contributing to the 1.64 MeV radiation. The components resulting from this fit to the decay data are indicated in the figure by the solid lines. Extrapolation of the $\tau_{1/2} = 11.6$ sec and the $\tau_{1/2} = 37.5$ sec curves to the zero-time axis provided a unique determination of the relative initial activities of these two radioactive products at the termination of bombardment and ascertained that, under the experimental condition utilized herein, $85 \pm 2\%$ of the 1.64 MeV radiation originated from F^{20} beta decay and $15 \pm 2\%$ originated from Na^{23} beta decay. The experimentally determined halflives and the halflives of Ne^{23} and F^{20} known from previous decay measurements[1] were in excellent agreement and provided further evidence that the identification of the dominant radioactive components as Ne^{23} and F^{20} was indeed correct.

(a) Deexcitation branching ratio of the 2.08 MeV state: The relative intensities of the cascade 2.08 → 0.44 → 0 MeV transition and the direct 2.08 → 0 MeV transition were determined from the direct gamma radiation spectrum to be $97 \pm 3\%$ and $3 \pm 3\%$, respectively. Included in this data analysis were considerations of both the energy dependent efficiency[63] of the NaI spectrometer and the contributions of the 1.64 + 0.44 MeV sum to the 2.08 MeV photopeak region. The sum correction was estimated from the compilations of Vegors et al.[63] to be 1.2% of the total photopeak counts. To provide experimental justification for the sum corrections used, the direct radiation spectrum from a Na^{22} source mounted in a position approximating that of the gas target was examined in detail; the 0.511 + 1.28 MeV

sum peak was found to be within 15% of that expected on the basis of the above referenced efficiency tabulations. The deexcitation branching of the 2.08 MeV state established by this work is presented in Figure IV-13.

Incidental to the branching ratio measurement was a determination of the intensities of the Ne^{23} ground state beta decay branches to the low-lying states of Na^{23}. The relative beta decay intensities were found to be 1% and 27 ± 2% to the 2.08 and 0.44 MeV states, respectively, compared to the values 1% and 32% deduced previously from direct beta decay studies[2].

(b) 2.08 → 0.44 → 0 MeV angular correlation: The same irradiate-count time cycle as before was employed in the 2.08 → 0.44 → 0 MeV angular correlation measurement. Two 3 x 3 inch NaI(Tl) crystals were mounted at 10 cm from the target center on the angular correlation table previously described; one of these was positioned at a fixed angle of 90° to the incident particle beam whereas the second, whose angular position was variable, was aligned to within ± 0.1 cm of the target center by direct detection of the necessarily isotropic radioactive-source radiation. Two voltage gates of equal width were established on the output signal of the fixed spectrometer. One gate (A) contained the energy region of the 1.64 MeV photopeak and the second gate (B) was positioned directly above the energy region of the photopeak. The corresponding coincidence spectra are presented in Figure IV-9. The gamma radiation spectra in coincidence with the voltage gates at each of the angles $\theta = 90^{\circ}$, 180°, 135°, 150°, and 120° were recorded in separate analyzers. As with all radioactive source measurements, the correlation of the radiations depended only on the angle θ between the axes of the detectors. The random coincidence contribution to each spectrum was determined to be less than 5% by insertion of a fixed 0.4 μs time delay into one side of the coincidence circuit.

The angular correlation of the 1.64 and 0.44 MeV radiations was extracted from raw data such as that of Figure IV-9. The area under each 0.44 MeV photopeak was calculated, normalized to the number of 1.64 MeV counts observed in both the fixed and the moving crystals (the ratio of these two numbers was found throughout the run to be constant to within statistical errors), and finally

Figure IV-9. Gamma radiation spectra in time coincidence with radiation in the energy ranges of 1.64 MeV (solid circles) and just above 1.64 MeV (open circles) following deuteron bombardment of Ne^{22}.

Figure IV-10. Angular correlation as a function of $\cos^2\theta$ of the $2.08 \rightarrow 0.44 \rightarrow 0$ MeV cascade members originating in Na^{23} following beta decay of Ne^{23}. The solid curve results from a least squares fit to the data of the correlation function given by Equation III-1.

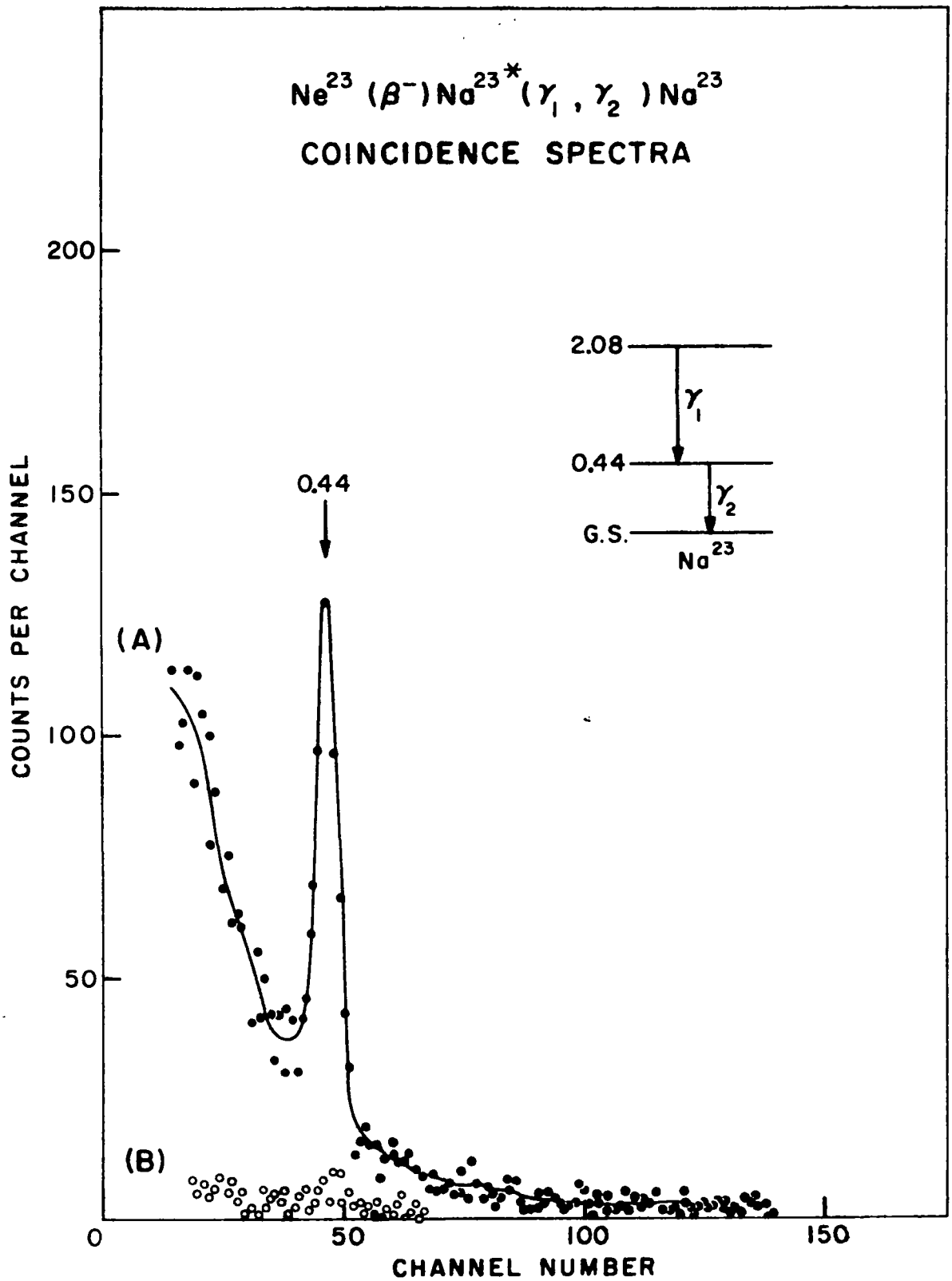
Ne23 (β−) Na23* (γ1 , γ2) Na23
COINCIDENCE SPECTRA
2.08
γ1
0.44
γ2
G.S.
Na23
0.44
(A)
(B)
COUNTS PER CHANNEL
CHANNEL NUMBER
200
150
100
50
0
50
100
150

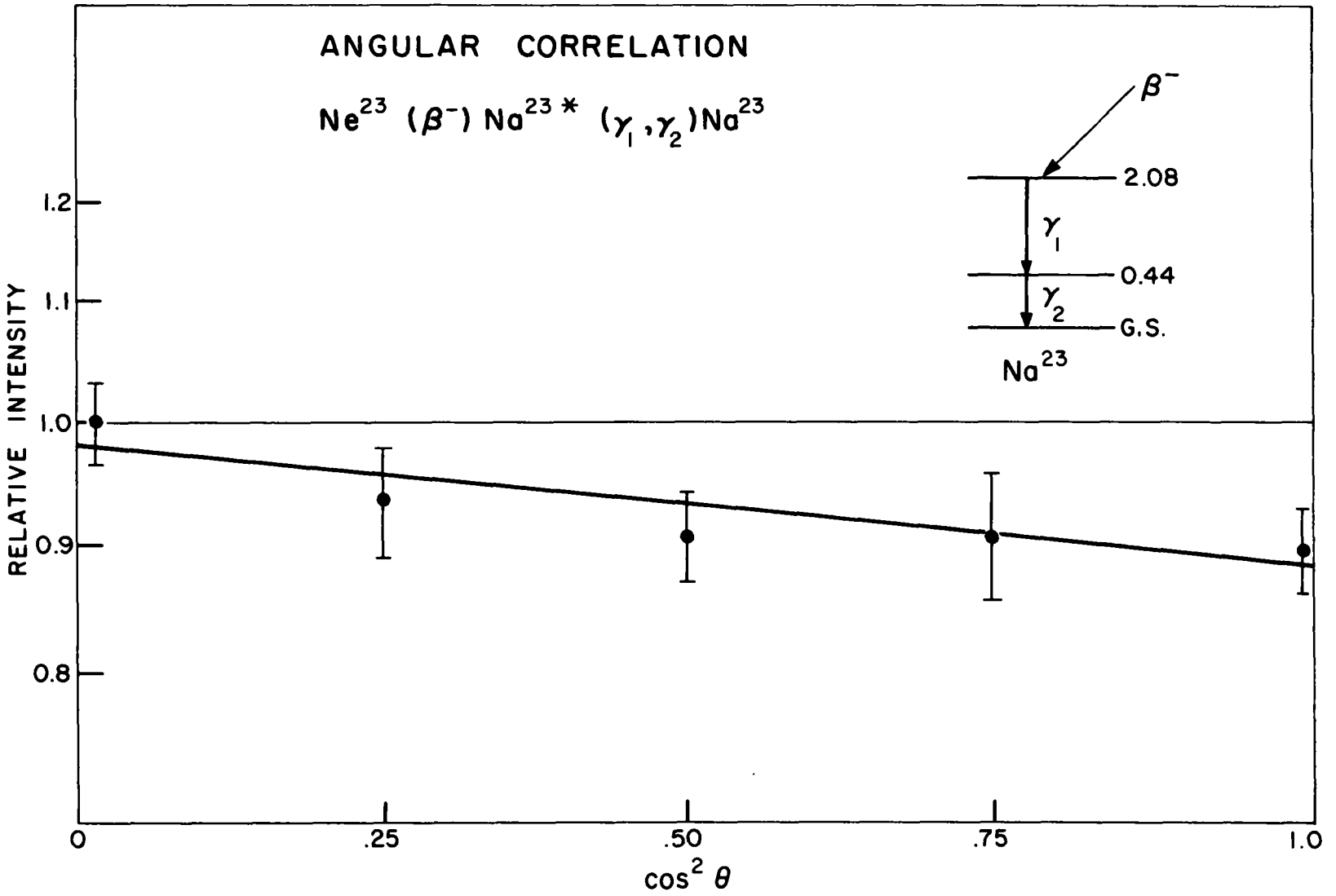
ANGULAR CORRELATION
Ne^{23} (β^-) Na^{23*} $(\gamma_1, \gamma_2)Na^{23}$
β^-
2.08
γ_1
0.44
γ_2
G.S.
Na^{23}
RELATIVE INTENSITY
1.2
1.1
1.0
0.9
0.8
0
.25
.50
.75
1.0
$\cos^2 \theta$

normalized to the 0.44 MeV gamma intensity observed at $\theta = 90^{o}$. The correlation results are presented in Figure IV-10.

A least squares fit to the previously introduced correlation function led to the coefficient ratios $A_2/A_0 = -0.083 \pm 0.032$ and $A_4/A_0 = 0$ which includes the appropriate finite solid angle correction factor[64] of 15% for the A_2/A_0 case. This theoretical fit is indicated in Figure IV-10 by the solid line.

D. Interpretation and Discussion of Experimental Results.

1. 2.80 MeV state in Ne^{21}:

The Ne^{20} (d, p γ) Ne^{21} coincidence measurement has established the deexcitation branching of the 2.80 MeV state as $10 \pm 2\%$ E2 radiation to the $5/2^{+}$ first excited state with the remaining $90 \pm 2\%$ being M1 - E2 radiation to the ground state. This determination is in excellent quantitative accord with the measurement of Howard et al.[107] in which the deexcitation of this level, populated by the Ne^{20} (d, p) Ne^{21} reaction, was investigated with both single crystal and three crystal pari spectrometers. However, the results stated above are in marked disagreement with two further recent measurements; Pelte et al.[112] have populated the 2.80 MeV Ne^{21} state with the reaction F^{19} (He^{3}, p) Ne^{21} and have found it to deexcite 50% to the first excited state and 50% to the ground state, Bent et al.[113] have used the Be^{9} (O^{16}, α) Ne^{21} reaction to form the 2.80 MeV state and have determined its branching as 40% to the first excited state and 60% to the ground state.

The reason for the marked discrepancies involved in these sets of measurements is not known. One explanation would be the existence of a second, as yet un unresolved, state of excitation at 2.80 ± 0.02 MeV which is more strongly populated by the (He^{3}, p) and (O^{16}, α) reaction than by the (d, p) reaction. Since the assignment $J^{\pi} = 1/2^{+}$ was made specifically to the state populated predominantly through the (d, p) reaction, the postulated "2.80" MeV state need not have equivalent values. Indeed, it is very unlikely that the J^{π} of this state is $1/2^{+}$ because of the strong mixing between the two states which would necessarily result if the states had identical spins and parities. Furthermore, the well known perturbations existing between similar closely spaced states would tend to move them farther apart in

energy than the 20 keV range within which they apparently lie.

Lacking particle measurements of sufficient resolution, the postulated state may, in fact, reveal itself in a non-isotropic distribution of any of its deexcitation branches. Work is now in progress to investigate this possibility using both the F^{19} (He^3, p) Ne^{21} and the Ne^{22} (He^3, α) Ne^{21} reactions to populate the 2.80 MeV states(s).

2. Distribution of 3.57 MeV radiation in Na^{21}:

The distribution of the 3.57 MeV radiations corresponding to the 3.57 $\rightarrow$0 MeV transition in Na^{21}, has been measured by a number of investigators. The Legendre expansion coefficients obtained in each of these studies are listed in Table IV-1.

TABLE IV-1

Experimental distribution coefficients of the 3.57 MeV to ground state transition in Na^{21}.

Authors	A_2/A_0	A_4/A_0
Val' ter et al.	-0.21	+0.02
Benenson and Lidofsky	-0.31	~0
Howard	-0.52 ± 0.04	$+0.11 \pm 0.04$
present work	-0.26 ± 0.02	0.0 ± 0.03

The values of A_2/A_0 and A_4/A_0 of the present study are in qualitive agreement with both the work of Val' ter et al[115] and the work of Benenson and Lidofsky[100]. The measurement of Howard[124] should be withdrawn, however, because of incorrect background subtraction in the data analysis.

The theoretical proton-gamma radiation correlation function[69] for the capture of a d-wave proton into a spin 5/2 state and the subsequent M1-E2 deexcitation radiation into a spin 3/2 state is given in Figure IV-11. The experimentally determined coefficients are indicated by the horizontal bands; the corresponding allowed values of the M1-E2 parameter δ are indicated by the vertical band.

Figure IV-11. Angular distribution coefficient ratios as a function of the E2-M1 mixing parameter δ for the spin sequence indicated. The shaded bands show the values of the coefficient ratios determined by experiment; the dashed vertical lines enclose values of δ compatible with the measured A_2/A_0 and A_4/A_0 ratios.

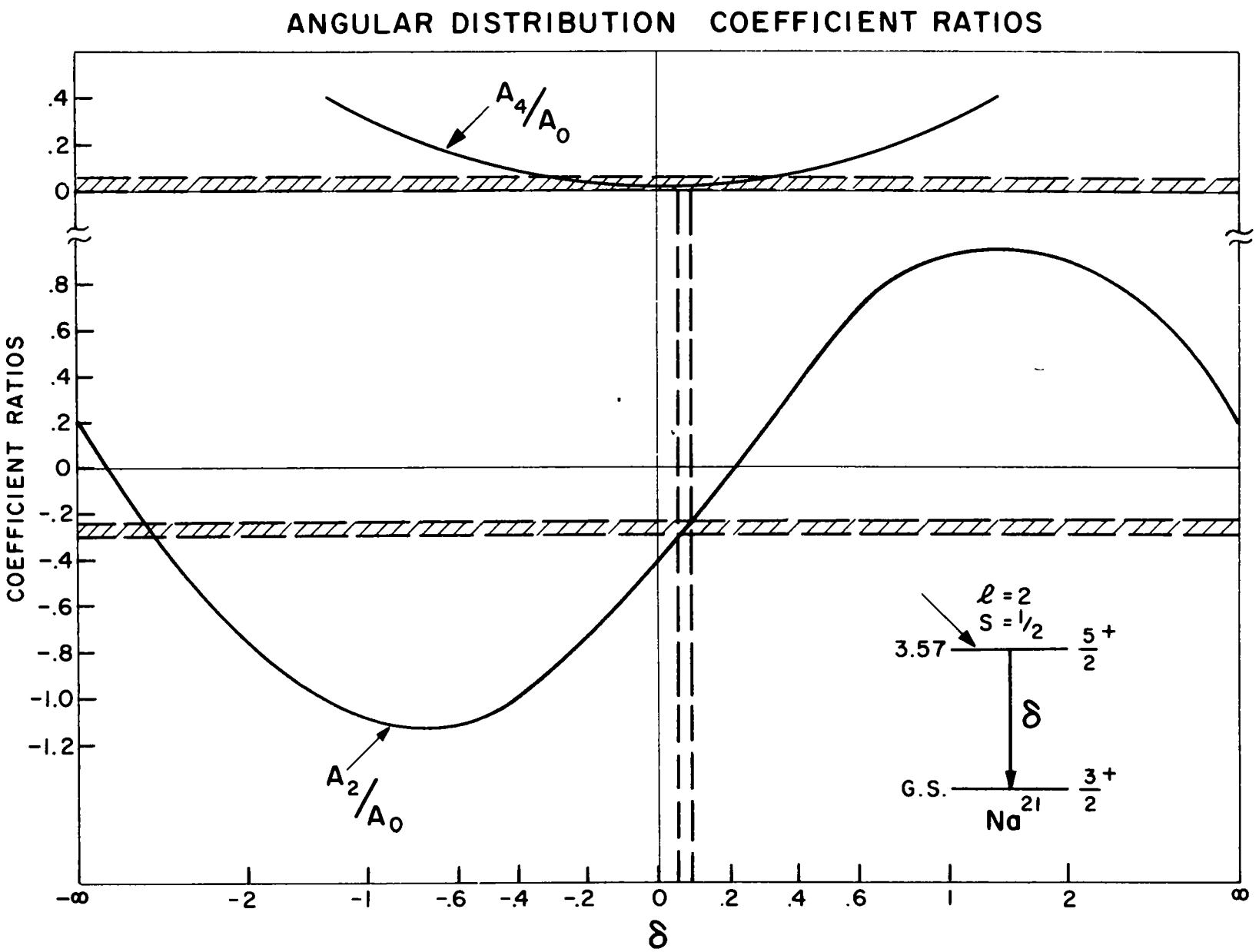
ANGULAR DISTRIBUTION COEFFICIENT RATIOS
COEFFICIENT RATIOS
.4
.2
0
.8
.6
.4
.2
0
-.2
-.4
-.6
-.8
-1.0
-1.2
A_4/A_0
A_2/A_0
$\ell = 2$
$S = 1/2$
3.57
$\frac{5}{2}^+$
δ
G.S.
$\frac{3}{2}^+$
Na^{21}
$-\infty$
-2
-1
-.6
-.4
-.2
0
.2
.4
.6
1
2
∞
δ

The mixing parameter is thus established as $0.05 \leq \delta \leq 0.09$ for the 3.57 MeV Na^{21} radiation.

3. Deexcitations of the second excited states in Ne^{21}, Na^{21}, and Na^{23}.

The angular momentum value $7/2^+$ has been previously assigned[105] to the 2.08 MeV Na^{23} state on the basis of an angular distribution measurement of the weak 2.70 MeV deexcitation branch cascading from the 4.78 MeV Na^{23} state through the 2.08 MeV state. The large uncertainty connected with this measurement indicates, however, the desireability of further studies to corroborate this probable $7/2^+$ assignment, although from examination of the known deexcitation cascades through the 2.08 MeV state it seems entirely reasonable to limit the possible angular momentum assignments to either 5/2 or 7/2.

Since the electric quadrupole—magnetic dipole amplitude ratio for the 0.44 to 0 MeV transition in Na^{23} has been established with some precision as $0.03 \leq \delta \leq 0.06$ by the $(p,p'\gamma)$ studies of Mizobuchi et al.[125] only the spin sequences $5/2 \rightarrow 5/2 \xrightarrow{0.03 \leq \delta \leq 0.06} 3/2$ and $7/2 \rightarrow 5/2 \xrightarrow{0.03 \leq \delta \leq 0.06} 3/2$ need be considered in the analysis of the correlation data from the cascade deexcitation of the 2.08 MeV state. The corresponding theoretical correlation functions[69] and the measured A_2/A_0 correlation coefficient of -0.083 ± 0.032 are shown in Figure IV-12. As is evident from the vertical bands which indicate the values of ρ allowed by experiment for each spin sequence, the angular correlation of the radiations from the 2.08 MeV state does not provide information sufficient for an unambiguous angular momentum assignment to this state; for spin 7/2 of the 2.08 MeV state the multipole mixing parameter in the 1.64 MeV deexcitation branch is given by $-0.65 \leq \rho \leq -0.25$ or $-2.5 \leq \rho \leq -1.3$ whereas for spin 5/2 of the 2.08 MeV state the multipole mixing parameter is given by $-0.24 \leq \rho \leq 0.02$ or $1.5 \leq \rho \leq 3.0$.

The particular deexcitation branching measurements determined in the present studies, as well as electric quadrupole–to– magnetic dipole mixing ratios established in previous measurements, are summarized in Figure IV-13. Reference to the figure indicates (i) ground state spins of 3/2 in all cases which alone strongly suggest the applicability of collective model formulations since

Figure IV-12. Angular correlation coefficient ratios for the spin sequences $5/2 \rightarrow 5/2 \rightarrow 3/2$ and $7/2 \rightarrow 5/2 \rightarrow 3/2$ as functions of the E2-M1 mixing parameter ρ at particular values of the E2-M1 mixing parameter δ. The experimentally determined values of A_2/A_0 are indicated by the shaded bands; the dashed vertical lines enclose values of ρ compatible with the correlation measurements.

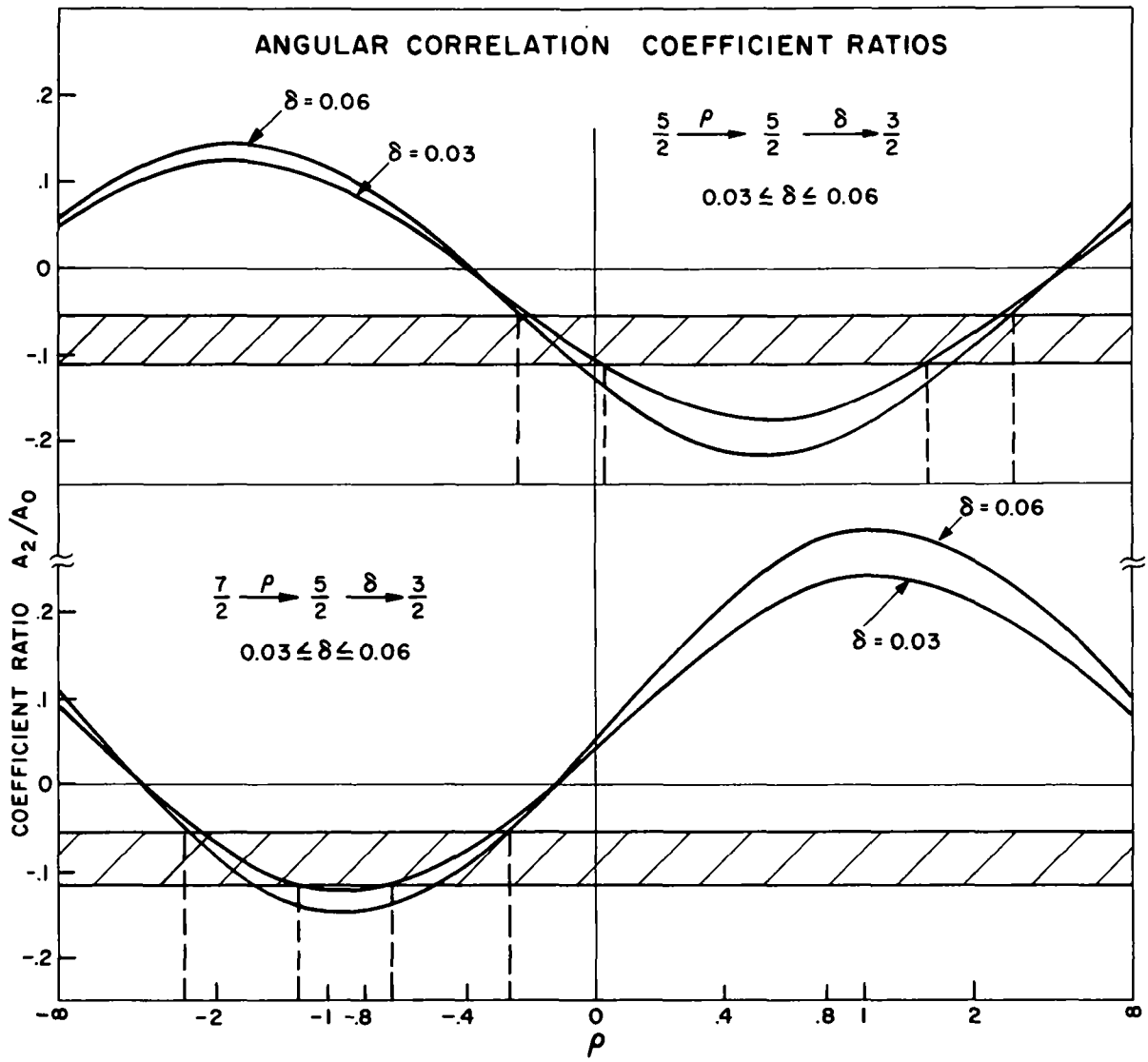
ANGULAR CORRELATION COEFFICIENT RATIOS
δ = 0.06
δ = 0.03
5/2 → ρ → 5/2 → δ → 3/2
0.03 ≤ δ ≤ 0.06
7/2 → ρ → 5/2 → δ → 3/2
0.03 ≤ δ ≤ 0.06
δ = 0.06
δ = 0.03
COEFFICIENT RATIO A2/A0
.2
.1
0
-.1
-.2
-∞
-2
-1
-.8
-.4
0
.4
.8
1
2
∞
ρ

these formulations correctly predict the ground state assignment $J^{\pi} = 3/2^{+}$ in contrast to the simple spherical shell model predictions of $J^{\pi} = 5/2^{+}$; (ii) first excited state energies of 0.453, 0.335, and 0.439 MeV for Ne^{21}, Na^{21}, and Na^{23}, respectively, and spins of 5/2 in all cases; (iii) first excited state deexcitation mixing ratios of $0.004 \leq \delta \leq 0.03$, $0 \leq \delta \leq 0.10$, and $0.03 \leq \delta \leq 0.06$, respectively; (iv) second excited energies of 1.75, 1.73, and 2.08 MeV; and finally (v) second excited state crossover deexcitation intensities of 7 ± 1, 11 ± 2, and $3 \pm 3\%$ in the respective cases. The striking similarities in both the static and dynamic properties of these low-lying states provides considerable evidence in support of the Nilsson model interpretation of these nuclei as having equivalent structure; furthermore, the similarity of behavior of the 2.08 MeV Na^{23} state with that of the known $7/2^{+}$ states in Ne^{21} and Na^{21} is perhaps the firmest evidence yet available for a $7/2^{+}$ assignment to the state. The angular correlation measurement would in this case limit the E2-M1 mixing parameter of the 1.64 MeV deexcitation radiation from the 2.08 MeV state to the values $-0.65 \leq \rho \leq -0.25$ or $-2.5 \leq \rho \leq -1.3$.

It is of interest to examine the applicability of the Nilsson model to the intraband deexcitation branching of the three $7/2^{+}$ second excited states of Ne^{21}, Na^{21}, and Na^{23} which is summarized in Figure IV-13. The branching ratio for a $7/2^{+}$ state deexciting by M1-E2 radiation to a $5/2^{+}$ state and by E2 radiation to a $3/2^{+}$ state is given by the expression

$$\text{B.R.} = \frac{T(E2,\ 7/2 \rightarrow 3/2)}{T(E2,\ 7/2 \rightarrow 5/2) + T(M1,\ 7/2 \rightarrow 5/2)} \quad . \tag{IV-1}$$

In the Nilsson notation[32] the magnetic dipole transition probability T(M1) between states of spins J_i and J_f within the rotational band based on Nilsson orbit 7 is

$$T(M1) = \frac{1}{3\hbar} \left[\frac{E}{\hbar c}\right]^3 \left[\frac{e\hbar}{2Mc}\right]^2 \left[\left(J_i 1 \tfrac{3}{2} 0 \mid J_f \tfrac{3}{2}\right)\right]^2 G_{M1}^2 \ \text{sec}^{-1} \tag{IV-2}$$

where $$G_{M1}(\eta) = 3g_1 - 3g_R + (g_s - g_1)\left[a_{21}(\eta)^2 - a_{22}(\eta)\right] . \tag{IV-3}$$

Figure IV-13. Partial energy level spectra, deexcitation branchings, and E2-M1 multipole mixtures observed experimentally in the Ne^{21}, Na^{21}, and Na^{23} nuclear systems. Excitation energies are indicated in MeV. The deexcitation branching of the 2.08 MeV state of Na^{23} should read $97 \pm 3\%$ to the 0.44 MeV state and $3 \pm 3\%$ to the ground state.

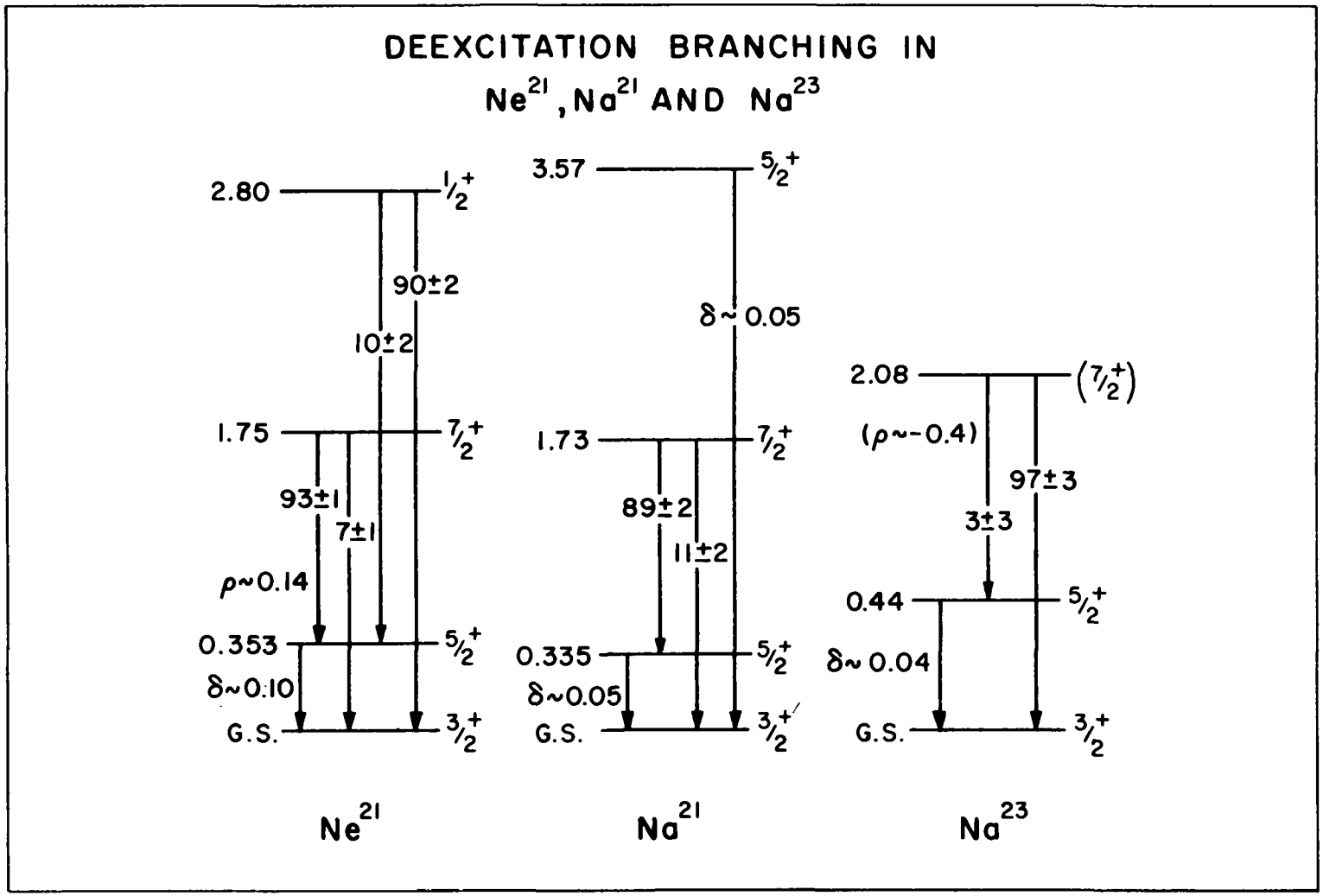
DEEXCITATION BRANCHING IN
Ne21, Na21 AND Na23
2.80
1/2+
90±2
10±2
1.75
7/2+
93±1
7±1
ρ~0.14
0.353
5/2+
δ~0.10
G.S.
3/2+
Ne21
3.57
5/2+
δ~0.05
1.73
7/2+
89±2
11±2
0.335
5/2+
δ~0.05
G.S.
3/2+
Na21
2.08
(7/2+)
(ρ~-0.4)
97±3
3±3
0.44
5/2+
δ~0.04
G.S.
3/2+
Na23

In these expressions $a_{21}(\eta)$ and $a_{22}(\eta)$ are the normalized Nilsson eigenfunction coefficients, g_l and g_s are respectively the orbital and the intrinsic angular momentum gyromagnetic ratios associated with the odd nucleon and g_R is the gyromagnetic ratio associated with the rotation of the core, M is the nucleon mass, and E is the energy of the transition.

The expression for the corresponding electric quadrupole transition probability including both single particle and collective contributions has been derived by McManus and Sharp and reported by Bromley et al.[126]. For transitions within the rotational band based on Nilsson orbit 7, the expression becomes

$$T(E2) = \frac{e^2}{15\hbar}\left[\frac{E}{\hbar c}\right]^5\left[\frac{\hbar}{M\omega_o}\right]^2\left[\left(J_i 2 \tfrac{3}{2} 0 \,|\, J_f \tfrac{3}{2}\right)(1 + y^c_{E2})\right]^2 G^2_{E2} \qquad \text{(IV-4)}$$

wherein

$$G_{E2} = 0.50\, a_{21}(\eta)^2 - a_{22}(\eta)^2 \,, \qquad \text{(IV-5)}$$

$$y^c_{E2} = \frac{\varkappa Z A^{1/3}}{G_{E2}}\,\eta\,(1 + \tfrac{2}{3}\delta) \,, \qquad \text{(IV-6)}$$

and

$$\hbar\omega_o \cong 41 A^{-1/3}\,(1 - \tfrac{4}{3}\delta^2 - \tfrac{16}{27}\delta^3)^{-1/6} \,. \qquad \text{(IV-7)}$$

Once again, $a_{21}(\eta)$ and $a_{22}(\eta)$ are the normalized Nilsson eigenfunction coefficients, Z and A are the atomic and mass numbers, and η and δ are the core distortion parameters related (as shown in Equation I-28) by the spin-orbit coupling parameter $\varkappa$.

As previously mentioned, the equations above are to be applied to electromagnetic transitions between members of the $K^\pi = 3/2^+$ rotational band based on Nilsson orbit 7. Although the $7/2^+$, $5/2^+$, and $3/2^+$ states being considered herein are not expected to be of pure $K^\pi = 3/2^+$ configuration, the collective effect of E2 transition enhancements is known to be most pronounced for intraband transitions, thus these E2 transitions should dominate the calculated deexcitation branching. On this basis, the possible band mixing to these states has been neglected in the following calculation.

Quantitative predictions[127] of the detailed branching ratio of interest in each of the systems under consideration require further information concerning the size and magnitude of the nuclear core deformation (parameterized by η),

the strength of the spin-orbit coupling term (parameterized by $\varkappa$), and the value of the gyromagnetic ratio of the core (parameterized by g_R).

(i) The collective model calculations[36, 71, 100, 101, 103, 105, 106] previously used to represent the static characteristics such as level spacing and spin assignments of the systems Ne^{21}, Na^{21}, and Na^{23} have indicated a core deformation parameter of $3 < \eta < 4$ for all three of these nuclei. Furthermore, Nilsson model interpretations[45] of properties of F^{19} suggest $\eta \cong 3$ for this nucleus, and similar considerations[36, 127] of the nuclei Mg^{25}, Al^{25}, and Al^{27} indicate $\eta \cong 3.5$ for these systems; thus the systematic behavior of η in this mass region provides further evidence in support of the $3 < \eta < 4$ range of values suggested above.

(ii) The value 0.05 was originally chosen for the spin-orbit coupling parameter $\varkappa$ in order to reproduce for zero deformation ($\delta = 0$) the level spectrum sequence which was first proposed by Klinkenberg[11] on the basis of empirical data interpreted in terms of the spherical shell model. Subsequent considerations, however, indicate that a more realistic estimate for this parameter may be based upon the observed static electric quadrupole moment Q_s of a given system. Q_s and u are related by the expression[128]

$$Q_s = \frac{3K^2 - J(J+1)}{(J+1)(2J+1)} 1.15\, ZA^{2/3} \varkappa\eta\left(1 + \frac{2}{3}\varkappa\eta\right) 10^{-26} \text{cm}^2 . \qquad \text{(IV-8)}$$

The experimentally measured values[1,2] of Q_s are 0.093 and 0.101 barns for the respective systems Ne^{21} and Na^{23}. If η is restricted to the region $3 < \eta < 4$ as suggested above, then the values of $\varkappa$ are determined in both cases to be $0.14 < \varkappa < 0.11$; this result is qualitatively consistent with the value of $\varkappa$ adduced from similar considerations of adjacent nuclei, for example $\varkappa = 0.08$ has been shown[36] to lead to a successful representation of Mg^{25} and Al^{25}. There is also some evidence[36] that $\varkappa = 0.13$ is the most appropriate value in the collective model interpretation of O^{17}.

(iii) If irrotational flow is assumed for the core of the Nilsson model, the value for the gyromagnetic ratio of the core is given[32] by $g_R \cong Z/A \cong 0.5$. However, experimental evidence currently available for sd-shell nuclei suggests that a value of 0.3 is perhaps more appropriate for this parameter. Finally,

the expression[32] which relates g_R to the measured static dipole moment μ of a nucleus through the collective model framework, although known to be of limited validity because of non-negligible mesonic contributions to μ ignored in its derivation, may nevertheless be employed to indicate an approximate value of g_R;

$$g_R = \frac{\mu}{J} - \frac{G_{M1}(\mu)}{2J(J+1)} \quad . \tag{IV-9}$$

Dipole moments of -0.661 and 2.216 nm have been observed experimentally for the ground states of Ne^{21} and Na^{21}, respectively. These values are best reproduced by Equation IV-9 when $\eta \cong 2.2$ and $g_R = 0.23$.

The deexcitation branching from the second excited $7/2^+$ states in Ne^{21}, Na^{21}, and Na^{23} have been computed using Equations IV-2 and IV-4 with the assumed values of $\varkappa$ and g_R indicated above. The results of these calculations are presented in Figures IV-14, 15, and 16 in which the theoretical value of the branching ratio is plotted as a function of deformation parameter η over the range $-6 < \eta < 6$; the corresponding branching ratios determined experimentally herein are indicated by the shaded bands. The value of η compatible with the considerations presented above are indicated by the dashed vertical lines.

In the case of Ne^{21}, reasonable quantitative agreement between the predicted and the measured branching ratio of the deexcitation of the second excited state occurs for $3.0 < \eta < 3.5$, $0.1 < \varkappa < 0.08$, and $0.23 < g_R < 0.5$ in accordance with the limitations of these parameters which were previously deduced. Qualitative theoretical and experimental agreement is also obtained in the deexcitation branching of the second excited state of Na^{23} although uncertainties assigned to the experimental measurement of this branching preclude more meaningful quantitative comparison.

Agreement is not as good for the predicted branching of the $7/2^+$ state in Na^{21} since the measured value of this deexcitation is about a factor of 2 larger than that generated by the model with values of parameters η, $\varkappa$, and g_R consistent with previous considerations. This disagreement in the Na^{21} system could be "removed" by increasing $\varkappa$ from a value of 0.1 to a value of about 0.12; however, in view of the considerable uncertainties already associated with the

Figure IV-14. Relative radiative widths Γ_B/Γ_A of the cascade and cross-over deexcitations of the $7/2^+$, second excited, Ne^{21} state as predicted by the Nilsson model for various values of the model parameters κ, g_R, and η. The radiative widths are related to the transition probabilities defined in the text according to $\Gamma_B/\Gamma_A = T_B(E2) / (T_A(M1) + T_A(E2))$. The shaded band indicates the experimentally determined ratio Γ_B/Γ_A; the dashed vertical lines enclose values of the deformation parameter η compatible with other experimentally determined properties of Ne^{21}.

Figure IV-15. Relative radiative widths Γ_B/Γ_A of the cascade and cross-over deexcitations of the $7/2^+$, second excited, Na^{21} state as predicted by the Nilsson model.

Figure IV-16. Relative radiative widths Γ_B/Γ_A of the cascade and cross-over deexcitations of the $7/2^+$, second excited, Na^{23} state as predicted by the Nilsson model.

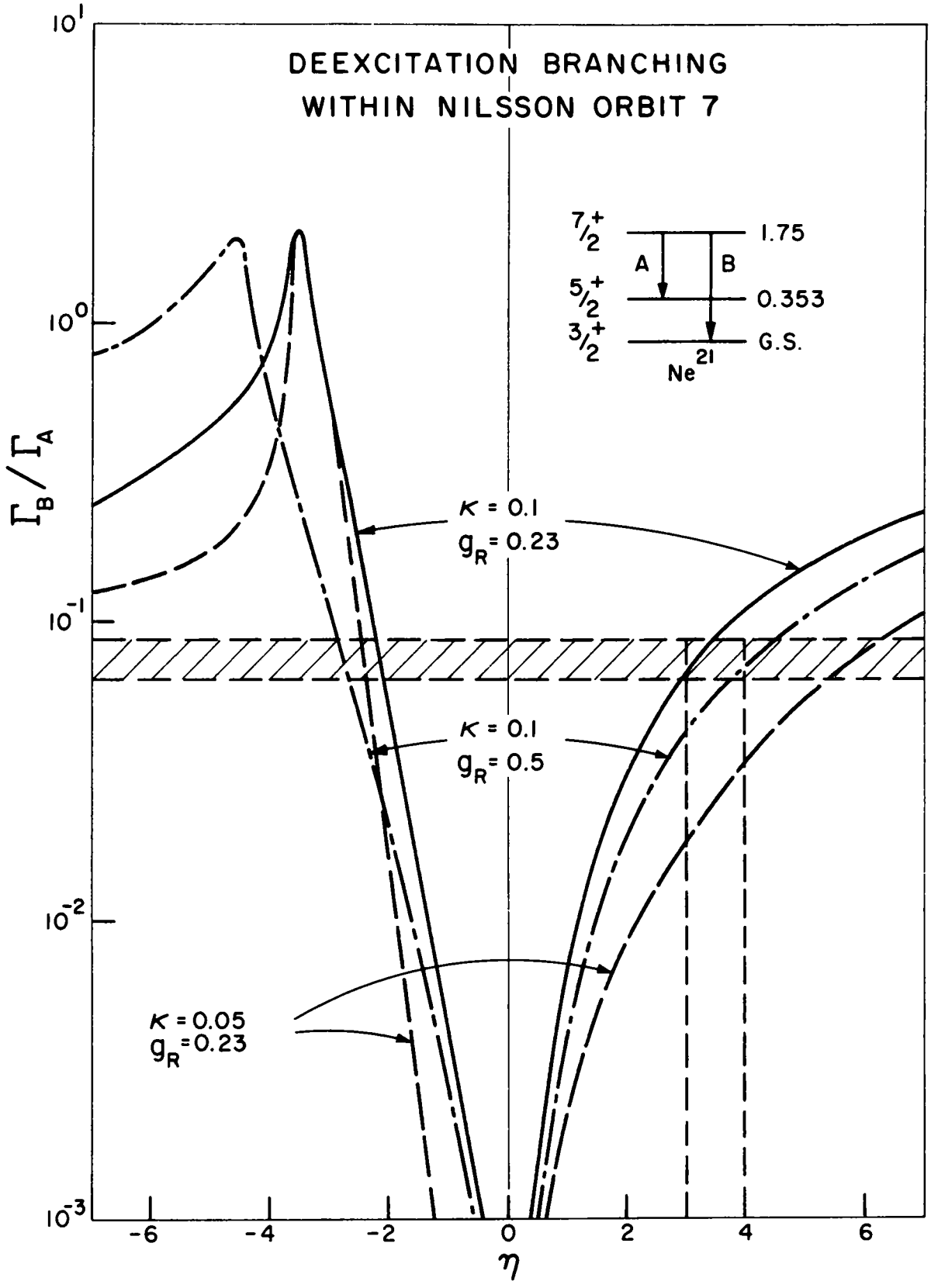
DEEXCITATION BRANCHING
WITHIN NILSSON ORBIT 7
$7/2^+$
1.75
A
B
$5/2^+$
0.353
$3/2^+$
G.S.
Ne^{21}
$\kappa = 0.1$
$g_R = 0.23$
$\kappa = 0.1$
$g_R = 0.5$
$\kappa = 0.05$
$g_R = 0.23$
Γ_B / Γ_A
10^1
10^0
10^{-1}
10^{-2}
10^{-3}
-6
-4
-2
0
2
4
6
η

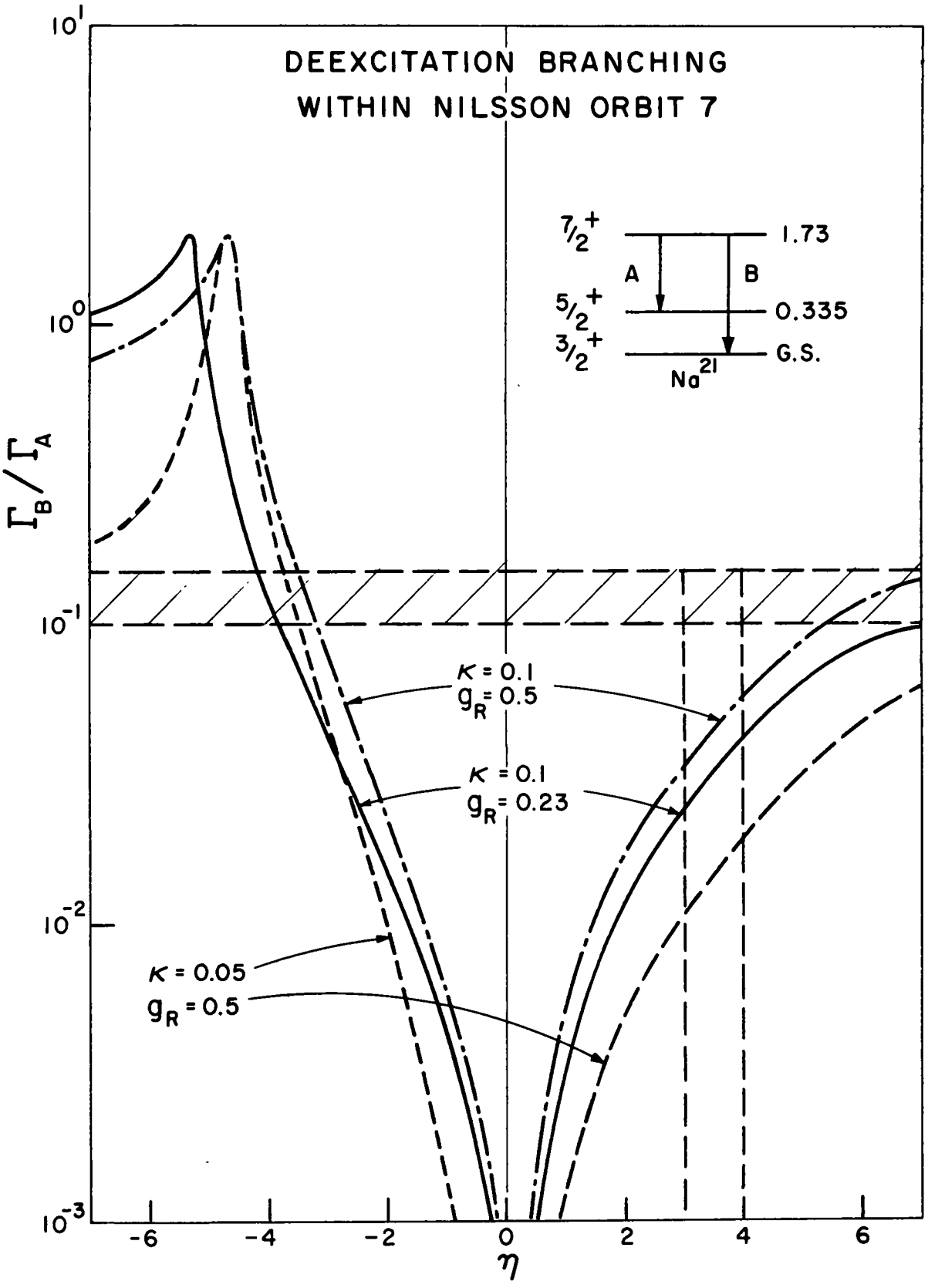
DEEXCITATION BRANCHING
WITHIN NILSSON ORBIT 7
7/2+
1.73
A
B
5/2+
0.335
3/2+
G.S.
Na21
10^1
10^0
10^-1
10^-2
10^-3
Γ_B / Γ_A
κ = 0.1
g_R = 0.5
κ = 0.1
g_R = 0.23
κ = 0.05
g_R = 0.5
-6
-4
-2
0
2
4
6
η

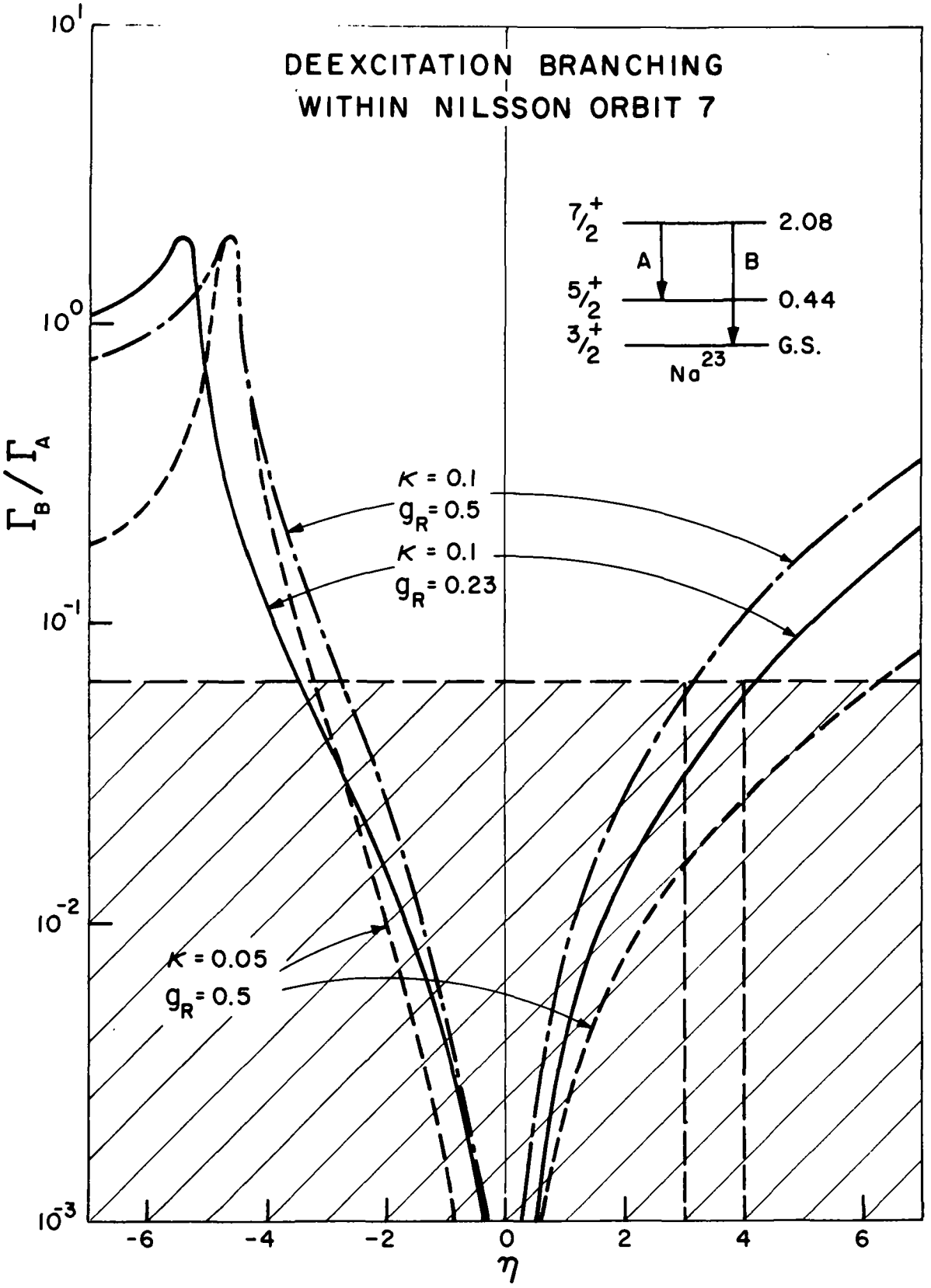
DEEXCITATION BRANCHING
WITHIN NILSSON ORBIT 7
7/2+
2.08
A
B
5/2+
0.44
3/2+
G.S.
Na23
κ = 0.1
gR = 0.5
κ = 0.1
gR = 0.23
κ = 0.05
gR = 0.5
ΓB / ΓA
η
10¹
10⁰
10⁻¹
10⁻²
10⁻³
-6
-4
-2
0
2
4
6

model parameters, and because of the lack of more precise systematic measurements of dynamic level properties in these and neighboring nuclei, it is doubtful whether further calculations of this type would be of value at present in elucidating in more detail the significance of the Nilsson model in these nuclear systems. When more extensive experimental information becomes available, it will certainly be of interest to examine the model predictions in a more comprehensive way.

E. Summary

Studies on the $Ne^{20}(d,p)Ne^{21}$ reaction with coincident proton-gamma detection have permitted an accurate determination of the deexcitation branching of the Ne^{21} states at 2.80 and 1.75 MeV excitation. Comparison of the 2.80 MeV branching ratio with earlier measurements of several independent investigators suggests the existence of a second, as yet unresolved, excited state in Ne^{21} of nearly equivalent energy and of $J^{\pi} \neq 1/2^{+}$.

Measurements utilizing the $Ne^{20}(p,\gamma)Na^{21}$ resonance capture reaction with coincident gamma-gamma detection of the radiation depopulating the resonant state at 3.57 MeV have established the deexcitation branching of the 1.73 MeV state in Na^{21}. Angular distribution measurements of the direct 3.57 MeV to ground state deexcitation radiation limit the M1-E2 multipole mixing parameter of this transition to the range of values $0.05 < \delta < 0.09$ in fair agreement with the previous work of Benenson and Lidofsky[100].

Investigations of deexcitation gamma radiation following the beta decay of the Ne^{23} ground state have provided data on the halflife of Ne^{23} and the relative beta decay branching to the first two excited states in Na^{23} in excellent agreement with the corresponding values deduced in previously reported measurements.

Finally, studies of the cascade branching and angular correlation of the $2.08 \rightarrow 0.44 \rightarrow 0$ MeV deexcitation transitions in Na^{23} have established the spin of the 2.08 MeV state as most probably 7/2 but cannot rule out unambiguously the possibility of 5/2.

The experimentally determined gamma radiation branchings from the second excited $7/2^{+}$ states in all three systems Ne^{21}, Na^{21}, and Na^{23} have been inter-

compared within the Nilsson model framework. To the extent that the model formalism predicts similar deexcitation behavior throughout these nuclei, the calculated branching ratios are in agreement with experiment further indicating the definite significance of the collective model approaches in this mass region; however, only approximate quantitative agreement is obtained between the predicted and the measured branching ratios.

A more realistic evaluation of the model predictions with regard to these nuclear systems may be made when further experimental information concerning the static and dynamic properties of these nuclei becomes available.

V. INITIAL STUDIES OF THE REACTION $Ne^{22}(d,p)Ne^{23}$

A. Introduction

The successful description[36] of the low-lying states in Al^{25} and Mg^{25} as members of overlapping, strongly- coupled, rotational bands has prompted the extension of this description to many neighboring nuclei. A number of these calculations have been discussed in detail in preceding chapters; for example, the treatment of F^{19} by Paul[45], Ne^{21} by Freeman[101], Na^{23} by Paul and Montague[104], Al^{27} by Almqvist et al.[128], and Si^{29} by Bromley et al.[126]. These Nilsson model descriptions have been found to be in good qualitative accord with experiment; the best quantitative agreement, however, is still that found between the model predictions and the experimental measurements of nuclei of odd-nucleon number $\eta = 13$, e.g. Mg^{25}, Al^{25}, and Al^{27}. As pointed out by Litherland et al.[36] the success enjoyed by the model in these systems is undoubtedly due, in part at least, to the simplification resulting from the lack of Coriolis mixing between the $K = 5/2$ and $K = 1/2$ bands which lie lowest in intrinsic energy for these systems and, consequently, are predominant in the model representation of the nuclear states of the systems.

The experimental level diagrams for four of the $\eta = 13$ nuclei are shown in Figure V-1. The identification of the various states as analogous members of rotational bands is indicated schematically by the arrows where the solid line denotes members of the $K^{\pi} = 5/2^{+}$ band based on Nilsson orbit 5, the dashed line denotes members of the $1/2^{+}$ band based on orbit 9, and the broken line denotes members of the $1/2^{+}$ band based on orbit 11. The odd nucleon in each of these nuclei is, of course, the fifth nucleon after the closed O^{16} shell; consequently, Ne^{23} would be expected within the spirit of the Nilsson model to show the same sort of collective behavior as Al^{25}, Mg^{25}, and Al^{27}. Reference to Figure V-1 indicates, however, that in spite of the theoretical interest in intercomparing Ne^{23} with the mass-25 systems, the experimental information available[1] for this nucleus is so sparce as to provide essentially no evidence either for or against its anticipated rotational properties.

Figure V-1. Experimentally observed energy level spectra of the odd-nucleon count $\eta = 13$ nuclear systems Ne^{23}, Mg^{25}, Al^{25}, and Al^{27}. Energy levels corresponding to analogous members of rotational bands within the framework of the Nilsson model are indicated by the arrows where the solid, dashed, and broken lines correspond to bands based on orbits 5, 9, and 11, respectively. Arrows in parentheses connecting states of Ne^{23} and Mg^{25} are based on the work presented herein.

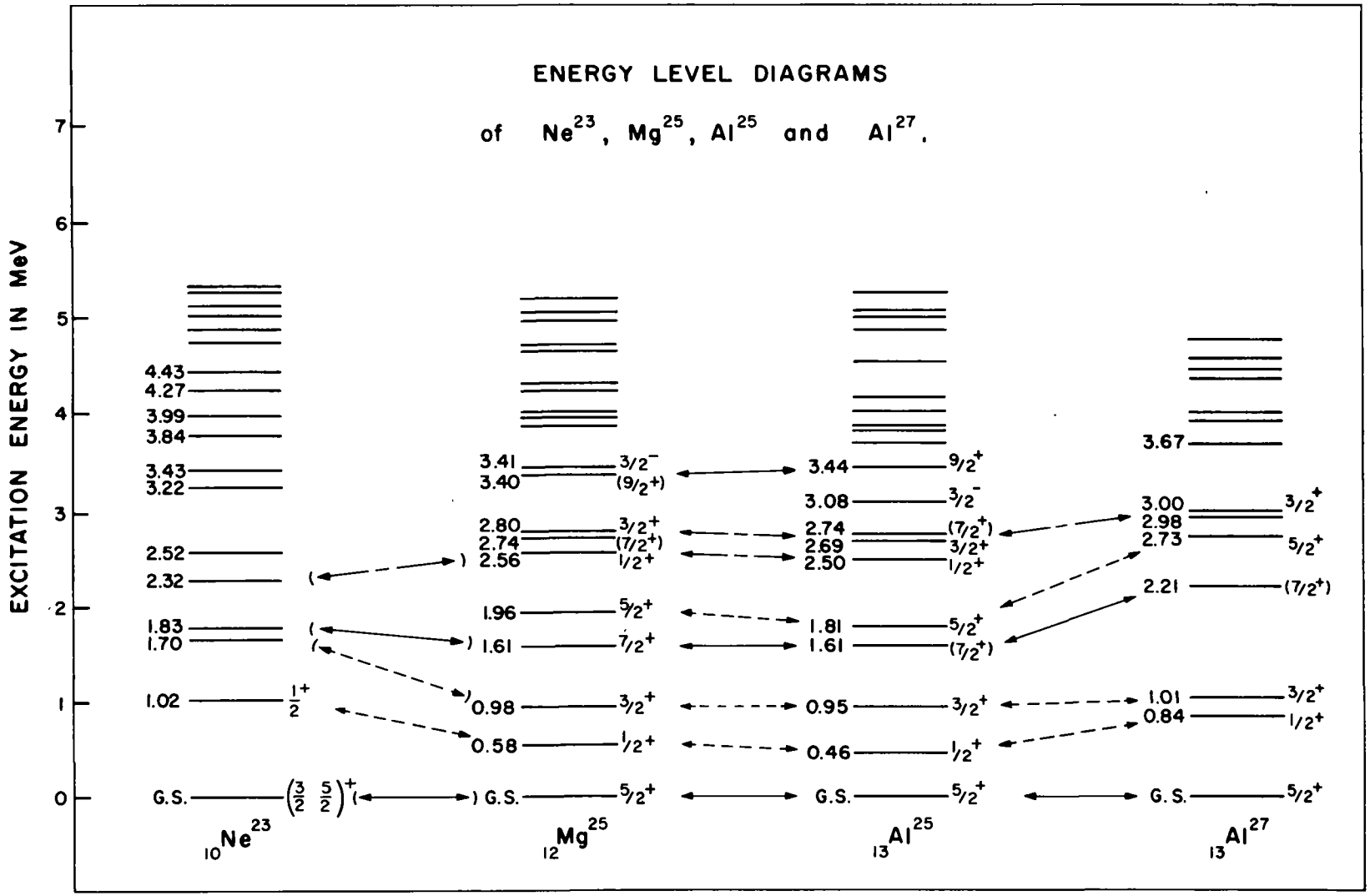
ENERGY LEVEL DIAGRAMS
of Ne23, Mg25, Al25 and Al27.
EXCITATION ENERGY IN MeV
0
1
2
3
4
5
6
7
G.S.
1.02
1.83
1.70
2.52
2.32
4.43
4.27
3.99
3.84
3.43
3.22
(3/2 5/2)+
1/2+
10Ne23
G.S.
0.98
0.58
1.96
1.61
2.80
2.74
2.56
3.41
3.40
5/2+
7/2+
3/2+
1/2+
(7/2+)
3/2+
(9/2+)
3/2−
12Mg25
G.S.
0.95
0.46
1.81
1.61
2.74
2.69
2.50
3.08
3.44
5/2+
3/2+
1/2+
(7/2+)
3/2−
9/2+
13Al25
G.S.
1.01
0.84
2.21
2.73
2.98
3.00
3.67
5/2+
1/2+
(7/2+)
5/2+
3/2+
3/2+
13Al27

A second motivation for obtaining experimental data concerning Ne^{23} is the possibility of comparing properties of the Ne^{23} and Na^{23} systems with corresponding properties of the previously investigated mass-21 systems, Ne^{21} and Na^{21}, and from such a comparison determining the degree to which the nuclear core, Ne^{20} in this particular case, is affected by the addition of two like nucleons to it.

Most of the experimental information presently available on Ne^{23} results from two experimental investigations. The energy levels shown in Figure V-1 were established by Freeman[101] in her studies of the reaction $Ne^{22}(d,p)Ne^{23}$ at a fixed laboratory angle. Burrows et al.[109] carried out an investigation of the angular distributions of the proton groups corresponding to population of the ground and first excited states which indicated the angular momenta of these states to be $(3/2, 5/2)^+$ and $1/2^+$, respectively. In addition to these measurements, a determination of the lifetime of the 1.02 MeV, $1/2^+$ state has been recently reported by McClelland et al.[129] and is consistent with an E2 transition to the ground state. Howard[61] has carried out a number of gamma radiation measurements involving deexcitations of Ne^{23} states populated via the $Ne^{22}(d,p)Ne^{23}$ reaction; however, interpretation of all gamma transition data is made difficult by the lack of proton angular distribution measurements for the states above 1.02 MeV excitation. A number of experimental measurements on this nucleus are badly needed.

The experiments to be reported herein were initiated in an attempt to provide gamma deexcitation information on the 1.70 and 1.83 MeV states in Ne^{23} and preliminary particle distribution data necessary for analysis of subsequent $(d,p\gamma)$ branching deexcitation studies. It was of course recognized from the outset that the deuteron beam energies available for the particle measurements were too low to permit any unambiguous extraction of spectroscopic information from the angular distributions. As will be later demonstrated, the distribution measurements do, however, provide gross information on several of the reaction characteristics involving the low-lying states of Ne^{23}.

B. Experimental Equipment

In the investigation of the deexcitation branching of the Ne^{23} states at 1.70 and 1.83 MeV, a proton-gamma coincidence was utilized. The same target cell and solid state detector assembly as described in Chapter III, Section B, was employed for the coincidence measurements; gamma radiation was detected in a 3 x 3 inch NaI(Tl) spectrometer.

The essential features of the scattering chamber used in the proton distribution measurements are shown in Figure V-2. As in the previously described gas target chambers, the beam entered through a 0.00025 cm Ni window. Two solid state particle detectors were independently mounted and operated directly within the target gas atmosphere contained by the chamber. The monitor counter was located at 90^{o} to the incident beam; the primary counter was fixed to a small externally controlled, angular distribution table whose position was continuously variable from 0^{o} to 160^{o} with respect to the beam axis. Angular position of this detector was determined to within $\pm 1^{o}$ by means of an external scale and pointer system.

Beam collimation and definition of the scattering volume was provided by sets of circular tantalum apertures; two of these apertures were located immediately after the entrance window to determine the beam profile, two more were placed before each of the detector units to define the extent of the effective reaction volume. The detector and collimator assemblies were aligned optically so that the scattering site was determined to within ± 0.3 mm of the axis of rotation of the primary counter. Because of the similar cross sections and Q-values for the reactions $Ne^{22}(d,p)Ne^{23}$ and $Ne^{22}(d,\alpha)F^{20}$, it was necessary to absorb the contaminant alpha particles in a section of 0.001 inch Al foil placed over the face of the primary detector at the cost of some energy resolution because of energy straggling in the foil.

After transversal of the entrance foil, tantalum collimators, and reaction volume, the beam was stopped in a tantalum liner placed around the inner circumference of the chamber. The entire target assembly was isolated electrically by a lucite spacer placed between it and the beam tube. This permitted integration

of incident beam current directly from the chamber.

C. Experimental Measurements and Results

1. Deexcitation Branching of the 1.80 MeV State:

The gamma deexcitation spectrum in coincidence with proton groups of energy corresponding to the population of states with 1.70 and 1.83 MeV of excitation in Ne^{23} is shown in Figure V-3. Energy calibration of the crystal spectrometer coupled with efficiency corrections of Vegors et al.[63] indicates that; (a) $68 \pm 10\%$ of the gamma deexcitations originate from the 1.83 MeV state and $32 \pm 10\%$ originate from the 1.70 MeV state which establishes a ratio of $\sim 2/1$ for the differential cross sections of formation for these two states by 2.5 MeV incident deuterons in satisfactory agreement with the results of Freeman[101], and (b) the 1.83 MeV state deexcites more than 95% of the time to the ground state with less than 5% intensity deexciting through the intermediate $1/2^+$ state in Ne^{23}.

2. Angular Distributions of the Proton Groups:

A typical particle spectrum obtained with a neon target (90% Ne^{22}, 10% Ne^{20}, and $< 0.01\%$ other contaminants) at a deuteron bombarding energy of 2.5 MeV is shown in Figure V-4. The energy resolution of the peaks taken as the full width at half maximum is of the order of 100 keV for the higher energy groups. This energy spread may be attributed to contributions from a number of sources; specifically, inherent detector resolution ~ 30 keV, electronic resolution ~ 30 keV, angular resolution at 90° to the beam direction ~ 40 keV, energy straggling and non-uniformity of the Ni entrance window ~ 40 keV, energy straggling in the target gas at 10 cm of Hg absolute ~ 20 keV, and energy straggling in the Al absorber foil ~ 60 keV. Additional peak broadening due to more severe energy straggling is evident in peaks of lower energy.

A series of particle spectra similar to the one shown in Figure V-4 were taken in 10° steps over the angular range 23° to 123° in the laboratory system. The energies of each of the particle groups were corrected for loss in the

Figure V-2. Gas target scattering chamber assembly.

Figure V-3. Gamma radiation in time coincidence with proton groups populating states at 1.70, 1.83 and 2.32 MeV in Ne^{23}. Energies of prominent peaks of the spectrum are indicated in MeV; intensity analysis of these peaks results in the partial scheme of deexcitation branching shown in the Ne^{23} level diagram

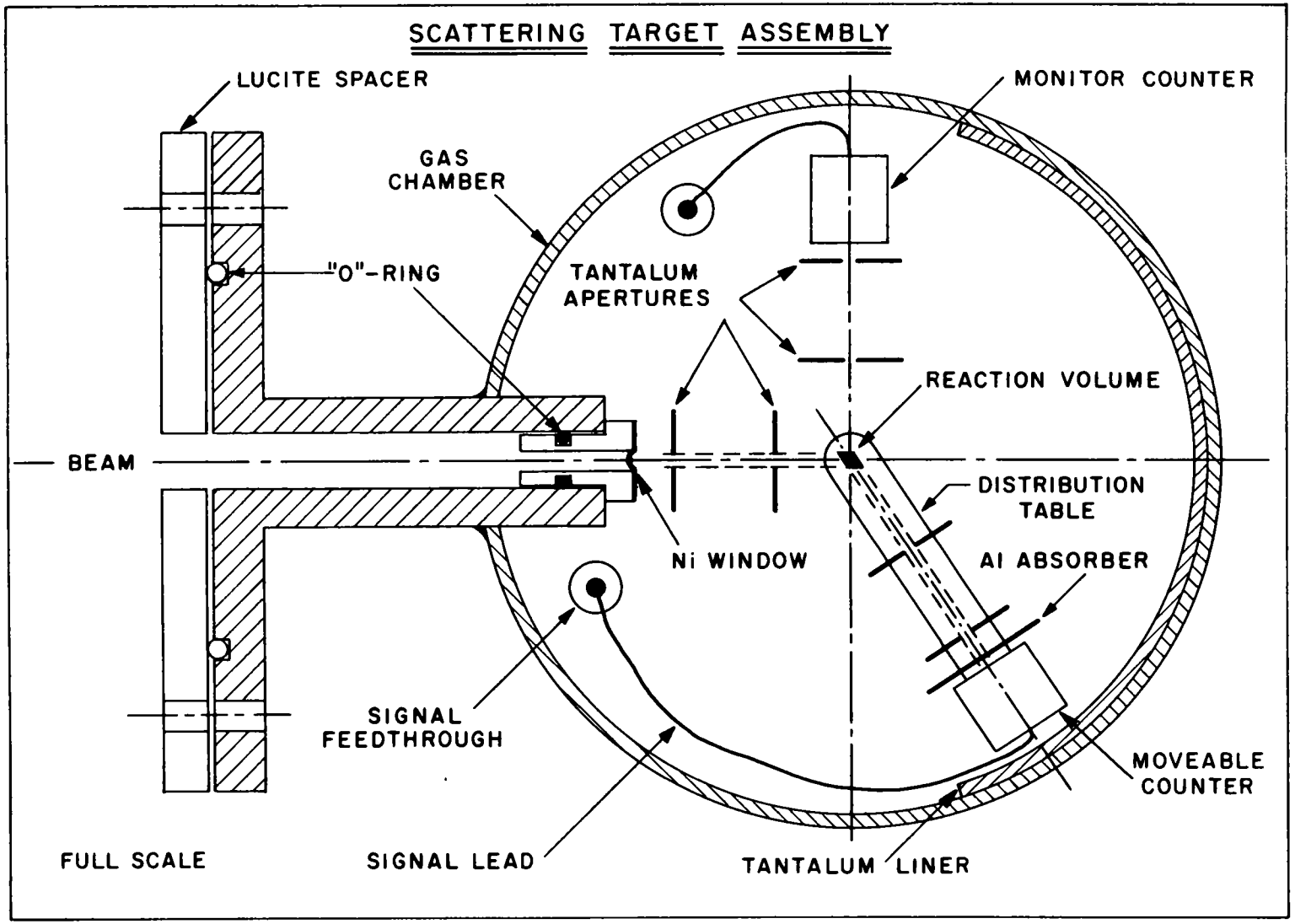
SCATTERING TARGET ASSEMBLY
LUCITE SPACER
MONITOR COUNTER
GAS CHAMBER
"O"-RING
TANTALUM APERTURES
REACTION VOLUME
BEAM
DISTRIBUTION TABLE
Ni WINDOW
Al ABSORBER
SIGNAL FEEDTHROUGH
MOVEABLE COUNTER
FULL SCALE
SIGNAL LEAD
TANTALUM LINER

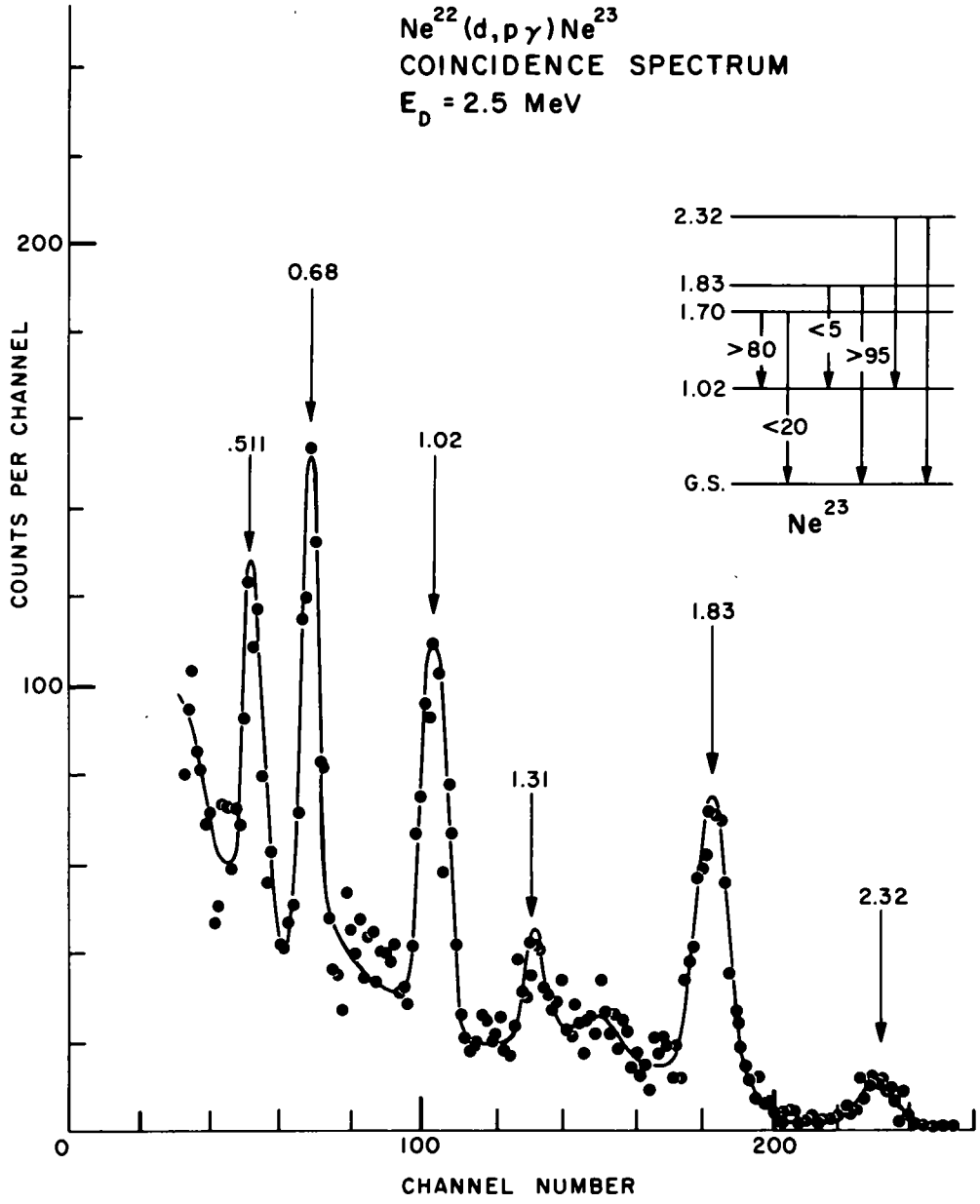
$Ne^{22}(d,p\gamma)Ne^{23}$
COINCIDENCE SPECTRUM
E_D = 2.5 MeV
2.32
1.83
1.70
1.02
G.S.
>80
<5
>95
<20
Ne^{23}
.511
0.68
1.02
1.31
1.83
2.32
COUNTS PER CHANNEL
200
100
0
100
200
CHANNEL NUMBER

target gas and absorber foil and then plotted against angle as illustrated in Figure V-5. The solid curves in this figure indicate the energy dependence of the first five $Ne^{22}(d,p)Ne^{23}$ proton groups reported by Freeman[101] and determined by the reaction kinematics; the dashed curves indicate the energy dependence of the three proton groups clearly visible in the direct spectrum and identified with known states in Ne^{21}. The good agreement between the experimentally measured and the kinematically expected energies of the particle groups permitted unambiguous identification of these groups. Each is labeled by the energy of the corresponding state populated in the residual nucleus.

The angular distributions of the proton groups resulting in the population of the 1.83 -1.70 MeV states, the 1.02 MeV state, and the ground state of Ne^{23} are shown on the left in Figures V-6, 7, and 8, respectively. The relative intensity of each group was determined by numerically integrating the number of counts in each peak, correcting the total for dead time in the multichannel analyzer, and multiplying the result by the sine of the detector-beam direction angle which corrects to first order for the angular dependent number of target nuclei inherent in gas target scattering. A final normalization of the data was made for the total integrated beam charge of each spectrum. The counting rate recorded at 90^{o} to the beam direction by the monitor counter was found to be constant with respect to the unit integrated beam to within the statistical errors of the measurement. From this, it was concluded that any relative errors in the beam integration or in the particle monitor system were not serious.

For comparative purposes, a series of particle spectra similar to those just described were taken for the reaction $Ne^{20}(d,p)Ne^{21}$ also with 2.5 MeV incident deuterons. Particle groups from known states of Ne^{21} were identified and their angular distributions analyzed as before; the results are presented on the right in Figures V-6, 7, and 8 where the ordinate scales have been adjusted by up to factors of 2 to facilitate comparison of the distribution patterns.

Figure V-4. Spectrum of charged particles resulting from the bombardment of a 90% Ne^{22} – 10% Ne^{20} target with 2.5 MeV deuterons. The prominent proton groups are identified by the excitation energy of the residual nucleus.

Figure V-5. Energy of proton groups resulting in the reactions Ne^{22}(d, p) Ne^{23} and Ne^{20} (d, p) Ne^{21} presented as a function of detector angle. The curves correspond to the energy-angle dependence expected for protons populating states of previously known energies in the residual nuclei Ne^{23} and Na^{23}.

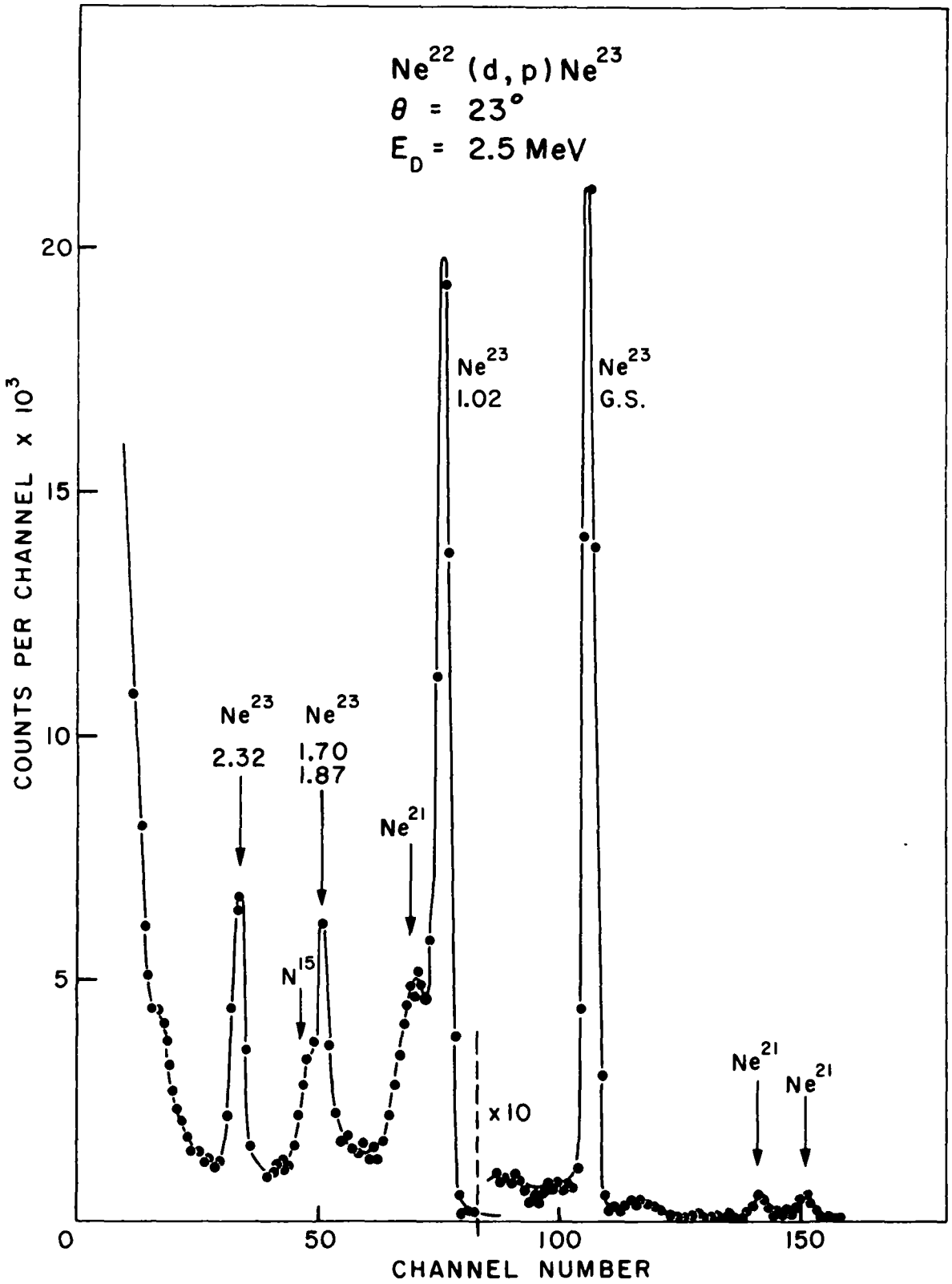
Ne22 (d, p) Ne23
θ = 23°
E_D = 2.5 MeV
COUNTS PER CHANNEL X 10^3
CHANNEL NUMBER
0
5
10
15
20
50
100
150
Ne23 2.32
Ne23 1.70 1.87
N15
Ne21
Ne23 1.02
Ne23 G.S.
x10
Ne21
Ne21

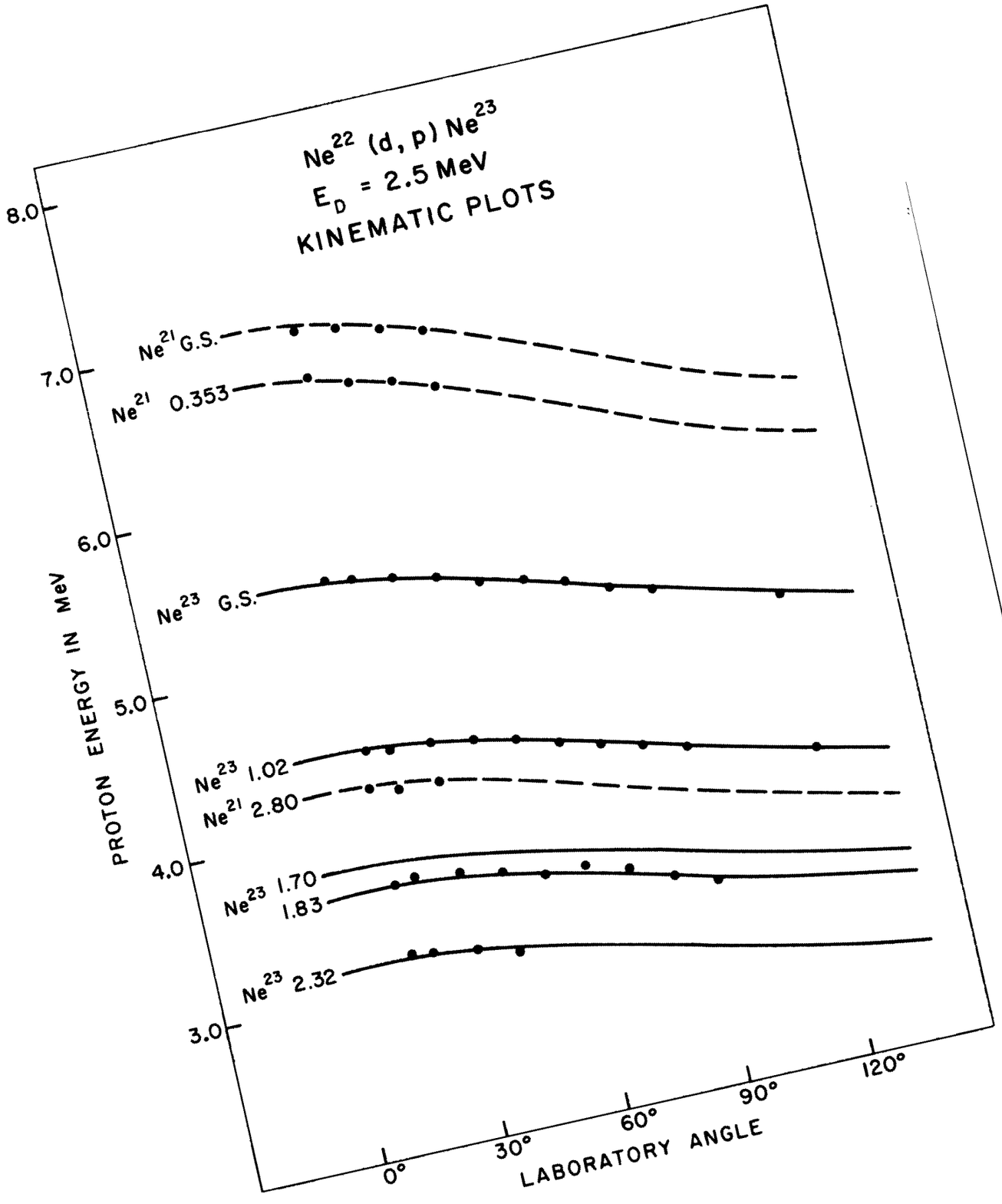
Ne^{22} (d, p) Ne^{23}
E_D = 2.5 MeV
KINEMATIC PLOTS
PROTON ENERGY IN MeV
8.0
7.0
6.0
5.0
4.0
3.0
Ne^{21} G.S.
Ne^{21} 0.353
Ne^{23} G.S.
Ne^{23} 1.02
Ne^{21} 2.80
Ne^{23} 1.70
1.83
Ne^{23} 2.32
0°
30°
60°
90°
120°
LABORATORY ANGLE

D. Discussion of Results

As suggested in the introduction of this chapter, an interesting test of the validity of the extreme single-particle assumption, which is critical to the simplest application of the Nilsson model in this mass region, would be the identification in Ne^{23} of rotational band structure similar to that seen in other $\eta = 13$ nuclei, Mg^{25}, Al^{25}, and Al^{27}. In each system the odd particle is the fifth outside the O^{16} core; thus, since rotational bands are determined by the configurations available for the last odd particle, a strict interpretation of the model predictions would make necessary a low-lying band with $K^{\pi} = 5/2^{+}$, two bands with $K^{\pi} = 1/2^{+}$, and a fourth band with $K^{\pi} = 1/2^{-}$. Of course, exact agreement in the intercomparison of these systems is not expected. Ne^{23} contains in its core two less protons than Mg^{25} and Al^{25} and two less protons and neutrons than Al^{27} which would certainly effect a difference in the value of β, the core distortion parameter, leading to corresponding differences between systems in both the energies of the intrinsic configurations, and in the moments of inertia which determine relative intra-band level spacings.

The primary purpose of the $Ne^{22}(d,p)Ne^{23}$ particle measurements was to determine the gross features of the proton group distributions necessary for the interpretation of subsequent $(d,p\gamma)$ coincidence branching ratio measurements. It was realized that spectroscopic information extracted by any analysis technique from the distribution data must be viewed with considerable suspicion because of the large distortions expected with incident deuterons of energy less than 3 MeV; consequently, no extensive analysis of the distribution data was carried through. On the other hand, several plausible arguments concerning the angular momentum assignments of the low-lying Ne^{23} states may be made from systematic comparisons of general characteristics of the particle distributions in the reaction $Ne^{22}(d,p)Ne^{23}$ to the characteristics of the particle distributions populating states of known J^{π} values in the reaction $Ne^{20}(d,p)Ne^{21}$. For this reason, these distributions were presented in the preceding section and will now be referred to.

The similarity of the curves B and A in Figure V-7, corresponding to the state at 2.80 MeV in Ne^{21} which is known to be $1/2^{+}$, and the state at 1.02 MeV

Figure V-6. Angular distributions of the proton groups populating the 1.80 MeV state of Ne^{23} and the 1.75 MeV state of Ne^{21}.

Figure V-7. Angular distributions of the proton groups populating the 1.02 MeV state of Ne^{23} and the 2.80 MeV state of Ne^{21}.

Figure V-8. Angular distributions of the proton groups populating the ground state of Ne^{23} and the 0.353 MeV state of Ne^{21}.

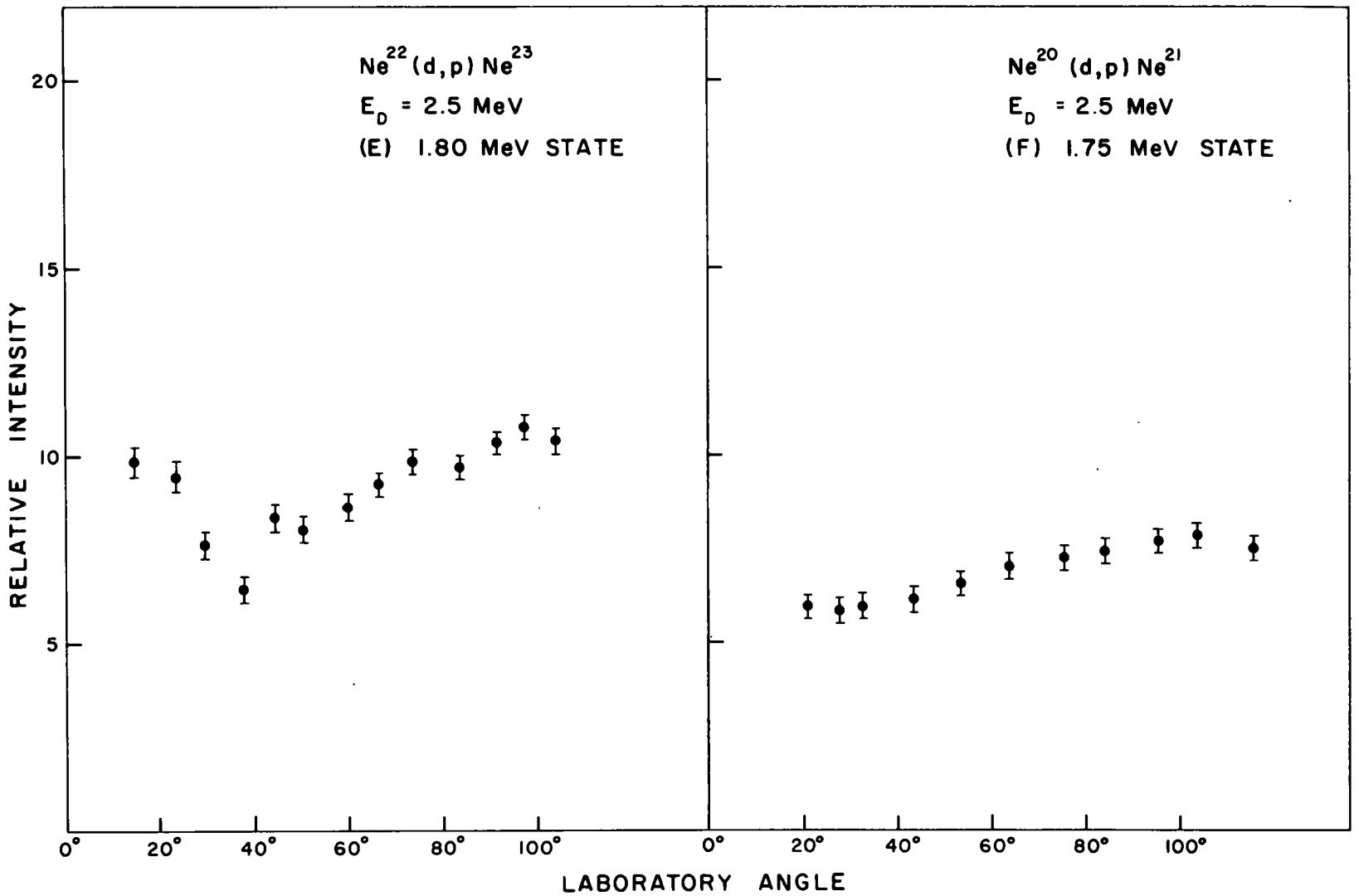
$Ne^{22}(d,p)Ne^{23}$
E_D = 2.5 MeV
(E) 1.80 MeV STATE
$Ne^{20}(d,p)Ne^{21}$
E_D = 2.5 MeV
(F) 1.75 MeV STATE
RELATIVE INTENSITY
20
15
10
5
0°
20°
40°
60°
80°
100°
LABORATORY ANGLE

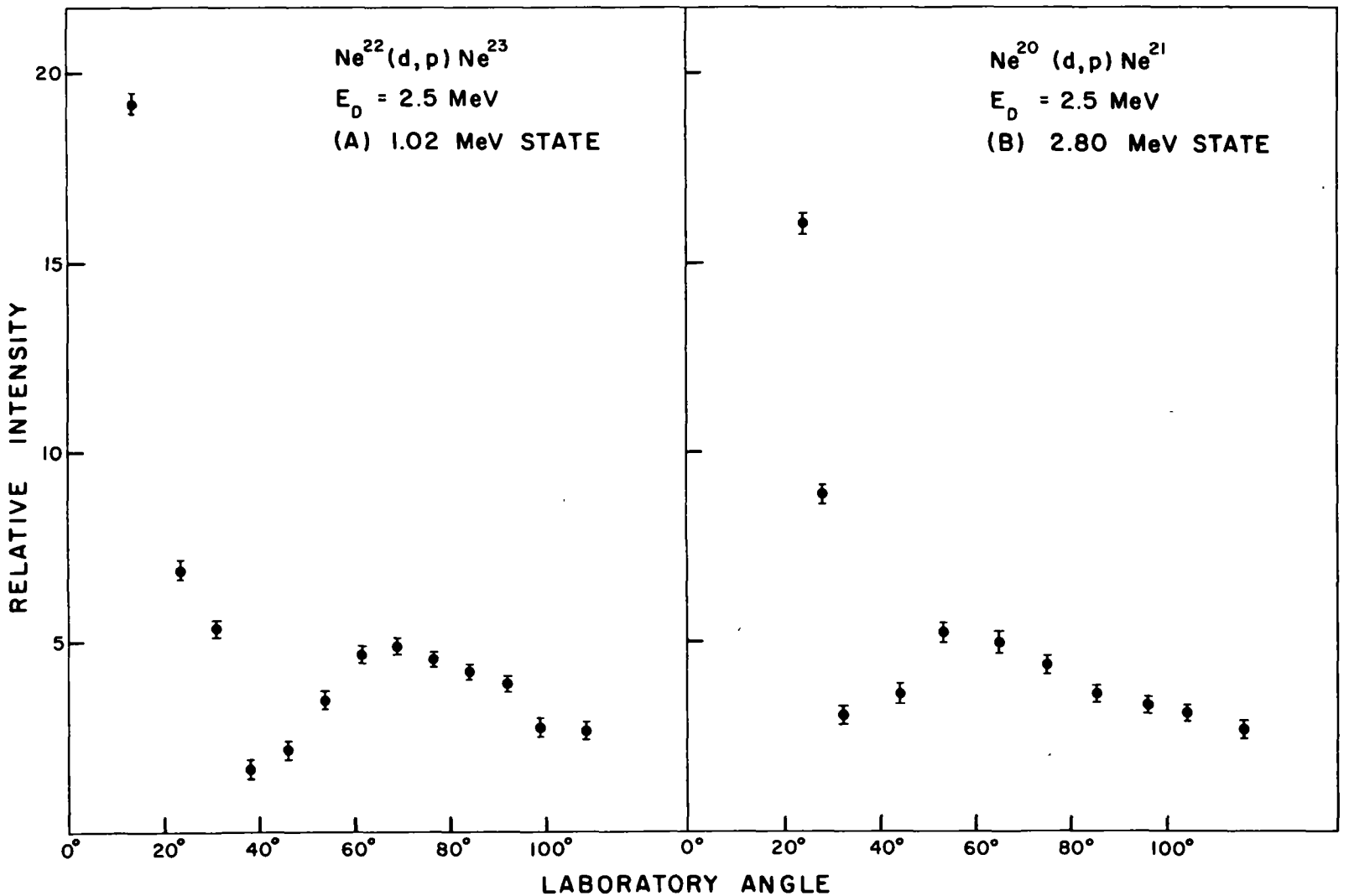
$Ne^{22}(d,p)Ne^{23}$
E_D = 2.5 MeV
(A) 1.02 MeV STATE
$Ne^{20}(d,p)Ne^{21}$
E_D = 2.5 MeV
(B) 2.80 MeV STATE
RELATIVE INTENSITY
20
15
10
5
0°
20°
40°
60°
80°
100°
LABORATORY ANGLE

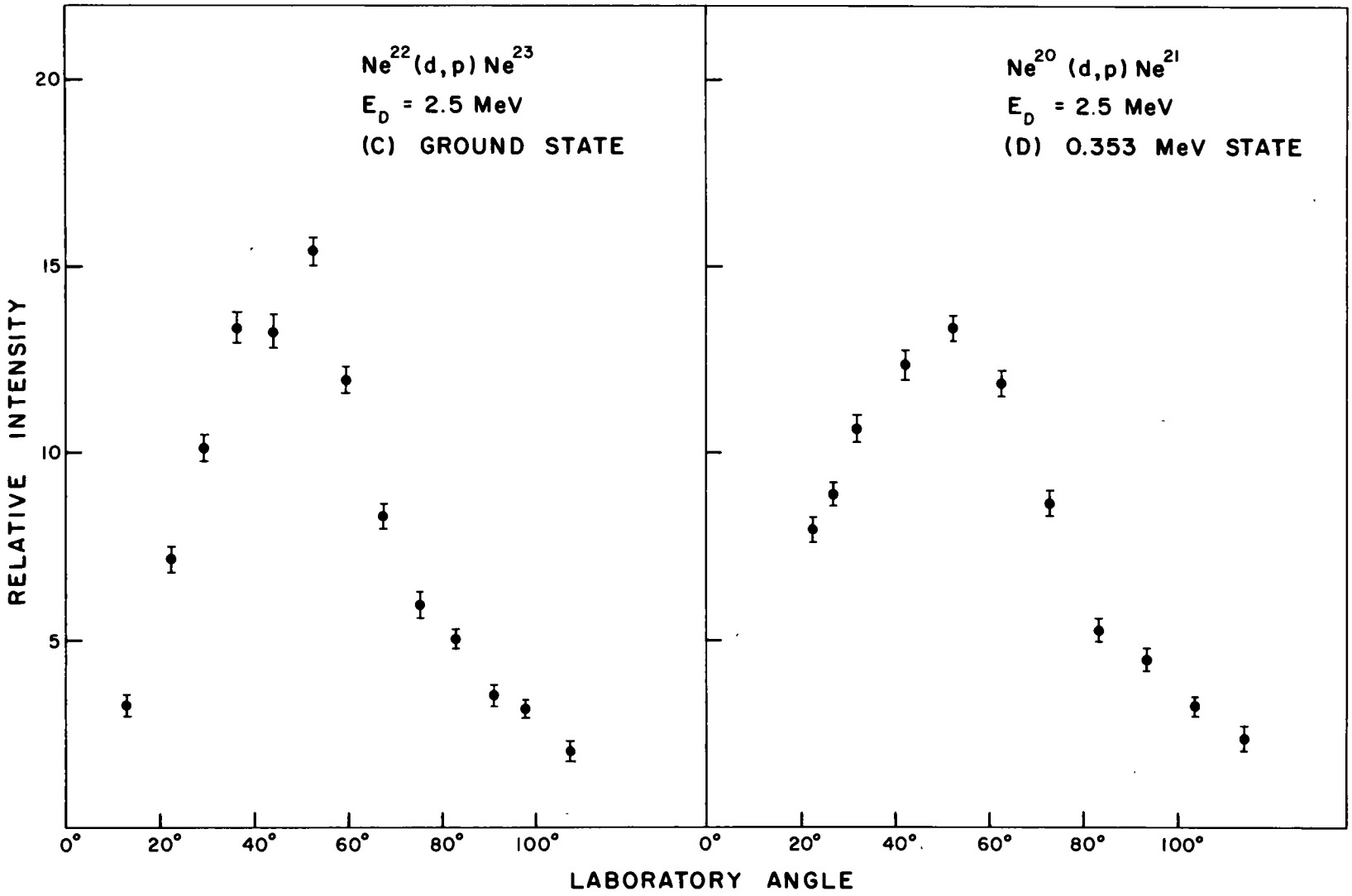
$Ne^{22}(d,p)Ne^{23}$
E_D = 2.5 MeV
(C) GROUND STATE
$Ne^{20}(d,p)Ne^{21}$
E_D = 2.5 MeV
(D) 0.353 MeV STATE
RELATIVE INTENSITY
LABORATORY ANGLE
0°
20°
40°
60°
80°
100°
5
10
15
20

in Ne^{23}, respectively, indicates the assignment of $1/2^+$ for the 1.02 MeV state and corroborates the results of Burrows et al.[109]. Likewise, comparison of curve C to curve D of Figure V-8 suggests angular momentum transfer of $l_n = 2$ to the ground state of Ne^{23} from the corresponding known value of angular momentum transfer, $l_n = 2$, to the first excited state in Ne^{21}.

The similar characteristics of the proton distributions E and F of Figure V-6, resulting primarily from population of the state at 1.83 MeV in Ne^{23} and the $J^\pi = 7/2^+$ state at 1.75 MeV in Ne^{21}, make the assignment of $J^\pi = 7/2^+$ to the 1.83 MeV Ne^{23} state seem entirely reasonable. The apparent lack of gamma deexcitation from this state to the $1/2^+$ level at 1.02 MeV as discussed in Section C provides further qualitative evidence for a spin assignment $\geq 5/2$ to the 1.83 MeV level, assuming that the Ne^{23} ground state spin of $5/2^+$ is correct. Finally, the similarity to both curves A and B of Figure V-7 of the angular distribution of the protons populating the 2.32 MeV state (not shown in the figures - only the protons in the angular range 0^o to 40^o were of sufficient energy to be adequately resolved in the particle spectra) indicated a probable angular momemtum transfer of $l_n = 0$ to, and thus the assignment $J^\pi = 1/2^+$ for, the 2.32 MeV state in Ne^{23}.

The tentative identifications of like members of analogous rotational bands between the neighboring nuclei Ne^{23} and Mg^{25}, to which the above considerations lead, are indicated in Figure V-1 by the arrows enclosed in parentheses. Although these identifications are somewhat speculative, the striking similarity between the level schemes of these systems is indicative of analogous structure between them and thus provides still further evidence for the applicability of the Nilsson model in this mass region. A quantitative interpretation of the Ne^{23} system must await further data on the properties of the Ne^{23} levels. Such measurements are planned for the near future in this laboratory.

VI. OPEN PROBLEMS

A. Orientation

The preceding chapters have described the experimental study of some very specific problems in the sd shell. Analysis of these experiments has suggested a number of further measurements important to the interpretation of nuclear models in this mass region. Moreover, in addition to these specific problems, a preliminary examination of the compilations[1,2] of sd-shell data shows quickly that much more experimental information in general is badly needed.

Of major interest would be data obtained through systematic surveys of the type carried out, for example, by Broude and Gove[130] on a number of even-even nuclei in the sd shell. Precise, systematic information would hopefully force still more critical examination of model relevance in this mass region and, at the same time, enable meaningful refinements of model formulations. Several examples are now given of where such general data would be of value.

(i) It would be instructive to increase the available information concerning the enhancement of E2 transitions within collective bands which now exists in nuclei of atomic weight 17 to 33 and, further, to extend this information to include nuclei in the upper end of the sd shell. The recent compilation[131] of E2 enhancement data indicates a pronounced trend away from collective behavior above atomic number 30, but the general lack of transition data in this region prevents quantitative interpretations of the trend.

(ii) It would be of interest to trace throughout the sd shell the approximate, intermediate-coupled shell model predictions of Bouten, Pullen, and Elliott[20]. At present such a comparison is greatly complicated by the fragmentary and incomplete nature of experimental J^{π} assignments available for a number of states of sd-shell nuclei.

(iii) It would be of interest to experimentally investigate phenomena which would be amenable to interpretation in terms of the sign and the magnitude of nuclear core deformation. Through such investigations the variation of core

distortion between atomic number 25 and 33 could be studied. Initial experiments and analyses of Bromley et al.[126] suggested, for example, a rapid change of deformation from prolate to oblate just before the Si^{29} system. Recent self-consistent model calculations[132] provide theoretical bases for, and predictions of, the same type of core deformation behavior. Unfortunately, still more experimental parameters are needed to evaluate these predictions adequately.

In addition to the preceding, rather general comments concerning open problems in the sd shell, a very brief list of specific spectroscopic investigations which would be of immediate interest follows.

B. O^{19}

As previously discussed, the shell model calculations of Talmi and Unna[21], among others, make very definite predictions concerning O^{19} which as yet remain untested. In particular, it would be extremely interesting to establish the existence (and, if it exists, the energy) of the $9/2^+$ state predicted by the shell model to lie somewhere between 2.6 and 3.2 MeV. Along with the $5/2^+$ ground state and the $3/2^+$ first excited state, the $9/2^+$ state would be the third and final member of the $(d_{5/2})^3$ triplet configuration. Its existence would be crucial to the validity of the initial assumptions on which the formulation of the independent particle shell model of O^{19} is based. Three unassigned levels have been reported[1] in the proper energy range; however, no characteristics of these states other than their energies are known.

General shell model considerations[133] show that comparison of the energy level spectra of cross conjugate pairs should provide a sensitive test of the coupling scheme of the extra-core nucleons. Thus the validity of the j-j coupling scheme, thought to be particularly good in nuclei of high T_z, could be directly investigated by comparison of the spectrum of O^{19} (3 neutrons outside the O^{16} core) with the spectrum of its cross conjugate, Na^{25} (3 proton holes in the Si^{28} core). Similarities in the two energy spectra would indicate that the j-j coupling approximation may be realistically made in carrying out shell model calculations of these nuclei; differences in the spectra would necessitate a

reevaluation of the validity of the approximation. Unfortunately, in addition to the paucity of information presently available on O^{19}, only very preliminary measurements on Na^{25} have been reported precluding completely such a comparison. With the availability of alpha particle beams of sufficient energy, many of the experimental techniques reported in this work could be used in conjunction with the $Ne^{22}(\alpha,p\gamma)Na^{25}$ reaction to provide substantially more information on the Na^{25} nucleus than is currently available.

C. F^{19}

As pointed out in Chapter II, it would be of considerable interest to establish the characteristics of the unassigned states at 4.00, 4.04, 4.39, 4.58, and 4.76 MeV in F^{19} to provide a more stringent test of the static predictions of the different models in this region. Identification of the $3/2^-$ band head of the second $[1\,0\,1]$ rotational system predicted by Harvey[51] would be of special interest.

A recent investigation[66] of the gamma deexcitation of states in F^{19} populated by the beta decay of the ground state of O^{19} shows a weak decay branch to the state at 4.39 MeV excitation. The 4.39 MeV level then deexcites partially through the $9/2^+$, 2.79 MeV state. The beta decay branch to the 4.39 MeV state together with the gamma deexcitation of this state suggests the assignment $J^\pi = 7/2^+$ for the state which is reportedly not inconsistent with the recent $(p,p'\gamma)$ triple correlation data of Thomas et al.[70]. It should be noted that once again the various collective model calculations predict a $7/2^+$ state to lie immediately in this energy region; this is not the case with the available shell model calculations.

The angular distribution measurements reported in Chapter II suggest a strongly enhanced E2 transition between the 9.07 MeV state and the $9/2^+$, 2.79 MeV state in F^{19}. There is no reason to expect a priori on the basis of any reasonable model such an enhancement; the particular transition is therefore of interest. Further angular distribution and correlation measurements are currently being carried out to provide more precise experimental information concerning this transition.

D. Ne^{19}

In contrast to the considerable experimental effort devoted to F^{19}, essentially no information, other that the level positions[134,135], has been obtained for the mirror nucleus Ne^{19}. Aside from small Coulomb and mass difference corrections, the numerous theoretical calculations of F^{19} apply equally to the Ne^{19} system. That the two nuclei are indeed similar is borne out by comparison of their energy level spectra shown in Figure VI-1. More complete experimental information on Ne^{19} clearly would be of interest. States of this nucleus will be accessible by the reactions $F^{19}(p,n)Ne^{19}$, $Ne^{20}(He^3,\alpha)Ne^{19}$, and $Ne^{20}(p,d)Ne^{19}$ using higher energy projectile beams. Many of the characteristics of the states may be investigated with standard distribution and correlation techniques. It is highly possible that even the modes of gamma deexcitation through the very closely spaced triplet members at 1.5 MeV in this nucleus could be measured with the newly developed, high resolution, lithium-drifted, germanium radiation detectors[136,137].

E. Ne^{21}, Ne^{23}, Na^{21}, Na^{23}

From the previously indicated interest in a large number of further parameter determinations within the Ne^{21}, Ne^{23}, Na^{21}, and Na^{23} systems, two specific measurements will be mentioned.

(i) A comprehensive interpretation of gamma radiation data from excited states of Ne^{23}, much of which is already at hand and awaiting analysis, cannot be carried out without the results of careful proton distribution measurements from the reaction $Ne^{22}(d,p)Ne^{23}$ at deuteron energies sufficient for meaningful stripping analyses. Such measurements would aid enormously subsequent experimental and theoretical studies of the Ne^{23} nucleus; they should be undertaken as soon as possible.

(ii) It would be of interest to investigate further and attempt to resolve the experimental discrepancy concerning the deexcitation branching of the 2.80 MeV state (or states) of Ne^{21}. Careful examination of the radiations originating from

Figure VI-1. Experimentally observed energy level spectra of the mirror nuclei F^{19} and Ne^{19}. Excitation energies are in MeV.

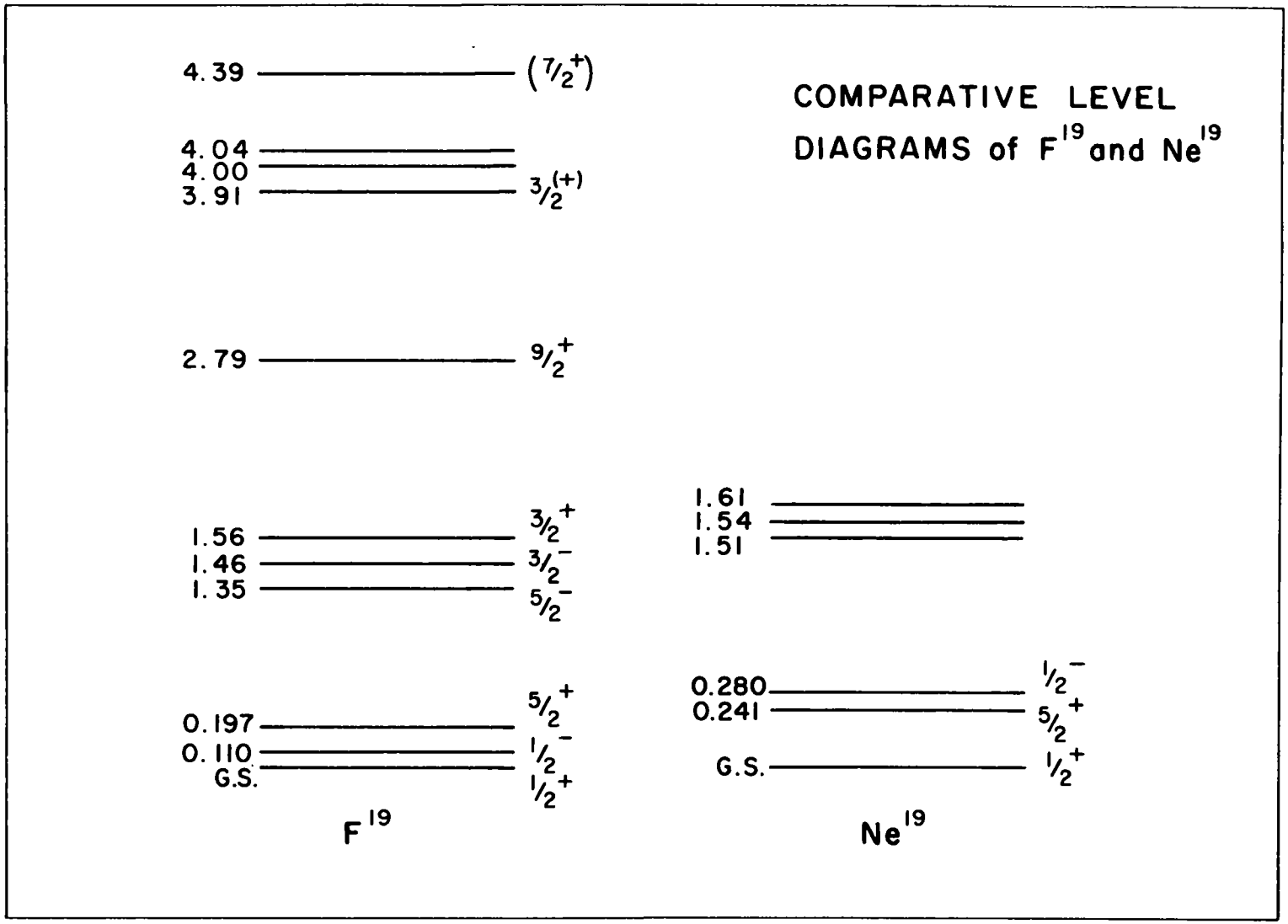
COMPARATIVE LEVEL
DIAGRAMS of F19 and Ne19
4.39
(7/2+)
4.04
4.00
3.91
3/2(+)
2.79
9/2+
1.56
1.46
1.35
3/2+
3/2−
5/2−
0.197
0.110
G.S.
5/2+
1/2−
1/2+
F19
1.61
1.54
1.51
0.280
0.241
G.S.
1/2−
5/2+
1/2+
Ne19

states in this energy region populated via the reactions $F^{19}(He^3,p)Ne^{21}$, $Ne^{20}(d,p)Ne^{21}$, and $Ne^{22}(He^3,\alpha)Ne^{21}$ are now underway. Since gas targets are being employed in all cases, nearly identical experimental conditions are being maintained throughout the measurements; this will simplify greatly the intercomparison of the resulting data and hopefully will lead to a satisfactory explanation of the as yet unexplained experimental discrepancy.

F. Upper End of the SD Shell

The recent availability[122] of usable quantities of nearly pure Ar^{36} and Ar^{40} gas samples makes feasible for the first time a long series of experimental investigations of odd-A nuclei at the upper end of the sd shell.

As pointed out by Elliott and Flowers[16], the locations of the single hole levels in the mass-39 nuclei are sufficient information on which to base extensive, intermediate-coupled, spherical shell model calculations predicting characteristic properties of the positive parity hole states in the mass-37 and mass-38 nuclear systems. Such calculations would be entirely analogous to those carried out by Elliott and Flowers[16] and by Inoue et al.[19] at the low end of the shell. Although not as complete as the Bouten, Pullen, and Elliott[20] calculations which span the entire shell, these hole state computations do not involve the approximations inherent in the former crude treatment. Some information[2] on Ca^{39} and K^{39} has already been reported; $Ca^{40}(p,d)Ca^{39}$ and $Ca^{40}(d, He^3)K^{39}$ measurements would undoubtedly supply still more. Then studies such as (p,p), (d,d), and (He^3, He^3) on Ar^{36}; $Ar^{36}(d,p)Ar^{37}$; $Ar^{36}(d,n)K^{37}$; $Ar^{36}(p,\gamma)K^{37}$; and $Ar^{40}(He^3,\alpha)Ar^{39}$, to mention just a few, could be used to provide copious amounts of experimental information with which to compare the shell model prodictions. Additional interest attaches to these measurements because of the small nuclear deformation, thus severe band mixing, thought to exist in this mass region. For this reason, collective model calculations may find only limited application in the regiom.

In addition to a general experimental survey of these nuclei, it would be of interest to attempt to answer several specific questions concerning them.

(i) The recent indications[78,138] that the doubly magic O^{16} nucleus becomes highly distorted from its normal symmetrical shape at excited energies, despite all intuitive assumptions to the contrary, suggest looking for evidence of the analogous situation in other magic number nuclei. It would be of utmost interest, for example, to search for experimental behavior reflecting core distortion in excited states of the next heaviest doubly magic nucleus, Ca^{40}, via the reaction analogous to that used in the O^{16} case, $Ar^{36}(\alpha,\alpha)Ar^{36}$.

(ii) Extensive calculations have been carried out by Bahcall[139] on the cross section of the neutrino capture reaction $Cl^{37} + \nu \rightarrow Ar^{37} + e^{-}$. The accuracy of these calculations depends on a number of assumptions including the estimation of several quantities which could be experimentally measured. For example, the calculation involves the correct identification and energy determination of the three $T = 1/2$ states in Ar^{37} with spins $1/2$, $3/2$, and $5/2$ formed from the shell model configuration of one $d_{3/2}$ neutron hole and two $d_{3/2}$ proton holes. A precise experimental knowledge of the energy position of the $T = 3/2$, $J^{\pi} = 3/2^{+}$ state in Ar^{37}, which is the analogue of the Cl^{37} ground state, is also of importance in the calculation together with the experimental values of various beta decay matrix elements.[140] Since the calculated cross section for neutrino absorption by Cl^{37} has direct application in the interpretation of several experiments[141] designed to measure the neutrino flux originating from the sun, experimental determinations of these quantities has astrophysical importance as well.

Preliminary work[142] has been carried out on several of the states in Ar^{37} using the reaction $Ar^{36}(d,p)Ar^{37}$ to populate the states of interest and the equipment described in previous chapters to obtain extensive proton angular distribution data and gamma-gamma and proton-gamma coincidence data. Interpretation of the experimental information is unfortunately made difficult by lack of higher energy deuteron beams which could provide proton distributions more amenable to straightforward stripping pattern analyses.

VII. SUMMARY

The preceding chapters have described in some detail several experimental measurements carried out to determine particular level parameters which represent the behavior of a number of selected states in the nuclei F^{19}, O^{19}, Ne^{21}, Na^{21}, Ne^{23}, and Na^{23}, all of which are odd-A members of the 2s-1d shell. Where possible, these experimental results have been compared with the corresponding predictions of a variety of model representations of the nuclear systems. From such intercomparisons, conclusions have been drawn concerning the relationships between the "model" nuclei and the actual nuclei.

In the F^{19} system, the angular momentum assignments of the 2.79 amd 3/91 MeV states have been established as 9/2 and 3/2, respectively, and the assignment of 7/2 to the 9.07 MeV state has been confirmed. Both shell and collective model formulations predict the correct level ordering of F^{19} up to and including this 9/2 state, but only the collective model calculations predict the existence of a 3/2 state in the correct energy region. The collective models further suggest positive parity for the 3.91 MeV state. Experimental deexcitation branching of the 8.76 and 3.91 MeV states have been determined in detail complementing the deexcitation branching of lower-lying states adduced in earlier measurements. Selection rules based on the collective Nilsson model provide an excellent qualitative description of these deexcitations indicating the utility of the asymptotic selection rules of this model even in so light a mass region and further suggesting the essential correctness of the collective picture of F^{19} as having strong, prolate deformation. Finally, the establishment of the assignment 9/2 to the 2.79 MeV state, when coupled with recently obtained information of the beta decay of the O^{19} ground state to the 4.39 MeV F^{19} state, has suggested the assignment $J^{\pi} = 7/2^{+}$ to the 4.39 MeV state. Once again, the collective model calculations predict a $7/2^{+}$ level in just this energy region providing still further evidence for the validity of the collective model with pronounced core deformation when applied to the F^{19} system.

Gamma radiation studies on the $O^{18}(d,p\gamma)O^{19}$ reaction have established that the 0.096 MeV state of O^{19} has an unambiguous assignment of $J^{\pi} = 3/2^{+}$

and, with slightly less certainty, that the ground state of O^{19} has the assignment of $J^+ = 5/2^+$.

The deexcitation of the 1.47 MeV state has been shown to have a branching ratio of $96.5 \pm 1.6\%$ to the 0.096 MeV state and $3.5 \pm 1/6\%$ to the ground state. The deexcitation branchings predicted by both the j-j coupled shell model wave functions and the intermediate-coupled shell model wave functions are in remarkably good quantitative agreement with this measured branching if the extra-core neutron is assumed to have effective charge of about one half the proton charge. This same effective charge also reproduces successfully other $1/2^+ \rightarrow 5/2^+$, E2 transition probabilities in neighboring nuclei, for example in N^{16} and O^{17}, indicating the relative ineffectiveness of the two neutrons added to the O^{17} core in increasing the polarizibility or the deformability of the core. This result is in direct contrast to the situation in F^{19} discussed above in which the two neutrons and one proton external to the O^{16} core result in strong prolate deformation. Both the pronounced core deformation in the case of F^{19} and the essential lack of this deformation in the case of O^{19} is, however, expected on the basis of recent self-consistent model calculations. A search for gamma deexcitation of energy 0.348 or 0.252 MeV originating in O^{19} has revealed no trace of the deexcitation of a previously reported 0.348 MeV state in O^{19} suggesting the possibility of confusion between this and the known 4.45 MeV state in O^{18} in the earlier measurement.

The deexcitation branching of the $1/2^+$, 2.80 MeV state of Ne^{21} has been determined as 90% to the $3/2^+$ ground state in excellent agreement with a previous measurement of Howard et al. but in marked disagreement with two other measurements of the same deexcitation. The reason for the experimental discrepancies is not known, but a possible explanation is the existence of an unresolved doublet of Ne^{21} states at energy $\sim$2.80 MeV which have radically differing level parameters and thus avoid the strong wave function admixing which would result necessarily in similar behavior as regards both the formation and the gamma deexcitation of the states.

Investigations of the gamma radiation originating from the $Ne^{20}(p,\gamma)\,Na^{21}$ reaction at $E_p = 1170$ keV have confirmed the spin assignment of 5/2 to the 3.57 MeV state of Na^{21} and have established the M1-E2 mixing parameter of the 3.57 MeV

state deexcitation to the ground state as $0.05 \leq \delta \leq 0.09$.

Angular correlation measurements of the 2.08 → 0.44 → 0 MeV cascade radiations were not sufficient to distinguish between earlier angular momentum limitations of 5/2 or 7/2 placed on the 2.08 MeV state of Na^{23}. However, a number of arguments based on experimentally measured properties of the 2.08 MeV state were presented for the validity of the 7/2 assignment. Incidental to this correlation measurement has been a redetermination of the relative intensities of the beta decay branches from the ground state of Ne^{23} to the 0.44 and 2.08 MeV Na^{23} states. These intensities were in satisfactory agreement with previous investigations of the beta decay.

The deexcitation branching of the second excited states of the $\eta = 11$ systems Ne^{21}, Na^{21}, and Na^{23} have been established in detail and compared to the corresponding branching predicted by the strongly-coupled Nilsson model. Approximate agreement between the measured and calculated quantities was obtained indicating again the qualitative validity of collective model approaches in this mass region.

Proton-gamma coincidence studies with the reaction Ne^{22} (d, pγ) Ne^{23} have been employed to determine the deexcitation branching of the 1.70 and 1.83 MeV states of Ne^{23}. These modes of deexcitation were combined with conclusions drawn from the gross features of angular distributions of the proton groups resulting in the same reactions to provide tentative angular momentum assignments of 5/2, 1/2, 7/2, and 1/2 to the ground, 1.02, 1.83, and 2.32 MeV states of Ne^{23}. These angular momentum assignments suggested the identification of analogous level sequences between $\eta = 13$ nuclei and thus provided evidence for the validity of the Nilsson formulation with respect to Ne^{23} which would indeed be anticipated from the well known successes of this model in the Al^{25}, Mg^{25}, and Al^{27} systems. However, the speculative nature of these results emphasized the need for much more experimental data in order to adequately assess the applicability of the collective model to the Ne^{23} nucleus.

In general, the comparisons presented above show in some cases remarkably quantitative agreement between model predictions and experimental results and in other cases only faint resemblences between experimental data and the general

characteristics of model predictions. Of most importance perhaps is the fact that the modest successes already achieved hint at the definite possibility of a yet more comprehensive understanding of the constitution of the atomic nucleus attainable in the future.

VII. REFERENCES

1. F. Ajzenberg-Selove and T. Lauritsen, Nucl. Phys. 11, 1 (1955): also F. Ajzenberg-Selove and T. Lauritsen, "Nuclear Data Sheets," Sets 5 and 6 (May, 1962).

2. P. M. Endt and C. Van der Leun, Nucl. Phys. 34, 21 (1962).

3. J. P. Elliott and A. M. Lane, in Handbuch der Physik, Vol. 39 (ed. by S. Flügge, Springer-Verlag, Berlin, 1957).

4. H. E. Gove, in "Proc. Intern. Conf. on Nucl. Structure" (ed. D. A. Bromley and E. W. Vogt, Univ. of Toronto Press, Kingston, Ontario, 1960) p. 438.

5. I. Talmi and I. Unna, Ann. Rev. of Nucl. Science 10, 353 (1960).

6. M. G. Mayer, Phys. Rev. 75, 1969 (1949); also M. G. Mayer, Phys. Rev. 78, 16 (1950).

7. O. Haxel, J. H. D. Jensen, and H. E. Suess, Phys. Rev. 75, 1766 (1949); also O. Haxel et al., Z. Physik 128, 295 (1950).

8. M. A. Preston, Physics of the Nucleus, (Addison-Wesley Publ. Co., Inc., Cambridge, 1962) p. 190.

9. P. Goldhammer, Rev. Mod. Phys. 35, 40 (63).

10. See, for example, Ref. 3, p. 248.

11. P. F. A. Klinkenberg, Rev. Mod. Phys. 24, 63 (1952).

12. L. A. Nordheim, Rev. Mod. Phys. 23, 322 (1951).

13. M. G. Mayer and J. H. D. Jensen, Elementary Theory of Nuclear Shell Structure, (John Wiley and Sons, Inc., New York, 1955).

14. D. R. Inglis, Rev. Mod. Phys. 25, 390 (1953).

15. D. Kurath, Phys. Rev. 101, 216 (1956).

16. J. P. Elliott and B. H. Flowers, Proc. R. Soc. 229, 536 (1955).

17. M. G. Redlich, Phys. Rev. 99, 1427 (1955).

18. B. H. Flowers and D. Wilmore, Proc. Phys. Soc. (London) 83, 683 (1964).

19. T. Inoue, T. Sebe, H. Hagiwara, and A. Arima (to be published).

20. R. Bouten, M. Pullen, and J. P. Elliott (private cummunication from J. P. Elliott, 1964).

21. I. Talmi and I. Unna, Nucl. Phys. 30, 28 (1962).

22. J. D. McCullen, B. F. Bayman, and L. Zamick, Phys. Rev. 134, B515 (1964).

23. P. W. M. Glaudemans, G. Wiechers, and P. J. Brussard, Nucl. Phys. 56, 529 (1964).

24. N. Bohr and J. A. Wheeler, Phys. Rev. 56, 426 (1939).

25. J. Rainwater, Phys. Rev. 79, 432 (1950).

26. A. Bohr, K. Danske Vid. Selsk, mat.-fys. Medd. 26, No. 14 (1952).

27. A. S. Davydov and G. F. Fillipov, Nucl. Phys. 8, 239 (1958).

28. A. S. Davydov and A A. Chaban, Nucl. Phys. 20, 499 (1960).

29. A. S. Davydov, Nucl. Phys. 24, 682 (1961).

30. See Ref. 8, p. 255.

31. A. K. Kerman, K. Danske Vid. Selsk. mat.-fys, Medd. 30, No. 15 (1956).

32. S. G. Nilsson, K. Danske Vid. Selsk, mat.-fys. Medd. 29, No. 16 (1955).

33. B. R. Mottelson and S. G Nilsson, K. Danske Vid. Selsk, mat.-fys. Skr. 1, No. 8 (1959).

34. D. Chasman and J. O. Rasmussen, University of California Radiation Laboratory Report UCRL - 3629 (1956).

35. G. Alaga, Phys. Rev. 100, 432 (1955); also G. Alaga, Nucl. Phys. 4, 625 (1957).

36. A. E. Litherland, E. B. Paul, G. A. Bartholomew, and H. E. Gove, Phys. Rev. 102, 208 (1956); also A. E. Litherland, H. McManus, E. B. Paul, D. A. Bromley, and H. E. Gove, Can. J. Phys. 36, 378 (1959).

37. T D. Newton, Can. J. Phys. 38, 700 (1960).

38. K. Gottfried, Phys. Rev. 103, 1017 (1956).

39. K. Kumar and M. A. Preston, Phys. Rev. 107, 1099 (1957).

40. B. E. Chi and J. P. Davidson, Phys. Rev. 131, 366 (1963); also B. E. Chi, "Asymmetric Core Collective Model with Application to 2s-1d Shell", Doctoral Dissertation, Rensselaer Polytechnic Institute (1963).

41. J. R. Roesser, "A Rotation-Vibration Model for Odd-A Atomic Nuclei", Doctoral Dissertation, Rensselaer Polytechnic Institute (1963).

42. C. A. Levinson, Phys. Rev. 132, 2184 (1963); also I. Kelson, Phys. Rev. 132, 2189 (1963).

43. D. R. Inglis, Phys. Rev. 96, 1059 (1964).

44. I. Kelson and C. A. Levinson, Phys. Rev. 134, B269 (1964).

45. E. B. Paul, Phil Mag. 15, 311 (1957).

46. M. G. Redlich, Phys. Rev. 110, 468 (1957).

47. D. Kurath and L. Picman, Nucl. Phys. 10, 313 (1959).

48. J. P. Elliott, Proc. Roy. Soc. (London) A245, 128 (1958).

49. J. P. Elliott, Proc. Roy. Soc. (London) A245, 562 (1958).

50. M. K. Banerjee, C. A. Levinson, and S. Meshkov, Phys. Rev. 130, 1064 (1963).

51. M. Harvey, Nucl. Phys. 52, 542 (1964); also M. Harvey, Phys. Lett. 3, 209 (1963).

52. R. M. Dreizler, Phys. Rev. 136, B321 (1964).

53. J. D. Prentice, N. W. Gebbie, and H. S. Caplan, Phys. Lett. 3, 201 (1963).

54. J. M. Freeman, Phil. Mag. 2, 628 (1957).

55. K. Huang, K. Yagi, T. Awaya, H. Ohnuma, M. Fujioka, and Y. Nogami, J. Phys. Soc. of Japan 18, 646 (1963).

56. H. Smotrich, K. W. Jones, L. C. McDermott, and R. E. Benenson, Phys. Rev. 122, 232 (1961).

57. R. R. Carlson, C. C. Kim, J. A. Jacobs, and A. C. L. Barnard, Phys. Rev. 122, 607 (1961).

58. K. Yagi, K. Katori, H. Ohnuma, Y. Hashimoto, and Y. Nogami, J. Phys. Soc. of Japan 17, 595 (1962).

59. J. W. Butler and H. D. Holmgren, Phys. Rev. 116, 1485 (1959).

60. J. W. Nelson and E. L. Hudspeth, Phys. Rev. 125, 301 (1962).

61. A. J. Howard, "Studies on the Mass-21 System", Doctoral Dissertation, Yale University (1963).

62. H. DeWaard, Nucleonics 13, 36 (1955); also J. A. Becker and E. K. Warburton, Phys. Rev. 134, B350 (1964).

63. S. H. Vegors, L. L. Marsden, and R. L. Heath, Phillips Petroleum Co. Report IDO-16370 (1958).

64. J. B. Marion, Nuclear Data Tables, Part 3, National Academy of Sciences - National Research Council (1960).

65. I. Unna, Phys. Rev. 132, 2225 (1963).

66. J. W. Olness and D. H. Wilkinson, (to be published).

67. K. Yagi, J. Phys. Soc. of Japan 17, 604 (1964).

68. G. Amsel and G. R. Bishop, Phys. Rev. 123, 957 (1961).

69. W. T. Sharpe, J. M. Kennedy, B. J. Sears, and M. G. Hoyle, "Tables of Coefficients for Angular Distribution Analysis", Chalk River Report CRT - 556 (1964).

70. M. F. Thomas, J. Lopes, R. W. Ollerhead, A. R. Poletti, and E. K. Warburton (private communication from R. W. Ollerhead, Oct., 1964).

71. G. Rakavy, Nucl. Phys. 4, 375 (1957).

72. G. Abraham and C. S. Warke, Nucl. Phys. 8, 69 (1958).

73. K. Wildermuth and Th. Kanellopoulos, Nucl. Phys. 9, 449 (1958).

74. S. A. Moszkowski, in Beta-and Gamma-Ray Spectroscopy (ed. K. Siegbahn, North Holland Publishing Co., Amsterdam, 1955) Chapter 13.

75. D. H. Wilkinson, in Nuclear Spectroscopy, Part B, (ed. F. Ajzenberg-Selove, Academic Press, New York, 1960) Chapter V. F.

76. D. Newton, A. B. Clegg, G. L. Salmon (to be published).

77. See Reference 30, p. 31-36.

78. E. B. Carter, G. E. Mitchell, and R. H. Davis, Phys. Rev. 133B, 1421(1964); also, E. B. Carter, B. E. Mitchell, and R. H. Davis, Phys. Rev. 133B, 1434(1964).

79. A. E. Litherland and H. E. Gove, Can. J. of Phys. 39, 471 (1961).

80. J. C. Armstrong and K. S. Quisenberry, Phys. Rev. 122, 150 (1961).

81. W. Zimmerman, Phys. Rev. 114, 837 (1959).

82. W. W. Givens, R. C. Bearse, B. C. Phillips, and A. A. Rollefson, Nucl. Phys. 46, 519 (1963).

83. K. Yagi, Y. Nakajima, K. Katori, Y. Awaya, and M Fujioka, Nucl. Phys. 41, 584 (1964).

84. G. Wickenberg, S. Hjorth, N. G. E. Johansson and B. Sjogren, Arkiv f. Fysik 25, 191 (1963).

85. F. A. El Bedewi, M. A. Fawzi, and N. S. Rizk, in "Proc. of the Paris Conference, 1964" (to be published, Dounod, Paris, 1964).

86. A. A. Rollefson, R. C. Bearse, W. W. Givens, and G. C. Phillips, Bull. Amer. Phys. Soc. 8, 126 (1963).

87. D. E. Alburger, A. Gallman, and D. H. Wilkinson, Phys. Rev. 116, 939(1959).

88. S. Hinds, H. Marchant, and R. Middleton, Nucl. Phys. 38, 81 (1962).

89. P. McWilliams, W. S. Hall, and H. E. Wegner, Rev. Sci. Instr. 33, 70 (1962).

90. S. K. Shah, Phys. Lett. 1, 261 (1962).

91. L. A. Sliv and I. M. Band, "Coefficients of Internal Conversion of Gamma Radiation", University of Illinois Report ICCK1 (1957).

92. See reference 72, p. 859.

93. The author is grateful to Dr. I. Kelson for helpful discussions regarding the deexcitation calculation in which shell model wave functions were employed.

94. J. M. Blatt and V. F. Weisskopf, Theoretical Nuclear Physics (John Wiley and Sons, New York, 1952) p. 595.

95. A. de-Shalit and I. Talmi, Nuclear Shell Theory (Academic Press Inc., New York, 1963).

96. B. J. Raz, Phys. Rev. 120,169 (1960).

97. J. A. Becker and D. H. Wilkinson, Phys. Rev. 134, B1201 (1964).

98. F. C. Barker, Phil Mag. 1, 329 (1959).

99. I. Kelson (private communication, September, 1964).

100. R. E. Beneson and L. J. Lidofsky, Phys. Rev. 123, 939 (1961).

101. J. M. Freeman, Phys. Rev. 120, 1436 (1960).

102. R. M. Dreizler, Phys. Rev. 132, 1166 (1963).

103. E. B. Paul and J. H. Montague, Nucl. Phys. 8, 61 (1958).

104. A. B. Clegg and K. J. Foley, Phil Mag. 7, 247 (1962).

105. D. W. Braben, L. L. Green, J. C. Willmott, Nucl. Phys. 32, 584 (1962).

106. W. Glöckle, Zeits. f. Phys. 178, 53 (1964).

107. K. H. Bhatt, Nucl. Phys. 39, 375 (1962).

108. M. Moshinsky, (private communication, November, 1964).

109. H. B. Burrows, T. S. Green, S. Hinds, and R. Middleton, Proc. Phys. Soc. (London) A69, 310 (1956).

110. S. Hinds and R. Middleton, Proc. Phys. Soc. (London) 74, 779 (1959).

111. A. J. Howard, D. A. Bromley, and E. K. Warburton, Phys. Rev. 136, (1964).

112. D. Pelte, B. Povh, and W. Scholz, Nucl. Phys. 55, 322 (1964).

113. R. D. Bent, J. E. Evans, G. C. Morrison, and I. J. Van Heerden, in "Proc. of Conf. on Reactions Between Complex Nuclei" (ed. A. Ghiorso, R. M. Diamond, and H. E. Conzett, University of California Press, 1963) p. 417.

114. F. Ajzenberg-Selove, L. Cranberg, and F. S. Dietrich, Phys. Rev. 124, 1548 (1961).

115. A. K. Val'ter, V. Yu. Gonchar, A. N. L'Vov, and S. P. Tsytko, Iszv. Akad. Navk. SSSR Ser. Fiz. 23, 298 (1959).

116. A. C. Thomas and N. W. Tanner, Proc. Phys. Soc. (London) 75, 498 (1960).

117. W. W. Beuchner and A. Sperduto, Phys. Rev. 106, 1008 (1957).

118. I. I. Rabi and V. W. Cohen, Phys. Rev. 43, 582 (1933).

119. T. H. Kruse, R. D. Bent, and L. J. Lidofsky, Phys. Rev. 119, 289 (1960).

120. J. J. Singh, V. W. Davis, and R. W. Krone, Phys. Rev. 115, 170 (1959).

121. E. B. Paul and J. H. Montague, Nucl. Phys. 54, 497 (1964).

122. A. J. Howard and W. W. Watson, J. Chem. Phys. 40, 1409 (1964).

123. W. L. Hafner, J. R. Huizenga, and R. Vandenbosch, Argonne National Laboratory Report ANL - 6662 (1962).

124. A. J. Howard (private communication, October, 1964).

125. A. Mizobuch, T. Katoh, J. Ruan, J. Phys. Soc. Japan 15, 1737 (1960).

126. D. A. Bromley, H. E. Gove, and A. E. Litherland, Can. Journ, of Phys. 35, 1057 (1957).

127. The author is grateful to Dr. A. J. Howard for helpful discussions concerning these branching ratio calculations.

128. E. Almqvist, D. A. Bromley, H. E. Gove, and A. E. Litherland, Nucl. Phys. 19, 1 (1960).

129. C. L. McClelland, J. Lowe, and A. J. Howard, Bull. Am. Phys. Soc. 8 , 47 (1963).

130. See reference 4, p.931.

131. H. E. Gove, Nucl. Instr. and Meth. 28, 180 (1964).

132. Dr. I. Kelson, (private communication, September, 1964).

133. See reference 21, p. 516.

134. J. Freeman and D. West, Nucl. Phys. 38, 89 (1962).

135. W. W. Givens, R. C. Bearse, B. C. Phillips and A. A. Rollefson, Nucl. Phys. 43, 553 (1953).

136. G. T. Ewan and A. J. Tavendale, Nucl. Instr. and Meth. (1963); also W. L. Hansen and B. V. Janett, Lawrence Radiation Laboratory Report UCRL - 11589 (1964).

137. J. P. Allen and C. P. Wu, Nucl. Structure Laboratory Report, Yale University, (1964).

138. J. Borysowicz and R. K. Sheline, Phys. Lett. 12, 219 (1964).

139. J. N. Bahcall, Phys. Rev. 135, B 137 (1964).

140. J. N. Bahcall and C. A. Barnes, Phys. Lett. 12, 48 (1964).

141. R. Davis, Phys. Rev. Lett. 12, 302 (1964).

142. J. P. Allen, A. J. Howard, and D. A. Bromley, Bull. Amer. Phys. Soc. 9, (1964).